

**Development of polylactide and polypropylene composites
reinforced with sisal fibres and halloysite nanotubes for
automotive and structural engineering applications**

Prakash Krishnaiah, M.Sc. M.Tech

**Thesis submitted to the University of Nottingham
for the degree of Doctor of Philosophy**

March 2017

Department of Chemical and Environmental Engineering

Faculty of Engineering

The University of Nottingham



**The University of
Nottingham**

UNITED KINGDOM · CHINA · MALAYSIA

Dedication;

To my beloved father and my family

Abstract

In recent decades, scientific research giving more attention to the development of bio-based polymer composites due to the extensive usage of petroleum based fillers as well as polymer matrices for the generation of polymer composites. It is a well-known fact that the petroleum derived polymer composites raise inevitable issues such as environmental pollution, waste management and depletion of petroleum resources etc. So it is important to develop fully or partially biodegradable polymer composites without compromising the mechanical, physical and thermal properties which are required for the end use applications. In this investigation, two different types of filler materials such as sisal fibres and halloysite nanotubes were used to prepare PLA polymer composites and their morphology, physical, mechanical, dynamic mechanical, thermal, water absorption and biodegradable properties were studied. This work also involves the preparation and properties of polypropylene composites reinforced with sisal fibres and halloysite nanotubes to compare the mechanical and thermal properties with PLA composites.

First, surface treatment was performed for sisal fibres in order to remove the amorphous materials such as hemicellulose, lignin and pectin from the surface of the fibres which enhances the fibre-matrix interfacial strength and mechanical properties of the fibres and their polymer composites. Sisal fibres were subjected to different surface treatments such as alkali, high intensity ultrasound (HIU), and the combination of alkali and HIU and their effects on the morphology, fibre diameter, moisture absorption, mechanical and thermal properties of untreated and surface treated sisal fibres were studied. Fourier transform infrared spectroscopy (FTIR) and field emission scanning electron microscopy (FE-SEM) results confirmed the removal

of amorphous materials after the combined treatments of alkali and ultrasound. Moisture absorption and diameter of the sisal fibres were significantly reduced by 40 and 200% respectively after the combination of alkali and HIU treatment as compared to untreated sisal fibres. TGA results revealed that the thermal stability of sisal fibres obtained with the combination of alkali and HIU treatment significantly increased by 38.5 °C as compared to the untreated fibres. Tensile properties of single fibre showed a reduction in the tensile strength and modulus by 25% and 26% respectively as compared to the untreated sisal fibre owing to surface treatments. A reduction in the tensile properties is mainly due to the removal of amorphous materials from the surface of sisal fibres which act as binding materials for cellulose.

Second, the effect of different surface treatments on the morphology, mechanical, thermal, water absorption and biodegradable properties of sisal fibres reinforced PLA (SF/PLA) composites has been investigated. For this, different ratio of untreated and surface treated sisal fibres was mixed with PLA polymer matrix by using an internal mixer. Compounded materials from the internal mixer were subjected to compression moulding to prepare the test specimens. FE-SEM analysis confirmed the good dispersion of different surface treated SF in the PLA composites. The tensile strength and modulus increased by 10 and 75.4% for 15 wt% and 30 wt% of fibre loading respectively with the combined treatment of alkali and HIU PLA composites as compared to the untreated fibre reinforced PLA composites. Young's modulus of the composites has also been predicted by using the theoretical models which fit well to the obtained experimental values. Dynamic-mechanical analysis (DMA) revealed that the combination of alkali and HIU treated SF/PLA composites showed an increase in the storage modulus by 15% and 30% as compared to the untreated fibre composites and pure PLA respectively. TGA and DSC analysis revealed that the thermal stability

and crystallinity increased significantly for the PLA composites reinforced with sisal fibres of combined treatment of alkali and HIU. Water absorption study showed a considerable reduction in the water absorption and coefficient of diffusion by 136% and 130% respectively for the combination of alkali and HIU treated SF/PLA composites as compared to untreated SF/PLA composites. The degradation of SF/PLA composites was studied by composting the samples into the soil. A significant weight loss of 17.87% could be observed for the addition of 30 wt% of untreated SF/PLA composites after soil composting for 120 days.

Apart from sisal fibres, halloysite (Hal) nanotubes were also used as reinforcement fillers to study their effectiveness in improving the mechanical and thermal properties of PLA nanocomposites. Hal nanotubes were surface modified with 3-aminopropyltriethoxysilane (APTES) to enhance the surface interaction of Hal nanotubes with PLA and to achieve good dispersion of Hal nanotubes across the PLA matrix. Nitrogen adsorption-desorption, FTIR and TGA analysis results were confirmed the successful modification of Hal nanotubes surface with APTES. The different wt% of unmodified and APTES modified Hal-PLA nanocomposites were prepared by using internal mixer and compression moulding machine. The resultant Hal-PLA nanocomposites were characterized for their morphology, thermal, mechanical and dynamic-mechanical properties. Tensile strength increased to 62.6 MPa with the addition of 4 wt% of APTES modified Hal-PLA nanocomposites which is 26.5% higher than pure PLA and 15% higher than unmodified (4 wt%) Hal-PLA nanocomposites. Impact strength of 4 wt% APTES modified Hal-PLA nanocomposites increased by 20% and 40% as compared to unmodified Hal-PLA nanocomposites and the pure PLA respectively. TGA analysis revealed that the thermal stability increased significantly by 17 °C with the addition of 4 wt % of

APTES modified Hal nanotubes onto PLA. Storage modulus increased by more than 10% with the addition of 4 wt% of APTES modified Hal nanotubes as compared to pure PLA.

To compare the PLA composites with conventional polymer matrix composites, composites of polypropylene (PP) were prepared by reinforcing with sisal fibres and Hal nanotubes and the effect of surface treatment of sisal fibres and surface modification of Hal nanotubes on the mechanical and thermal properties of SF/PP and Hal-PP nanocomposites were studied. Tensile properties were increased for the combined treated SF/PP composites as compared to the untreated and pure PP. Tensile modulus and strength increased by more than 50% and 10% respectively as compared to the untreated SF/PP composites. TGA and DSC results revealed that the combination of alkali and HIU treatments increased the thermal stability and crystallinity by 8 °C and 8% respectively as compared to untreated SF/PP composites. DMA analysis confirmed the significant enhancement of storage modulus for the combined treated SF/PP composites by 50% as compared to pure PP. Mechanical and thermal properties were studied for unmodified and APTES modified Hal nanotubes reinforced PP nanocomposites. The investigations suggest that the mechanical properties of APTES modified Hal-PP nanocomposites were found to be superior to the unmodified Hal-PP nanocomposites. The tensile strength and modulus increased by 31 and 72% with the addition of 6 wt% of APTES modified Hal-PP nanocomposites as compared to pure PP. Impact strength also increased by 44% than pure PP with 6 wt% loading of APTES modified Hal nanotubes. Thermal analysis revealed that the thermal stability and percentage crystallinity increased by 15 °C and 22% respectively for the Hal-PP nanocomposites with surface modification by

APTES. DMA analysis shows the improved storage modulus by 28% as compared to pure PP.

Based on the present work, it can be said that the sisal fibres and Hal nanotubes have potential as reinforcing materials in the generation of fully bio-based polymer composites. However, surface treatments and/or modification were playing an important role in order to tune the required mechanical and thermal properties of the polymer composites. This study also proved that in comparison to the conventional polymer matrix materials such as PP, PLA is a strong competitor with respect to its good mechanical properties and improved thermal stability apart from the fact that PLA is one of the best known biodegradable and biocompatible polymer matrices in the current market to use not only in medical application, but also in various commercial applications such as packaging, automotive and home appliances.

Publications

Prakash Krishnaiah, Sivakumar Manickam and C.T. Ratnam, 2017. “Enhancements in Crystallinity, Thermal stability, Tensile modulus and Strength of Sisal Fibres and their PP Composites Induced by the Synergistic Effects of Alkali and High Intensity Ultrasound (HIU) treatments”. *Ultrasonics Sonochemistry*. Vol 34, P 729-742.

Prakash Krishnaiah, Sivakumar Manickam and C.T. Ratnam, 2016. “Development of silane grafted halloysite nanotube reinforced polylactide nanocomposites for the enhancement of mechanical, thermal and dynamic-mechanical properties”. *Applied Clay Science*. Vol 135, P 583-595.

Conference presentations

Prakash Krishnaiah, Sivakumar Manickam and C.T. Ratnam, 2015. “Simultaneous Effects of Alkaline and Ultrasound Treatments on the Thermal and Morphological Properties of Sisal fibres”. *In: 2nd Asia-Oceania Sonochemical Society (AOSS-2) Conference, Kuala Lumpur, Malaysia, 25-28 July, 2015.*

Prakash Krishnaiah, Sivakumar Manickam and C.T. Ratnam, 2014. “Effect of silane compatibilizers on morphological, mechanical and thermal properties of Halloysite nanoclay reinforced PLA polymer nanocomposites”. *Postgraduate Research Week 22-26 September 2014, The University of Nottingham Malaysia campus, Semenyih, Malaysia.*

Manuscripts under submission

Prakash Krishnaiah, Sivakumar Manickam and C.T. Ratnam, 2017. “Improved Mechanical Properties and Theoretical Prediction of Young’s modulus of PLA Composites Reinforced with Sisal Fibres”.

Prakash Krishnaiah, Sivakumar Manickam and C.T. Ratnam, 2017. “Synergistic effects of alkali and high intensity ultrasound treatments on thermal stability, water absorption and soil biodegradation of polylactide based bio-composites reinforced sisal fibres”.

Prakash Krishnaiah, Sivakumar Manickam and C.T. Ratnam, 2017. “Bio-composites based on polypropylene reinforced with surface treated sisal fibres: Investigation of dynamic-mechanical, water absorption and thermal properties”.

Acknowledgement

I would like to express my profound gratitude and deep appreciation to my academic chief supervisor **Professor Sivakumar Manickam** for his valuable guidance, support, patience and enthusiastic encouragement throughout the entire period of this research which enabled me to complete the important milestone in my life.

I am also thankful to my co-supervisor **Dr. Chantara Theyy Ratnam** for her valuable guidance, support and suggestions throughout this research work.

I would like to thank **Dr. Ibrahim Alzorqi** for his encouragement and support during his stay as a PhD student in the University of Nottingham.

I would also like to thank to **Dr. Abdul Khaliq Rasheed** and **Mr. Debabrata Panda** for their help during this research work.

Special thanks to **Ms. Noor Fatimah Suhaimi** and **Mr. Ahmad Fareez Mohd Rawi** (laboratory technical staff, faculty of engineering) for their valuable support for completing this work.

Many thanks to all my friends and well-wishers for their encouragement which inspired me to complete the assignment.

Table of contents

Abstract.....	iii
Publications.....	viii
Acknowledgement.....	ix
Table of contents.....	x
List of figures.....	xviii
List of tables.....	xxvii
Abbreviations.....	xxix
CHAPTER I.....	001
Introduction.....	001
1.1 Background.....	001
1.2 Problem statement.....	003
1.3 Scope of the work.....	004
1.4 Objectives.....	005
1.5 Outline of the thesis.....	006
CHAPTER II.....	008
Literature review.....	008

2.1 Polymer composites.....	008
2.2 Natural fibres.....	009
2.2.1 Properties of natural fibres.....	010
2.2.2 Composition of natural fibres.....	012
2.2.2.1 Cellulose.....	014
2.2.2.2 Hemicellulose.....	015
2.2.2.3 Lignin.....	016
2.2.2.4 Pectin.....	018
2.2.3 Sisal fibres.....	018
2.3 Major concern over usage of natural fibres.....	022
2.4 Surface treatments on natural fibres.....	022
2.4.1 Alkali treatment.....	024
2.4.2 High intensity ultrasound (HIU) treatment.....	026
2.4.3 The combined treatment of alkali and HIU.....	028
2.5 Clay based nanofillers.....	029
2.5.1 Halloysite (Hal) nanotubes.....	030
2.6 Polymer matrix materials.....	032
2.6.1 Polylactide or Poly lactic acid (PLA).....	032
2.6.2. Polypropylene (PP).....	037

2.7 Methods used for the processing of polymer composites.....	038
2.7.1 Melt mixer.....	038
2.7.2 Compression moulding.....	039
2.8 Factors affecting the properties of fibre reinforced composites.....	040
2.8.1 Dispersion of fibres in the composites.....	040
2.8.2 Fibre orientation.....	041
2.8.3 Aspect ratio of fibres.....	041
2.8.4 Fibre volume fraction.....	042
2.9 Theoretical predictions of Young’s modulus.....	042
2.9.1 Parallel and series model.....	043
2.9.2 Hirsch model.....	045
2.9.3 Bowyer and Baber model.....	046
2.10 Summary of literature review.....	047
CHAPTER III.....	048
Experimental.....	048
3.1 Introduction.....	048
3.2 Materials.....	048
3.3 Surface treatment methods.....	049
3.3.1. Fibre surface treatments.....	049

3.3.1.1 Alkali treatment.....	049
3.3.1.2 Treatment with high intensity ultrasound (HIU).....	049
3.3.2 Surface modification of Halloysite (Hal) nanotubes.....	050
3.4 Fabrication of composites.....	052
3.4.1 Sisal-PLA composites.....	052
3.4.2 Sisal-PP composites.....	053
3.4.3 Hal-PLA nanocomposites.....	054
3.4.4 Hal-PP nanocomposites.....	055
3.5 Characterisation techniques.....	055
3.5.1 FTIR analysis.....	055
3.5.2 FE-SEM analysis.....	056
3.5.3 Nitrogen absorption-desorption analysis.....	056
3.5.4 XRD analysis.....	057
3.5.5 Tensile properties of single sisal fibre.....	057
3.5.6 Density measurement.....	058
3.5.7 Tensile properties of the composites.....	059
3.5.8 Impact properties of the composites.....	059
3.5.9 TGA analysis.....	059
3.5.10 DSC analysis.....	060

3.5.11 DMA analysis.....	061
3.5.12 Water absorption studies.....	061
3.5.13 Biodegradability analysis.....	062
CHAPTER IV.....	064
Results and discussion: surface treatments and characterisation of sisal fibres.....	064
4.1 Effects of alkali and HIU treatments on sisal fibres.....	064
4.2 FTIR analysis.....	068
4.3 Morphology of sisal fibres.....	071
4.4 Analysis of moisture absorption.....	073
4.5 Analysis of fibre diameter.....	075
4.6 XRD analysis.....	077
4.7 TGA analysis.....	081
4.8 Tensile properties of single sisal fibre.....	085
4.9 Conclusions.....	088
CHAPTER V.....	089
Results and discussion: Sisal-PLA composites.....	089
5.1 FE-SEM analysis.....	089

5.2 FTIR analysis.....	092
5.3 Tensile properties.....	094
5.4 Predictions of Young’s modulus.....	098
5.5 Impact properties.....	103
5.6 DMA analysis.....	104
5.7 TGA analysis.....	109
5.8 DSC analysis.....	111
5.9 Water absorption studies.....	114
5.10 Biodegradability analysis.....	118
5.11 Conclusions.....	122
CHAPTER VI.....	123
Results and discussion: Hal-PLA nanocomposites.....	123
6.1 Nitrogen absorption-desorption analysis.....	123
6.2 FTIR analysis.....	124
6.3 FE-SEM analysis.....	129
6.4 FE-SEM with EDX analysis for Hal nanotubes.....	131
6.5 Tensile and impact properties.....	132
6.6 DMA analysis.....	137

6.7 TGA analysis.....	140
6.8 DSC analysis.....	143
6.9 Conclusions.....	146
CHAPTER VII.....	147
Results and discussion: Sisal-PP composites.....	147
7.1 FE-SEM analysis.....	147
7.2 Tensile and impact properties.....	148
7.3 TGA analysis.....	153
7.4 DSC analysis.....	155
7.5 DMA analysis.....	158
7.6 Water absorption studies.....	162
7.7 Conclusions.....	167
CHAPTER VIII.....	168
Results and discussion: Hal-PP nanocomposites.....	168
8.1 FE-SEM analysis.....	168
8.2 Tensile and impact properties.....	169
8.3 TGA analysis.....	174

8.4 DSC analysis.....	175
8.5 DMA analysis.....	177
8.6 Conclusions.....	181
CHAPTER IX.....	183
Conclusions and future work.....	183
9.1 Conclusions.....	183
9.2 Suggestions for future work.....	185
References.....	186
Appendices.....	216

List of figures

Figure 2.1 General classifications of natural fibres.....	010
Figure 2.2 Constituents and structural arrangements of plant cell wall.....	014
Figure 2.3 Haworth projection formula of cellulose.....	015
Figure 2.4 Chemical structure of hemicellulose.....	016
Figure 2.5 Chemical structure of lignin.....	016
Figure 2.6 Chemical structure of three main precursors of lignin.....	017
Figure 2.7 Chemical structure of pectin.....	018
Figure 2.8 Photograph of sisal plant.....	019
Figure 2.9 Cross sectional view of sisal leaf and ribbon-fibre bundles.....	020
Figure 2.10 Schematic diagram showing the mechanism of HIU treatment on natural fibres.....	027
Figure 2.11 Pictorial representations of chemical and ultrasound treatments on natural fibres.....	028
Figure 2.12 The two stereo-isomeric forms of lactic acid.....	034
Figure 2.13 Synthesis of PLA from L- and D-lactic acids.....	034
Figure 3.1 Schematic diagram of the method followed to determine the tensile strength of single fibre.....	058

Figure 4.1 Schematic representation of the effects of alkali and HIU treatments on the sisal fibres.....	066
Figure 4.2 Visual examination of sisal fibres: (A) Untreated (UT), (B) High intensity ultrasound treated (ULT), (C) Alkali treated (ALKT), (D) Combination of alkali and high intensity ultrasound treated (ALKT-ULT) sisal fibres.....	067
Figure 4.3 FTIR spectra of untreated (UT), ultrasound treated (ULT), alkali treated (ALKT) and the combination of alkali and ultrasound treated (ALKT-ULT) sisal fibres.....	070
Figure 4.4 FE-SEM micrographs of sisal fibres: (A) Untreated (UT) (B) Ultrasound treated (ULT) (C) Alkali treated (ALKT) (D) the combination of alkali and ultrasound treated (ALKT-ULT).....	072
Figure 4.5 Moisture content of untreated (UT), ultrasound treated (ULT), alkali treated (ALKT) and the combination of alkali and ultrasound treated (ALKT-ULT) sisal fibres.....	074
Figure 4.6 FE-SEM images of sisal fibres with the diameter for different concentration of alkali treatment and combination of alkali and ultrasound treatments (A) Untreated (B) HIU treated (C) Alkali treated (D) the combination of alkali and HIU treated.....	076
Figure 4.7 X-ray diffractogram of untreated (UT), alkali treated (ALKT) and the combination of alkali and HIU treated (ALKT-ULT) sisal fibres (A: Untreated, B: HIU treated, C-G: Alkali treated (3, 5, 7, 9 and 15 wt% of alkali), H-L: Combination of alkali and HIU treated (3, 5, 7, 9 and 15 wt% of alkali).....	079

Figure 4.8 Percentage of crystallinity as a function of percentage of alkali concentration for untreated (UT), high intensity ultrasound treated (ULT), alkali treated (ALKT) and the combination of alkali and high intensity ultrasound treated (ALKT-ULT) sisal fibres.....	080
Figure 4.9 TGA curves of untreated (UT), ultrasound (ULT) and alkali treated (ALKT) sisal fibres.....	081
Figure 4.10 TGA curves of untreated (UT), ultrasound treated (ULT) and the combination of alkali and ultrasound treated (ALKT-ULT) sisal fibres.....	083
Figure 4.11 Thermal stability of untreated (UT), alkali (ALKT) and the combination of alkali and ultrasound treated (ALKT-ULT) sisal fibres.....	084
Figure 4.14 Typical stress-strain curves of single sisal fibre.....	085
Figure 4.15 Tensile properties of untreated (UT), high intensity ultrasound treated (ULT), alkali treated (ALK) and the combination of alkali and high intensity ultrasound treated (ALKTULT) sisal fibres: (A) tensile strength (B) tensile modulus.....	087
Figure 5.1 FE-SEM images of (A) untreated (UT), (B) ultrasound treated (ULT), (C) alkali treated (ALK) and (D) the combination of alkali and ultrasound treated (ALKTULT) SF/PLA composites.....	090
Figure 5.2 FTIR spectra of sisal fibre, pure PLA and SF/PLA composites.....	092
Figure 5.3 Tensile strength of untreated (UT), ultrasound treated (ULT), alkali treated (ALK) and the combination of alkali and ultrasound treated (ALKTULT) sisal fibres reinforced PLA composites.....	094

Figure 5.4 Tensile modulus of untreated (UT), HIU treated (ULT), alkali treated (ALK) and the combination of alkali and HIU treated (ALKULT) SF/PLA composites.....	096
Figure 5.5 Tensile elongation at break of untreated (UT), HIU treated (ULT), alkali treated (ALK) and the combination of alkali and HIU treated (ALKULT) sisal fibres reinforced PLA composites.....	098
Figure 5.6 Variations of theoretical and experimental values of tensile modulus for the untreated sisal fibre reinforced PLA composites.....	099
Figure 5.7 Variations in the theoretical and experimental values of tensile modulus for the HIU treated SF/PLA composites.....	100
Figure 5.8 Variations in the theoretical and experimental values of tensile modulus of alkali treated SF/PLA composites.....	101
Figure 5.9 Variations in the theoretical and experimental values of tensile modulus of the combination of alkali and HIU treated SF/PLA composites.....	102
Figure 5.10 Impact strength of untreated (UT), ultrasound treated (ULT), alkali treated (ALK) and the combination of alkali and HIU treated (ALKULT) SF/PLA composites.....	103
Figure 5.11 Storage modulus (E') of untreated (UT), HIU treated (ULT), alkali treated (ALK) and the combination of alkali and HIU treated (ALKULT) sisal fibres reinforced PLA composites.....	105

Figure 5.12 Loss modulus (E'') curves of untreated (UT), HIU treated (ULT), alkali treated (ALK) and the combination of alkali and HIU treated (ALKULT) SF/PLA composites.....	107
Figure 5.13 Tan delta curves of untreated (UT), HIU treated (ULT), alkali treated (ALK) and the combination of alkali and HIU treated (ALKULT) SF/PLA composites.....	108
Figure 5.14 TGA of untreated (UT), HIU treated (ULT), alkali treated (ALK) and the combination of alkali and HIU treated (ALKULT) SF/PLA composites.....	110
Figure 5.15 DSC thermograms of pure PLA, untreated (UT), HIU treated (ULT), alkali treated (ALK), and the combination of alkali and HIU treated (ALKULT) SF/PLA composites.....	112
Figure 5.16 Effect of fibre loading on water absorption of untreated SF/PLA composites.....	114
Figure 5.17 Effect of high intensity ultrasound (ULT), alkali (ALK) and the combination of alkali and HIU (ALKULT) surface treatments on the water absorption of SF/PLA composites.....	116
Figure 5.18 Biodegradation of untreated (UT), HIU treated (ULT), alkali treated (ALK) and the combination of alkali and HIU treated (ALKULT) sisal fibre reinforced PLA composites with different weight percentage of fibre loading.....	119
Figure 5.19 FE-SEM images of outer surface of the soil buried samples (A) Pure PLA before soil burial, (B) Pure PLA after 60 days, (C) Pure PLA after 120 days, (D) 15 wt% untreated sisal fibre (UT) + PLA composites before soil burial, (E) 15UT+PLA	

after 60 days, (F) 15UT+PLA after 120 days, (G) 15 wt% of alkali and HIU treated sisal fibre (ALKULT) + PLA composites before soil burial, (H) 15ALKULT+PLA after 60 days, (I) 15ALKULT+PLA after 120 days.....	121
Figure 6.1 Nitrogen adsorption-desorption isotherms of unmodified (uHal) and APTES modified Hal nanotubes (mHal).....	124
Figure 6.2 FTIR spectra of unmodified (uHal) (A) and APTES modified Hal nanotubes (mHal) (B).....	125
Figure 6.3 FTIR spectra of PLA/unmodified Hal nanotubes (PLAuHal) (A) and PLA/APTES modified Hal nanotubes (PLAmHal) (B).....	127
Figure 6.4 FE-SEM images of impact fractured samples of unmodified (uHal) and APTES modified (mHal) Hal-PLA nanocomposites: (A) Hal nanotubes (B) Pure PLA (C) 4 wt% uHal (D) 4 wt% mHal.....	130
Figure 6.5 FE-SEM images of (A) unmodified (uHal) and (B) APTES modified Hal nanotubes (mHal).....	131
Figure 6.6 Tensile strength of unmodified and APTES modified Hal-PLA nanocomposites.....	133
Figure 6.7 Tensile modulus of Hal nanotubes (unmodified (uHal) and APTES modified Hal nanotubes (mHal)) PLA nanocomposites.....	134
Figure 6.8 Impact strength of Hal nanotubes (unmodified (uHal) and APTES modified (mHal)) PLA nanocomposites.....	136
Figure 6.9 storage modulus of Hal (unmodified (uHal) and APTES modified (mHal)) PLA nanocomposites.....	138

Figure 6.10 Comparison of Tan delta values of Hal nanotubes (unmodified (uHal) and APTES modified (mHal)) PLA nanocomposites.....	139
Figure 6.11 TGA curves of (A) unmodified (uHal) and (B) APTES modified Hal nanotubes (mHal).....	140
Figure 6.12 TGA curves of Hal nanotubes (modified and unmodified) PLA nanocomposites.....	142
Figure 6.13 DSC curves of Hal nanotubes (unmodified (uHal) and APTES modified (mHal)) PLA nanocomposites.....	143
Figure 7.1 FE-SEM micrographs of sisal fibres reinforced PP composites (A) Untreated (UT), (B) HIU treated (ULT), (C) Alkali treated (ALKT), (D) Combined treatment of alkali and HIU (ALKT-ULT).....	148
Figure 7.2 Tensile strength of untreated and treated sisal fibre reinforced PP composites 1) Untreated (UT) 2) HIU treated (ULT) 3) Alkali treated (ALKT) 4) combined treatment of alkali and HIU (ALKT-ULT).....	149
Figure 7.3 Elongation at break of untreated and treated sisal fibre reinforced PP composites.....	151
Figure 7.4 Tensile modulus of untreated and treated sisal fibre reinforced PP composites.....	152
Figure 7.5 TGA of untreated (UT), HIU treated (ULT), alkali treated (ALK) and the combination of alkali and HIU treated (ALKULT) SF/ PP composites.....	153

Figure 7.6 DSC endothermic heating curves of untreated (UT), HIU treated (ULT), alkali treated (ALK), and the combination of alkali and HIU treated (ALKULT) SF/PP composites.....	156
Figure 7.7 DSC exothermic cooling curves of untreated (UT), HIU treated (ULT), alkali treated (ALK), and the combination of alkali and HIU treated (ALKULT) SF/PP composites.....	157
Figure 7.8 Storage modulus (E') of untreated (UT), HIU treated (ULT), alkali treated (ALK), and the combination of alkali and HIU treated (ALKULT) SF/PP composites.....	159
Figure 7.9 Tan δ curves of untreated (UT), HIU treated (ULT), alkali treated (ALK), and the combination of alkali and HIU treated (ALKULT) SF/PP composites.....	160
Figure 7.10 Loss modulus curves of untreated (UT), HIU treated (ULT), alkali treated (ALK), and the combination of alkali and HIU treated (ALKULT) SF/PP composites.....	162
Figure 7.11 Effect of fibre loading on the water absorption of untreated SF/PP composites.....	163
Figure 7.12 Effect of HIU (ULT), alkali (ALK) and the combination of alkali and HIU (ALKULT) surface treatments on the water absorption of SF/PP composites.....	164
Figure 8.1 FE-SEM image of unmodified (a) and APTES modified (b) Hal nanotubes reinforced PP nanocomposites.....	168
Figure 8.2 Tensile strength of untreated and APTES modified Hal nanotubes reinforced PP nanocomposites.....	170

Figure 8.3 Tensile modulus of unmodified and APTES modified Hal nanotubes reinforced PP nanocomposites.....	171
Figure 8.4 Elongation at break of unmodified and APTES modified Hal nanotubes reinforced PP nanocomposites.....	172
Figure 8.5 Izod impact strength of notched unmodified and APTES modified Hal-PP nanocomposites.....	173
Figure 8.6 TGA thermo-grams of pure PP, unmodified and APTES modified Hal-PP nanocomposites.....	174
Figure 8.7 DSC melting curves of pure PP, unmodified and APTES modified Hal-PP nanocomposites.....	176
Figure 8.8 DSC cooling curves of pure PP, unmodified and APTES modified Hal-PP nanocomposites.....	177
Figure 8.9 Storage modulus (E') curves of unmodified and APTES modified Hal nanotubes reinforced PP nanocomposites.....	179
Figure 8.10 Loss modulus curves of unmodified and APTES modified Hal nanotubes reinforced PP nanocomposites.....	180
Figure 8.11 Tan δ curves of unmodified and APTES modified Hal nanotubes reinforced PP nanocomposites.....	181

List of tables

Table 2.1 Mechanical and physical properties of few important natural fibres.....	011
Table 2.2 Chemical composition of few important natural fibres.....	013
Table 2.3 Comparison of physical and mechanical properties PLA and other commodity polymers.....	036
Table 3.1 Composition of untreated and treated sisal fibres reinforced PLA composites.....	052
Table 3.2 Composition of PP/Sisal composites.....	053
Table 3.3 Composition of Hal nanotubes (APTES modified/unmodified) PLA nanocomposites.....	054
Table 3.4 Composition of Hal nanotubes (APTES modified/unmodified) PP nanocomposites.....	055
Table 4.1 FTIR transmittance peaks of the constituents of sisal fibres.....	069
Table 4.2 Diameter of untreated and different surface treated sisal fibres.....	077
Table 5.1 Effects of surface treatments on thermal stability of SF/PLA composites.	111
Table 5.2 Thermal properties of pure PLA and SF/PLA composites.....	113
Table 5.3 Water absorption properties of SF/PLA composites.....	118
Table 6.1 Nitrogen adsorption and desorption data of surface area (S_{BET}), Langmuir surface area, volume (V_{pore}) and width (W_{pore}) for unmodified (uHal) and APTES modified Hal nanotubes (mHal).....	123

Table 6.2 FTIR bands and assignments for uHal, mHal and Hal-PLA nanocomposites.....	128
Table 6.3 EDX results of unmodified and APTES modified Hal nanotubes.....	131
Table 6.4 Mechanical properties of Hal nanotubes (unmodified and APTES modified) PLA nanocomposites.....	135
Table 6.5 storage modulus (at room temperature) and peak temperature of $\tan \delta$ (Tg) of Hal nanotubes (unmodified (uHal) and APTES modified (mHal)) PLA nanocomposites.....	139
Table 6.6 Thermal properties of Hal nanotubes (unmodified (uHal) and APTES modified (mHal)) PLA nanocomposites.....	143
Table 6.7 DSC results of Hal nanotubes (unmodified (uHal) and APTES modified (mHal)) PLA nanocomposites.....	145
Table 7.1 Thermal properties of PP and untreated and different surface treated SF/PP composites.....	157
Table 7.2 Storage modulus of SF/PP composites.....	159
Table 7.3 Water absorption properties of SF/PP composites.....	166
Table 8.1 TGA and DSC data of melting temperature (T_m), cold crystallization temperature (T_c) and percentage of crystallinity (X_c).....	177

List of Abbreviations

APTES	3-Aminopropyltriethoxysilane
ASTM	American society for Testing and Materials
CPN	Clay Polymer Nanocomposites
DMA	Dynamic Mechanical Analysis
DSC	Differential Scanning Calorimetry
exo	Exothermic
FTIR	Fourier Transform Infrared spectroscopy
FE-SEM	Field-emission scanning electron microscopy
Fig	Figure
GPa	Giga Pascal
h	Hours
Hal	Halloysite
HDPE	High-density Polyethylene
HIU	High intensity ultrasound
ISO	International Standard Organisation
KBr	Potassium Bromide
kHz	Kilohertz
LDPE	Low-density Polyethylene
mg	Milligram
MPa	Mega Pascal
ml	Millimetre
Mw	Molecular weight
NaOH	Sodium hydroxide
nm	Nanometre
OH	Hydroxide

Pa	Pascal
PE	Polyethylene
PLA	Poly lactide or Poly (lactic acid)
PP	Polypropylene
PS	Polystyrene
PVC	Polyvinyl Chloride
SF	Sisal Fibres
s	Second
TGA	Thermo-gravimetric analysis
Wt%	Weight Percentage
W/v	Weight/volume ration
°C	Celsius

CHAPTER I

Introduction

1.1 Background

Polymer composite materials are playing an important role in our day-to-day life from aerospace industries to common household applications due to their low density, high strength, easy processability, easy availability and more importantly low cost as compared to metal matrix composites. However, extensive usage of petroleum based fibres such as glass fibres, Kevlar fibres, carbon fibres, and phenolic based fibres etc. as reinforcement fillers in the generation of polymer composites raises many issues such as depletion of petroleum resources, waste management due to non-degradable fillers and matrices used and environmental pollution etc. Thus, it is important to develop fully or partially biodegradable polymer matrices as well as fillers to produce the biodegradable polymer composites to combat the above-mentioned challenges (Raquez et al., 2013).

Currently researchers focus on the development of bio-derived polymer matrix and filler materials to produce biodegradable polymer composites. Poly (lactic acid) or Polylactide (PLA) is one such polymer matrix with high potential to replace many conventional synthetic polymer matrices. It is derived from the renewable resources such as corn, starch and sugarcane (Raquez et al., 2013). PLA is getting wide attention owing to its attractive mechanical properties, recyclability, biocompatibility and biodegradability (Wu et al., 2013; Arrieta et al., 2014). However, PLA has limitations of low thermal stability, low toughness and extreme brittleness (Pandey et al., 2005; Lim et al., 2008). It is therefore necessary to improve the mechanical and

thermal properties of PLA when we aim for specific applications more importantly on a large scale (Raquez et al., 2013).

To overcome the limitations of PLA, it is necessary to incorporate different types of filler materials into PLA matrix. Natural fibres and natural clay materials are the two different types of fillers which are highly cost-effective and offer many benefits such as improved mechanical and thermal properties of the composites, easy processing, light weight, recyclability, biodegradability and biocompatibility. Over the last few decades, natural fibres are emerging as one of the best reinforcing fillers in the production of polymer composites due to their properties that are environmentally favourable (Dittenber and Gangarao, 2012). Some of the important properties of natural fibres as compared to their synthetic counterparts are ready availability with low cost, good mechanical properties, low weight, eco-friendly, biocompatibility and biodegradability (Azwa et al., 2013).

Natural fibres are derived from plant based materials such as banana, hemp, sisal, jute, kenaf blast, flax, bamboo, palm sugarcane, date etc. (Sudhakara et al., 2013; Šutka et al., 2013; Saba et al., 2016). Amongst all cellulosic fibres, sisal fibres are the well accepted natural fibres to use them as reinforcing fillers in the generation of polymer composites due to their higher cellulosic content (>78%), high stiffness and good tensile strength (>600MPa). Sisal fibres are hard and stiff and are extracted from the leaves of sisal plant (Li et al., 2000).

However, unlike many other synthetic fibres, natural fibres have limitations due to their hydrophilic nature which causes incompatibility with hydrophobic nature of polymer matrices to use them as reinforcing fillers. This is mainly due to the presence of amorphous materials such as hemicellulose, lignin, pectin and other waxy materials

on the surface of natural fibres. These amorphous materials have the tendency of absorbing moisture which leads to a significant reduction in the mechanical, thermal and structural properties of natural fibre reinforced polymer composites (John and Thomas, 2008). Thus, it is important to remove the amorphous materials from the surface of natural fibres in order to achieve the targeted mechanical, thermal and structural properties depending on the end use applications. Surface treatment is often the used method in the removal of amorphous materials which enhances the interfacial adhesion between the reinforcing fillers and polymer matrices which leads to improved mechanical and thermal properties of the composites (Kabir et al., 2012).

It has already been proved that the incorporation of nanofillers onto PLA matrix increases crystallization ability, elongation and thermal properties. The incorporation of exfoliated graphite onto PLA matrix increased the tensile strength and thermal stability by 12% and 14 °C respectively as compared to pure PLA (Evagelia et al., 2011; Kim and Jeong, 2010). The clay based nanofillers as plasticizer are good substitutes which also improved the thermal properties of PLA more than 20% as compared to pure PLA (Liu et al., 2013).

1.2 Problem statement

In recent years, there are growing concerns of environmental pollution due to extensive usage of synthetic polymer composites which are derived from petroleum resources. These synthetic polymer composites are completely non-degradable which cause a huge threat to environment. Since these polymeric materials are non-degradable, waste management is the major issue. It is reported that more than 275 million metric tons of plastic wastage is getting generated from 192 countries in which around 12 million metric tons entering to the ocean every year (Jambeck et al.,

2015) which cause severe environmental pollution. Another major problem by using the petroleum based polymers is the depletion of petroleum resources. It is therefore important to develop fully or partially biodegradable polymer composites in order to overcome the above-said environmental issues.

1.3 Scope of the work

PLA is an important biodegradable polymer which has good tensile properties, biodegradability, biocompatibility and derived from renewable sources such as corn, starch etc. However, PLA has major drawbacks such as high brittleness, lower impact strength, low thermal stability and high cost as compared to conventional polymers which cause limitations to its usage in many technical applications. The main scope of this work is to improve the mechanical and thermal properties of PLA with the incorporation of different types of fillers.

Among many natural fibres, sisal fibres are gaining good attention owing to their good tensile strength, easy availability, low density, low cost and biodegradability. However, sisal fibres are hydrophilic in nature due to the presence of amorphous materials on the surface of fibres which cause incompatibility between sisal fibres and polymer matrix leading to a major issue in employing the sisal fibres as fillers in the generation of PLA polymer composites. Amorphous materials from the surface of sisal fibres can be removed by using different surface treatments which are effective in removing the amorphous materials and enhance the interfacial adhesion between sisal fibres and polymer matrices.

On the other hand, halloysite (Hal) nanotubes are naturally occurring aluminosilicates having the formula, $\text{Al}_2\text{Si}_2\text{O}_5(\text{OH})_4 \cdot n\text{H}_2\text{O}$. Their tubular structure in nano dimension with high aspect ratio makes them as unique materials to be used as fillers in the

generation of clay-polymer nanocomposites (CPN). However, similar to other nanoparticles, dispersion of Hal nanotubes into polymer matrix is challenging (Kim and Jeong, 2010; Raquez et al., 2013). Modification or functionalization of nanofillers is a way to enhance their dispersion into polymer matrix. Functionalization of Hal nanotubes can enhance the surface properties and leads to good dispersion into PLA matrix of the CPN. Surface modification of Hal nanotubes with different types of silane coupling agents is the most common method to improve the surface properties of Hal nanotubes. This method is referred as the grafting of silanes and is carried out via condensation between hydrolysed silanes and surface hydroxyl groups of Hal nanotubes. The modification of Hal nanotubes with silane coupling agent enhanced the dispersion of Hal nanotubes into polymer matrix and improved the mechanical properties and thermal stability of the resultant nanocomposites (Rooj et al., 2010).

1.4 Objectives:

- ❖ To study the effect of different surface treatments such as alkali, high intensity ultrasound (HIU) and the combination of alkali and HIU treatments on the removal of amorphous materials from the surface of sisal fibres and characterising the structural and morphological changes of sisal fibres. This study also involves the investigations of crystallinity, thermal stability and tensile properties of untreated and different surface treated sisal fibres.
- ❖ To prepare sisal fibre reinforced PLA composites and to study the effect of alkali, HIU and the combination of alkali and HIU surface treatments on morphology, mechanical, thermal, water absorption and biodegradability properties of sisal fibres reinforced PLA biocomposites. This study also involves the theoretical predications of Young's modulus of the effect of different surface treatments of sisal fibres reinforced with PLA biocomposites.

- ❖ To study the effect of silane coupling agent i.e., 3-Aminopropyltriethoxy silane (APTES) on the surface of Halloysite (Hal) nanotubes and characterising APTES modified Hal nanotubes and their PLA nanocomposites for their structural modifications, morphology, mechanical and thermal properties.
- ❖ To study the effect of different surface treatments of sisal fibres and their polypropylene (PP) composites on their morphological, mechanical, thermal and water absorption properties.
- ❖ To investigate the effect of APTES modified Hal nanotubes on the mechanical, dynamic mechanical, thermal and water absorption properties of PP nanocomposites reinforced with Hal nanotubes.

1.5 Outline of the thesis:

This thesis consists of nine chapters. Chapter one is the introduction which describes the background and objectives of the present study and also summarises the outline of the thesis. Chapter two consists of a comprehensive literature review which addresses the relevant background of the present work. Chapter three gives the details of materials, experimental procedures and characterisation techniques used in this investigation. Chapter four represents the results and discussion of the effects of different surface treatments such as alkali, HIU, and the combination of alkali and HIU treatments on the structural, mechanical and thermal properties of sisal fibres. Chapter five deals with the results and the detailed discussion of the effect of fibre surface treatments and fibre loading on the morphology, mechanical, physical, thermal, water absorption properties as well as the biodegradability of sisal fibres reinforced PLA composites. Chapter six describes the results and discussion of the effect of surface modification on the morphology, structural changes and thermal

properties of APTES modified Hal nanotubes. This chapter also deals with the results and discussion of the effect of surface modification and filler loading on the morphological, mechanical and thermal properties of Hal nanotubes reinforced PLA nanocomposites. Chapter seven gives the results and detailed discussion of the morphological, mechanical, thermal and water absorption properties of untreated and different surface treated sisal fibre reinforced PP composites. Chapter eight presents the results and discussion of the effect of APTES modified Hal nanotubes on the morphology, mechanical and thermal properties of PP composites reinforced with Hal nanotubes. Chapter nine draws the conclusions of this investigation and also gives the suggestions for the further investigation on this specialised area.

CHAPTER II

Literature Review

2.1 Polymer composites

Composites are combining and orienting of two or more different materials to achieve superior properties which is a well-known and proven concept. There are many examples for natural composites such as teeth, bones, bird feathers and plant leaves. Composites can be produced with ceramics, metal or polymers which are used as matrices and for the reinforcement phases different fibres can be used such as ceramic, metallic or polymeric (Malhotra et al., 2012). However, a more common classification relates to whether they are synthetic or natural (Gibson, 2010).

Polymer composites are low in strength and stiffness compared to metallic and ceramic composites but their density is low and are easily formed. The reinforcing phase of a composite can be either fibrous or particulate, the difference being that a particle has almost equal dimensions in all the directions, whilst a fibre has a greater length than its cross-sectional area and both of these reinforcements have been used to produce composites. Fibre materials are receiving much attention in recent years due to their high tensile strength and young's modulus, low density and ability to give better mechanical and thermal properties to end use applications. In the fibre reinforced composite materials, fibres are used to carry the loads while the matrices are used to bind the fibres together. Many fibre reinforced polymer matrix composites offer a combination of strength and stiffness that are comparable to, or even better than some of the traditional metallic composite materials (Tjong, 2013).

Different types of fibrous materials are used in the reinforcement phase of the composites in order to get good mechanical properties. Generally fibres are classified as natural and synthetic fibres. Few examples of synthetic fibres are carbon, acrylic, phenolic, aramid and glass fibres. Synthetic fibres are strong and stiff as compared to natural fibres (Diez-Pascual et al., 2014). However, synthetic fibres have drawbacks such as high density, non-degradability, non-biocompatibility and also concern about depletion of petroleum resources, waste management issues etc., so it is important to develop biodegradable and renewable fibre materials such as natural fibres as reinforcement fillers in the polymer composites (Mantia and Morreale, 2011).

The use of natural fibres as reinforcement fillers in the polymer composites to replace conventional fibres like glass is the current trend. The usage of natural fibres gives much attention to the materials engineers mainly because of the growing environmental issues and advantages of natural fibres over their conventional counterparts (Koronis et al., 2013a). In the last few years, research activities are focussing on the application of natural fibres as reinforcement materials in the polymer composites. The use of natural fibres in the generation of polymer composites offers many advantages such as economically cheaper, their ability to recycle and their good mechanical properties by which they compete with many synthetic fibres (John et al. 2008).

2.2 Natural fibres

Natural fibres can be derived from plant, animal and minerals. General classification of natural fibres is shown in **Fig. 2.1**. Plant or cellulosic fibres are the most commonly used natural fibres in the generation of fibre reinforced polymer composites. According to literature, apart from the wood based fibres, there are more than 1000

different types of natural fibres are available (Mwaikambo and Ansell, 2002). Natural fibres can be extracted from different parts of the plant such as stem, leaves, fruits etc. Fibres which are extracted from the stem are called as bast fibres. Few examples of bast fibres are hemp, Ramie, Kenaf, flux, jute etc. Sisal, pineapple and abaca are the common leaf fibres (Dittenber and Gangarao, 2012). Since the last two decades, the production of natural fibres is being increased significantly due to awareness that non-renewable resources are getting depleted.

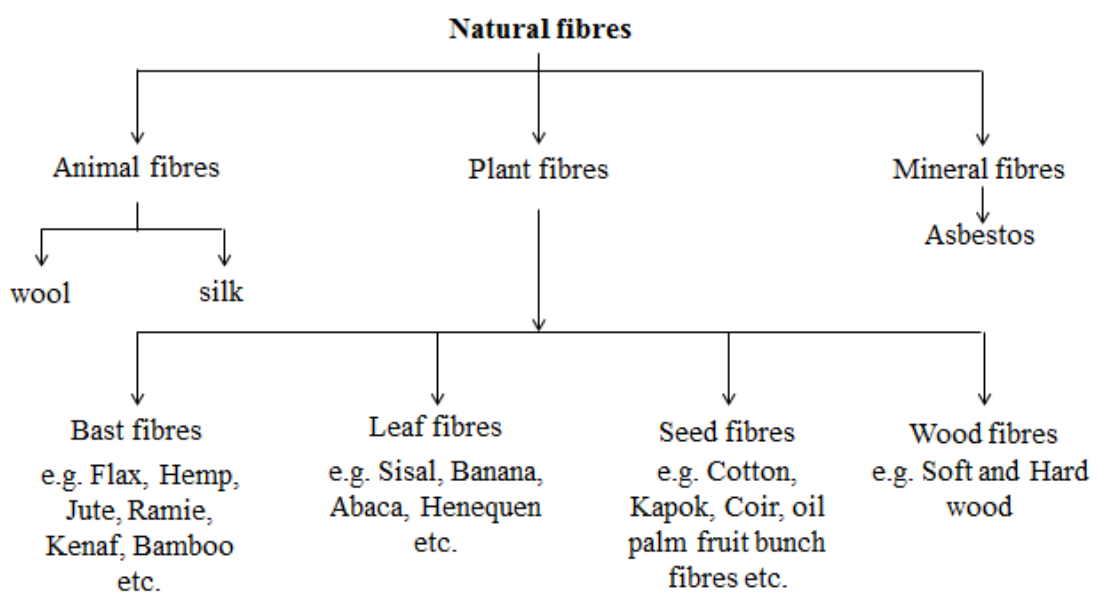


Fig. 2.1 General classification of natural fibres (Abdul Khalil et al., 2012)

2.2.1 Properties of natural fibres

Natural fibres tend to be stronger and stiffer as compared to their animal counterparts which make them useful as reinforcement materials to produce polymer composites. Moreover naturally available fibre materials having advantages over animal fibres such as easy processing, comparatively cheaper and are readily available. Natural fibres reinforced polymer composites possess lower tensile strength as compared to glass fibre composites though the modulus is of the same order of magnitude

(Pickering et al., 2016). **Table 2.1** shows the mechanical and physical properties of different natural fibres in order to have a broader view of their properties to compare with their synthetic counterparts.

Table 2.1 Mechanical and physical properties of few important natural fibres (Dicker et al., 2014; Dittenber and Gangarao, 2012; Ho et al., 2012; Koronis et al., 2013b)

Fibre type	Density (g/cm³)	Diameter (µm)	Tensile strength (MPa)	Tensile modulus (GPa)	Moisture content (wt%)	Price (USD/kilo)
Abaca	1.5	10 – 30	430 – 980	6 – 20	5 – 10	0.345
Bamboo	0.6 – 1.1	25 – 40	140 – 800	11 – 32	-	0.5
Banana	1.35	12 – 30	140 – 800	12 – 30	8.7 – 12	-
Coir	1.2	10 – 460	130 – 240	4 – 6	8	0.25 – 0.5
Cotton	1.5 – 1.6	10 – 45	350 – 800	7 – 12	7.85 – 8.5	2.1 – 4.2
Flax	1.5	12 – 600	750 – 940	75 – 90	8 – 12	2.1 – 4.2
Hemp	1.47	25 – 250	550 – 900	38 – 70	6.2 – 12	1.55
Jute	1.3 – 1.4	20 – 200	393 – 800	13 – 26	12 – 13	0.925
Kenaf	1.5 – 1.6	2.6 – 4	350 – 930	40 – 53	-	0.378
Oil palm	0.7 – 1.5	150 – 500	80 – 248	0.5 – 3.2	-	-
Ramie	1.0 – 1.5	20 – 80	400 – 1000	24.5 – 128	7.5 – 17	2
Sisal	1.3 – 1.5	8 – 200	360 – 700	9 – 25	10 – 22	0.6 – 0.7
E-glass	2.55	15 – 25	345 – 1500	27 – 39	-	1.6 – 3.5
Carbon	1.8	<17	4400 – 4800	225 – 260	-	124 – 166

Mechanical and physical properties of natural fibres vary depending on factors such as crop production, temperature, soil condition in which plants are growing and the weather conditions. Fibre selection plays an important role in the achievement of specific required properties. The location of the fibres within the plant influences the properties of fibre materials (Dittenber and Gangarao, 2012). However, when the specific modulus of natural fibres is considered, natural fibres show values that are comparable to or even better than glass fibres. Savings on the material cost due to the use of natural fibres and high fibre filling levels, coupled with the advantage of being non-abrasive to the mixing and moulding equipment make natural fibres important materials in the production of polymer composites. These benefits mean natural fibres could be used in many applications which include building, automotive, household appliances and others (Gurunathan et al., 2015; Yan et al., 2016b).

2.2.2 Composition of natural fibres

Chemical composition as well as structure of the natural fibres mainly depend on several factors such as nature of the plant source, growing conditions of the plant, climate, age of the plant and extraction process of the fibres (Faruk et al., 2012). **Table 2.2** shows the percentage composition of different natural fibres. A single natural fibre filament has a diameter approximately in the range of 10 to 650 μm , which itself is a kind of natural composite. It consists of three major components, namely cellulose, hemicellulose and lignin in different proportions in different fibres. From 80 to 90% of natural fibres made up of cellulose, hemicellulose, lignin and pectin. Apart from these, natural fibres also have minerals, waxes and other water-soluble components (Majeed et al., 2013). The inner cell wall contains rigid cellulose component which is embedded in a soft lignin and hemicellulose matrix in the secondary cell wall of the fibre materials (Dittenber and Gangarao, 2012).

Table 2.2 Chemical composition of few important natural fibres (John and Anandjiwala, 2008; Abdul Khalil et al., 2012; Dittenber and Gangarao, 2012; Dicker et al., 2014; Yan et al., 2016b)

Cellulosic fibres	Composition (wt%)			
	Cellulose	Hemicellulose	Lignin	Pectin
Hard wood	43 – 47	25 – 35	16 – 24	-
Soft wood	40 – 44	25 – 29	25 – 31	-
Abaca	56 – 63	20 – 25	7 – 13	0.8
Bagasse	32 – 55	30	20	10
Coir	32 – 43	10 – 20	43 – 49	4
Cotton	95	2	1	6
Oil palm	50	30	17	-
Flax	62 – 72	18.6 – 20.6	2 – 5	0.9
Hemp	68 – 74.4	15 – 22	3.7 – 10	0.9
Henequen	60 – 77	4 – 28	8 – 13	-
Jute	71	14	13	0.2
Kenaf	31 – 72	20.3 – 21.5	8 – 19	2
Ramie	76	17	1	2
Sisal	60 – 78	10 – 14	8 – 11	1.2

Composition and structural arrangements of plant fibre cell wall have been shown in **Fig. 2.2**. The lignin material in the secondary cell wall bonds together with cellulose and hemicellulose and it acts as a cementing material. Pectin is another component which helps to attach the cellulose fibre with all other component together. Both

lignin and pectin are the weak amorphous polymers as compared to cellulose (Dicker et al., 2014).

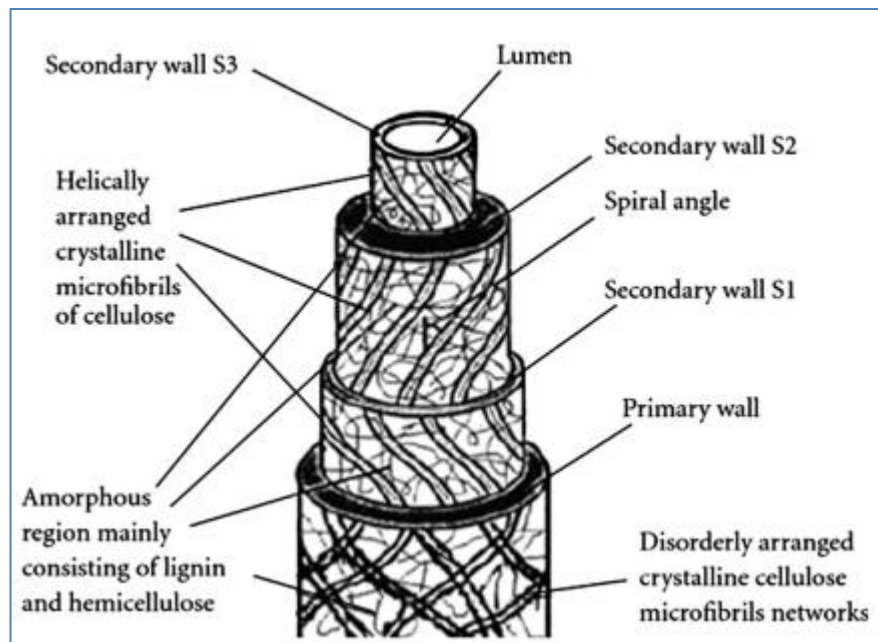


Fig. 2.2 Constituents and structural arrangements of plant cell wall (Rong et al., 2001)

2.2.2.1 Cellulose

Cellulose is one of the most abundant polymers on the earth and it is commercially exploited in the form of wood. In the natural fibres, cellulose is the main structural component and the mechanical properties of these fibres mainly depend on the percentage of cellulose content. The crystalline cellulose is the elementary building material which is responsible to give the strength to the plant stem and the variation in strength is attributed to growth conditions of the plant such as botanical origin, soil characteristics and weather conditions (Majeed et al., 2013). Cellulose is a linear, semi-crystalline polysaccharide composed of polymer chains consisting of the repeating units of anhydro-glucose linked via 1,4- β -D-glucosidic linkages as shown in

Fig. 2.3. The repeating units of these monomers are called as cellobiose (Zhu et al., 2016). The molecular weight of these 1,4- β -D-glucosidic linkages depends on the

source of cellulose. General lignocellulosic fibres have the degree of polymerisation (number of glucose units) up to 10000 (Abdul Khalil et al., 2012). The glucose monomers in the cellulose chain form the hydrogen bonds within the chain forming fibrils as well as neighbouring chains. The formation of these intra and intermolecular hydrogen binding leads to the formation of linear crystalline structure (Eichhorn et al., 2010).

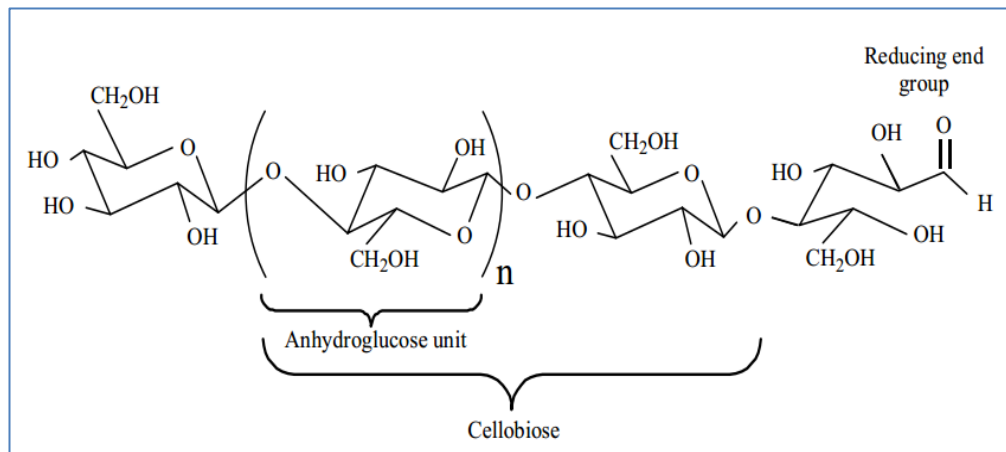


Fig. 2.3 Haworth projection formula of cellulose (Bledzki and Gassan, 1999; Sawpan, 2009)

2.2.2.2 Hemicellulose

Hemicellulose is a heterogeneous branched polysaccharide composed of many different glucose monomers whereas cellulose contains only 1,4- β -D-glucopyranose repeating units. **Fig. 2.4** shows the chemical structure of hemicellulose. Unlike cellulose, hemicellulose constituents differ from one plant source to another. Hemicellulose contains high degree of chain branching which confirms that amorphous nature of hemicellulose. The degree of polymerisation for hemicellulose is as low as 200 as compared to the cellulose molecule which has more than 10000 (Bledzki and Gassan, 1999).

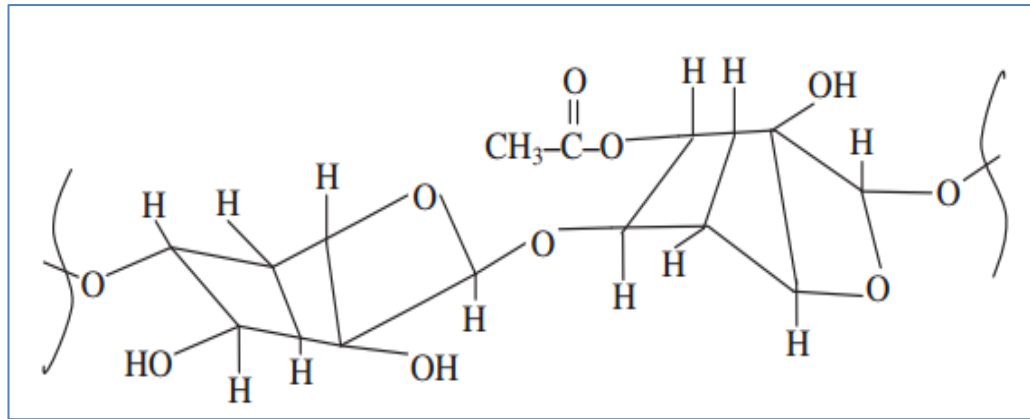


Fig. 2.4 Chemical structure of hemicellulose (Kabir et al., 2012)

2.2.2.3 Lignin

Lignin is a complex hydrocarbon polymer which contains both aliphatic and aromatic constituents. Along with cellulose, lignin is the most abundant organic polymer on the earth. The chemical structure of lignin is shown in **Fig. 2.5**.

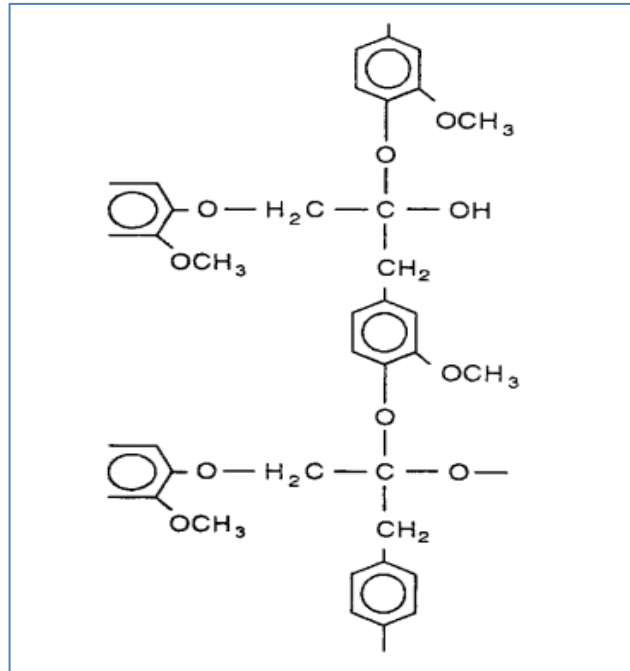


Fig. 2.5 Chemical structure of lignin (Bledzki and Gassan, 1999)

Lignin gives the compression strength to the plant by binding the fibres together to form a stiff structure of the fibre surface (Bledzki and Gassan, 1999). The chemical structure of lignin consists of phenylpropane units derived from an enzyme-initiated dehydrogenate polymerisation of three different primary precursors namely trans-coniferyl, trans-sinapyl and trans-p-coumaryl as shown in **Fig. 2.6**. These phenolic substructures are also called p-hydroxyphenyl monolignols which form a complex 3-dimensional chemical structure during the biological lignification process via radical coupling reactions (Stephanie, 2014).

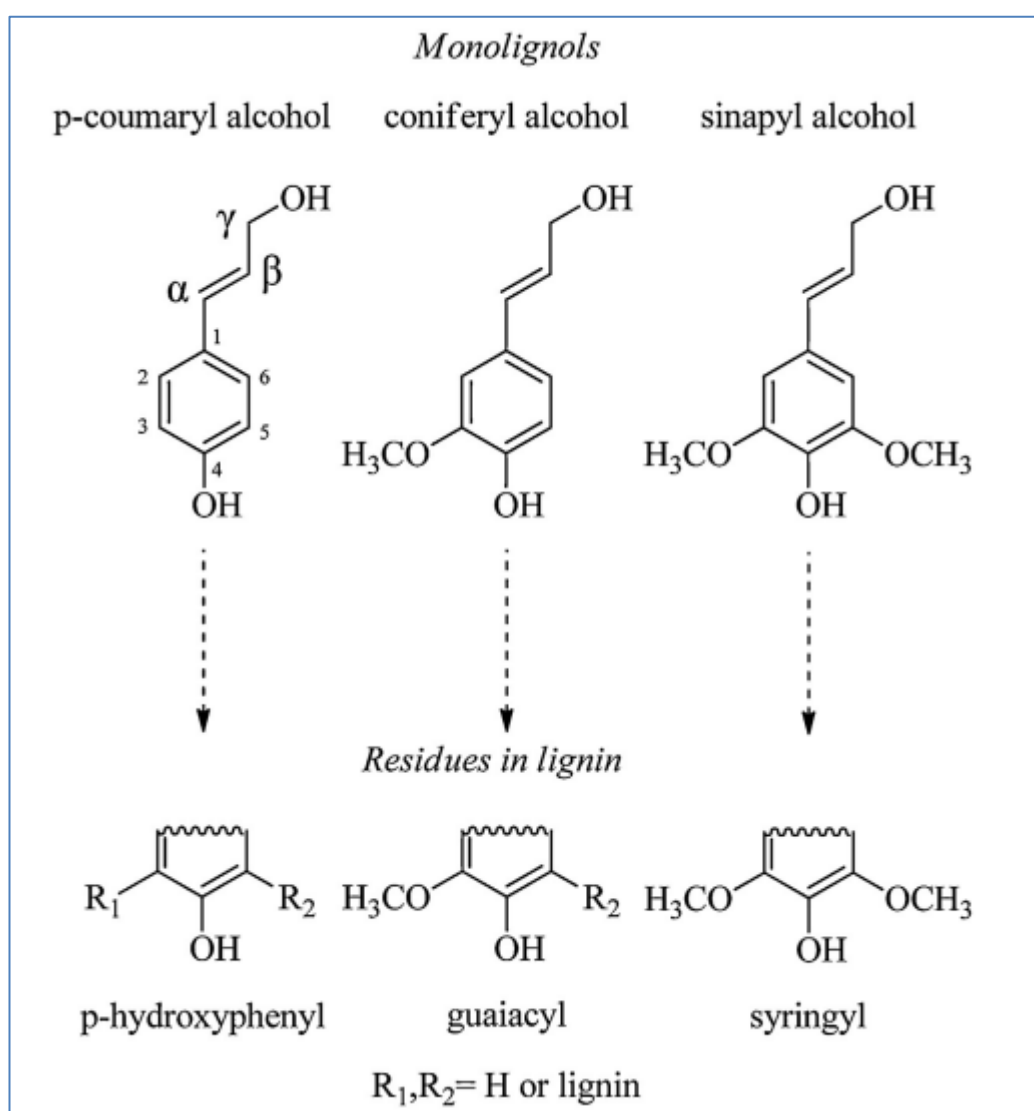


Fig. 2.6 Chemical structure of three main precursors of lignin (Stephanie, 2014)

2.2.2.4 Pectin

Pectin is a component of acidic polysaccharides with complex branched structure. The pectin mainly consists of homopolymeric acid and partially residues of methylated poly- α -(1-4)-D-galacturonic acid (**Fig. 2.7**). Pectin will become water soluble polymer only after a partial neutralisation with alkali or ammonium hydroxide solution (Bledzki and Gassan, 1999). Pectin acts as a binding material inside the natural fibres. It binds the cellulose, hemicellulose and lignin along with pectin itself to form as bundles. High concentration of pectin can be seen in the primary cell wall and the middle lamella of natural fibres (Li et al., 2007). Most of the pectin removed during retting process of the natural fibres. It is important to remove the pectin in order to get technical fibres in the application of fibre reinforced polymer composites as reinforcement material (Gurunathan et al., 2015).

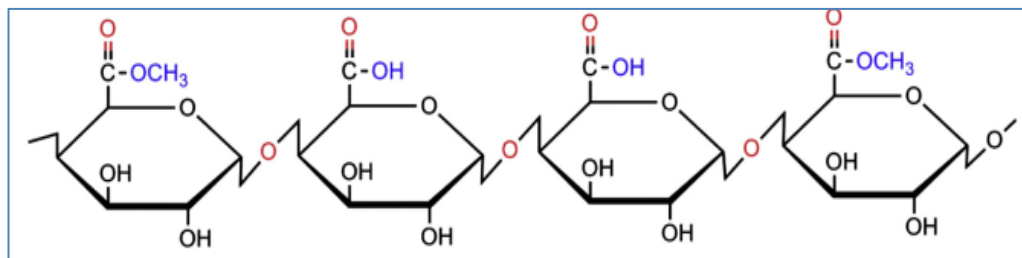


Fig. 2.7 Chemical structure of pectin (Gurunathan et al., 2015)

2.2.3 Sisal fibres

Many different types of natural fibres are being exploited for the production of biodegradable polymer composites (Herrmann et al., 1998; Satyanarayana et al., 2009; Abdul Khalil et al., 2012; De Rosa et al., 2010; Kabir et al., 2012). More than thousand types of natural fibres are already available (Mwaikambo and Ansell, 2002). Among these, sisal fibres are one of the best reinforcing materials for polymer

composites owing to their higher cellulose content (78%), good tensile strength (>600MPa), easy availability and low cost (Li et al., 2000). Sisal fibres tend to be hard and stiff and extracted from the sisal plant (*Agave sisalana*) (**Fig. 2.8**). Sisal plants are mainly growing in tropical and sub-tropical countries like Brazil, Tanzania, India, West Indies etc. A single sisal plant can produce 200-250 leaves in which 150 kilograms of fibres can be extracted in a year (Mishra et al., 2004).



Fig. 2.8 Photograph of sisal plant (<http://www.flickrriver.com/photos/40295335@N00/5219408347/>)

The processing methods for the extraction of sisal fibres from sisal leaves include retting followed by scrapping and mechanical methods by using decorticators. By using mechanical extraction methods only 2-3% of good quality fibres can be extracted. Whereas, a large quantity of fibres can be extracted by means of retting methods. However, retting method gives poor quality of fibres with less lustrous colour. Sisal fibres consist of 60-78% of cellulose, 10-14% of hemicellulose, 8-11% of lignin and about 1.2% of pectin (Barkakaty, 1976). Three different types of fibres

can be extracted from the sisal leaf namely mechanical, ribbon and xylem fibres. Mechanical fibres are extracted easily from the periphery part of the sisal leaf during retting process.

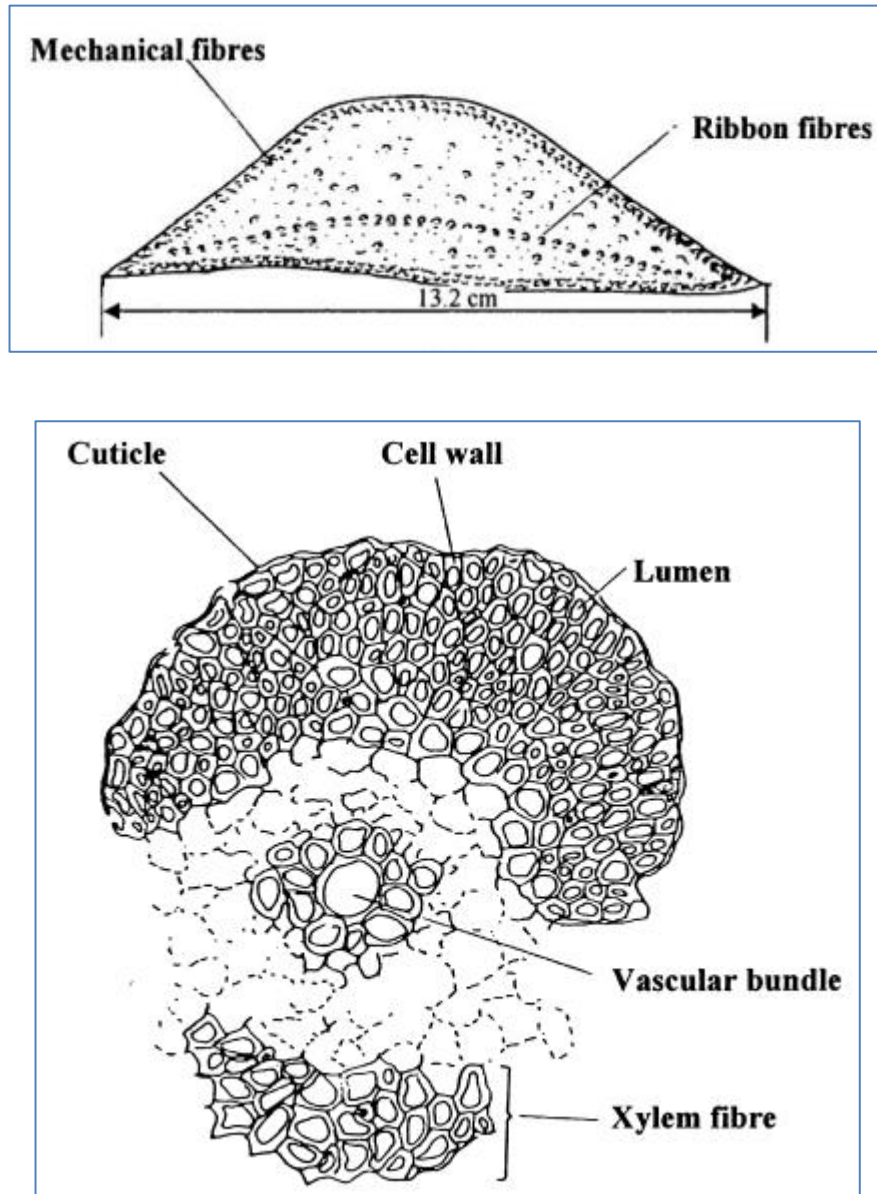


Fig. 2.9 Cross sectional view of sisal leaf and ribbon-fibre bundles (Li et al., 2000)

These mechanical fibres are the commonly used sisal fibres for commercial purpose. Ribbon fibres are extracted from the conducting tissues in the median line of the sisal leaf. Ribbon fibres are the lengthy fibres as compared to mechanical fibres and they

are easily split longitudinally from the leaf during mechanical extraction process. Xylem fibres are irregular in shape with very thin cell wall due to which they have low strength and easily broken during processing. Xylem fibres are extracted from the vascular bundles of the sisal leaf just opposite of the ribbon fibres as shown in **Fig. 2.9** (Li et al., 2000). The sisal fibre cell wall itself is a form of composite structure with spirally oriented cellulose in a hemicellulose and lignin matrix (Mishra et al., 2004). The strength and stiffness of natural fibres mainly depending on the percentage of cellulose content in the fibres. Since the sisal fibres have relatively high percentage of cellulose content (60-78%), they demonstrate good mechanical properties (Li et al., 2000). **Table 2.2** compares the mechanical and physical properties of sisal fibres and other natural fibres. Sisal fibres are one of the widely used natural fibres for the generation of fibre reinforced polymer composites and Joseph et al. (1996) studied the interfacial adhesion on the mechanical properties and fracture behaviour of short sisal fibre reinforced polymer composites. They found that the tensile strength increased significantly by 66%, 55%, 50% and 60% for sisal fibre reinforced LDPE, epoxy, phenolic and polyester composites respectively.

Joseph et al. (2003) studied the thermal and crystallisation properties of short sisal fibres reinforced polypropylene composites. They noticed that the thermal stability and crystallinity increased by 14 °C and 23% respectively as compared to pure polypropylene resin. The increased thermal and crystallinity were due to significant enhancement of interfacial adhesion between the sisal fibre and the polypropylene matrix. Dynamic mechanical properties of short sisal fibre reinforced polymer composites were also studied extensively (Joseph et al., 2003; Nair et al., 2001).

2.3 Major concern over the usage of natural fibres

Similar to the advantages of natural fibres as reinforcement fillers in the generation of polymer composites they also pose many drawbacks such as poor consistency in their performance, hydrophilic nature, and inconsistency in the physical dimensions in a specific period. Physical properties of natural fibres vary with different harvesting methods and the season of harvesting. Moreover, the physical properties are surprisingly depending on the soil conditions, rain pattern and the maturity of the plant. So the selection of fibre materials plays an important role to achieve the specific engineering properties of the composites.

In addition to the above mentioned drawbacks, natural fibres are incompatible with many polymeric matrices which causes the poor fibre dispersion within the polymer matrix of the polymer composites and leads to severe reduction in the mechanical and physical properties of the final composite materials. More importantly plant fibres are chemically hydrophilic in nature and most of the polymeric matrices are hydrophobic materials (similar to water and oil which never mix together). In order to improve the compatibility and enhance the interfacial adhesion between the natural fibres and the polymer matrices, surface treatments have to be employed on the surface of natural fibres.

2.4 Surface treatments on natural fibres

Natural fibres are highly hydrophilic in nature due to the presence of amorphous materials such as hemicellulose, lignin and pectin on the surface. These amorphous materials are responsible for incompatibility between fibres and the matrix materials which result in lowering of mechanical performance of the fibre reinforced composites. In addition to this, amorphous materials absorb moisture due to their

hydrophilic nature which leads to a significant reduction in the mechanical and thermal properties (Faruk et al., 2012). Fibre surface treatments are essential in order to improve the interfacial adhesion between the fibre and matrix. Fibre surface treatment also helps to improve the fibre dispersion across the matrix material in the composites. In addition, surface treatments decrease the water absorption by removing amorphous materials from the surface of fibres which are responsible for the absorption of moisture. Many different types of surface treatment methods are employed in order to remove the amorphous materials from the surface of natural fibres. Surface treatments can be classified as chemical, physical and biological treatments (Kabir et al., 2012).

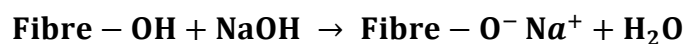
Chemical surface treatments are employed by using chemicals to treat the fibre surface. Few examples of chemical treatments which utilise alkali (Fiore et al., 2015), acetylation (Mokaloba and Batane, 2014; Pothan et al., 2003), silanisation (Pothan et al., 2003), esterification, benzoyl peroxide (Kaushik et al., 2012), acrylic acid (Vilay et al., 2008), potassium permanganate and bleaching (Rosa et al., 2009). Biological treatments involve using naturally occurring microorganisms such as bacteria, fungi (Li et al., 2009; Li and Pickering, 2009) and enzyme (Cao et al., 2012). These treatments are performed in the aqueous medium and are relatively cheaper as compared to other surface treatments. Physical surface treatments are employed by using ionised gas or heat energy. Few examples of physical treatments are corona (Ragoubi et al., 2012), heat (Wootthikanokkhan et al., 2013) and ultrasound (Batalha et al., 2011). The following sections give a brief review on some of the important fibre surface treatment methods.

2.4.1 Alkali treatment

Alkali treatment is one of the common and widely used chemical surface treatments for the removal of amorphous materials from the surface of natural fibres. Alkali treatment is also called mercerisation in which different concentration of sodium hydroxide solution is used to treat the fibre surfaces. Alkali surface treatment reduced the fibre diameter by removing or dissolving amorphous materials such as lignin, hemicellulose, pectin and other waxy materials which bind on the surface of natural fibres.

A reduction on the fibre surface due to alkali treatment leads to an increase in the fibre aspect ratio (i.e. ratio of width to length) and surface roughness. In addition, alkali treatment also helps to expose active hydrogen molecules of cellulose which enhance the surface adhesion of fibres with hydrophobic matrix materials in the fibre reinforced polymer composites. Hydrophilic hydroxyl groups on the surface of natural fibres are reduced due to alkali treatment and this enhances the moisture resistance property. Alkali treatment also enhances the uniformity of fibre surface by dissolving the waxy and gummy materials on the surface of natural fibres (Kabir et al., 2012). During alkali treatment, natural fibres go through swelling reaction which leads to relaxation of the structure of natural cellulose.

The native cellulose is called as cellulose as it occurs in the nature which is the monoclinic crystalline lattice of cellulose-I structure. This cellulose-I structure can be changed to alkali-cellulose (Na-cellulose-I) after reaction with alkali solution as shown in **Scheme 1** (Oh et al., 2005). Na-cellulose-I is an intermediate phase of the native cellulose. Na-cellulose-I is transformed to cellulose-II after washing alkali cellulose with distilled water (Cai et al., 2015).



Scheme 1 Chemical reaction of alkali solution with natural fibres

Since last few years, many research activities focussed on the effect of alkali treatment on the mechanical and thermal properties of natural fibres and their polymer composites (Ray et al., 2002; Le Troedec et al., 2008; Mokaloba and Batane, 2014; Chikouche et al., 2015). Kabir et al. (2013) studied the effects of chemical treatments on the tensile properties of hemp fibres. They noticed that a significant reduction in the tensile strength by 35% due to the removal of hemicellulose, lignin and pectin components from the surface of hemp fibres which were acting as binding materials for the cellulose. Removal of these binding materials leads to least support to withstand the tensile loading. Yan et al. (2016a) investigated the effect of alkali treatment on the microstructure and mechanical properties of coir fibres and their epoxy and cementitious composites. They noticed that the interfacial adhesion between the fibre and the matrix enhanced significantly which was confirmed by SEM analysis. A considerable increase in the tensile strength and modulus was also observed i.e. 17.8% and 6.9% respectively after alkali treatment. Cai et al. (2015) studied the influence of alkali treatment on the internal microstructure and tensile properties of abaca fibres. They used three different concentration of NaOH solution (5, 10 and 15 wt%) to conduct the alkali treatments. They found that the native cellulose (cellulose-I) of abaca fibres was partially converted into cellulose-II which was confirmed by XRD. FTIR analysis revealed that the removal of amorphous materials from the surface of abaca fibres after the application of alkali treatment. They also reported that the Young's modulus increased by 41% after subjected to an alkali treatment using 5 wt% of NaOH. However, the Young's modulus significantly decreased by 24 and 29% when the concentration of NaOH was 10 and 15 wt%

respectively. These results confirmed that higher concentration of alkali not only removes the amorphous materials from the surface of natural fibres but also causes severe damage of cellulose structure which leads to a significant reduction in the mechanical properties of natural fibres.

2.4.2 High intensity ultrasound (HIU) treatment

In recent years, high intensity ultrasound (HIU) treatment is gaining more attention owing to its effective removal of amorphous materials from the surface of natural fibres. Moreover, HIU treatment is more effective in the separation of cellulose nanofibers from its bundles which enhances the surface area of fibres and leads to improve the interfacial adhesion between the fibres and the matrix in the fibre reinforced polymer composites (Chen et al., 2011). Ultrasound refers to a sound spectrum in the range of 20 kHz to 10 MHz generated by using transducer which converts the electrical energy into high frequency sound waves. Ultrasound transducer can produce high energy microscopic air bubbles in the solution and causes cavitation (Siquin and Wang, 2009). Cavitation is the physical phenomenon which refers to the formation, expansion and violent collapse of the microscopic air bubbles on the surface of materials in the solution. The energy produced by the violent implosion of cavitation is approximately equal to hydrogen bond energy (10-100 kJ/mol). Thus, the HIU treatment can disintegrate the hydrogen bonds between the cellulose and the amorphous materials which results in the removal of amorphous materials from the surface of natural fibres (Chen et al., 2011). For the better understanding of the action of HIU treatment, a schematic diagram of the mechanism of HIU treatment on the surface of natural fibre is shown in **Fig. 2.10**.

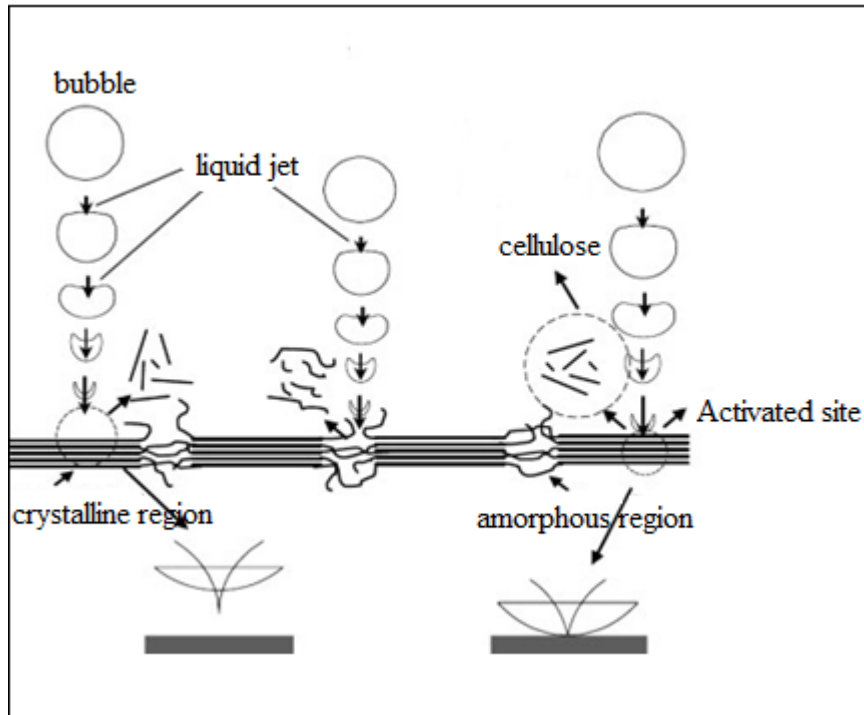


Fig. 2.10 Schematic diagram showing the mechanism of HIU treatment on natural fibres (Li et al., 2012)

Siquin and Wang. (2009) studied the effect of HIU treatment on the isolation of cellulose nanofibrils from the natural fibres. They optimised the time, temperature, distance of the probe from the fibres, fibre size and fibre concentration. They reported that HIU treatment is effective for the isolation of cellulose nanofibers from the natural fibres. Li et al. (2012) produced the nanocellulose from microcellulose by using HIU treatment and studied the mechanical and thermal properties of nanocellulose and their poly (vinyl alcohol) (PVA) composites. They reported that HIU treatment is highly effective to remove amorphous materials from the surface of fibres. A significant increment (145%) in the storage modulus was observed with HIU treated nanocellulose as compared to pure PVA resin.

2.4.3 The combined treatment of alkali and HIU

HIU treatment is emerged as an effective treatment for the separation and isolation of crystalline cellulose from the natural fibres. However, its effectiveness is limited to microcrystalline cellulose (MCC) materials and HIU treatment alone is not an effective treatment for the removal of amorphous materials from the surface of natural fibres.

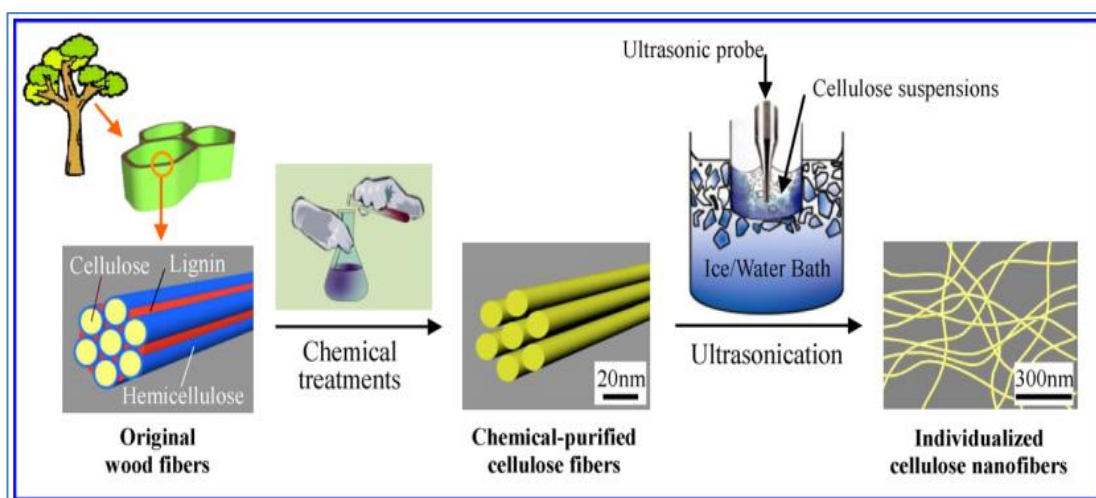


Fig. 2.11 Pictorial representation of chemical and ultrasound treatments on natural fibres (Chen et al., 2011)

Chen et al. (2011) studied the isolation of cellulose nanofibers by using HIU treatment from chemically pre-treated wood fibres, where the wood fibres were subjected to chemical pre-treatment before the application of HIU treatment. They have optimised the HIU treatment in terms of varying the time, temperature and output power. They noticed that the separation of cellulose nanofibers increased with a gradual increase in the power output. Crystallinity of the isolated cellulose nanofibers was increased by 69% as compared to pure wood fibres. **Fig. 2.11** shows the graphical representation of stages in the surface treatments for the wood fibres. Lee et al. (2008) studied the effect of combined treatment of alkali and ultrasound treatment on the interfacial and

mechanical properties of henequen fibre reinforced polypropylene (PP) composites. Henequen fibres were soaked with both water as well as alkali solution before the application of ultrasound. They noticed that the alkali pre-treated fibre composites showed a significant increment in the interfacial shear strength, flexural strength and modulus by 48%, 38% and 49% respectively as compared to the untreated henequen fibres/PP composites. Moshiul Alam et al. (2012) studied the combined effects of alkali and ultrasound treatments on oil palm empty fruit bunch fibres and reinforced them with poly (lactic acid), where they observed a significant improvement of tensile strength, modulus and impact strength by 33%, 62% and 53.8% respectively for the combination of alkali and ultrasound treated fibre composites as compared to untreated fibre composites.

2.5 Clay based nanofillers

Last few decades, natural clay minerals such as halloysite (Hal) nanotubes, kaoline, and montmorillonite (MMT) etc. are also used extensively owing to their easy availability, biocompatibility and good thermal and physical properties. Clay as nanofillers offers a variety of advantages in the polymer nanocomposites such as high thermal stability, good barrier, thermomechanical, and fire-retardant properties. It is worth noted that the high mechanical and thermal properties could be achieved by introducing a very small content of clay nanofillers (Raquez et al., 2013).

It has already been proved that the incorporation of nanofillers onto PLA matrix increases the crystallization ability, elongation and thermal properties. The incorporation of exfoliated graphite onto PLA matrix increased the tensile strength and thermal stability by 12% and 14 °C respectively as compared to pure PLA (Kim and Jeong, 2010; Evagelia et al., 2011). It is reported that the introduction of a smaller

amount (0.2 wt%) of carbon nanotubes (CNTs) as nanofillers into PLA enhanced the tensile strength and modulus by 25% and 12% respectively (Park et al., 2013). However, nanofillers such as graphene, CNTs, fullerenes and oxide nanoparticles are toxic to the environment and therefore using them as fillers in the polymer matrix again causes pollution (Nel, 2007).

It is reported that clay based nanofillers as plasticizer are good substitutes which also improved the thermal properties of PLA by more than 20% as compared to pure PLA (Liu et al., 2013). Aluminosilicate-based nanofillers are also widely used in the polymer nanocomposites to enhance the mechanical and thermal properties. Aluminosilicates are also called as layered silicate nanocomposites which are a new class of hybrid materials, making them more interesting in academic and industrial realms due to their excellent thermal barrier, thermo-mechanical and fire-resistance properties which have been achieved at a lower loading of fillers (<5 wt%). However, improvements in the desired properties rely on how well the dispersion of nanofillers within the polymer matrix (Sinha Ray and Okamoto, 2003).

2.5.1 Halloysite (Hal) nanotubes

Hal nanotubes are naturally occurring aluminosilicates having the formula, $\text{Al}_2\text{Si}_2\text{O}_5(\text{OH})_4 \cdot n\text{H}_2\text{O}$. Their tubular structure in nano dimension with high aspect ratio makes them as unique materials to be used as fillers in the generation of CPN (clay polymer nanocomposites). Hal nanotubes are chemically similar to kaolinite group which consist of multiple layers of hollow cylinders with nanometre dimensions (Joussein et al., 2005). Hal nanotubes consist of gibbsite like array of aluminol groups (Al-OH) which are located inside the lumen while the outer surface covered with siloxane (Si-O-Si) groups. These two unit layers are separated by a barrier of water molecules

which lead to hydrated Hal nanotubes with a basal spacing of 10 Å which is larger than that of kaolinite (~3 Å) (Yuan et al., 2008, 2015). Hal nanotubes are naturally formed in the earth crust over millions of years and having unique and versatile mechanical and thermal properties (Du et al., 2010; Rooj et al., 2010). However, the presence of a large number of hydroxyl groups on the surface of Hal nanotubes leads to its hydrophilic nature which limits its applications to use them as fillers in the generation of CPN (Yuan et al., 2008; Pasbakhsh et al., 2010; Jin et al., 2015).

In recent times, a sizeable number of reports being published on Hal nanotubes reinforced CPN (Liu et al., 2014). The loading of Hal nanotubes into PLA matrix significantly improved the mechanical properties. Tensile and flexural strength increased by 34% and 25% respectively with the addition of 30phr of unmodified Hal nanotubes into PLA as compared to pure PLA. Thermal stability of 30phr loaded unmodified Hal-PLA nanocomposite slightly increased by 4.4 °C as compared to pure PLA (Liu et al., 2013). However, similar to other nanoparticles, dispersion of Hal nanotubes into polymer matrix is challenging (Kim and Jeong, 2010; Raquez et al., 2013). Modification or functionalization of nanofillers is a way to enhance their dispersion into the polymer matrix. Functionalization of Hal nanotubes can enhance the surface properties and leads to good dispersion into PLA matrix of CPN. Surface modification of Hal nanotubes with different types of silane coupling agents is the most common method to improve the surface properties of Hal nanotubes. This method is referred as the grafting of silanes and is carried out via condensation between hydrolysed silanes and surface hydroxyl groups of Hal nanotubes. The modification of Hal nanotubes with silane coupling agent enhanced the dispersion of Hal nanotubes into natural rubber (NR) matrix and improved the thermal stability by 64 °C as compared to unmodified Hal nanotubes (Rooj et al., 2010). The modified Hal

nanotubes with silane coupling agent enhanced its dispersion in Ethylene propylene diene monomer (EPDM) matrix and increased the mechanical properties. 30phr of silane modified Hal nanotubes into EPDM matrix increased the tensile strength, modulus and elongation at break by 360%, 65% and 135% respectively as compared to unmodified Hal-EPDM composites (Pasbakhsh et al., 2010).

2.6 Polymer matrix materials

Polymers are mainly classified into three classes of thermoplastics, thermosets and elastomers. Elastomers are the rubbery materials which have both viscous and elastic nature. Few important elastomers are natural polyisoprene, polybutadiene, chloroprene, etc., Thermoset polymers are polymers which are interlinked by covalent bonds and possess a three dimensional network structure. Thermoset polymer composites cannot be remoulded and recycled. On the other hand, thermoplastic polymers possess linear and branched molecular chains with weak intermolecular bonding such as van der Waals force or hydrogen bonding. Thermoplastic polymer composites can be recycled. In this work, polylactide or poly lactic acid (PLA), a bio-derived thermoplastic polymer is compared with polypropylene (PP) which is a petroleum based synthetic thermoplastic polymer matrix.

2.6.1 Polylactide or Poly lactic acid (PLA)

The term poly lactic acid is a misinterpretation. PLA is synthesized from ring opening polymerisation of lactide, a dimer of lactic acid. Thus, it should be referred as polylactide instead of poly lactic acid. PLA is an important semicrystalline thermoplastic polyester biopolymer derived from annual renewable resources such as corn, sugarcane etc. (Lim et al., 2008; Pandey et al., 2005). The developmental history of PLA biopolymer dates back to 1893 when Bischoff and Walden published lactide

formulas. Carothers and his co-workers started producing low molecular weight PLA in 1932. In 1954, medical grade PLA was produced and marketed by DuPont de Nemours and Ethicon, Inc. In 1994, Japan started the production of commercial PLA fibres. PLA derived from the starch was produced by Cargill Dow LLC, USA under the trade name of NatureWorks at a capacity of 140,000 tons/year in 2002 (Rasal et al., 2010). More recently NatureWorks has changed the trade name of commercial PLA as Ingeo™.

PLA draws more interest owing to its renewability, biodegradability, biocompatibility and good mechanical properties (Raquez et al., 2013). Moreover, PLA degradation releases non-toxic gases at a lower level (Nel, 2007). Besides, for packaging, automotive, and electronic applications it has comparable tensile strength and Young's modulus with several commercial polymers such as polypropylene, polyethylene, polystyrene etc. (Notta-cuvier et al., 2014). However, PLA has limitations of low thermal stability, low toughness and extreme brittleness (Lim et al., 2008; Pandey et al., 2005). It is therefore necessary to reduce the brittleness and to improve the mechanical and thermal properties of PLA when we aim for long-term applications more importantly on a large scale (Raquez et al., 2013).

The PLA polymer belongs to a family of aliphatic polyester which is derived from 2-hydroxy propionic acid (i.e. lactic acid). The basic monomer for the production of PLA is lactic acid which can be produced by either fermentation of carbohydrates or chemical synthesis route. Lactic acid has two stereo-isomeric forms which are L (Laevorotatory) – lactic acid and D (Dextrorotatory) – lactic acid (**Fig. 2.12**). Both the forms of lactic acid can be produced from either petrochemical or agricultural by-products (Lim et al., 2008). Lactic acid produced from petrochemical synthesis route gives 50:50 ratios of both L-lactide and D-lactide forms.

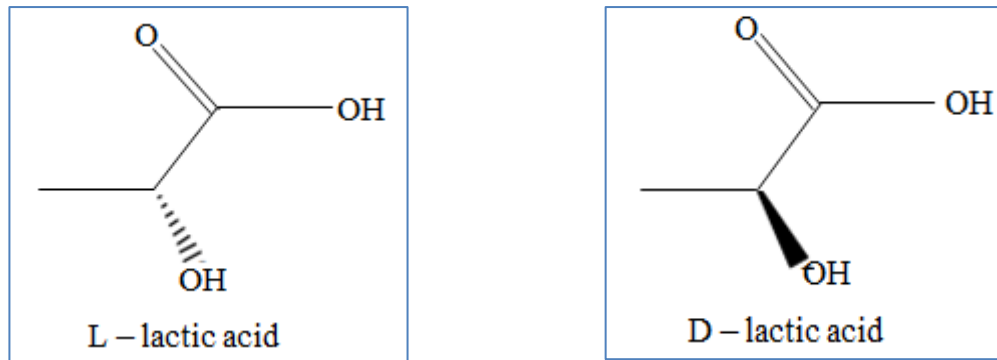


Fig. 2.12 The two stereo-isomeric forms of lactic acid

In contrast to the petrochemical route, lactic acid produced from agricultural by-products exists mainly in L-lactic acid stereo-isomeric form. Currently lactic acid which is used to produce PLA comes from agricultural by-products by using a fermentation process (Rasal et al., 2010). Polymerisation of lactic acid can be achieved by two main methods. **Fig. 2.13** shows the different types of PLA synthesis.

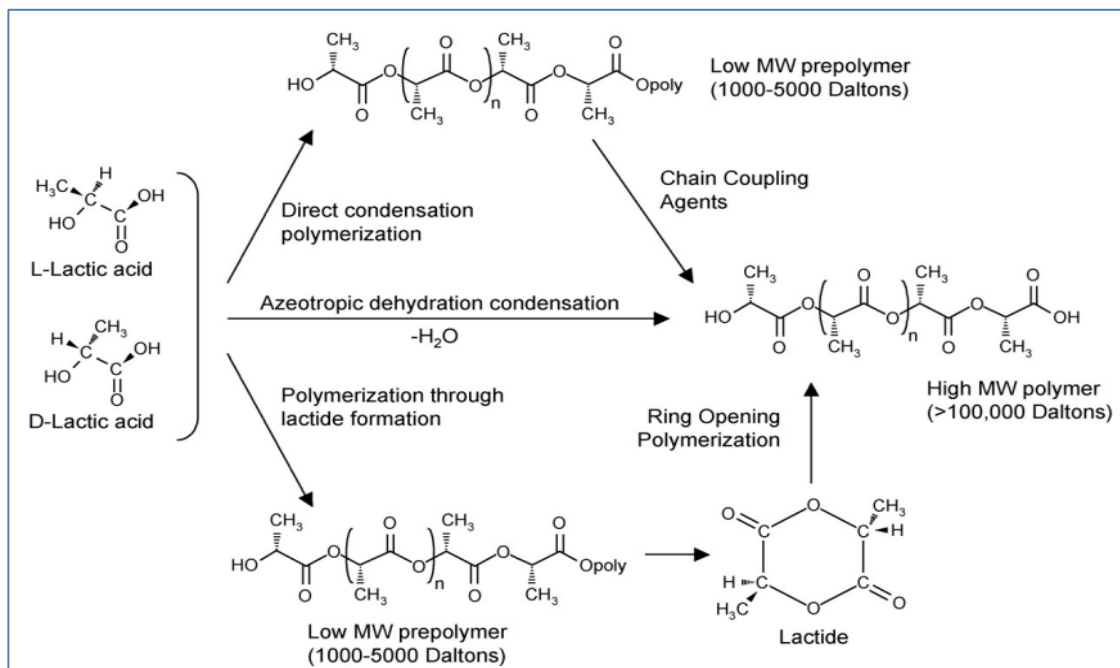


Fig. 2.13 Synthesis of PLA from L- and D-lactic acids (Lim et al., 2008)

The first method involves the direct condensation of lactic acid under high temperature and vacuum. However, only low molecular weight PLA can be produced

with this method mainly due to the presence of water as a by-product in this reaction which is difficult to separate from the polymer. The second method of producing PLA from lactic acid involves two steps. First the low molecular weight pre-polymer was produced with the condensation polymerisation reaction of lactic acid.

The low molecular weight pre-polymer is then catalytically depolymerised to form intermediate of lactic acid called dilactide which is the primary feedstock to produce high molecular weight PLA. Finally the dilactide is polymerised in the solvent free ring opening polymerisation (ROP) to produce high molecular weight PLA polymer (Rathin Datta and Michael Henry, 2006). PLA is a semicrystalline polymer having the glass transition temperature (T_g) ranging from ~55 to 65 °C available from amorphous glassy grades to highly crystalline grades with melting temperature from ~160 to 180 °C (Nampoothiri et al., 2010; Saeidlou et al., 2012; Raquez et al., 2013). Physical and mechanical properties of PLA are mostly superior and are comparable to many commodity polymer matrices such as polypropylene (PP), polystyrene (PS), polyethylene terephthalate (PET) etc. Comparison of mechanical and physical properties of PLA and other conventional polymer matrices are represented in **Table 2.3**.

Until last few years, the application of PLA was mainly focused on packaging, diapers, planting and in other sanitary products. However, several reports suggested that PLA is a potential bio-derived polymer matrix for a wide range of applications such as structural, automotive etc. with the incorporation of fibrous filler. Natural fibres as fillers for the generation of PLA polymer composites offer many advantages such as light-weight, lower manufacturing cost, easy to handle, good thermal and acoustic insulation properties (Dittenber and Gangarao, 2012). Porras and Maranon. (2012) studied the mechanical properties of laminate composite material of PLA and

woven bamboo fabric. They noticed that the tensile strength and modulus significantly increased by 43 and 47% respectively as compared to pure PLA. Yu et al. (2014) reported that the incorporation of short ramie fibres into PLA matrix increased the tensile strength and modulus by 42% and 73% respectively as compared to pure PLA.

Table 2.3 Comparison of physical and mechanical properties PLA and other commodity polymers (Carrasco et al., 2010; NatureWorks LLC, 2013)

Properties	PLA	Polystyrene (PS)	Polypropylene (PP)	Polyethylene terephthalate (PET)
Density (g/cm ³)	1.24	1.04 - 1.06	0.91	1.37
Clarity	Transparent	Transparent	Translucent	Transparent
Tensile yield strength (MPa)	48 – 110	34 – 46	21 – 37	47
Tensile modulus (GPa)	3.5 – 3.8	2.9 – 3.5	1.1 – 1.5	3.1
Tensile elongation (%)	2.5 – 100	3 – 4	72	79
Impact strength (J/m)	13		72	79
Glass transition temperature (°C)	60	95	0	75
Melting temperature (°C)	153		163	250
Heat distortion temperature (°C)	55 – 60	84 – 106	80 – 140	74 – 200
Processing temperature (°C)	210	230	225	255

Environmental conditions such as humidity, temperature, pH, salinity, supply of different nutrients and presence and absence of oxygen etc., have important role on the polymer degradation directly as well as influence the microbial population to degrade it. Degradation of PLA initiates with scission of main or side chains of the macromolecules. Biodegradation by soil burial of PLA and natural fibre reinforced PLA composites have been reported by several authors (Ohkita and Lee, 2006; Dong et al., 2014; Rajesh et al., 2015). Dong et al. (2014) studied the soil biodegradation of coir fibre reinforced PLA composites. They found that the degradation of pure PLA is much slower than coir fibre reinforced PLA composites. Higher the fibre loading faster the degradation of fibre reinforced polymer composites. It was found that PLA composites reinforced with 10 wt% of coir fibres showed a significant reduction in the weight by 34.9% as compared to pure PLA which showed a weight loss of 18% after 18 days of open soil burial.

2.6.2 Polypropylene (PP)

PP is one of the most widely used thermoplastic polymers in the applications such as automotive, home appliances, packaging, construction, etc. owing to its ease of processing, low cost and high recyclability (Pérez et al., 2013). However, in recent years, plastic waste management is a major issue due to an extensive usage of petroleum based synthetic polymers (Azwa et al., 2013). Natural fibres are the best alternatives as reinforcing materials into thermoplastic polymers such as PP to address the issue of waste management owing to their environmentally friendly properties (Abdul Khalil et al., 2014; Azwa et al., 2013; El-Sabbagh, 2014). Kaewkuk et al. (2013) studied the effect of interfacial modification and fibre content on the physical properties of sisal fibre reinforced PP composites. They found that the tensile modulus increased significantly by more than 90% with the addition of 30 wt% of

alkali treated sisal fibres in the fibre reinforced PP composites as compared to pure PP. Elkhaoulani et al. (2013) studied the mechanical and thermal properties of Moroccan hemp fibres reinforced PP composites. They reported that the tensile modulus of the hemp fibre reinforced PP composites increased by 50% as compared to pure PP resin. Yao et al. (2013) studied the mechanical and thermal properties of furfural modified clam shell waste reinforced PP composites. They found that the addition of modified clam shell waste into PP composites resulted in a significant enhancement of flexural modulus and impact strength both by 50% as compared to pure PP resin.

2.7 Methods used for the processing of polymer composites

Selection of a suitable processing method for the generation of fibre reinforced polymer composites is an important task in order to enhance the mechanical, physical and thermal properties of the final product. Same processing methods were used to produce both synthetic and natural fibre reinforced polymer composites. Currently there are no separate processing methods developed for the natural fibre composites. Common processing methods to generate fibre reinforced thermoplastic polymer composites are melt mixing, injection moulding, extrusion, and compression moulding.

2.7.1 Melt mixer

An enhancement in the mechanical properties of short fibre reinforced polymer composites directly depends on how well the fibre materials disperse into polymer matrix. Conventional processing methods such as single screw extruder is not useful in order to improve the dispersion of the fibre materials in the fibre reinforced polymer composites. Twin screw mixer such as melt mixer is an ideal equipment for

the better achievement of fibre dispersion across the polymer matrix (Lim et al., 2008). Melt mixer is a very common polymer mixing equipment for the mixing especially for the generation of short fibres reinforced thermoplastic polymer composites. Initially thermoplastic polymer was heated to its melting temperature and then the short fibrous materials were added to the mixing chamber to disperse the fibres into polymer matrix. Mixing time and rotor speed depend on the dispersion of short fibres across the polymer matrix which directly affects the mechanical properties of polymer composites (Gareth Beckermann, 2007). It is well reported in the literature that the lower mixing time (<10 min) and lower rotor speed (< 50 rpm) cause poor dispersion of the fibre materials across the polymer matrix which leads to a high level of fibre agglomeration in the polymer composites. Lower mixing temperature also causes severe damage of the fibres during melt mixing (Joseph et al., 1999). Melt mixing method is widely used in the small scale scientific investigations due to its good mixing and results in the lab scale production of short fibre reinforced polymer composites. However, the major drawbacks of using the melt mixer are the limited usage of materials per batch and the melt mixer can be used only for mixing and further processing equipment is required in order to generate the composites.

2.7.2 Compression moulding

Compression moulding also called as hot pressing is a commonly used method for the processing of polymer composites. Composite materials produced by using compression moulding possess relatively good mechanical properties as compared to other processing techniques. Larger and simpler composite materials can be produced by using compression moulding. Composite materials are generated by using compression moulding by placing a weighed amount of mixed fibre-matrix stack in between two pre-heated mould cavity. The temperature and applied pressure of the

mould cavities are fixed according to the types of matrix and filler materials used and thickness of composite samples. The top of the mould cavity moves at a constant speed and touches the lower mould cavity. After reaching the set compression time, composite samples are cooled by placing them under the cooling plates with same pressure and then the composite samples are removed from the mould (Gareth Beckermann, 2007; Ho et al., 2012).

2.8 Factors affecting the properties of fibre reinforced composites

It is important to choose specific fibres and processing methods in order to achieve the desired engineering properties of the fibre reinforced polymer composites. Several factors such as fibres dispersion, orientation of the fibres inside the composites, length and width (aspect ratio) of the fibres, volume of the fibres and key properties of the fibres are the major areas to consider in the natural fibres which are used as reinforcement fillers in the polymer composites for achieving specific engineering properties.

2.8.1 Dispersion of fibres in the composites

Filler dispersion is one of the key factors which affect the mechanical properties of the fibre reinforced polymer composites specifically in the short fibre reinforced composites. It is well reported in the literature that a significant reduction in the tensile and impact properties occurs due to poor dispersion of fibres across the composites. Poor fibre dispersion causes the fibre agglomeration in the composites which creates stress concentration points and leads to sudden mechanical failure. Compatibility between the natural fibres (hydrophilic nature) and polymer matrices (hydrophobic) is the major reason for the poor dispersion of the fibres. Compatibility between natural fibres and the polymer matrices can be improved by subjecting to a

suitable surface treatment of either natural fibres or polymer matrices. Another important reason which causes the poor dispersion is mixing time during the processing of composites. Higher mixing time gives better dispersion of the fibres across the polymer matrix (Thomason, 1997).

2.8.2 Fibre orientation

Fibre orientation also called as fibre direction is an important factor to consider for achieving specific engineering applications of the fibre reinforced composites. It is a well-known fact that the mechanical properties are superior for the unidirectional long fibre reinforced polymer composites as compared to short randomly orientated fibre composites. It is very rare to achieve the fibre orientation in the short fibre reinforced composites. Fu and Lauke (1996) studied the effect of fibre length and fibre orientation distribution on the tensile strength of short fibre reinforced polymer composites. They noticed that the strength of the composites increased with an increase in the fibre orientation coefficient.

2.8.3 Aspect ratio of fibres

Aspect ratio of the fibres is defined as the ratio between length and width of the fibres. It is an important factor which directly affects the mechanical properties of the fibre reinforced polymer composites. Ashori and Nourbakhsh (2010) studied the chemical composition and particle size of the oak and pine wood particle reinforced PP composites. It was found that the pine fibre had significant impact on the improvement of mechanical properties of pine wood fibre reinforced PP composites as compared to oak fibre wood reinforced PP composites. It was found that the aspect ratio of pine fibre wood was higher than the oak fibre wood which enhances the interfacial adhesion between the fibre and matrix in the fibre reinforced composites.

2.8.4 Fibre volume fraction

Fibre volume fraction plays an important role in improving the mechanical and thermal properties of the fibre reinforced composites. It is well reported that the mechanical properties of natural fibre reinforced polymer composites decreased significantly with low volume fraction of fibres. This is because at low fibre content it created flaws between the fibre and the matrix materials and led to mechanical failure. At higher fibre volume fractions, short fibres cause agglomeration of the fibres across the matrix in the composites which cause stress concentration points and leads to a reduction in the mechanical properties. However, optimisation of fibre loading is important in order to achieve the maximum mechanical properties of the natural fibre reinforced polymer composites. López et al. (2013) studied the effect of fibre loading on the mechanical properties of thermoplastic starch (TPS) bio-composites reinforced with newspaper fibre. They noticed that the tensile strength significantly increased by 150% with the addition of 15 wt% of newspaper fibres as compared to pure TPS resin. However, with the further addition of fibre materials the tensile strength started decreasing. In addition, cellulosic fibres have thermal stability due to the presence of amorphous materials on the surface of fibres. Thus, increasing the fibre loading in the fibre reinforced composites leads to lower the thermal stability.

2.9 Theoretical predictions of Young's modulus

The mechanical and elastic properties of fibres reinforced polymer composites depend on many different parameters such as fibre length, fibre orientation, fibre geometry, fibre dispersion and interfacial adhesion between fibre and matrix. Young's modulus is an important intrinsic property of the composite materials which solely depends on the volumetric fibre fractions of the composites, Young's modulus of the matrix

materials and intrinsic Young's modulus of the fibres are used for the generation of the composites.

In order to predict the theoretical values of the Young's modulus of natural fibres reinforced polymer composites the Young's modulus for the natural fibres has to be measured experimentally. However, it is quite difficult to measure the elastic properties of natural fibres due to their characteristic properties such as fibre length, orientation and fibre geometry (Kalaprasad et al., 1997; Joseph et al., 2003; Cabral, 2005; Granda et al., 2016). The mechanical properties of fibres could be predicted by theoretical models which are based on different assumptions and experimental data. Several researchers were also used these theoretical models to predict the Young's modulus of the fibres reinforced composites (Kalaprasad et al., 1997; Nayak et al., 2013; Serrano et al., 2014).

2.9.1 Parallel and series model

Parallel or Voigt model and Series or Reuss model are the simplest and widely used models to predict the experimental data of Young's modulus of short fibres reinforced composite materials (Kalaprasad et al., 1997; Cabral, 2005; Nayak et al., 2013). The Young's modulus of the short sisal fibre reinforced PLA composites could be calculated by using the following eqns. 2.1 and 2.2:

Parallel model

$$M_c = \eta_\epsilon \cdot M_f \cdot V_f + (1 - V_f) \cdot M_m \quad (\text{eqn. 2.1})$$

Series model

$$M_c = \frac{M_m M_f}{M_m V_f + M_f (1 - V_f)} \quad (\text{eqn. 2.2})$$

Where M_c , M_m and M_f are the Young's modulus of the composites, matrix and the fibres respectively and V_f is the volume fraction of the fibres. η_e is the fibre efficiency or compatibility factor for the strength of the composite which is used to correct the contribution of semi-aligned short fibres in the composites. Fibre efficiency factor (η_e) is the product of fibre orientation efficiency factor (η_0) and fibre length efficiency factor (η_1) (Fu and Lauke, 1996). According to Cox-Krenschel's model, the fibre length efficiency factor is defined by the following eqn. 2.3 (Vilaseca et al., 2010):

$$\eta_1 = 1 - \frac{\tanh\left(\frac{\beta L^F}{2}\right)}{\frac{\beta L^F}{2}} \quad (\text{eqn. 2.3})$$

Where L^F is the weighted fibre length and β is the coefficient of stress concentration rate at the ends of the fibres according to the following eqn. 2.4:

$$\beta = \frac{1}{r} \sqrt{\frac{M_m}{M_f (1 - v_m) \text{Ln} \sqrt{\frac{\pi}{4V_f}}}} \quad (\text{eqn. 2.4})$$

Where r is the radius of the fibre, v_m is the Poisson's ratio of the matrix which is assumed to be 0.36 (Espinach et al., 2013). Fibre efficiency factor (η_0) can be calculated by considering the fibre orientation across the matrix in the composites. It is assumed to be a rectangular or square distribution of discontinuous phase of short

fibres inside the matrix phase. (Granda et al., 2016; Sanomura and Kawamura, 2003) studied the fibre orientation of short fibre reinforced thermoplastics. According to them, the function of orientation distribution is represented by the following eqn. 2.5:

$$\eta_0 = \begin{cases} 1/\alpha, & (0 \leq \alpha_0 \leq \alpha) \\ 0, & (\alpha < \alpha_0) \end{cases} \quad (\text{eqn. 2.5})$$

Where α is the average orientation angle of the fibres inside the matrix and α_0 is the fibre orientation limit angle.

The Young's modulus of the fibre reinforced polymer composites largely depends on the angle of fibre orientation inside the composite system. The angle of fibre orientations can be calculated by the following eqn. 2.6:

$$\eta_0 = \frac{\text{Sin } \alpha_0}{\alpha_0} \left(\frac{3 - \nu_m}{4} \frac{\text{Sin } \alpha_0}{\alpha_0} + \frac{1 + \nu_m}{4} \frac{\text{Sin } 3\alpha_0}{3\alpha_0} \right) \quad (\text{eqn. 2.6})$$

By using the eqns 2.2, 2.3, 2.4, and 2.5, the fibre efficiency factor (η_e) can be calculated.

2.9.2 Hirsch model

The intrinsic Young's modulus of the short sisal fibre reinforced PLA composites was predicted by using the Hirsch's model which is a combination of Parallel and Series models (Espinach et al., 2013; López et al., 2012).

According to this model, Young's modulus can be calculated by using the following eqn. 2.7:

$$M_c = x (M_f V_f + M_m (1 - V_f)) + (1 - x) \frac{M_m M_f}{M_m V_f + M_f (1 - V_f)} \quad (\text{eqn. 2.7})$$

Where M_c , M_m and M_f are the Young's modulus of the composites, matrix and the fibres respectively and V_f is the volume fraction of the fibres. Where x is an empirical parameter which is related to fibre-matrix interface.

2.9.3 Bowyer and Baber model

According to Bowyer and Baber model, the tensile properties of short fibre reinforced composites are the sum of contributions from subcritical and supercritical fibres and the matrix. According to this model, the Young's modulus can be calculated by using the following eqn. 2.8:

$$M_c = M_f K_1 K_2 V_f + M_m (1 - V_f) \quad (\text{eqn. 2.8})$$

Where K_1 is the fibre orientation factor which depends on the fibre orientation during the preparation of composite. K_2 is the fibre length factor. According to Fu and Lauke (1996), for short fibre composites, fibre length and fibre interface factor (K_2) can be calculated by using the following eqns. 2.9 and 2.10:

For fibre length $L > L_c$

$$K_2 = 1 - [(L_c / 2L)] \quad (\text{eqn. 2.9})$$

For fibre length $L < L_c$

$$K_2 = (L / L_c) \quad (\text{eqn. 2.10})$$

Where, L and L_c represent the length and the critical length of the fibres respectively. Critical length of the fibre is defined as the minimum length of the fibre required for the stress to reach the fracture stress of the fibre. Fibres which are shorter than critical

fibre length will not carry the maximum possible load and become inefficient (Lacroix et al., 1992).

2.10 Summary of literature review

From the literature survey, it could be noted that there are significant findings in PLA polymer nanocomposites especially for the medical applications. However, there is a lack of literature for tuning the mechanical and thermal properties of PLA composites for other applications especially for the automotive and structural applications. In addition, a detailed study of the effects of high intensity ultrasound (HIU) and the combination of alkali and HIU treatments on sisal fibres reinforced PLA composites are yet to be reported. Hence, in this study; PLA and PP composites reinforced with different fillers (sisal fibres and halloysite nanotubes) will be prepared and a detailed study of the effects of surface modification in tuning the mechanical and thermal properties will be attempted.

CHAPTER III

Experimental

3.1 Introduction

Sisal fibres and halloysite (Hal) nanotubes were used to produce polylactide and polypropylene composites. Surface modification methods were employed for both sisal fibres and Hal nanotubes in order to improve the surface interactions of fillers (sisal fibres and Hal nanotubes) with matrix materials to enhance the mechanical and thermal properties of the resultant composites. Physical, morphological, mechanical and thermal properties were investigated for untreated and surface treated sisal fibres. Untreated and 3-Aminopropyltriethoxysilane (APTES) modified Hal nanotubes were subjected to SEM, FT-IR, nitrogen absorption-desorption analysis and TGA to confirm the structural modifications of Hal nanotubes by the surface modification of APTES. A set of physical, morphological, mechanical, thermal and biodegradable properties were investigated for sisal fibres and Hal nanotubes reinforced polylactide and polypropylene composites. This chapter describes in brief the materials, surface treatment methods, composite processing and characterisation techniques.

3.2 Materials

Sisal fibres were obtained from vibrant nature, Chennai, India. PLA (trade name of Ingeo™ 2003D) was supplied by NatureWorks LLC Inc, USA. The melt flow index of PLA was 6 g/10 min (210 °C, 2.16 kg) with the density of 1.24 g/cm³. General purpose injection moulding grade polypropylene (Titanpro 6331) was used with the melt flow index of 14 g/ 10 min and the density of 0.9 g/cm³. Hal nanotubes were

purchased from Sigma-Aldrich, Malaysia. 3-Aminopropyltriethoxysilane (APTES) was supplied by Fisher Scientific, Malaysia. Dichloromethane was supplied by Merck. Commercial grade NaOH, ethanol, and acetic acid were supplied from RM Chemicals and were used for the alkali and silane treatments.

3.3 Surface treatment methods

3.3.1 Fibre surface treatment

Sisal fibres were subjected to different surface treatments such as alkali, HIU treatment and the combination of alkali and HIU treatments. Prior to the surface treatments, sisal fibres were washed with distilled water in order to remove dirt and impurities on the surface of sisal fibres and then fibres were dried at 80 °C using a hot air oven for 24 h.

3.3.1.1 Alkali treatment

The alkali solution was prepared with different concentrations of NaOH (w/v) (0%, 3%, 5%, 7%, 9% and 15%) with distilled water. At first, the clean and dried sisal fibres were soaked in an alkali solution at room temperature for 24 h with constant stirring. The fibres were then washed several times with distilled water containing acetic acid to neutralise the remaining NaOH in the fibres and then dried at 100 °C for 24 h using a hot air oven.

3.3.1.2 Treatment with high intensity ultrasound (HIU)

Untreated and sisal fibres that were treated with different concentrations of alkali were subjected to HIU for 90 min. An ultrasonic processor (Hielscher UIP1000hd, transducer tip diameter of 24 mm) with the frequency of 20 kHz, output power of 1000 W has been employed. Optimisation studies were also carried out of ultrasound

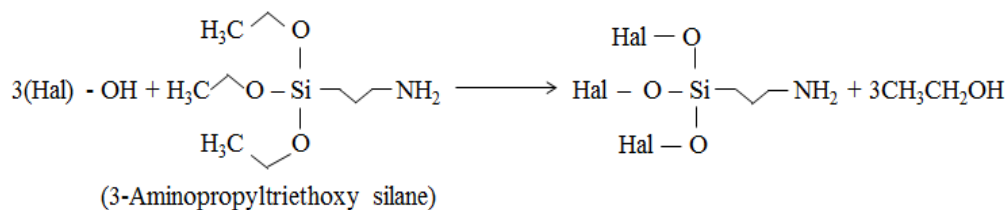
irradiation parameters such as for output power, frequency and time. Distilled water was used as the medium and the weight of fibres to water solution ratio was maintained as 1:20 (w/v). The total volume of the solution was 1000 ml and the transducer tip was dipped approximately 50% inside the solution medium. The temperature was maintained between 25 to 30 °C by using an ice/water bath. The optimization of ultrasound irradiation time and the temperature were also carried out as described in the literature (Lee et al., 2008; Moshiul Alam et al., 2012). The fibres were then washed with distilled water and dried at 100 °C in a hot air oven for 24 h and the resultant sisal fibres were then studied for their morphological and thermal properties.

3.3.2 Surface modification of Halloysite (Hal) nanotubes

The functionalisation of Hal nanotubes was carried out with the silane coupling agent, APTES. The amount of APTES was determined by using the eqn. 3.1 (MacMillan, 2009) to ensure the uniform distribution of silane onto the surface of Hal nanotubes. Typical surface area of Hal nanotubes is 65 m²/g and the specific surface area of APTES is 355 m²/g (Arkles, 1977).

$$\text{Amount of APTES (g)} = \frac{\text{Amount of Hal (g)} \times \text{surface area of Hal (m}^2\text{/g)}}{\text{Specific surface area of APTES (m}^2\text{/g)}} \quad (\text{eqn. 3.1})$$

12 g of silane coupling agent i.e. APTES was dissolved in 500 mL of ethanol (95%) solution and 1 mL of acetic acid was added to keep the pH between 4.5 and 5.5. This solution was then stirred vigorously at 60 °C for 15 min. 50 g of Hal nanotubes were added to the solution and stirred at 60 °C for 2 h. The silane modified Hal nanotubes were then filtered and washed with ethanol and dried at room temperature for 24 h and then dried under vacuum at 100 °C for 8 h to remove the moisture and ethanol.



Scheme 2: Reaction of APTES with Hal nanotubes (Arkles et al., 1992; Du et al., 2006)

In case of Hal nanotubes, the aluminol groups (Al-OH) on the surface of the inner layer of Hal nanotubes have high degree of chemical reactivity with organic compounds such as APTES (**Scheme 2**). Yuan et al. (2008) investigated the modifications of Hal nanotubes with APTES by grafting on the inner surface of Hal nanotubes. The external surface of Hal nanotubes consists of siloxane (Si-O-Si) groups and few aluminols (Al-OH) and silanols (Si-OH) at the edges and surface defects of Hal nanotubes. They reported that the amino-propyl groups as well as the hydroxyl groups of the hydrolysed APTES formed the covalent bonds between Al-OH groups of the inner surface of Hal nanotubes and the siloxane (Si-O-Si) groups at the edges or the surface defects of Hal nanotubes (Yuan et al., 2015). On the other hand, since the modification of Hal nanotubes was carried out using the mixture of water and ethanol solution, some of the hydrolysed APTES reacts with each other to form oligomers which grafted by hydrogen bonding. These oligomers were further reacted with aluminols and siloxanes to form the cross-linked network in the lumen of Hal nanotubes (Arkles et al., 1992; Yuan et al., 2008). It is also believed that more hydroxyl groups exist on the surface of Hal nanotubes due to surface defects. These hydroxyl groups are the potential reactive sites for the surface modification on the external surface of Hal nanotubes which increased the interaction of APTES with Hal nanotubes (Yuan et al., 2008).

3.4 Fabrication of composites

3.4.1 Sisal-PLA composites

Different ratio of untreated and different surface treated (HIU, alkali (7 wt%)) and the combination of alkali (7 wt%) and HIU treated) sisal fibres and PLA (**Table 3.1**) were mixed with an internal mixer (Brabender Plasticoder PL2000-6 equipped with co-rotating blades and a mixing head with a volumetric capacity of 69 cm³). The rotor speed and the blending temperature and time were set at 50 rpm, 180 °C and 15 min respectively.

Table 3.1 Composition of untreated and treated SF/PLA composites

S. No.	PLA (wt %)	Untreated sisal fibres (wt %)	Ultrasound treated sisal fibres (wt %)	Alkali treated sisal fibres (wt %)	Alkali + ultrasound treated sisal fibres (wt %)
1	100	0	0	0	0
2	90	10	0	0	0
3	85	15	0	0	0
4	80	20	0	0	0
5	75	25	0	0	0
6	70	30	0	0	0
7	90	0	10	0	0
8	85	0	15	0	0
9	80	0	20	0	0
10	75	0	25	0	0
11	70	0	30	0	0
12	90	0	0	10	0
13	85	0	0	15	0
14	80	0	0	20	0
15	75	0	0	25	0
16	70	0	0	30	0
17	90	0	0	0	10
18	85	0	0	0	15
19	80	0	0	0	20
20	75	0	0	0	25
21	70	0	0	0	30

Before mixing all the samples were dried under vacuum at 60 °C for 4 h to remove any moisture. Materials obtained from the internal mixer were compression moulded to obtain the test specimens. The compounded materials were placed onto a steel frame mould covered by aluminium plates on both sides. The materials were pressed into sheets of 1 and 3 mm thickness at 180 °C. The moulding cycles involved 3 min of preheating without any pressure, 20 sec of venting and 3 min of compression under 100 bar using hot and cold pressing machine (LP-S-50 Scientific Hot and Cold Press). Then the hot moulded samples were cooled immediately between two platens of cold press at 20 °C for 2 min.

3.4.2 Sisal-PP composites

Table 3.2 Composition of Sisal/PP composites

S. No.	PP (wt %)	Untreated sisal fibres (wt %)	Ultrasound treated sisal fibres (wt %)	Alkali treated sisal fibres (wt %)	Alkali + ultrasound treated sisal fibres (wt %)
1	100	0	0	0	0
2	90	10	0	0	0
3	85	15	0	0	0
4	80	20	0	0	0
5	70	30	0	0	0
6	90	0	10	0	0
7	85	0	15	0	0
8	80	0	20	0	0
9	70	0	30	0	0
10	90	0	0	10	0
11	85	0	0	15	0
12	80	0	0	20	0
13	70	0	0	30	0
14	90	0	0	0	10
15	85	0	0	0	15
16	80	0	0	0	20
17	70	0	0	0	30

Composites of PP reinforced with untreated and different surface treated (HIU treated, alkali (7 wt%) and the combination of alkali (7 wt%) and HIU treated) sisal fibres by using internal mixer and compression moulding at 175 °C as described in the section 3.4.1. **Table 3.2** shows the composition of SF/PP composites.

3.4.3 Hal-PLA nanocomposites

PLA nanocomposites were prepared with reinforcement of different weight percentage of unmodified and APTES modified Hal nanotubes by using internal mixer and compression moulding machine as described in the section 3.4.1. Before mixing, all the samples were dried under vacuum at 60 °C for 4 h to remove any moisture. **Table 3.3** shows the composition of PLA nanocomposites reinforced with unmodified and APTES modified Hal nanotubes.

Table 3.3 Composition of Hal nanotubes (APTES modified/unmodified) PLA nanocomposites

S. No.	Sample	PLA (wt%)	uHal (wt%)	mHal (wt%)
1	Pure PLA	100	0	0
2	2uHal	98	2	0
3	4uHal	96	4	0
4	6uHal	94	6	0
5	8uHal	92	8	0
6	2mHal	98	0	2
7	4mHal	96	0	4
8	6mHal	94	0	6
9	8mHal	92	0	8

uHal: unmodified Hal nanotubes and mHal: APTES modified Hal nanotubes

3.4.3 Hal-PP nanocomposites

PP nanocomposites were prepared with the incorporation of different ratio of unmodified and APTES modified Hal nanotubes by using internal mixer and compression moulding as described in the section 3.4.1. **Table 3.4** shows the composition of PP nanocomposites reinforced with unmodified and APTES modified Hal nanotubes.

Table 3.4 Composition of Hal nanotubes (APTES modified/unmodified) PP nanocomposites

S. No.	Sample	PP (wt%)	uHal (wt%)	mHal (wt%)
1	Pure PP	100	0	0
2	2uHal	98	2	0
3	4uHal	96	4	0
4	6uHal	94	6	0
5	8uHal	92	8	0
6	2mHal	98	0	2
7	4mHal	96	0	4
8	6mHal	94	0	6
9	8mHal	92	0	8

uHal: unmodified Hal nanotubes and mHal: APTES modified Hal nanotubes

3.5 Characterisation techniques

3.5.1 FTIR analysis

FTIR analysis was conducted in between 400 and 4000 cm^{-1} with 0.4 cm^{-1} resolution by using FTIR spectrophotometer (PerkinElmer Spectrum RX1) to confirm the surface modification of alkali, ultrasound and the combination of alkali and

ultrasound treated sisal fibres. FTIR was used to confirm the structural modifications of untreated and different surface treated sisal fibre reinforced PLA composites. FTIR was conducted in between 400 and 4000 cm^{-1} with 0.85 cm^{-1} resolution using FTIR (8300 Shimadzu, Japan) to confirm the structural modification of Hal nanotubes and Hal-PLA nanocomposites. For this, fibre samples were grounded well with KBr (~2% by weight) and pressed into a pellet with the thickness of about 1 mm. All FTIR spectra were recorded in Transmittance units.

3.5.2 FE-SEM analysis

The surface morphology of untreated, ultrasound treated and the combination of alkali and ultrasound treated sisal fibres and their PLA and PP composites of the tensile fractured surfaces were investigated by using Quanta 400 FE-SEM. The FE-SEM also used to measure the fibre diameter of the untreated and different surface treated sisal fibres. The morphology of tensile fractured surfaces of Hal-PLA and Hal-PP nanocomposites and the elemental analysis for the unmodified and APTES modified Hal nanotubes was carried out by using FE-SEM with EDX using Quanta 400 FE-SEM.

3.5.3 Nitrogen adsorption-desorption analysis

Nitrogen adsorption-desorption isotherm analysis was carried out for unmodified and APTES modified Hal nanotubes at $-196\text{ }^{\circ}\text{C}$ by using porosimeter (ASAP2020, Micromeritics). The specific surface area and total pore volume of both unmodified and APTES modified Hal nanotubes were calculated by Brunauer-Emmett-Teller (BET) method and Barrett-Joyner-Halenda (BJH) methods respectively by using MicroActive 4.0 software. Before measurements, samples of unmodified and APTES

modified Hal nanotubes were dried at 110 °C for 12 h and out-gassed at 100 °C under vacuum for 8 h (Barrientos-Ramirez et al., 2011).

3.5.4 XRD analysis

The crystallinity of cellulose in sisal fibres was analysed with X'Pert Pro MRD (PANalytical) diffractometer using CuK α (1.2405980Å) radiation Ni-filter and scintillation counter as detector at 45 kV and at 23 mA. Experiments were carried out in the continuous mode at a scan speed of 2° per min and with a step size of 0.02°. The X-ray diffractograms were recorded from 10 to 50° (Bragg angle). The crystallinity index and percentage of crystallinity (%C_r) of cellulose were calculated according to peak height method (eqn. 3.2) (Segal et al., 1959; Park et al., 2013).

$$C_r I (\%) = \frac{(I_{002} - I_{am})}{I_{002}} \times 100 \quad (\text{eqn.3.2})$$

Where I₀₀₂ is the peak intensity at a 2 θ angle close to 22° and I_{am} is the amorphous counter reading at a 2 θ angle at around 18°.

3.5.5 Tensile properties of single sisal fibre

Tensile properties of untreated and surface treated sisal fibres were carried out according to ASTM D3379-75 standard test method for a single filament. For this purpose, untreated and surface treated single fibre was fixed to the rectangular cardboard sheet with the dimensions of 50 mm \times 20 mm (length \times width) which has a 20 mm hole in the middle of the cardboard sheet as shown in **Fig. 3.1**. The single fibre was mounted on the cardboard sheet by using polyvinyl acetate glue. The mounted fibres were then placed in the grips of tensile testing machine (Toyoski tensile testing machine) and a cutter was used to cut the supporting sides of the cardboard. The

tensile test was carried out at a cross head speed of 0.5 mm/min using 10 N-cell load. The fibres were assumed to be cylindrical and the diameter of the fibres was measured at five different points using optical microscopy (Olympus SZX7). The obtained average diameter was then used to calculate the tensile properties of fibres considering twenty specimens.

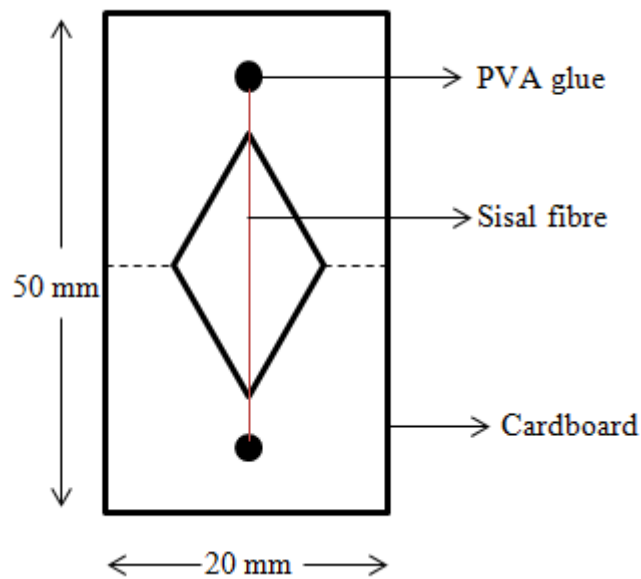


Fig. 3.1 Schematic diagram of the method followed to determine the tensile strength of single fibre

3.5.6 Density measurements

The density (ρ_c) of the composites was calculated by using a pycnometer which was carried out according to ISO 118-3. Distilled water was used as a reference liquid for this test at 23 °C. The density of the composites was then calculated by using the following eqn. 3.3

$$\rho_c = \frac{w_c}{(w_m / \rho_m) + (w_f / \rho_f)} \quad (\text{eqn.3.3})$$

Where W_c , W_m and W_f are the weights of the composites, matrix and fibres respectively, whereas ρ_m and ρ_f are the density of matrix and fibres respectively.

3.5.7 Tensile properties of the composites

Dumb-bell shaped specimens were punched from the moulded sheets of pure PLA, pure PP, untreated and different surface treated sisal fibres reinforced PLA and PP composites after 24 h of storage. Tensile properties were also evaluated for the unmodified and APTES modified Hal nanotubes reinforced PLA and PP composites. Ultimate tensile strength (maximum stress), elongation at break and Young's modulus were measured according to ASTM D638 standard using Toyoski tensile testing machine at a constant crosshead speed of 5 mm/min. Six specimens were tested and at least five replicate specimens have been presented as an average of tested specimens.

3.5.8 Impact properties of the composites

Impact tests were performed for pure PLA, pure PP, untreated and different surface treated sisal fibres reinforced PLA and PP composites after 24 h of storage. Impact properties were also evaluated for the unmodified and APTES modified Hal nanotubes reinforced PLA and PP composites by using CEAST Izod impact tester (Model CE UM-636) with a 4 J hammer according to ASTM D256 standard. For this, samples with the final dimensions of 3 x 25 x 150 mm³ were cut and the impact strength was performed at room temperature for six notched samples taken from each nanocomposite and the average values and the standard deviation have been reported.

3.5.9 TGA analysis

TGA was conducted using Perkin-Elmer (STA6000 TA instrument) from room temperature to 600 °C at a heating rate of 10 °C/min under nitrogen atmosphere at a

flow rate of 20 ml/min and the sample weight was taken as an average of 8 mg for each sample.

3.5.10 DSC analysis

DSC analysis was carried out for pure PLA, pure PP, and untreated and different surface treated sisal fibres reinforced PLA and PP composites. DSC test was also carried out for unmodified and APTES modified Hal nanotubes reinforced PLA and PP composites. For this purpose computerised DSC (Mettler Toledo DSC 1/32 equipped with STARe System) was used to determine the crystallization and melting temperatures, heat of fusion and degree of crystallinity of the samples. The tests were conducted by heating the samples in a covered aluminium pan from room temperature to 120 °C at 10 °C/min followed by cooling to 30 °C at a cooling rate of 10 °C/min to remove the thermal history. Second heating was carried out at a rate of 10 °C/min up to 120 °C to obtain heat flow vs. temperature thermogram. All the analysis was carried out using 5 to 10 mg of samples in an atmosphere of nitrogen (20 ml/min). First heating scan was omitted from the data analysis. The crystallinity of PLA and PP in the composites was calculated by using the following eqn. 3.4

$$\text{Crystallinity (\%)} = \frac{\Delta H_m - \Delta H_{cc}}{\Delta H_m^0 - C} \times 100 \quad (\text{eqn. 3.4})$$

Where ΔH_m and ΔH_m^0 are the endothermic enthalpy of samples and that of 100% crystallized PLA and PP (heat of fusion of 100% crystallinity of PLA and PP are 93 J/g and 209 J/g respectively) (Avella et al., 1992; Arbelaiz et al., 2006; Battezzore et al., 2011). ΔH_{cc} is the enthalpy of cold crystallization and C is the mass percentage of pure PLA and PP composites respectively.

3.5.11 DMA analysis

DMA was measured by using a dynamic mechanical analyser (Perkin-Elmer DMA8000). The samples were subjected to a cyclic tensile strain with the force amplitude of 0.1 N at a frequency of 1.0 Hz. Storage modulus, tan delta and loss modulus were determined from room temperature to 120 °C at a heating rate of 3 °C/min.

3.5.12 Water absorption studies

Water absorption tests were carried out according to ASTM D570-98. The composite samples were cut into square shape with the dimensions of 20 mm × 20 mm × 3 mm. The composite samples were first dried in an oven at 70 °C for 24 h to remove the moisture and then the composite samples were weighed and soaked in a beaker with distilled water. The water soaked samples were taken out at regular time intervals and the experiments were continued over a period of 60 days. Composite samples were dried using tissue paper after taken out from the beaker and the samples were weighed by using a digital balance. A digital weighing scale (Mettler Toledo model: XS204-3) with a weighing precision of 0.0001 g was used to weigh the samples. The percentage weight of water absorbed (W_A) was calculated by using the following eqn. 3.5

$$W_A(\%) = \frac{W_f - W_i}{W_i} \times 100 \quad (\text{eqn. 3.5})$$

Where, W_i and W_f are the initial and final weights of the composite samples respectively. Water or moisture absorption is an important property in which the mechanical properties of fibre reinforced composite materials decrease greatly with increasing water absorption (Chow et al., 2007). The diffusion properties of composite materials could be explained by Fick's law. The coefficient of diffusion

(D) is defined as the rate of diffusion takes place with respect to unit area of sample and square root of time (Dhakal et al., 2007b; Sreekala and Thomas, 2003). Diffusion coefficient (D) behaviour of untreated and treated SF/PLA composites was calculated by the following eqn. 3.6.

$$D = \pi \left[\frac{kh}{4M_m} \right]^2 \quad (\text{eqn. 3.6})$$

Where k is the initial slope of a plot $M(t)$ versus $t^{1/2}$; M_m is the maximum weight gain and h is the thickness of the sample.

3.5.13 Biodegradability analysis

The biodegradability of the untreated, HIU treated, alkali treated and the combination of alkali and HIU treated SF/PLA polymer composites were conducted by natural soil burial test for a period of 4 months (January to April 2016). This biodegradability test was carried out according to Kim et al. (2005). For this purpose, samples were cut into square shape with the dimensions of 20 mm × 20 mm × 3 mm. Each month, one set of samples were dig out from the soil and washed with distilled water and then dried at 60 °C in an oven for 24 h before subjecting the samples to morphological studies and weight loss measurements. The weight loss was estimated with an electronic digital balance with the precision of 0.0001.

Weight loss was calculated by using following eqn. 3.7.

$$\text{Weight loss (\%)} = \frac{W_i - W_f}{W_i} \times 100 \quad (\text{eqn. 3.7})$$

Where W_i and W_f are the initial and final weight of the samples. Morphological aspects of the exposed area of the samples were analysed by using Quanta 400 FE-SEM.

CHAPTER IV

Results and Discussion: Surface treatments and characterisation of sisal fibres

4.1 Effects of alkali and HIU treatments on sisal fibres

Alkali treatment is one of the most common and efficient chemical methods used for cleaning and/or mercerising the surface of natural fibres (Gurunathan et al., 2015). On the surface of sisal fibres, free space exists between the cellulose and amorphous materials, which is responsible for the absorption of moisture. Absorption of moisture leads to the reduction in the mechanical and thermal properties of fibres. **Scheme 1** (section 2.4.1) shows the alkali reaction with sisal fibres in which Na^+ ions from the alkali solution replace the hydroxyl groups on the surface of fibres whereby the fibre surface becomes hydrophobic which leads to the enhancement of moisture resistance property of the fibre surface (Kabir et al., 2012). Alkali treatment also dissolves the waxy and oily materials that cover the surface of fibres thereby making the surface to become cleaner. Besides, micro-voids are eliminated due to the clean surface and the stress transfer property of fibres is increased (John and Anandjiwala, 2009; Mwaikambo et al., 2007). With the removal of these amorphous materials from the surface of fibres, mechanical and thermal properties of the fibre reinforced composites increased (Mwaikambo et al., 2007; Lu et al., 2013; Kabir et al., 2013b; Mahjoub et al., 2014). However, improvement of these properties mainly depends on the concentration of alkali solution. It is proved that the optimized percentage of alkali treatment can only remove the amorphous materials partially from the surface of natural fibres (Mwaikambo and Ansell, 1999; Cai et al., 2015). If the concentration of

alkali is higher than the optimum, delignification takes place and the fibres become weakened or damaged, which leads to the reduction in the mechanical and thermal properties of the reinforced composites (John and Anandjiwala, 2009; Kabir et al., 2012).

On the other hand, in recent years, HIU has gained wide popularity as an effective method for the surface modification of natural fibres especially for the separation of fibres (Chen et al., 2011b). HIU waves can produce powerful mechanically oscillating bubbles which lead to cavitation that consists of formation, expansion and violent collapse of bubbles in the water and result in the generation of high pressure and temperature locally. The energy produced by the cavitation during violent collapse is approximately equals to hydrogen bond energy (10-100 kJ/mol). Thus, the ultrasonic impact can gradually disintegrate the complicated multilayer structure and separates the cellulose fibrils from the amorphous materials (Tischer et al., 2010). The effect of HIU treatment of sisal fibres was studied without alkali pre-treatment. It was noticed that the ultrasound treatment alone not effective in the removal of amorphous materials from the surface of fibres and to reduce the fibre diameter. This may be due to the strong intermolecular hydrogen bonding of hemicellulose and lignin present on the surface of fibres with the cellulose molecule. However, alkali treatment replaces the hydrogen bonding as shown in the **scheme 1** (section 2.4.1). This is in agreement with the results of FE-SEM, FTIR and tensile strength and modulus. Similar results were reported by other researchers (Lee et al., 2008; Moshiul Alam et al., 2012; Beg et al., 2015).

Application of HIU treatment for the alkali treated sisal fibres significantly improved the aspect ratio due to well-separated fibre strands which leads to improve the mechanical and thermal properties of the fibre reinforced polymer composites. **Fig.**

4.1 shows the schematic representation of the effects of alkali and HIU treatments on the surface of fibres. Chen et al. (2011) described the key effects of HIU for the chemically pre-treated wood fibres. They mentioned that HIU with an output power equals to 1000 W or more was efficiently individualised the fibres and significantly increased the aspect ratio of fibres. Tischer et al. (2010) reported the pre-treatment of bacterial cellulose with 0.1M NaOH solution before applying HIU treatment. They found that the combination of alkali and HIU treatments were effective in promoting the removal of amorphous materials from the surface of bacterial cellulose.

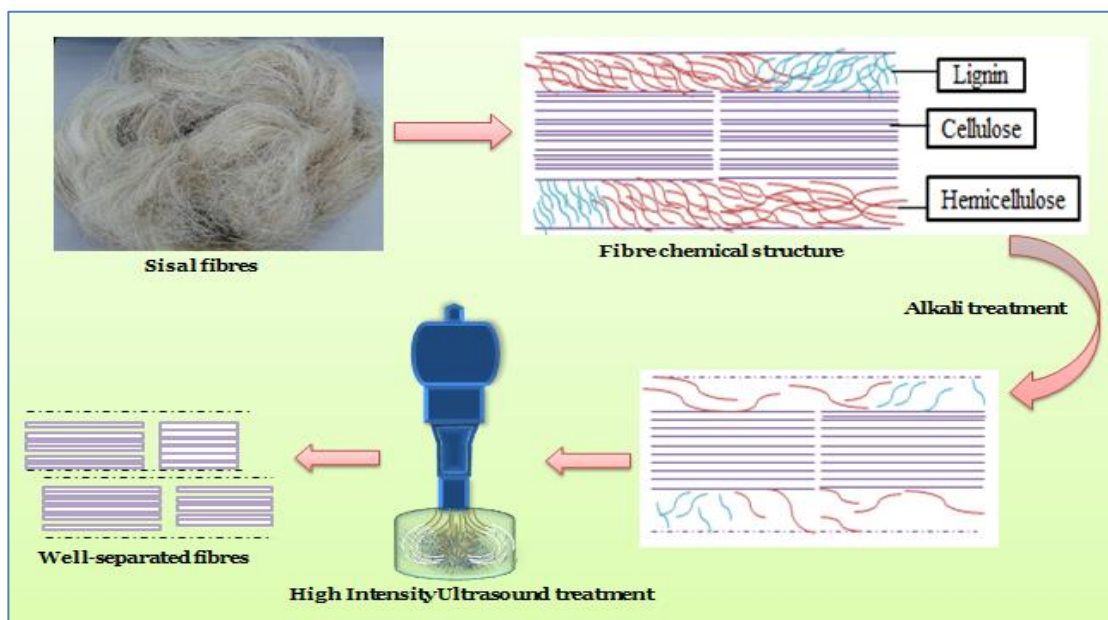


Fig. 4.1 Schematic representation of the effects of alkali and HIU treatments on the sisal fibres

A significant reduction of water absorption by 50% and an increase in the tensile strength by 4.52% were found out with alkali and ultrasound treated banana fibres reinforced vinyl ester composites as compared to untreated banana fibre composites (Ghosh et al., 2014). Combined treatments of alkali and ultrasound treatments were applied to oil palm empty fruit bunch fibres reinforced PLA composites and the

mechanical and thermal properties were evaluated. It was noticed that the tensile strength, modulus and impact strength increased by 33%, 62% and 53.8% respectively for the combined treatments of alkali and ultrasound as compared to pure PLA (Moshiul Alam et al., 2012). **Fig. 4.2** shows the visual examination of untreated and different surface treated sisal fibres. It can be seen that the untreated fibres (**Fig. 4.2A**) possess higher diameter as compared to alkali and the combined treatment of alkali and HIU (**Figs. 4.2C and D**). HIU treatment (**Fig. 4.2B**) could remove the impurities whereby the fibres become cleaned.



Fig. 4.2 Visual examination of sisal fibres: (A) Untreated (UT), (B) High intensity ultrasound treated (ULT), (C) Alkali treated (ALKT), (D) Combination of alkali and high intensity ultrasound treated (ALKT-ULT) sisal fibres

Abdul Khalil et al. (2014) and Iskalieva et al. (2012) have also studied the HIU effects on the separation of hemicellulose and lignin from the fibre surface and indicated that the pre-treatment of fibres with high power input of ultra-sonication enhanced the removal of amorphous materials from the surface of natural fibres along with individualisation of fibre strands. This is in agreement with the observed results from FE-SEM and tensile strength.

4.2 FTIR analysis

The chemical structure of untreated, ultrasound, alkali and the combination of alkali and ultrasound treated sisal fibres was analysed through FTIR. The functional groups of cellulose, hemicellulose, pectin and lignin present on these fibres and their respective IR bands have been listed in **Table 4.1** (Boopathi et al., 2012; Ramadevi et al., 2012; Cai et al., 2015). FTIR spectrum is useful to investigate the shifted functional groups within the fibre constituents after subjected to surface treatments (Carrillo et al., 2004; Abidi et al., 2014).

Fig. 4.3 shows the FTIR spectra of untreated, ultrasound, alkali and the combination of alkali and ultrasound treated sisal fibres. The broad peaks at 3431 cm^{-1} and at 3434 cm^{-1} are attributed to the hydroxyl groups of cellulose and hemicellulose. In the untreated fibres, the band at 2916 cm^{-1} indicates the C-H stretching of lignin which shifted to 2893 cm^{-1} with the treatment of ultrasound, alkali and the combination of alkali and ultrasound on the sisal fibres and this clearly indicates the removal of lignin (Zhou et al., 2014). In the untreated fibres, the band appearing at 1742 cm^{-1} indicates the C=O groups of hemicellulose and pectin which disappeared with the alkali treatment (Ramadevi et al., 2012). However, with ultrasound treatment the sisal fibres

still indicates the peak at 1742 cm^{-1} , which confirms that ultrasound treatment alone is not effective in removing hemicellulose and lignin from the surface of fibres.

Table 4.1 FTIR transmittance peaks of the constituents of sisal fibres

Wavenumbers (cm^{-1})	Functional groups	Possible assignment
3431, 3434	-OH stretching vibrations	Cellulose, hemicellulose and lignin
2916, 2921, 2893	C-H stretching vibrations	Lignin, hemicellulose and cellulose
1742	C=O stretching vibrations	Carboxyl groups of hemicellulose and pectin
1636	-OH bending mode	Presence of water in hemicellulose
1376	C-H bending and C-O stretching	Hemicellulose
1261	C-O stretching	Acetyl groups of lignin
1053, 1060	C-O stretching	Lignin and cellulose

Similarly, the peak corresponding to C-O stretching of acetyl groups of lignin at 1261 cm^{-1} no longer appears with the combined treatment of alkali and ultrasound. The characteristic peak at 1053 cm^{-1} represents the C-O stretching of lignin in the untreated fibres which shifted to a higher wavelength at 1060 cm^{-1} due to the removal of lignin from the surface of sisal fibres with the treatments of alkali and the combination of alkali and ultrasound (Kabir et al., 2013a; Belaadi et al., 2014; Cai et al., 2015).

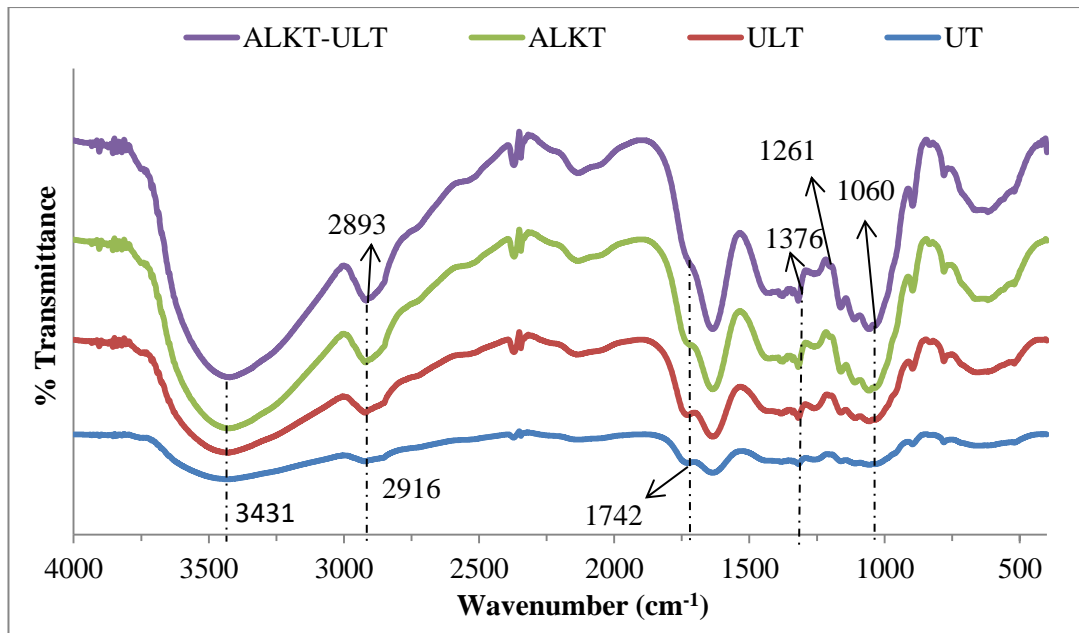


Fig. 4.3 FTIR spectra of untreated (UT), ultrasound treated (ULT), alkali treated (ALKT) and the combination of alkali and ultrasound treated (ALKT-ULT) sisal fibres

From these observations it could be noted that hemicellulose, pectin and lignin from the surface of sisal fibres could be removed when they were subjected to alkali and the combined treatment of alkali and ultrasound. Previous studies indicated that ultrasound treatment alone did not cause any significant effect on the removal of hemicellulose and pectin (Chen et al., 2011). On the other hand, alkali treatment alone found to have good impact on the removal of amorphous materials such as hemicellulose, lignin and pectin from the surface of sisal fibres (Lu et al., 2013; Cai et al., 2015).

In this investigation no difference was observed between the spectra of alkali treated and the combination of alkali and ultrasound treated sisal fibres. This indicates the importance of alkali in removing the amorphous components from the surface of fibres. Besides, it confirms that the molecular structure of cellulose was not changed

with any of the above treatments. Thus, alkali as well as the combination of alkali and ultrasound treatments successfully removed the amorphous materials such as hemicellulose, lignin and pectin from the surface of sisal fibres. Similar observations were reported on the preparation of cellulose I nanofibers from bamboo fibres (Chen et al., 2011).

4.3 Morphology of sisal fibres

The changes in the morphology of sisal fibres with alkali, ultrasound and their combined treatments were studied using FE-SEM (**Fig. 4.4**). **Fig. 4.4A** clearly shows that the surface of untreated fibres contains impurities such as waxy and gummy materials which are attached onto the surface. Whereas, the partial removal of impurities, waxy and gummy materials could be seen in the case of ultrasound treated sisal fibres as compared to the untreated fibres (**Fig. 4.4B**). Thus, ultrasound treatment alone is not effective to remove the hemicellulose, lignin and pectin from the surface of sisal fibres owing to the strong hydrogen bonding between lignin and cellulose structure. Whereas, alkali treatment helps to dissolve the oily, waxy and other impurities which stick onto the surface of sisal fibres and results in the cleaning of fibre surface (**Fig. 4.4C**).

Besides, the alkali treatment reduced the fibre diameter owing to the removal of hydrogen bonding between the cellulose and lignin materials on the surface of fibres and leads to their easy separation (Li et al., 2007). A reduction in the fibre diameter enhances the aspect ratio (length/diameter) of sisal fibres which assists in the improvement of mechanical and thermal properties of fibre reinforced polymer composites (Vilay et al., 2008; Dong et al., 2014; Shukor et al., 2014). These

observed results of removal of amorphous components from the fibre surface are in agreement with FTIR results.

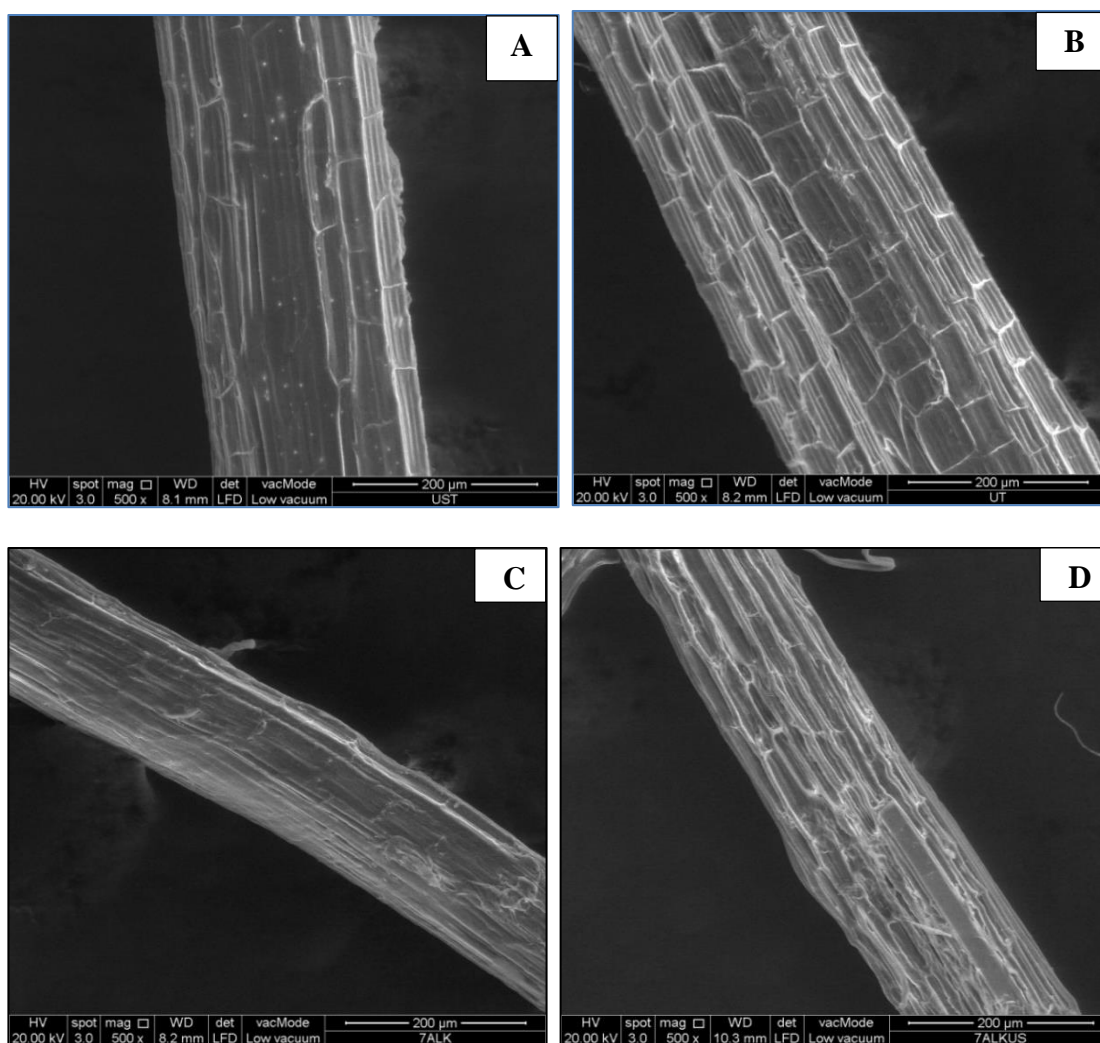


Fig. 4.4 FE-SEM micrographs of sisal fibres: (A) Untreated (UT) (B) Ultrasound treated (ULT) (C) Alkali treated (ALKT) (D) the combination of alkali and ultrasound treated (ALKT-ULT)

With the combined treatment of alkali and ultrasound, the fibre surface becomes highly rough with loosened structure (**Fig. 4.4D**) as compared to the untreated, ultrasound and alkali treated fibres. Thus, alkali treatment removed the waxy, oily and other impurities present on the surface of fibres whereby fibres become swollen and soft. Whereas, the application of HIU causes the removal of amorphous materials as

well as the separation or disintegration of cellulose effectively which in turn enhances the surface roughness of sisal fibres.

An increase in the surface roughness is very important to enhance the adhesion or mechanical interlocking between fibre surface and polymer matrix to improve the mechanical and thermal properties of fibre reinforced polymer composites (Cheng et al., 2010; Chen et al., 2011a, 2011b). Other researchers also noted similar results using different natural fibres where they have observed the removal of wax and pectin from the fibre surface after alkali and ultrasound treatments. Besides, they observed an irregularity in the structure on the fibre surface which increased the adhesion of fibre and matrix of polymer composites (Mwaikambo and Ansell, 2002; Chen et al., 2011b; Kaushik et al., 2012; Moshiul Alam et al., 2012; Zhang et al., 2013; Cai et al., 2015).

4.4 Analysis of moisture absorption

Similar to other natural fibres, sisal fibres absorb moisture, mainly due to the presence of amorphous materials on the surface of fibres which induce the absorption of moisture from the atmosphere. With the absorption of moisture, the mechanical and thermal properties of fibres are reduced. Besides, it causes poor compatibility between the polymer matrix and fibre. Analysis of moisture content of the untreated, HIU treated, alkali treated and the combination of alkali and HIU treated fibres have been shown in **Fig. 4.5**. It is obvious that the untreated fibres show a higher moisture content, as discussed in the earlier sections where the large gap between the cellulose and amorphous materials such as hemicellulose, lignin and pectin on the surface of sisal fibres absorb the moisture in the untreated fibres (Somerville et al., 2004).

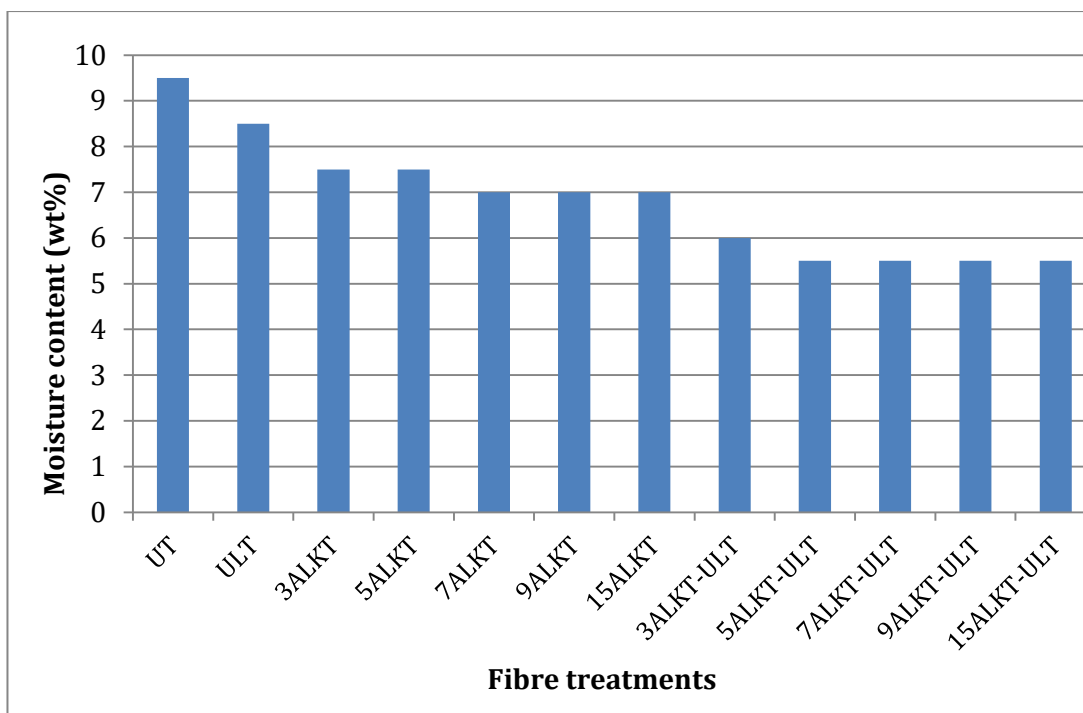


Fig. 4.5 Moisture content of untreated (UT), ultrasound treated (ULT), alkali treated (ALKT) and the combination of alkali and ultrasound treated (ALKT-ULT) sisal fibres

Alkali treatment replaces the hydroxyl groups of amorphous materials with Na^+ ions and the fibres become O^-Na^+ which makes the fibre surface hydrophobic and reduces its moisture absorption (Cai et al., 2015). Whereas the combination of alkali and ultrasound treated fibres exhibited a lower moisture content where the alkali treatment makes the fibre surface to swollen and soft; high intensity ultrasound effectively removed the remaining amorphous materials and increased the exposure of crystalline cellulose to the outer surface. Higher exposure of crystalline cellulose makes the fibres to resist moisture (Chen et al., 2011a) which leads to lower its moisture content.

These results further support the observations obtained from FTIR and FE-SEM. **Fig. 4.5** illustrates the moisture content of treated and untreated sisal fibres. Untreated sisal fibres show a moisture content of 9.5% which reduced to 7.5% when the sisal fibres

were treated with NaOH (3 wt%). Moisture content further reduced to 7% when the conc of NaOH increased to 7%. Whereas, for the combined alkali and ultrasound treated fibres, the moisture content significantly dropped to 5.5% which reveals that the combined treatments of alkali and ultrasound made significant effects on the fibre surface. Boopathi et al. (2012) reported that the absorption of moisture significantly reduced (30%) after alkali treatment of Borassus fibres. Moisture absorption is an important property as it modifies the mechanical and thermal properties of fibres. A lower moisture content of the fibres enhances the adhesion between the fibres and the matrix which results in its wider applications as reinforcing fillers in the production of polymer composites.

4.5 Analysis of fibre diameter

Fibre diameter analysis was carried out by taking 25 samples each of untreated, alkali treated, HIU treated and the combination of alkali and HIU treated sisal fibres. **Fig. 4.6** shows the FE-SEM images from which the diameter of sisal fibres could be established. A reduction in the fibres diameter was observed and the obtained results have been summarised in **Table 4.2**. Untreated fibres show a higher fibre diameter (240-305 μm) as compared to HIU treatment, alkali and the combination of alkali and HIU treated sisal fibres. In case of HIU treatment, a slight reduction in the fibre diameter was observed which is due to the effect of ultrasonication. In case of alkali treated fibres, a considerable reduction in the fibre diameter was observed which clearly indicated the removal of amorphous materials as well as waxy, oily and other impurities from the surface of fibres. It is noteworthy that the diameter of fibre decreased constantly with an increase in the concentration of NaOH from 3 to 15 wt%. Similar observations were also noted for the simultaneous treatment of alkali and HIU.

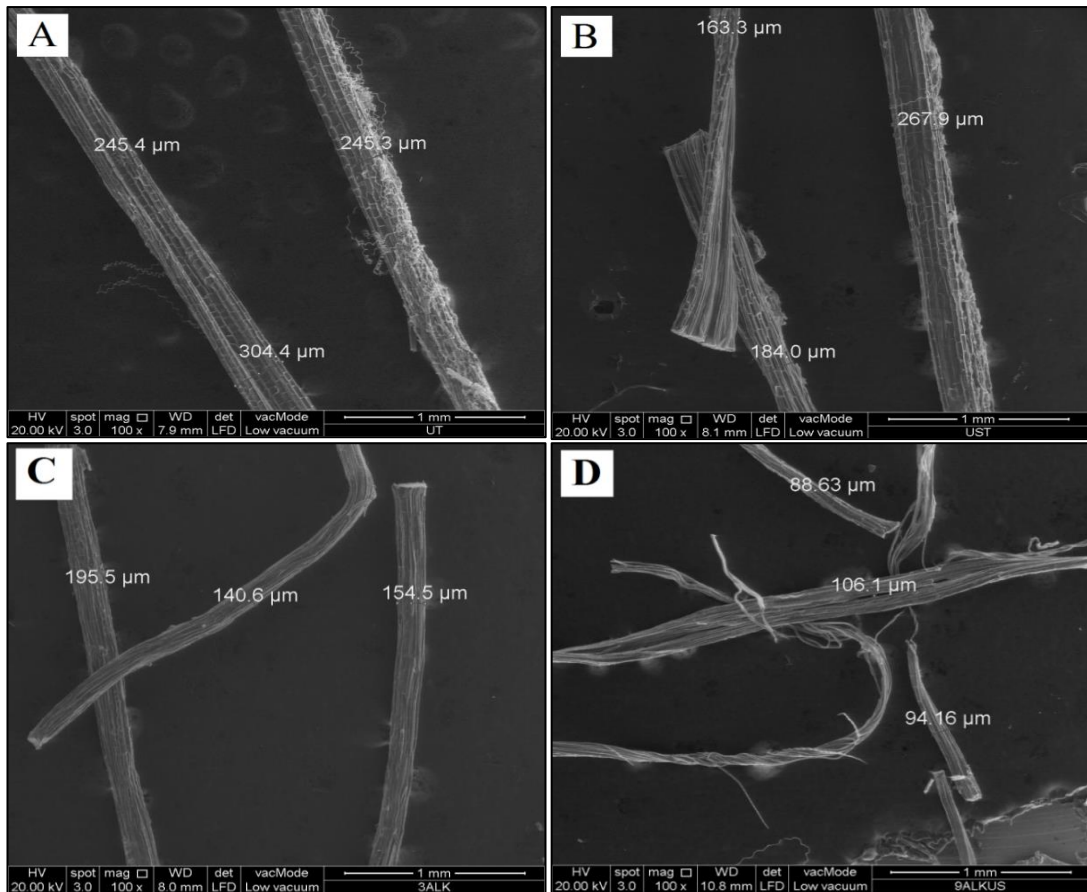


Fig. 4.6 FE-SEM images of sisal fibres with the diameter for different concentration of alkali treatment and the combination of alkali and ultrasound treatments (A) Untreated (B) HIU treated (C) Alkali treated (D) the combination of alkali and HIU treated

In case of the combination of alkali and HIU treated sisal fibres, the fibre diameter reduced by about 200% (**Table 4.2**), implying an increased aspect ratio. These observations show that the combined treatments of alkali and HIU affect the fibre diameter of the sisal fibres. Kabir et al. (2013) observed the same trends in the hemp fibres where the diameter of fibres reduced to 20% of their original diameter after subjecting the fibres to NaOH (10 wt%) which is due to the removal of hemicellulose and lignin from the surface of fibres. Mahjoub et al. (2014) determined the fibre

diameter after alkali treatment and observed a reduction in the fibre diameter by 15 to 25%.

Table 4.2 Diameter of untreated and different surface treated sisal fibres

S. No.	Fibre type	Maximum diameter (μm)	Minimum diameter (μm)	Average diameter (μm)
1	UT	305	240.0	275.25
2	ULT	285	175	240.50
3	3ALKT	245.50	135.84	185.67
4	5ALKT	206.52	136.33	155.95
5	7ALKT	195.30	92.22	147.40
6	9ALKT	190	103.52	136.50
7	15ALKT	175.20	97.60	133.99
8	3ALK-ULT	228.60	187.35	195.60
9	7ALK-ULT	187	122.68	145.70
10	9ALK-ULT	125	85.50	105.00
11	15ALK-ULT	120	85	97.50

4.6 XRD analysis

XRD is an important technique to investigate the crystallinity of materials. **Fig. 4.7** shows the diffraction patterns of untreated, HIU, alkali and the combination of alkali and HIU treated sisal fibres. The X-ray spectrum of untreated and treated sisal fibres show three main peaks at 15.3° , 23.0° and 35.0° , which are assigned to (101), (002) and (040) reflection planes of cellulose I structure. The untreated sisal fibre shows a broad peak at 15.3° which is related to the amorphous phase of lignin and

hemicellulose. The sharp peak with high intensity refers to the crystalline cellulose phase of sisal fibres (Ouajai and Shanks, 2005; Mohan and Kanny, 2012). After alkali treatment, cellulose in the sisal fibres converted into alkali cellulose. Formation of alkali cellulose purely depends on the concentration of alkali and the treatment conditions. Na⁺-cellulose I and Na⁺-cellulose II are the commonly existing types of alkali cellulose with the alkali treatment. Na⁺-cellulose I is formed at room temperature with the concentration of alkali between 3-5%. Whereas, Na⁺-cellulose II is formed at a higher concentration of alkali (7% and higher) and at higher temperatures (60-100⁰C). Subsequent washing of Na⁺- cellulose leads to the formation of Na⁺-cellulose II which is of a crystalline structure. Nishiyama et al. (2000) reported that the alkali treatment involves rearrangement of amorphous form of cellulose molecules into crystalline phase. Cai et al. (2015) also observed similar results in abaca fibres using higher concentrations of alkali.

The crystalline index (C_rI) of untreated, HIU, alkali and the combination of alkali and HIU treated sisal fibres was calculated by using the Segal method and the obtained values of C_rI have been shown in **Fig. 4.8**. Segal method is simple and effective and is based on the intensity measured at two points of XRD according to eqn. 3.2 (Park et al., 2010). Crystallinity index of untreated sisal fibres was 64.67% which slightly increased to 66.21% for the HIU treated sisal fibres and this indicates the partial removal of amorphous materials from the surface of sisal fibres. However, with the treatment of alkali, crystallinity index of the sisal fibres increased gradually. The crystallinity continuously increased with an increase in alkali from 3 wt% up to 7 wt%, and resulted in about 10% higher crystallinity than the untreated sisal fibres.

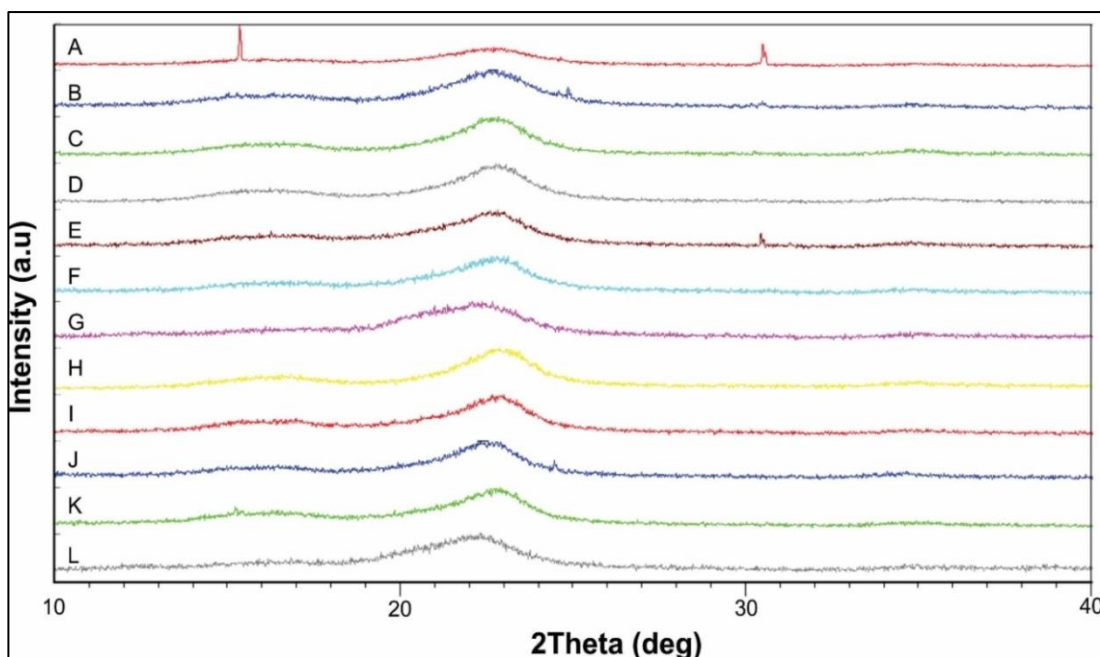


Fig. 4.7 X-ray diffractogram of untreated (UT), alkali treated (ALKT) and the combination of alkali and HIU treated (ALKT-ULT) sisal fibres (A: Untreated, B: HIU treated, C-G: Alkali treated (3, 5, 7, 9 and 15 wt% of alkali), H-L: Combination of alkali and HIU treated (3, 5, 7, 9 and 15 wt% of alkali))

However, a further increase in the concentration of alkali (9 wt% and above), a decrease in the crystallinity was observed which may be due to the disintegration of cellulose structure. Similar results have been reported in the literature (Cao et al., 2012; Kaushik et al., 2012; Mokaloba and Batane, 2014; Chikouche et al., 2015). Mokaloba and Batane. (2014) noticed an increase in the crystallinity index (C_rI) of sisal fibres by 8% with the treatment of 6 wt% alkali. Kaushik et al. (2012) observed that the crystallinity index of raw sisal fibres was 71.7% and with the alkali treatment (5 wt%) the crystallinity index increased to 74.3%; however it reduced to 62% when the concentration of alkali finally increased to 10 wt%. These observations revealed that crystallinity index depends on the concentration of alkali employed.

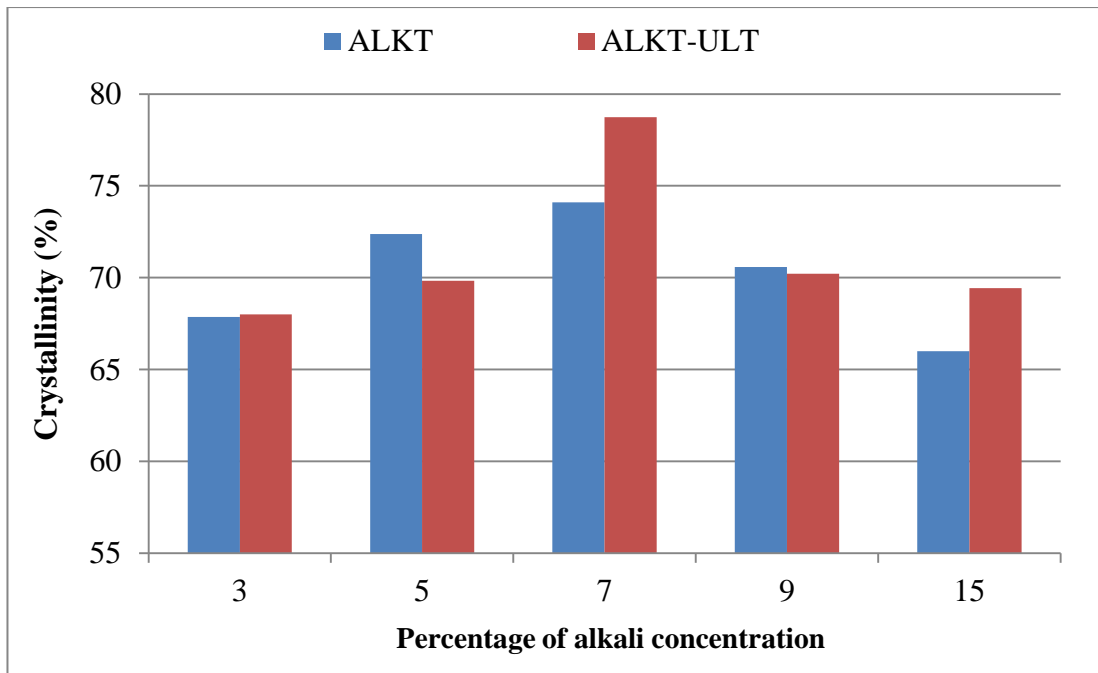


Fig. 4.8 Percentage of crystallinity as a function of percentage of alkali concentration for alkali treated (ALKT) and the combination of alkali and high intensity ultrasound treated (ALKT-ULT) sisal fibres

With the combined treatment of alkali and HIU, the crystallinity index improved further and reached the maximum of 78.74% for alkali concentration of 7 wt% and HIU combination as compared to individual HIU and alkali treated sisal fibres which is associated with the swelling of sisal fibres after the alkali treatment. With the swelling and smooth surface of sisal fibres after alkali treatment, it becomes easy for the HIU treatment to remove the amorphous materials effectively. Thus, 7 wt% alkali and HIU treated sisal fibres shows 14% higher crystallinity as compared to the untreated sisal fibres. However, similar to alkali treated sisal fibres, the combination of alkali (9 and 15 wt%) and HIU treated sisal fibres resulted into a slight reduction in the crystallinity of 70.21 and 69.43% respectively, which is due to the disintegration of cellulose structure. These observations indicate that the fibre surface becomes more crystalline upon the removal of amorphous materials with the combination of alkali

and HIU treatments. These results are in agreement with the observations from FTIR and FE-SEM results.

4.7 TGA analysis

Fig. 4.9 shows the TGA curves of alkali treated sisal fibres with untreated and HIU treated sisal fibres respectively. Whereas, **Fig. 4.10** shows the TGA curves of combined treatment of alkali and HIU with untreated and HIU treated sisal fibres respectively.

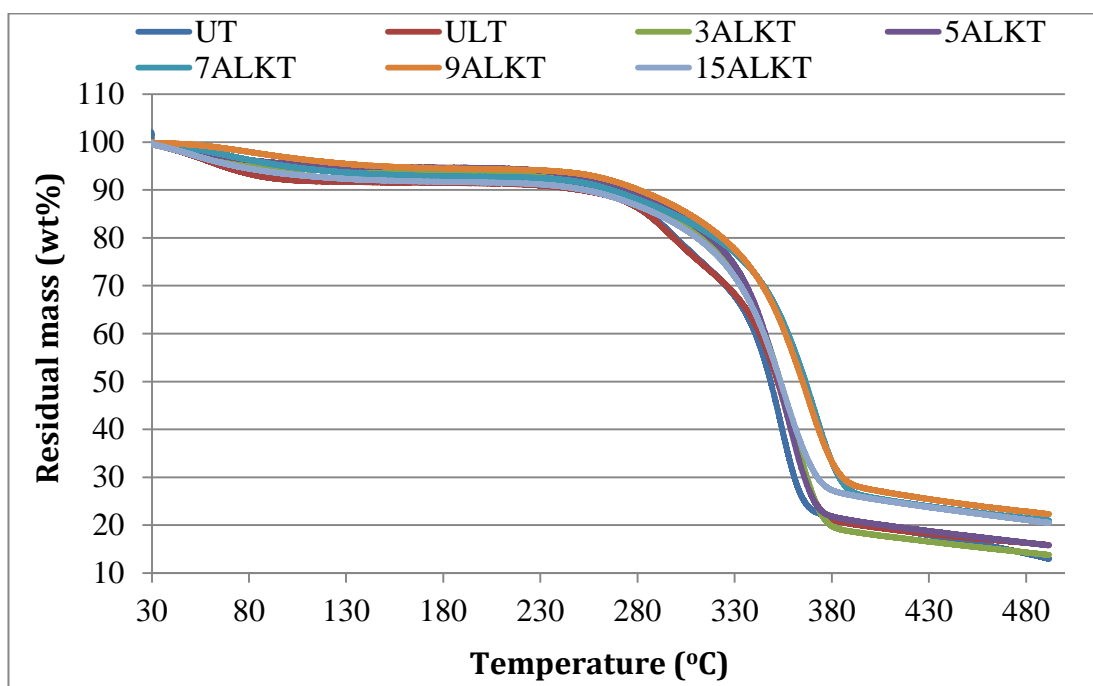


Fig. 4.9 TGA curves of untreated (UT), ultrasound (ULT) and alkali treated (ALKT) sisal fibres

It could be observed that the untreated sisal fibres show a primary weight loss in the temperature range of 90 to 110 °C which is due to the evaporation of surface water (De Rosa et al., 2010; Orue et al., 2016). HIU treated sisal fibres also show a similar weight loss in the temperature range of 90 to 110 °C which clearly indicates that the ultrasound alone could not be effective for the removal of amorphous materials from

the surface of fibres, since the amorphous materials are responsible for the absorption of moisture. However, this primary degradation peak reduced with an increase in the concentration alkali from 3 wt% and completely disappeared at an optimum concentration of alkali (7 wt%). This observation strongly supports the reduction in the moisture after alkali treatment which is due to the removal of amorphous materials as well as surface impurities i.e. wax and oil which lead to make the fibre surface becomes cleaned and enhances the thermal stability of fibres. Secondary thermal degradation peak could be noticed around 300 °C for the untreated and ultrasound treated sisal fibres which is due to the thermal degradation of hemicellulose. However, this secondary degradation peak could not be observed in the alkali and the combination of alkali and ultrasound treated sisal fibres which confirms the removal of hemicellulose. This is further supported by FTIR analysis.

Similar observations were noted for the untreated sisal fibres which show a second degradation peak around 190 to 220 °C due to the degradation of hemicellulose which starts degrading around 190 °C owing to the amorphous characteristics of hemicellulose (Rosa et al., 2009; Wu et al., 2013; Hossain et al., 2014; Orue et al., 2015). In case of alkali treated sisal fibres, a weight loss of 10% could be seen at 282 °C which is 25 °C higher than the untreated fibres. This indicates that the alkali treatment influenced the removal of hemicellulose and pectin considerably. However, in case of combined treatments of alkali and ultrasound, a weight loss of 10% could be noticed at 295.5 °C, which is 38.5 °C and 25 °C higher than the untreated and alkali treated sisal fibres respectively (**Fig. 4.11**). This again clearly confirms that the thermal stability is significantly increased in the combined alkali and ultrasound treated fibres.

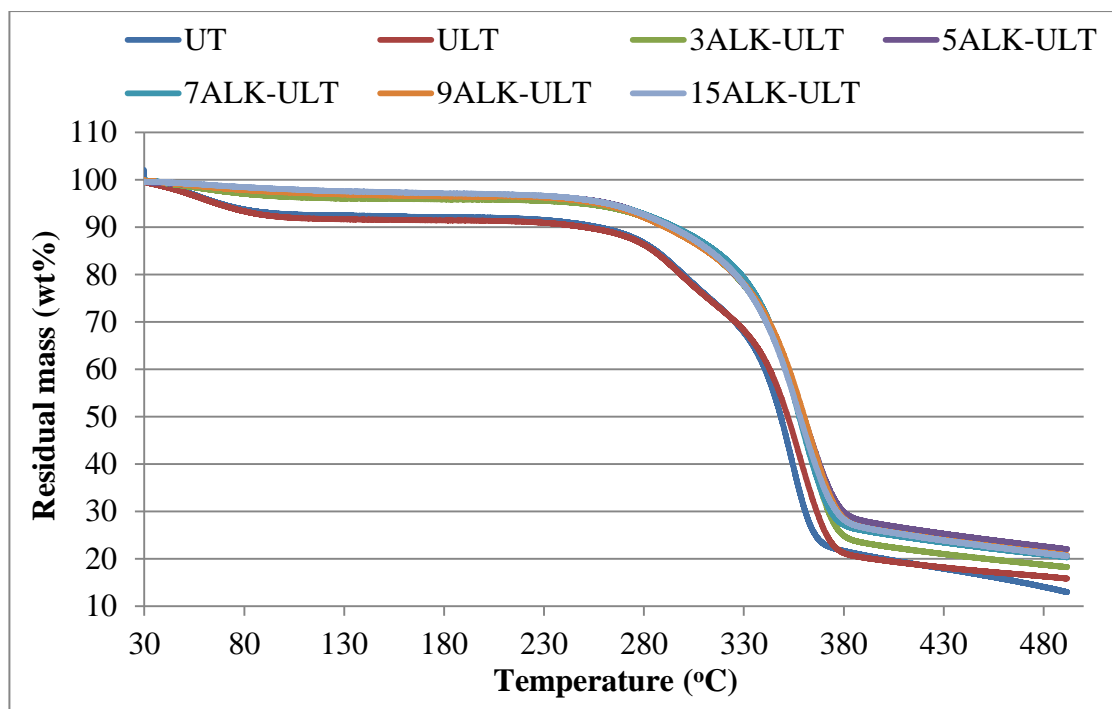


Fig. 4.10 TGA curves of untreated (UT), ultrasound treated (ULT) and the combination of alkali and HIU treated (ALK-ULT) sisal fibres

The combined alkali and ultrasound treated sisal fibres show better thermal stability as compared to untreated, ultrasound treated and alkali treated fibres. As discussed in the earlier section 4.3, this may be due to the ultrasound of high intensity which may induce the disintegration of sisal fibres to increase the overall surface area of fibres and to enhance the surface roughness. Kabir et al. (2013b) reported that the thermal stability of pure cellulose was much higher than lignin and hemicellulose. They observed that the thermal stability of cellulose was 350 °C, whereas hemicellulose degraded at 290 °C and lignin degraded at 320 °C. Hence, these observations confirm that the thermal stability of cellulose is higher than hemicellulose and lignin.

Besides, in the combined treatment of alkali and HIU, HIU treatment effectively exposes the crystalline cellulose to the outer surface by disintegrating the fibre which makes these fibres to become more hydrophobic with improved thermal stability

(Cheng et al., 2009; Chen et al., 2011b). This supports the observations made from FE-SEM and FTIR. 50% weight loss could be observed in the temperature range from 350 to 370 °C (**Fig. 4.11**) which shows an increase in the thermal stability by 19 °C for the alkali treated as compared to the untreated sisal fibres.

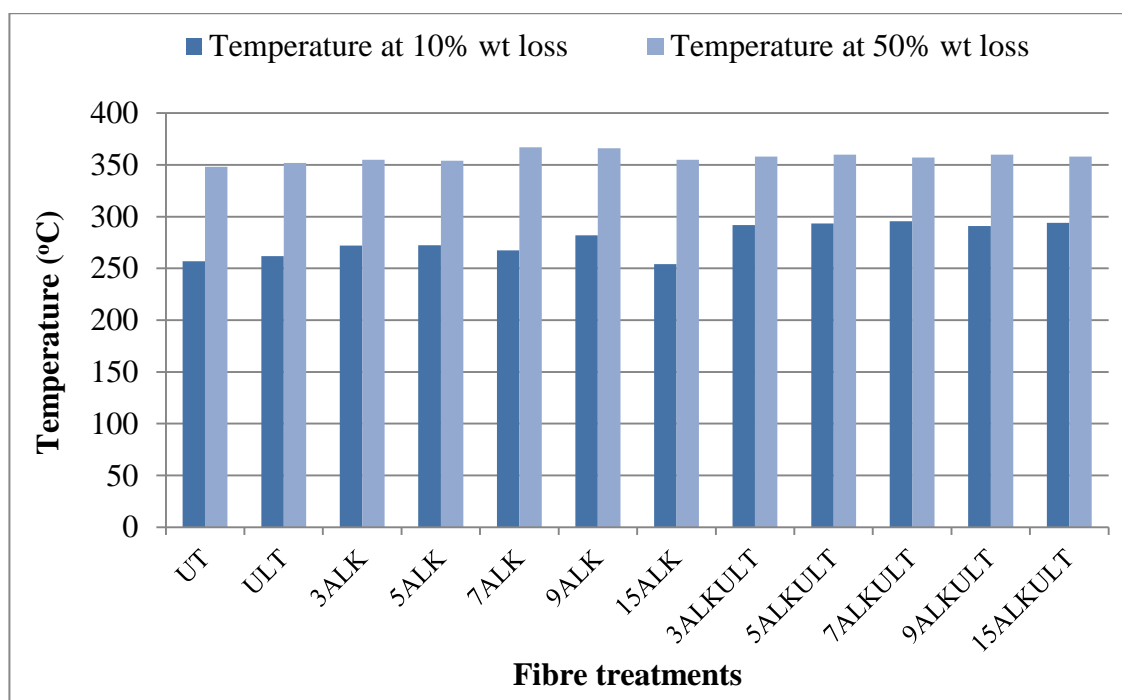


Fig. 4.11 Thermal stability of untreated (UT), alkali (ALKT) and the combination of alkali and ultrasound treated (ALKT-ULT) sisal fibres

However, thermal stability decreased slightly to 357 °C (10 °C) at 50% weight loss for the combination of alkali and HIU treated fibres which may be due to the disintegration of small portion of cellulose structure of sisal fibres caused by high intensity ultrasonication. Similar observations of an increased thermal stability with alkali treatment have been reported by several researchers (Mohan and Kanny, 2012; Hossain et al., 2014; Zhou et al., 2014; Orue et al., 2015). It could also be observed that the char residue obtained with the combination of alkali (9 wt%) and HIU treated sisal fibres is 22%, whereas for the untreated sisal fibres it is 12% which is 10 wt%

higher char residue as compared to the untreated sisal fibres. This again confirms that the combined treatment of alkali and HIU is better in the removal of hemicellulose, lignin and pectin from the surface of sisal fibres and causes the exposure of cellulose to the outer surface.

4.8 Tensile properties of single sisal fibre

Fig. 4.12 shows the typical stress-strain curve obtained from the tensile tests. Similar to other natural fibres, sisal fibres showed brittle nature under tensile test conditions and a sudden drop in the load was observed when the fibres break. It is evident from **Fig. 4.12** that the stress-strain curves were initially linear until the fibre fracture occurred and the failure strain was found to be approximately 1-3%. It is difficult to analyse the results of tensile test obtained from single filament due to its very small size and brittleness.

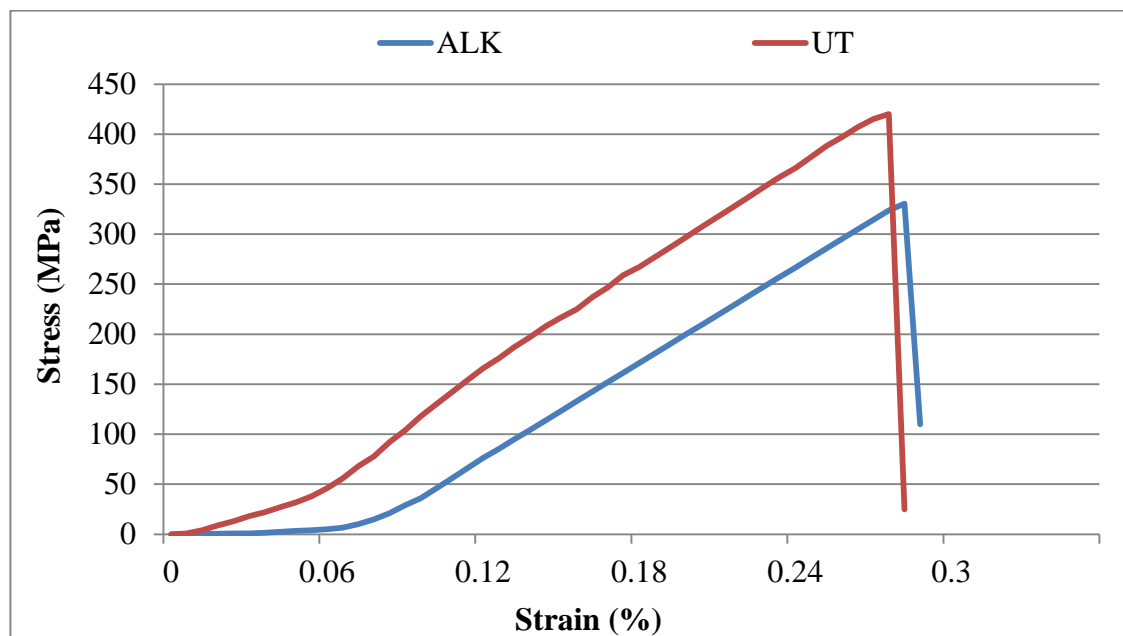
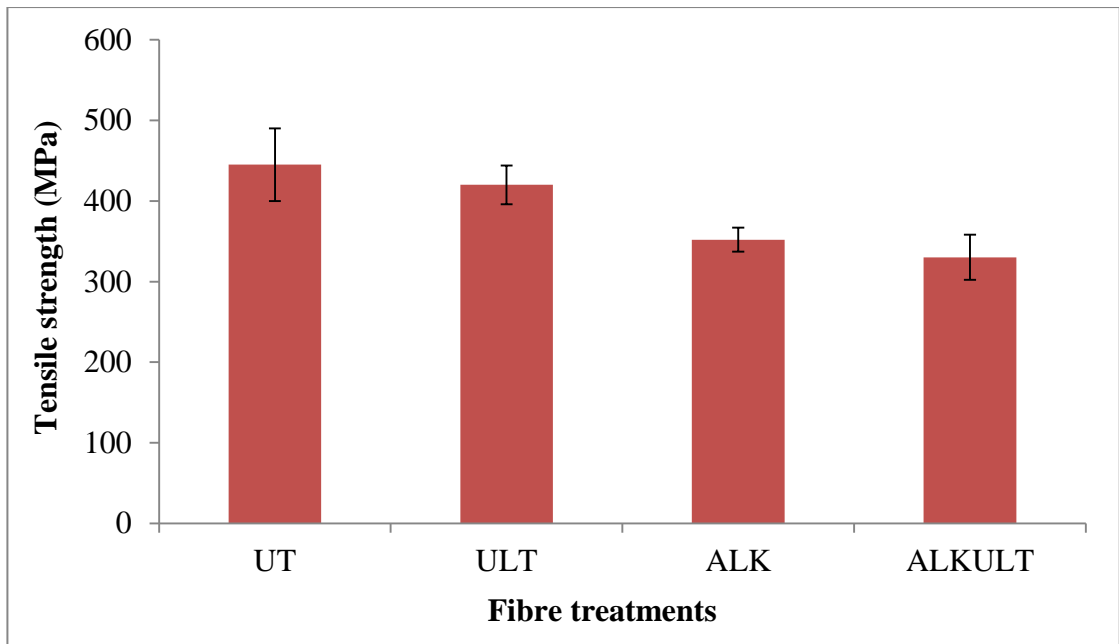


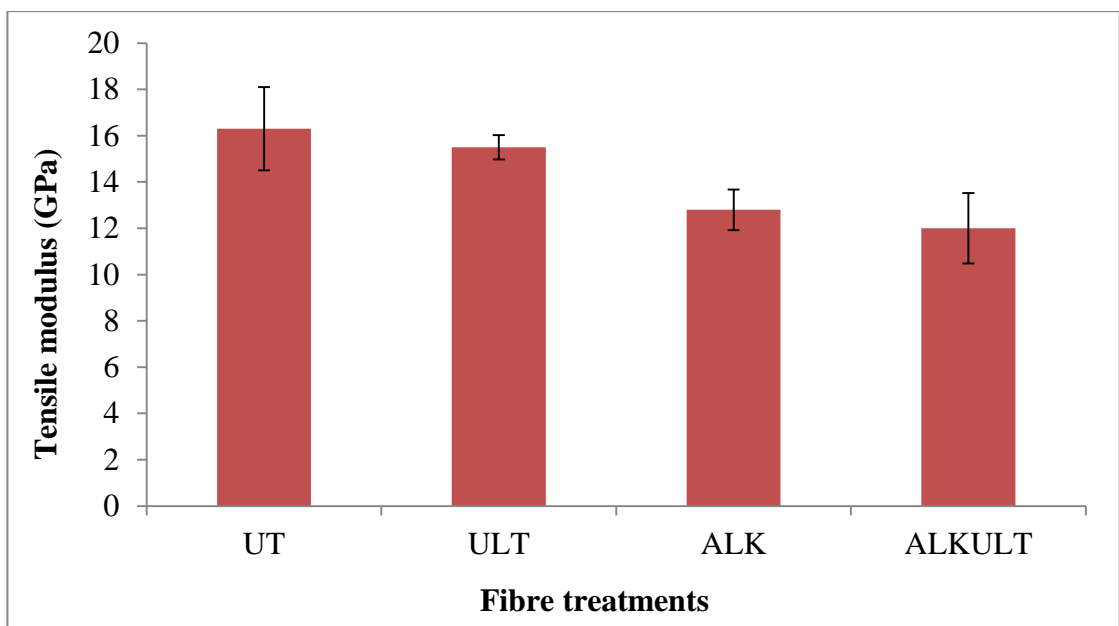
Fig. 4.12 Typical stress-strain curves of single sisal fibre

The results of tensile test of single fibre depend on three main factors: the test parameters/conditions, plant characteristics and the area measurements. The plant age, source, mechanism of fibre extraction and the presence of defects are the few which affect the mechanical properties of fibres (Silva et al., 2008; Belaadi et al., 2014). **Figs. 4.13 (A) and (B)** show the plot of tensile strength and modulus values against different surface treatments of sisal fibres respectively. Tensile strength and modulus of HIU treated sisal fibres showed a slight decrease by 5.6% and 5% respectively as compared to the untreated fibres. However, a significant reduction in the tensile strength and modulus was observed for the alkali and the combination of alkali and HIU treated sisal fibres.

The tensile strength and modulus reduced by 25% and 26% respectively for the combination of alkali and HIU treated sisal fibres as compared to untreated sisal fibres. This is mainly due to the removal of amorphous materials such as hemicellulose, lignin and other waxy materials from the surface of fibres. Hemicellulose and lignin are the two main components on the cell wall structure of natural fibres which tightly bound to the cellulose. Removal of these amorphous materials due to alkali treatment causes fibre degradation and leads to the reduction in the mechanical properties of fibres (Mahjoub et al., 2014; Haameem et al., 2016; Orue et al., 2016). Moreover, the application of HIU for alkali pre-treated sisal fibres significantly damages the surface of fibres and reduces the fibre diameter which significantly reduces the mechanical properties (Chen et al., 2011b; Iskalieva et al., 2012). These observations are in agreement with the obtained results of FE-SEM.



(A)



(B)

Fig. 4.13 Tensile properties of untreated (UT), ultrasound treated (ULT), alkali treated (ALK) and the combination of alkali and ultrasound treated (ALKTULT) sisal fibres:

(A) tensile strength (B) tensile modulus

4.9 Conclusions

In this investigation, sisal fibres were subjected to different surface treatments such as alkali, HIU and the combination of alkali and HIU treatments in order to remove the amorphous materials such as hemicellulose, pectin and lignin from the surface of sisal fibres by which the interfacial strength, mechanical and thermal properties of PLA and PP matrix composites were enhanced. FTIR analysis confirmed the removal of amorphous materials from the fibre surface with alkali and the combination of alkali and HIU treatments. FE-SEM indicated the removal of amorphous materials by which the fibre surface became rougher and enhanced the adhesion. The fibre diameter and moisture absorption significantly decreased for the combination of alkali and HIU treatment by 200% and 40% as compared to untreated sisal fibres. Crystallinity index increased to 10 % and 14 % for alkali treatment (7 wt%) and the combined treatment of alkali (7 wt%) and HIU respectively as compared to the untreated sisal fibres. This again supports the removal of amorphous materials from the surface of fibres which increased the crystalline phase. The thermal stability found to increase significantly by 38.5 °C for the combined treatments of alkali (7 wt%) and HIU as compared to the untreated fibres. This is in agreement with FTIR and FE-SEM analysis which confirmed the removal of amorphous materials whereby the fibres become more crystalline and thermally more stable. Tensile properties of single sisal fibre showed a reduction in the tensile strength and modulus by 25% and 26% respectively for the combined treatment of alkali and HIU as compared to the untreated sisal fibre owing to surface treatments.

CHAPTER V

Results and Discussion: Sisal-PLA Composites

5.1 FE-SEM analysis

FE-SEM was used to analyse the morphology and failure mechanism of sisal fibres reinforced PLA composites. **Fig. 5.1** shows the morphology of impact fractured samples of untreated, HIU treated, alkali treated and the combination of alkali and HIU treated (15 wt% loading) SF/PLA composites. Large voids could be noted at the fibre-matrix interface of untreated SF/PLA composites (**Fig. 5.1 A**). These large voids maybe due to fibre pull-out from the matrix phase when impact force was applied which indicates the poor interfacial adhesion between the fibre and matrix interface in the untreated SF/PLA composites. In addition, a large number of cracks could also be observed on the fractured surface which is mainly due to the presence of amorphous materials such as hemicellulose, pectin, lignin and other waxy materials on the surface of untreated sisal fibres. These amorphous materials are responsible for the absorption of moisture causing incompatibility between untreated sisal fibres and PLA. It is a well-known fact that the interfacial adhesion between fibre and matrix plays an important role on the mechanical properties of fibre reinforced composites (Asumani et al., 2012). Treatment of sisal fibres with HIU helps to remove the amorphous materials from the surface of fibres which reduces the incompatibility between the fibres and matrix (**Fig. 5.1 B**). However, the agglomeration of fibre and a large number of voids on the surface of HIU treated sisal fibre composites confirm that HIU treatment alone could not be sufficient to reduce the amorphous materials from the surface of sisal fibres. **Fig. 5.1 C** shows the surface morphology of alkali treated

SF/PLA composites, where a reduction in the number of voids and air bubbles could be noticed.

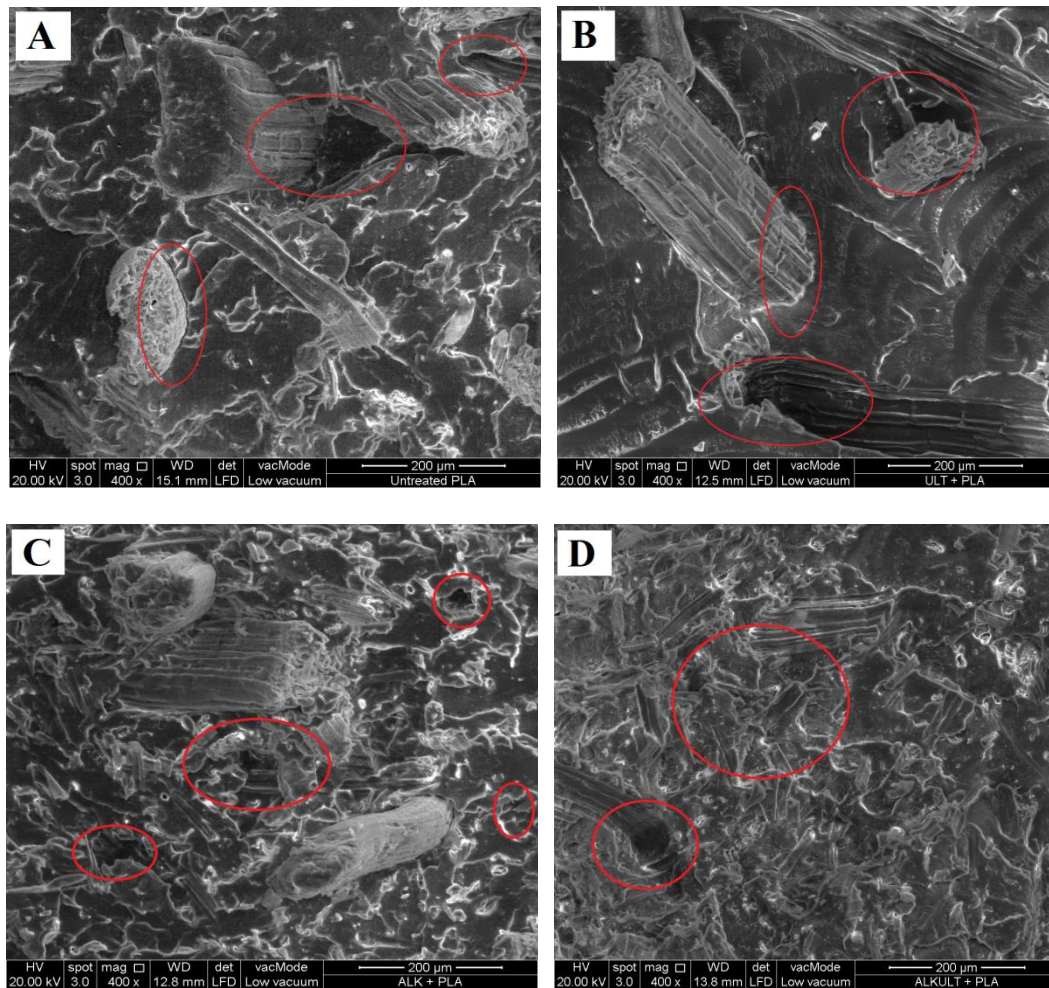


Fig. 5.1 FE-SEM images of impact fractured samples of (A) untreated (UT), (B) ultrasound treated (ULT), (C) alkali treated (ALK) and (D) the combination of alkali and ultrasound treated (ALKTULT) SF/PLA composites

This may be due to the mercerisation effects of alkali which dissolves the amorphous and other impurities that stick on the surface of sisal fibres. However, in the alkali treated composites, micro voids and cracks could be seen in the matrix phase which is mainly due to fibre agglomeration. In the case of combination of alkali and HIU treated sisal fibres composites (**Fig. 5.1 D**), the fibres are well dispersed across the

matrix and the interfacial adhesion increases between the fibre-matrix phases. This is mainly due to the effects of combined treatment of alkali and HIU which resulted in good fibre separation across the PLA matrix. It could also be noticed that the FE-SEM images of the impact fractured samples show that fibres are fractured rather than pull out when sudden impact force was applied for the combination of alkali and HIU treated SF/PLA composites. This confirms that the stress transfers from the matrix to the fibres. Similar results have been reported by other authors (Silva et al., 2009; Das and Satapathy, 2011; Li et al., 2011; Zhong et al., 2011; Asumani et al., 2012; Dong et al., 2014; Shanmugam and Thiruchitrambalam, 2013).

Moshiul Alam et al. (2012) studied the effect of combined treatment of alkali and ultrasound on oil palm empty fruit bunch fibres reinforced PLA composites. They noticed that in case of untreated fibres surface, fibres seem to be pulled out due to poor interfacial adhesion between the fibre and matrix. However, fibres were fractured rather than pull out for the simultaneous treatment of alkali and ultrasound. Chen et al. (2011) reported that the combined treatment of alkali and HIU is an effective way to remove the amorphous materials and to reduce the diameter of the fibres in which the aspect ratio of the fibres increased which leads to improving the mechanical properties of fibre reinforced composites. Dong et al. (2014) observed large voids on the tensile fractured surface of untreated coir fibres PLA composites due to the presence of amorphous materials and other impurities on the surface of coir fibres. The large voids in the untreated coir fibres composites tend to decrease the load bearing capacity of composites and lead to lowering the mechanical strength. In contrast, numbers of voids were reduced in the alkali treated coir fibres which improved the interfacial bonding between the fibre and matrix. This again confirms the removal of amorphous and other waxy materials with alkali treatment.

5.2 FTIR analysis

FTIR spectroscopy is an important technique to study the structural changes of composite materials. This technique was used in the investigation of structural modification SF/PLA composites. The FTIR spectra of SF, PLA and SF/PLA composites have been represented in **Fig. 5.2**.

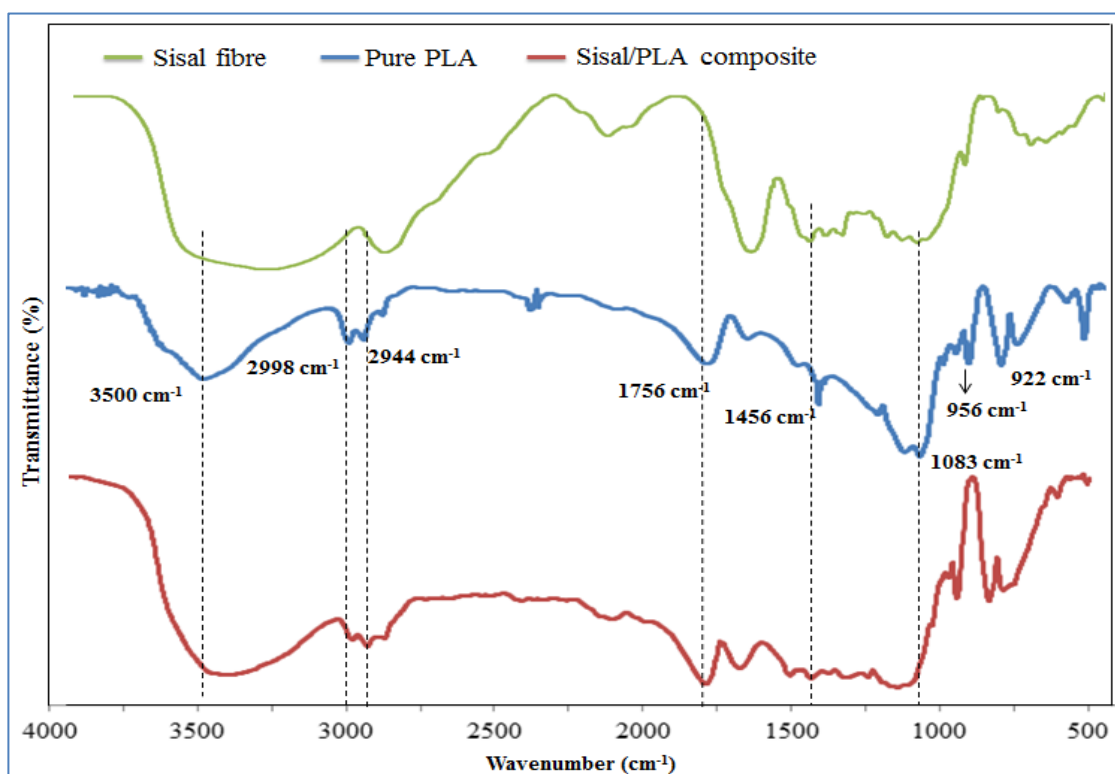


Fig. 5.2 FTIR spectra of sisal fibre, pure PLA and SF/PLA composites

The peaks obtained in the FTIR spectra of PLA are as follows: the peak of asymmetric mode of the ester group (O-C) appeared at 1083 cm⁻¹; a sharp peak at 1456 cm⁻¹ could be assigned to symmetric bending vibrations of CH₃ and the peaks obtained at 956 and 922 cm⁻¹ could be attributed to the rocking mode of CH₃ group. A relatively smaller peak appeared at around 3500 cm⁻¹ from PLA is related to the stretching deformation of hydroxyl group. However, the characteristic peak of PLA (i.e. 3500 cm⁻¹) found to be different for the composites (3437 cm⁻¹) and for the sisal

fibres (3410 cm^{-1}). This peak disappeared for the composites with the incorporation of sisal fibres and appeared as a broad peak which is similar to sisal fibres. This indicates that the OH groups from the fibres formed hydrogen bonds with the carbonyl groups (C=O) of PLA. Similar results have been reported for the rice starch reinforced PLA composites (Yew et al., 2005). There is no change in the peaks appeared at 2998 and 2944 cm^{-1} could be assigned to asymmetric and symmetric mode of C-H stretching respectively.

The C=O stretching appeared approximately at 1756 cm^{-1} is assigned for the ester group of PLA. This ester peak has higher intensity for the composites than for PLA. This is due to the esterification reaction which took place between OH groups of sisal fibres and terminal carboxylic acid groups (COOH) of PLA. This agrees with the observations reported by Semba et al. (2006). They noted that the peak intensity of C=O group at 1756 cm^{-1} increased due to the reaction between dicumyl peroxide and PLA. It is already reported that similar to any other natural fibres sisal fibres are made-up of cellulose as a main component. It is assumed that majority of physicochemical bonding interactions occur between the hydroxyl groups of cellulose from the surface of sisal fibres with the carbonyl groups (C=O) of PLA matrix. The untreated sisal fibres contain amorphous materials such as hemicellulose, pectin and other waxy materials on the surface of fibres which allow limited hydroxyl groups to interact with the carbonyl groups (C=O) and carboxyl groups (COOH) of PLA. However, in case of alkali and the combination of alkali and HIU treated sisal fibers, these amorphous materials are removed from the surface of fibres thereby exposing more number of hydroxyl groups of cellulose for hydrogen and covalent bonding with the carbonyl groups (C=O) and the carboxyl groups (COOH) of PLA (Sawpan et al., 2011).

5.3 Tensile properties

Tensile strength of untreated, HIU treated, alkali treated and the combination of alkali and HIU treated SF/PLA composites was evaluated and is illustrated in **Fig. 5.3**. It could be noted from this figure that the tensile strength decreased with an increase in the fibre loading as compared to pure PLA except for 15 wt% of fibre loading for which the tensile strength slightly increased to 54.24 MPa (10% higher than pure PLA). However, as compared to the untreated sisal fibre composites, surface treated sisal fibres composites showed a gradual increment in the tensile strength at all the percentages of fibre loading. Combination of alkali and HIU treated SF/PLA composites showed superior tensile properties. PLA composites with the fibre loading of 15 wt% showed higher tensile strength among all other fibre content.

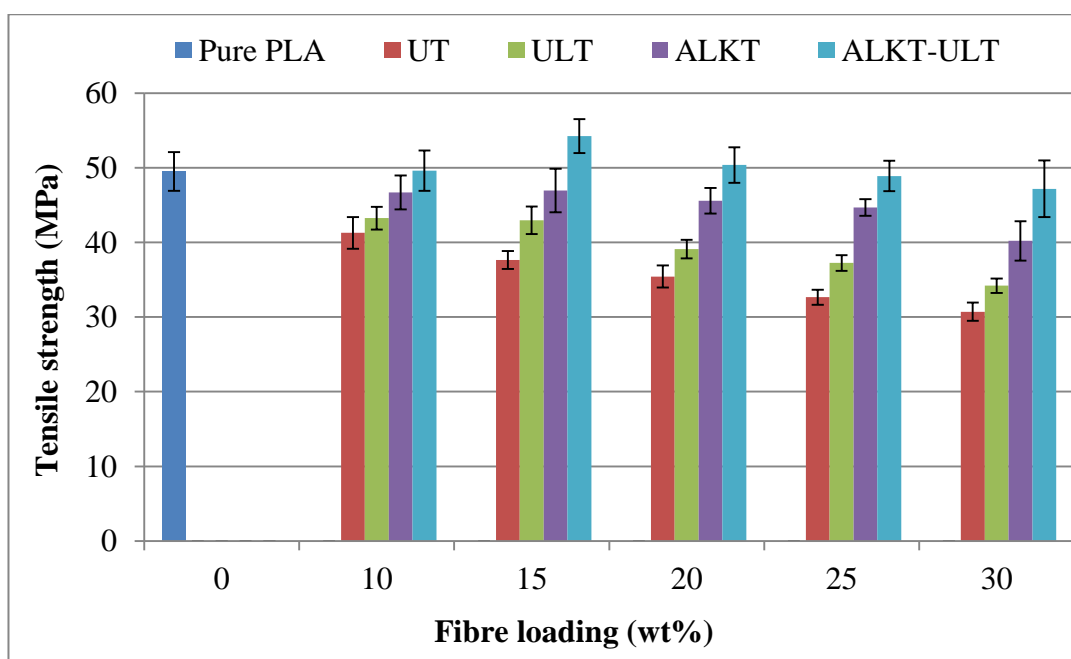


Fig. 5.3 Tensile strength of untreated (UT), ultrasound treated (ULT), alkali treated (ALK) and the combination of alkali and ultrasound treated (ALKTULT) sisal fibres reinforced PLA composites

The tensile strength of HIU treated, alkali treated and the combination of alkali and HIU treated SF/PLA composites were 43 MPa, 47 MPa and 54.24 MPa respectively as compared to the untreated sisal fibre composites, which were 10%, 20% and 33% higher than the untreated fibres composites with the same weight percentage (15 wt%) of fibre loading. This trend is almost the same at all fibre loading. An increase in the tensile strength for the treated sisal fibres composites as compared to the untreated sisal fibre composites indicates the removal of non-cellulosic (amorphous) materials and other impurities from the surface of sisal fibres during surface treatment (Arrakhiz et al., 2012; Dong et al., 2014). These results further support the observations obtained from FTIR and FE-SEM. Ma and Joo. (2011) reported that the bamboo fibres reinforced PLA composites with different surface treatments such as Plasma, UV irradiation and direct silane treatments showed an increase in the tensile strength by 43.7%, 60.7% and 71.1% respectively.

As compared to pure PLA, the tensile strength decreased for the SF/PLA composites with an increase in the fibre loading from 10 to 30% irrespective of the surface treatments. This may be due to an increase in the fibre agglomeration in the fibre-matrix interface which leads to poor interfacial adhesion between the fibres and matrix. Similar results have already been reported. Tisserat et al. (2013) observed that the tensile strength of PLA composites decreased significantly by 20% with the addition of 25 wt% of paulownia wood filler as compared to pure PLA. They also indicated that the aspect ratio of filler materials play an important role in improving the mechanical properties of composite materials. Lee et al. (2012) observed a reduction in the tensile strength by 10% with the addition of 20 wt% of sisal fibres in the PLA composites as compared to pure PLA. They also indicated that the poor

interfacial adhesion between the fibre and matrix and the agglomeration of fibres across the matrix resulted in reducing the tensile strength.

In contrast to the tensile strength, tensile modulus enhanced significantly with the incorporation of sisal fibres into PLA matrix at all the fibre loading as compared to pure PLA. It can be seen from **Fig. 5.4** that the sisal fibre loading of 30 wt % on the PLA composite increased the tensile modulus by 25%, 46%, 54% and 75.4% for the untreated, HIU treated, alkali treated and the combination of alkali and HIU treated sisal fibres PLA composites respectively as compared to pure PLA. These results are in agreement with the observations of Ragoubi et al. (2012). They reported that the tensile modulus increased by 19% and 31% for miscanthus grass fibres reinforced PLA composites with and without fibre surface treatments respectively as compared to pure PLA.

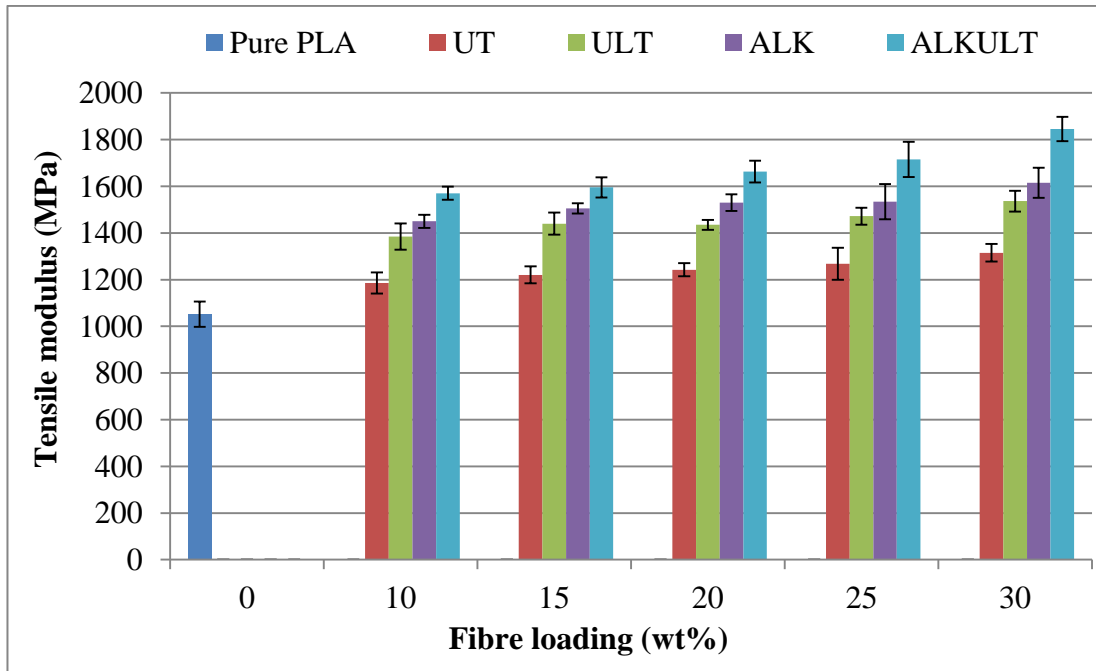


Fig. 5.4 Tensile modulus of untreated (UT), HIU treated (ULT), alkali treated (ALK) and the combination of alkali and HIU treated (ALKULT) SF/PLA composites

A significant enhancement in the observed tensile modulus is attributed to improved interfacial adhesion between the sisal fibres and PLA matrix which enhances the load transfer from the matrix phase to filler phase (Ma and Whan Joo, 2011; Asumani et al., 2012; Lee et al., 2012; Cran et al., 2014).

Arrakhiz et al. (2012) reported that the tensile modulus increased significantly by more than 70% and 100% for the alkali and esterification treatments respectively for the same fibre loading (20 wt%). They also observed an improved interfacial adhesion between the alfa fibres and the PP matrix due to the effective removal of non-cellulosic materials from the surface of fibres during the surface treatments which leads to improve the tensile properties. The aspect ratio of the fibres playing an important role in altering the mechanical properties of fibre reinforced polymer composites. Tisserat et al. (2013) observed that the tensile modulus increased by 35% for smaller filler size as compared to larger filler particles.

On the other hand, the percentage of elongation at break reduced with an increase in the sisal fibres content in the PLA composites (**Fig. 5.5**). A significant reduction of more than 50% could be seen with an addition of even 10 wt% of untreated sisal fibres. It is further reduced with an increase in the fibre content. Addition of fibre materials into the PLA matrix restricts the mobility of polymer chain and making it more resistant to elongation at break as compared to pure PLA. This is in agreement with the reports of Petinakis et al. (2009) and other researchers (Cran et al., 2014; Lee et al., 2012; Ragoubi et al., 2012; Tisserat et al., 2013).

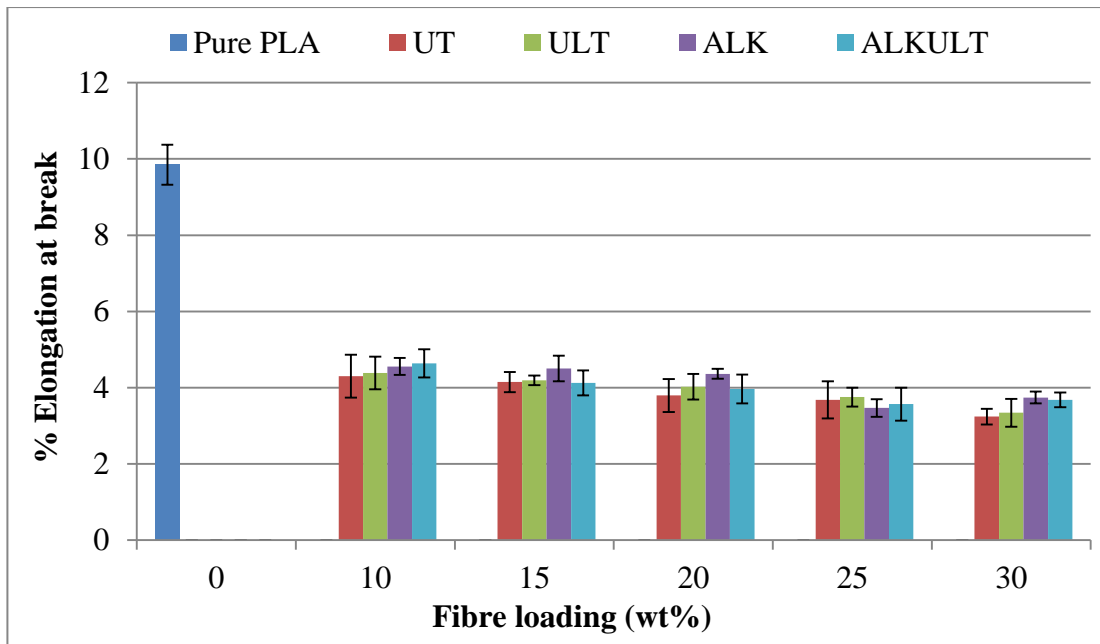


Fig. 5.5 Tensile elongation at break of untreated (UT), HIU treated (ULT), alkali treated (ALK) and the combination of alkali and HIU treated (ALKULT) sisal fibres reinforced PLA composites

5.4 Predictions of Tensile modulus

Practically, it is very difficult to calculate the experimental values of tensile or Young's modulus of natural fibre reinforced polymer composites accurately due to large variation in the matrix and fibres parameters such as aspect ratio of fibres, fibre orientation, surface treatments of fibres etc., However, intrinsic tensile modulus of the reinforcing fibres is the key parameter to predict the modulus or strength of the fibre reinforced composites (López et al., 2012). Mathematical models are commonly used to estimate the theoretical values of the tensile or flexural modulus of natural fibre reinforced polymer composites (Serrano et al., 2014).

Figs. 5.6-5.9 show the comparison of tensile modulus obtained from the experimental values of different surface treated (untreated, HIU treated, alkali treated and the combination of alkali and HIU treated) SF/PLA composites with the theoretical

values calculated by using different mathematical models. It can be seen that Young's modulus gradually increases with an increase in the volume fraction of fibres. It is well-known that the stiffness of the fibre reinforced composites increases with the addition of filler materials to the polymer matrix.

The modulus mainly depends on the intrinsic rigidity of the fibres and the matrix (López et al., 2012; Granda et al., 2016). The fibre efficiency factor (η_e) was calculated using the eqns 2.3, 2.4, 2.5 and 2.6 which was 0.53. This theoretically calculated value of the fibre efficiency factor was found to fit with the experimental values. It could be seen from **Figs. 5.6-5.9** that at initial fibre loading there is a good agreement between the experimental and theoretical values in all the models. This may be due to low volume of fibre loading.

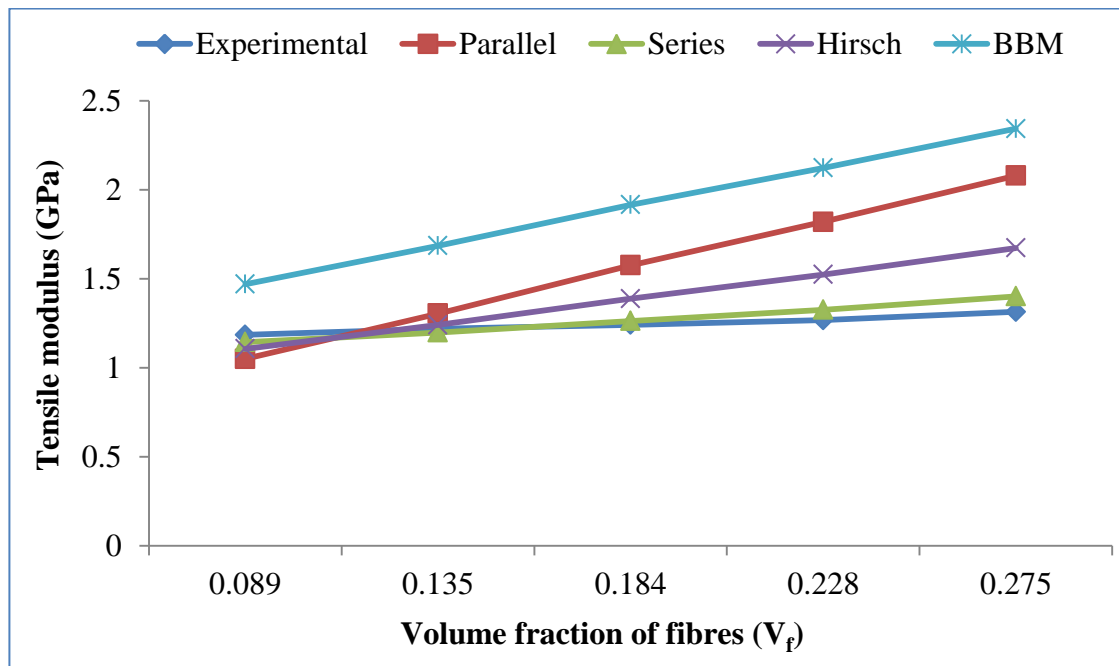


Fig. 5.6 Variations of theoretical and experimental values of tensile modulus for the untreated sisal fibre reinforced PLA composites

It is well known that at low volume fractions of fibres, it can be assumed to be a uniform distribution of stress and strain which results in better load transformation across the fibres from the matrix phase in the composite which leads to improving the mechanical properties of fibre reinforced polymer composites.

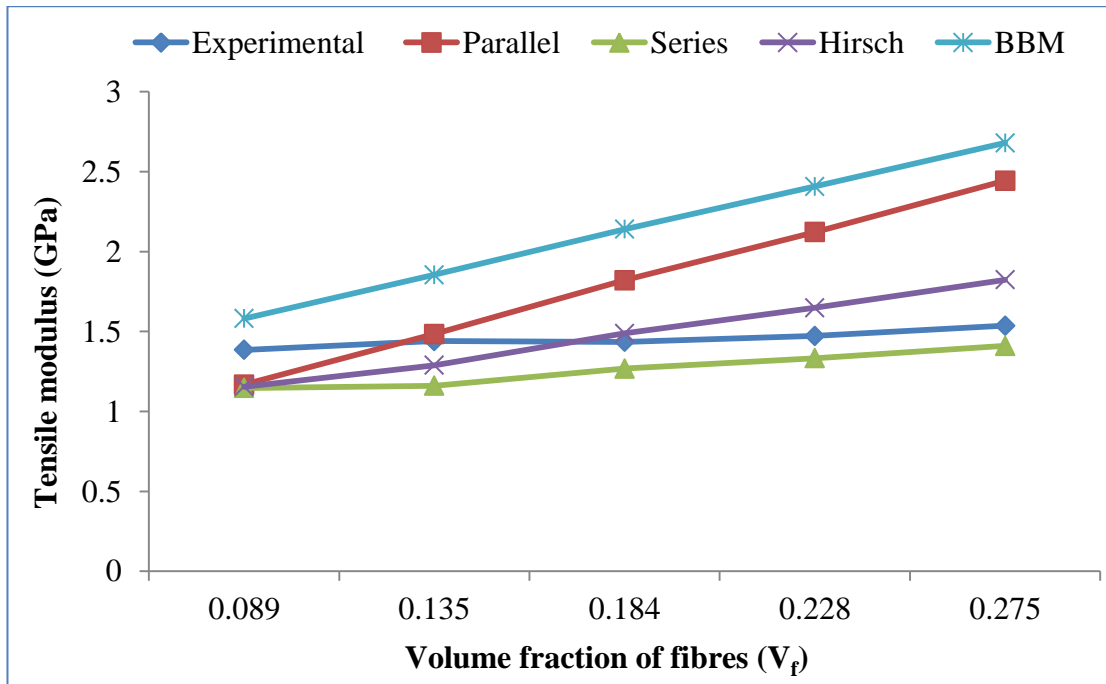


Fig. 5.7 Variations in the theoretical and experimental values of tensile modulus for the HIU treated SF/PLA composites

However, in case of higher fibre volume fractions, there could be large variations between experimental and theoretical values. This may be due to more possibilities for the fibre agglomeration across the matrix which causes an uneven distribution of stress and strain and leads to a reduction in the mechanical properties. Kalaprasad et al. (1997) studied the theoretical modelling of tensile properties of short sisal fibres reinforced low density polyethylene composites. Parallel and series models were commonly used for continuous fibre reinforced polymer composites, where the stress transfer mechanism is different as compared to short fibre reinforced polymer

composites. In short fibre composites, the stress transfer largely depends on the fibre orientations inside the composite, stress concentration at the end of the fibres as well as on the critical fibre length.

It could be seen from **Figs. 5.6-5.9** that the experimental values of surface treated SF/PLA composites do not show much variation as compared to theoretical values. However, there is a marginal agreement between the experimental and theoretical values for the alkali treated and the combination of alkali and HIU treated SF/PLA composites (**Figs. 5.8-5.9**). Hirsch model is a combination of parallel and series models which shows a good agreement between theoretical and experimental values in all the cases. It is mentioned that the prediction of Hirsch model largely depends on the value of x in **eqn. 2.7** (López et al., 2012; Serrano et al., 2014).

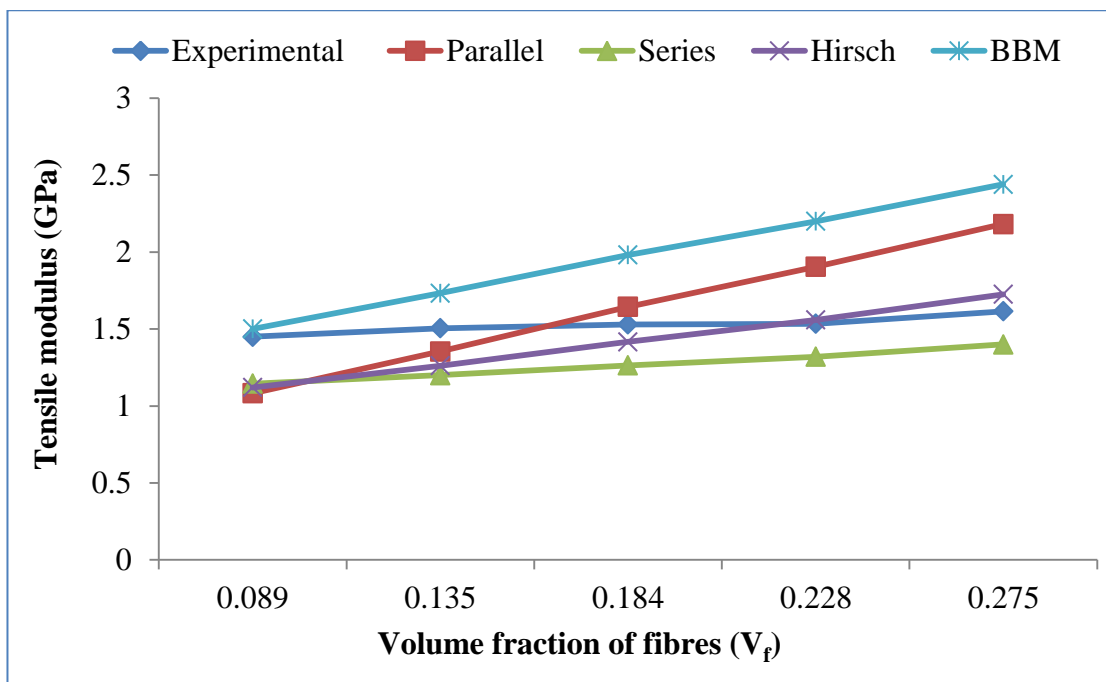


Fig. 5.8 Variations in the theoretical and experimental values of tensile modulus of alkali treated SF/PLA composites

The factors which control the x values are: fibre orientation, fibre length and the effect of stress concentration of the fibres. The stress transfer factor x is approximately 0.4 which is in agreement with the semi-aligned fibre reinforced polymer composites (Kalaprasad et al., 1997). The theoretical values of tensile modulus of modified Bowyer and Bader model (BBM) were calculated using the **eqn. 2.8**. The values of K_2 and K_1 were calculated to be 0.5 and 1 respectively by using **eqns. 2.9 and 2.10**. These values are in agreement with the observations of Joseph et al. (2003). It was noticed that there is a marginal variation with the experimental and theoretical values when BBM model was applied for predicting the Young's modulus of SF/PLA composites. Unlike other theoretical models, BBM model exhibits higher values as compared to the experimental values. This may be due to variations in the fibre orientation factor (K_1) and fibre length factor (K_2) for the untreated and HIU treated SF/PLA composites.

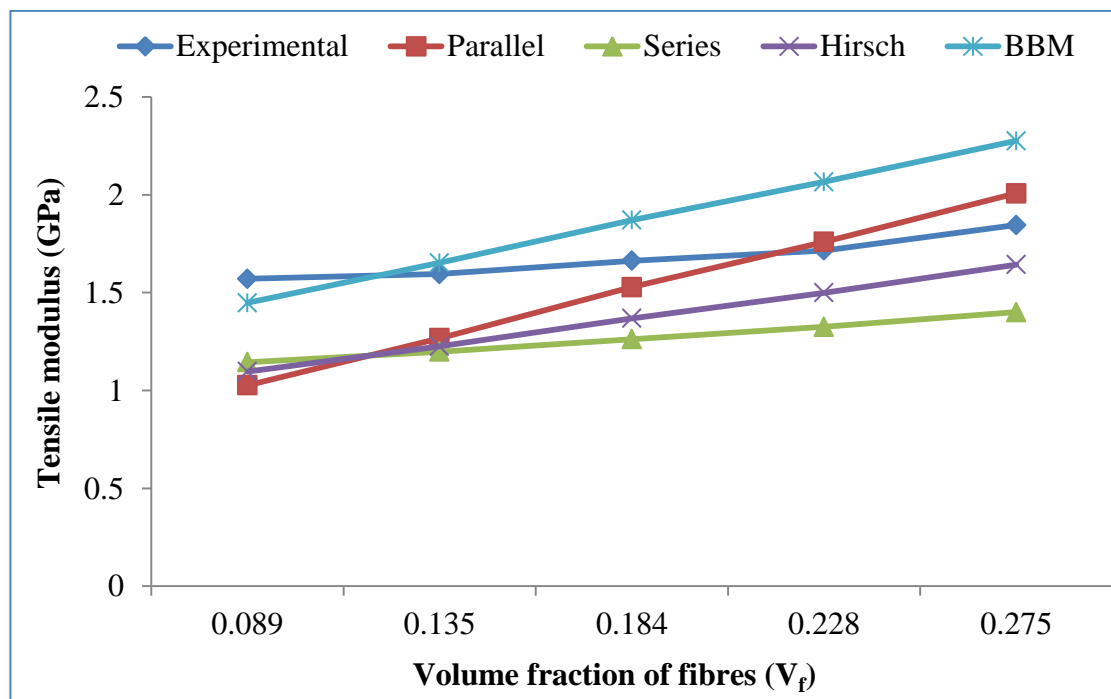


Fig. 5.9 Variations in the theoretical and experimental values of tensile modulus of the combination of alkali and HIU treated SF/PLA composites

From these observations, it is noticed that the values of Young's modulus of theoretical models are in reasonable correlation with the experimental values in all the models except a little variation in the BBM model. A good agreement in the experimental and theoretical values of Young's modulus of untreated and different surface treated SF/PLA composites reveals better utilization of sisal fibres and PLA matrix for the generation of SF/PLA composites.

5.5 Impact properties

The impact property of SF/PLA composites was also investigated. **Fig. 5.10** shows the impact strength of untreated, HIU treated, alkali treated and the combination of alkali and HIU treated SF/PLA composites. It could be observed that the impact strength of sisal fibre reinforced composites for the entire fibre loading from 10 to 30 wt% was higher than pure PLA.

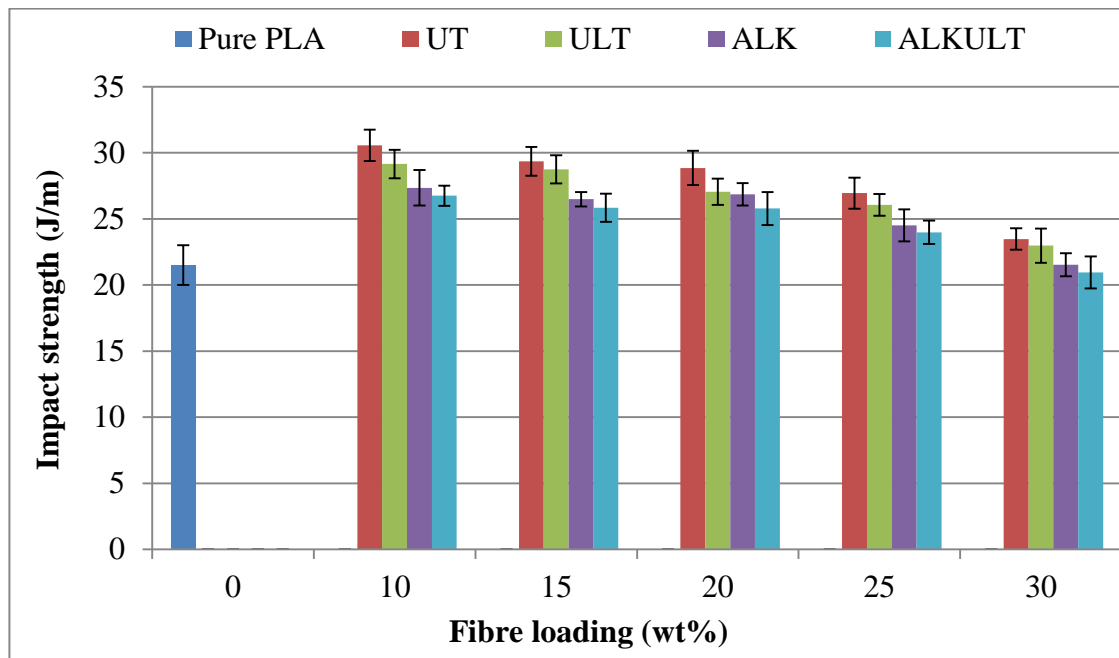


Fig. 5.10 Impact strength of untreated (UT), ultrasound treated (ULT), alkali treated (ALK) and the combination of alkali and HIU treated (ALKULT) SF/PLA composites

It is notable that the impact strength of notched samples of SF/PLA composites increased to 30.5 J/m which is 42% higher as compared to pure PLA. However, the impact strength decreased gradually with an increase in the loading of sisal fibre. This may be due to an increase in the brittleness of the composite with an increase in the fibre content. Similar results have been reported (Mwaikambo et al., 2007; Li et al., 2011; Luo et al., 2014). It is worth noted that the impact strength decreased to 12.5%, 10.5% and 4.5% for the combined treated, alkali treated and HIU treated sisal fibre composites respectively as compared to untreated sisal fibre composites. A decrease in the impact strength of treated sisal fibre composites was noticed. This is may be due to the surface treatment of sisal fibres which increased the interfacial adhesion between the fibre and matrix. Sisal fibres in the composites were fractured instead of pull-out from the matrix when applied with sudden impact force. This is due to an increase in the adhesion between fibre and matrix phase. Similar results were reported by other researchers (Mwaikambo et al., 2007; Luo et al., 2014). Luo et al. (2014) reported similar results where they noticed a decrease in the impact strength by approximately 14% and 8% for the alkali and sizing treated corn fibre reinforced PLA composites as compared to untreated fibre composites. Mwaikambo et al. (2007) also reported that the impact strength decreased by more than 50% for the alkali treated hemp fibre reinforced euphorbia composites than the untreated one.

5.6 DMA analysis

DMA measurements were carried out to evaluate the effect of different surface treatments on the visco-elastic behaviour of SF/PLA composites. The dynamic-mechanical properties of the fibre reinforced composites can be expressed in terms of storage modulus (E'), loss modulus (E'') and damping factor ($\tan \delta$) which depend on time, temperature and frequency. **Fig. 5.11** shows the effect of different surface

treatments and temperature on the storage modulus (E') of SF/PLA composites as a function of temperature. It could be seen that in all the cases the storage modulus decreased as the temperature increased at constant frequency (1.0 Hz). Pure PLA showed the lowest storage modulus as compared to SF/PLA composites.

The increased storage modulus for the fibre reinforced composites is due to the restriction in the free mobility of polymer chains which leads to an increased stiffness (Poathan et al., 2003; Li et al., 2011; Das and Satapathy, 2011; Lavoratti et al., 2015). It is also worth noted that the surface treated SF/PLA composites showed higher storage modulus as compared to untreated fibre composites.

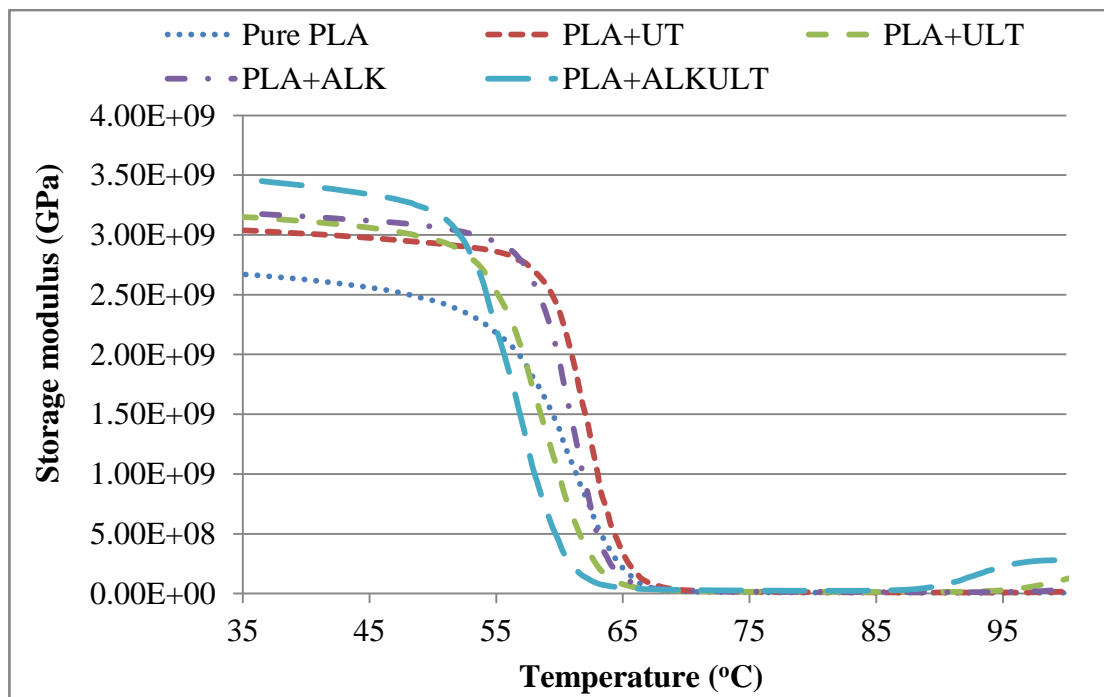


Fig. 5.11 Storage modulus (E') of untreated (UT), HIU treated (ULT), alkali treated (ALK) and the combination of alkali and HIU treated (ALKULT) sisal fibres reinforced PLA composites

The storage modulus of SF/PLA composites resulted from the combination of alkali and HIU treatment was 3.50 GPa which is 30% and 15% higher as compared to pure

PLA and untreated fibre composites respectively. These results show that the surface treatment of sisal fibres increased the compatibility and interfacial adhesion between SF and PLA matrix which leads to an increased stiffness of the resultant composites (Ray et al., 2002; De Rosa et al., 2011). Sreenivasan et al. (2015) studied the effect of different surface treatment on the dynamic-mechanical properties of sisal fibre reinforced polyester composites and found that the sisal fibres treated with alkali increased the storage modulus by more than 30% as compared to untreated fibre composites. They also mentioned that the increased storage modulus for the treated fibre composites is due to an enhancement in the interfacial adhesion between the fibres and the matrix.

Loss modulus (E'') is defined as the ability of a material to dissipate the absorbed energy as heat owing to viscous motions within the material. Loss modulus could be associated to impact strength and internal friction of the composite materials. It is sensitive to molecular motions, transitions and relaxation processes. When the temperature increased gradually, the material changes from rigid to more elastic state depending on the movement of its fillers and main polymer chain (Saba et al., 2016).

Fig. 5.12 shows the loss modulus (E'') of the untreated and different surface treated SF/PLA composites as a function of temperature. It could be seen that the loss modulus peak increased by more than 15% as compared to pure PLA with the addition of 15 wt% of sisal fibres into PLA matrix.

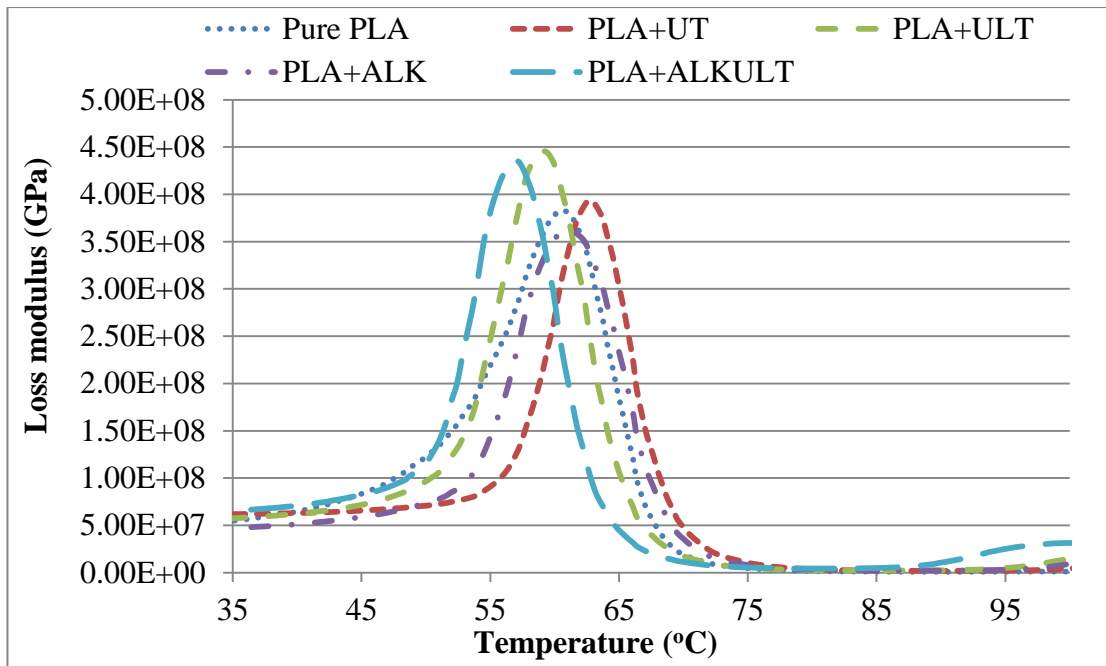


Fig. 5.12 Loss modulus (E'') curves of untreated (UT), HIU treated (ULT), alkali treated (ALK) and the combination of alkali and HIU treated (ALKULT) SF/PLA composites

An increase in the loss modulus with the addition of sisal fibres into PLA matrix gives the evidence that the reduction of brittleness and uniform dispersion of fibres across the matrix material which leads to increased mechanical and thermal properties (Poathan et al., 2003). It is worth noted that the loss modulus was 25% higher for the combination of alkali and HIU treated fibre composites as compared to untreated SF/PLA composites. These results confirmed the increased interfacial adhesion between the fibres and the matrix for the combination of alkali and HIU treated SF/PLA composites.

Tan δ or damping factor is a dimensionless number and is the ratio of storage modulus to loss modulus of the material (Saba et al., 2016). **Fig. 5.13** shows the Tan δ peaks of untreated and different surface treated SF/PLA composites as a function of temperature.

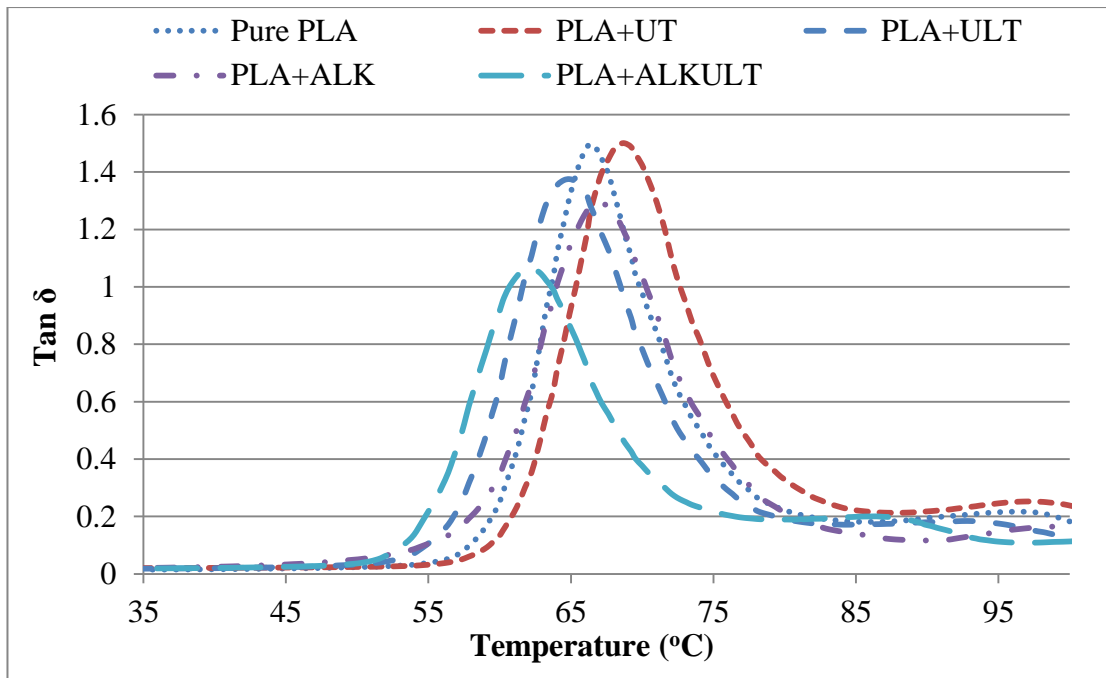


Fig. 5.13 Tan δ curves of untreated (UT), HIU treated (ULT), alkali treated (ALK) and the combination of alkali and HIU treated (ALKULT) SF/PLA composites

It could be noticed that the peaks of tan delta reduced significantly by 50% for the combination of alkali and HIU treated SF/PLA composites as compared to pure PLA. A reduction in the tan δ peak indicates that the combination of alkali and HIU treated SF/PLA composites have high elasticity and good interfacial bonding between fibre and matrix since the mobility of the polymer chains decreased. Pure PLA showed a higher Tan δ peak which clearly indicates the non-elastic and highly brittle nature (Lee et al., 2012). It is to be noted that the peak of damping factor decreased gradually for HIU treated, alkali treated and the combination of alkali and HIU treatments.

Similar results have been reported by other researchers (Ray et al., 2002; Sreenivasan et al., 2015). Vilay et al. (2008) studied the effect of fibre surface treatment and fibre loading on the properties of bagasse fibre reinforced unsaturated polyester composites. They reported that the peak of loss modulus decreased significantly by 90% for the alkali treated bagasse fibre composites as compared to pure resin. Lee et

al. (2012) studied the dynamic-mechanical properties of short sisal fibre reinforced bacterial cellulose polylactide composites and noted the amplitude of damping peak was higher for pure PLA as compared to sisal fibre reinforced composites. They mentioned that the higher damping peak indicates the poor interfacial adhesion between the fibres and matrix whereas the lower tan delta peak represents the good interfacial adhesion of fibres and matrix.

DMA results also revealed that the temperature of $\tan \delta$ peak slightly increased with the addition of untreated sisal fibre into PLA matrix. This is due to the restriction of molecular mobility of PLA polymer with sisal fibres. However, in case of surface treated sisal fibres, the temperature of $\tan \delta$ shifted to lower temperature as compared to pure PLA. For the combined treatment of alkali and HIU treatments, a significant reduction of $\tan \delta$ peak temperature was observed. This may be due to the increased compatibility between the surface treated sisal fibres and PLA matrix which increased the interfacial adhesion between the fibre and matrix. Similar results were reported by other researchers (Liu Xiaohui, 2001; Vilay et al., 2008; Guo et al., 2009)

5.7 TGA analysis

The effect of different surface treatments on the thermal stability of SF/PLA composites was evaluated by using TGA. **Fig. 5.14** shows the TGA curves of untreated, HIU treated, alkali treated and the combination of alkali and HIU treated SF/PLA composites. A relatively smaller degradation could be observed in the temperature range from 90 to 150 °C in case of SF/PLA composites due to the presence of moisture in the sisal fibres. However, this step could not be seen in case of pure PLA. Pure PLA shows degradation in a single stage between 280 and 390 °C with the maximum degradation occurred at 375 °C. From **Fig. 5.14** it is clearly seen

that the degradation temperature of SF/PLA composites decreased with the addition of fibres as compared to pure PLA. For the untreated sisal fibre composites, 10% weight loss could be noticed at 313 °C for the untreated SF/PLA composites which is 20 °C lower than pure PLA (333 °C).

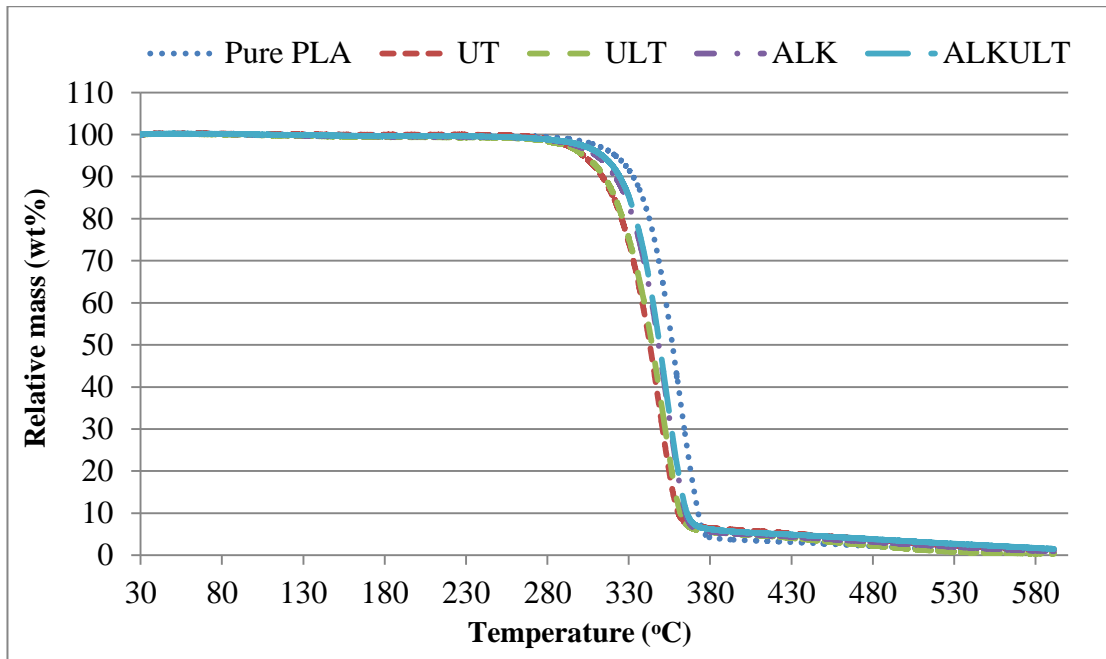


Fig. 5.14 TGA of untreated (UT), HIU treated (ULT), alkali treated (ALK) and the combination of alkali and HIU treated (ALKULT) SF/PLA composites

This trend was same for the ultrasound treated sisal fibre composites which is in agreement with FE-SEM results. It is well known that any type of natural fibres will exhibit lower thermal stability as compared to polymer matrices. Adding fibres of low thermal stability into polymer matrix leads to a reduction in the thermal stability of the composite materials (Ohkita and Lee, 2006; Yussuf et al., 2010; Cran et al., 2014; Dong et al., 2014). Yussuf et al. (2010) investigated the thermal stability of pure PLA and kenaf fibre reinforced PLA composites with 20 wt% loading of kenaf fibres. They noticed that the composite degraded at 321 °C as compared to pure PLA which degraded at 323 °C with a weight loss of 10%. However, the thermal stability

considerably increased for the alkali and the combination of alkali and HIU treated SF/PLA composites as compared to untreated SF/PLA composites.

Table 5.1 Effects of surface treatments on thermal stability of SF/PLA composites

S No	Fibre treatments	T _{10% wt loss} (°C)	T _{50% wt loss} (°C)	T _{90% wt loss} (°C)
1	Pure PLA	332.7	356.8	372.7
2	UT	313.7	343	360.5
3	ULT	315.2	344	362
4	ALK	321.6	348	365
5	ALKULT	324.5	349	367

10% weight loss occurred at 321 °C and at 325 °C for the alkali treated and the combination of alkali and HIU treated SF/PLA composites respectively which are 8 °C and 12 °C higher than the untreated SF/PLA composites. It is also interesting to note that the addition of 15 wt% of alkali and the combination of alkali and HIU treated SF/PLA composites showed an increase in the char residue by 4% and 6% respectively as compared to pure PLA. This is in agreement with the observations as reported by Yussuf et al. (2010) and Mitra et al. (1998).

5.8 DSC analysis

The thermal properties of PLA and SF/PLA composites were studied by DSC analysis and the obtained DSC thermograms have been presented in **Fig. 5.15**. The glass transition temperature (T_g), the cold crystallisation temperature (T_{cc}) and melting temperature (T_m), melting enthalpy (ΔH_m) and percentage of crystallinity (X_c) were obtained from the DSC analysis and have been summarised in **Table 5.1**.

The percentage crystallinity was calculated by using the **eqn. 3.4**. As seen from **Fig. 5.15**, peaks observed around 60 °C are considered as T_g of PLA due to the thermal

transition from glossy state to rubbery. The pure PLA exhibits higher T_g as compared to SF/PLA composites. The T_{cc} was found to be around 117 °C and for pure PLA T_m was at 155.2 °C which supports that the PLA is a semi-crystalline polymer (Cran et al., 2014).

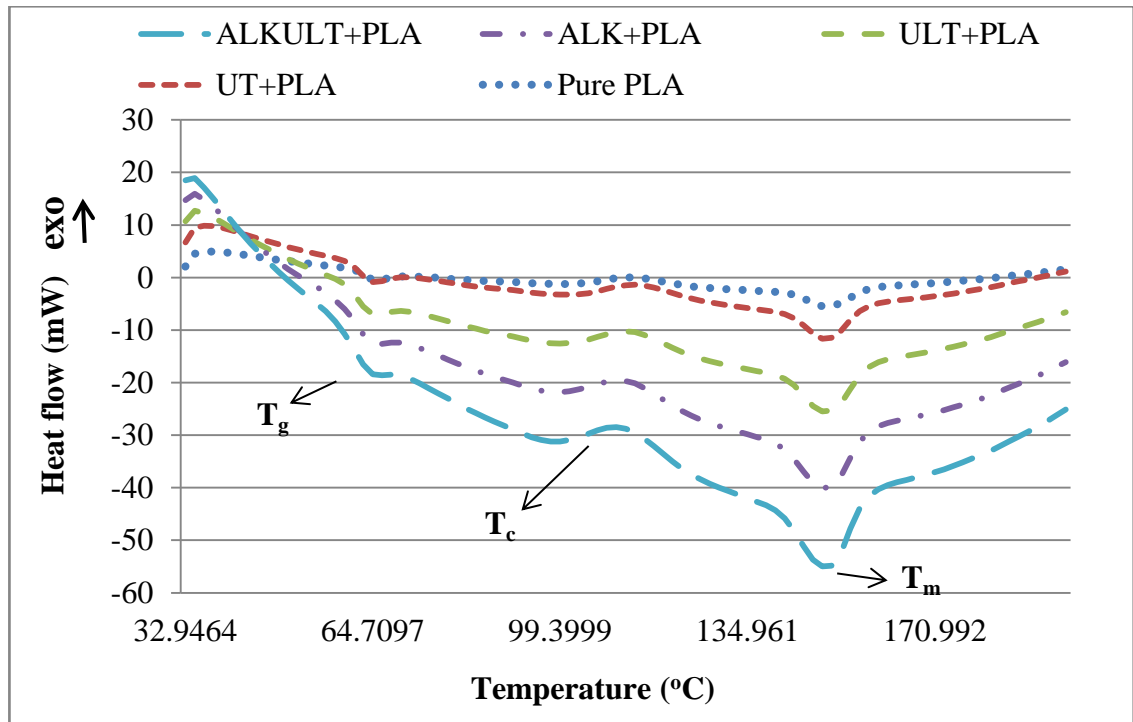


Fig. 5.15 DSC thermo-grams of pure PLA, untreated (UT), HIU treated (ULT), alkali treated (ALK), and the combination of alkali and HIU treated (ALKULT) SF/PLA composites

The T_g increased gradually with the addition of sisal fibres into SF/PLA composites. This is mainly due to the reinforcement effect with the addition of sisal fibres which causes the restriction of polymer chain mobility in PLA (Khalid et al., 2008). The T_{cc} significantly decreased with an increase in the sisal fibres into PLA. The percentage crystallinity decreased by more than 50% with the addition of 15 wt% of untreated sisal fibres as compared to pure PLA (**Table 5.2**). The percentage crystallinity decreased mainly because of an increase in the amorphous region and due to the

disruption in the crystalline structure of PLA polymer (Wootthikanokkhan et al., 2013; Yu et al., 2014). However, it was found that the percentage crystallinity increased significantly for the sisal fibre composites with surface treatments. The percentage crystallinity drastically increased by 75% for the combination of alkali and HIU treated SF/PLA composites as compared to untreated SF/PLA composites (**Table 5.2**).

Table 5.2 Thermal properties of pure PLA and SF/PLA composites

Samples	T _g (°C)	T _{cc} (°C)	T _m (°C)	ΔH _m (J/g)	X _c (%)
Pure PLA	63.05	114.25	148.2	14.22	15.5
15UT+PLA	63.52	113.6	149.5	11.54	6.86
15ULT+PLA	64.2	111.8	149.6	10.72	7.67
15ALK+PLA	64.7	110.5	150.5	12.5	9.51
15ALKULT+PLA	66.3	108.6	151.85	16.35	11.97

This may be due to an increase in the cellulose content of sisal fibres in the treated SF/PLA composites after the combined treatment of alkali and HIU. It is also believed that the increased interfacial adhesion between the surface treated sisal fibres and PLA matrix leads to increase the percentage crystallinity (Dong et al., 2014). This supports TGA, water absorption and DMA analyses.

5.9 Water absorption studies

The water absorption properties have been investigated for the untreated and different surface treated SF/PLA composites. **Figs. 5.16 and 5.17** show the effect of fibre loading and different surface treatments of sisal fibres on the percentage of water absorption for SF/PLA composites respectively. As seen in the **Figs. 5.16 and 5.17**, the water absorption graphs show linear curves for all the composites during the initial period of water immersion followed by saturation. According to Mishra et al. (2014) the water absorption graphs with linear curves obeyed Fick's law of diffusion. The water absorption purely depends on its rate of diffusion into the composite materials (Yew et al., 2005).

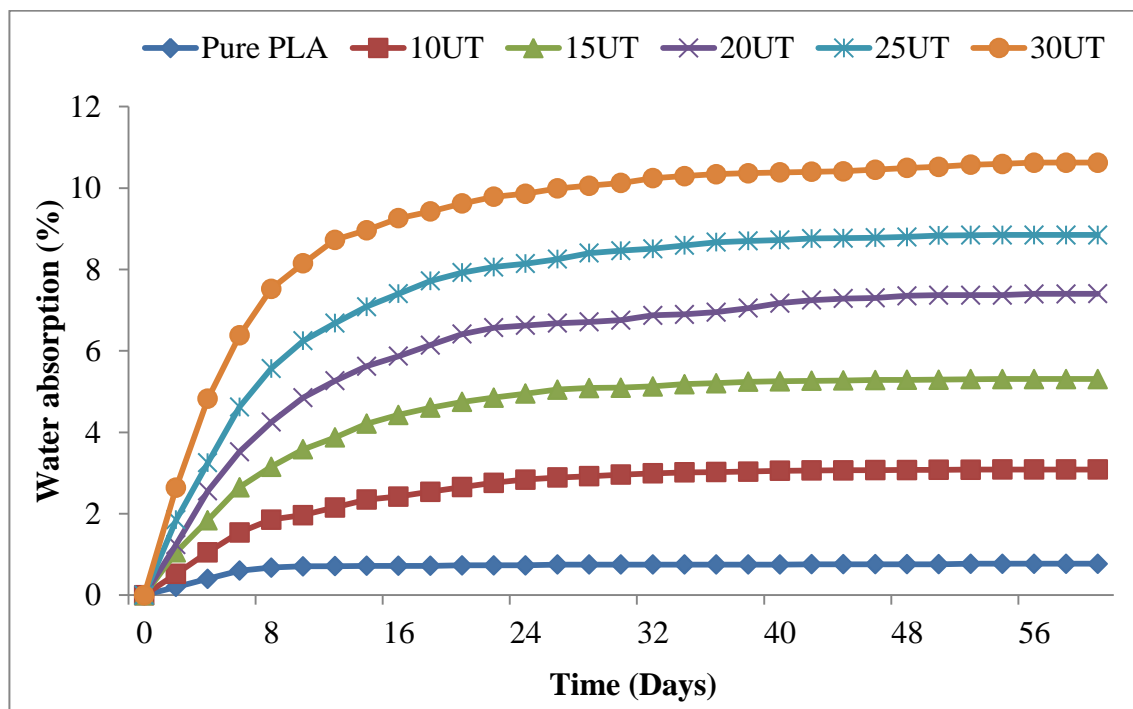


Fig. 5.16 Effect of fibre loading on the water absorption of untreated SF/PLA composites

The percentage of water absorption of pure PLA was 0.78% which is the lowest as compared to SF/PLA composites which confirms the hydrophobic nature of PLA

matrix. The percentage of water absorption gradually increased with an increase in the fibre loading (**Fig. 5.16**) which is in agreement with the results as reported by other researchers (Badia et al., 2014; Rajesh et al., 2015). The percentages of water absorption, initial slope versus $t_{1/2}$ and diffusion coefficient have been calculated by using **eqns. 3.5 and 3.6** and the obtained results have been summarised in **Table 5.3**. The composites with 30 wt% sisal fibre loading show the highest water absorption (10.62%) as compared to pure PLA. The presence of sisal fibres in the composites increases the water absorption which is due to the presence of amorphous materials on the surface of sisal fibres with a large number of hydroxyl groups. These hydroxyl groups attract the water molecules through hydrogen bonding (Alamri and Low, 2013). Dhakal et al. (2007b) reported that the composites show an increase in the trend of water absorption with an increase in the fibre loading. They observed an increase in the water absorption to 10.97% for 5 layers of hemp fibre mat reinforced unsaturated polyester composites as compared to pure unsaturated polyester resin which showed 0.87% of water absorption.

Similar observations have been reported (Yew et al., 2005; Badia et al., 2014; Rajesh et al., 2015). Alamri and Low (2013) studied the water absorption behaviour of recycled cellulose fibre reinforced with epoxy composites. They noticed that the water absorption significantly increased by more than 15% with the addition of 46 wt% fibre loading into epoxy matrix. These results proved that the addition of natural fibres into the hydrophobic nature of the polymer matrices resulting into higher water absorption and leads to decrease the mechanical and physical properties. Espert et al. (2004) reported that the addition of 30 wt% of cellulose fibres into PPEVA polymer increased the water absorption by 6% as compared to pure PPEVA polymer. The effect of different surface treatments on the water absorption has been studied and the

obtained results have been presented in **Fig. 5.17**. It was found that the surface treatment has a good impact on reducing the water absorption significantly for sisal fibres composites. The combined treatment of alkali and HIU on the composites showed the lowest water absorption by 2.24% which is 45% and 80% lower than the alkali and HIU treated SF/PLA composites. A significant reduction in the water absorption in the treated sisal fibre composites confirms the removal of amorphous materials from the surface of sisal fibres.

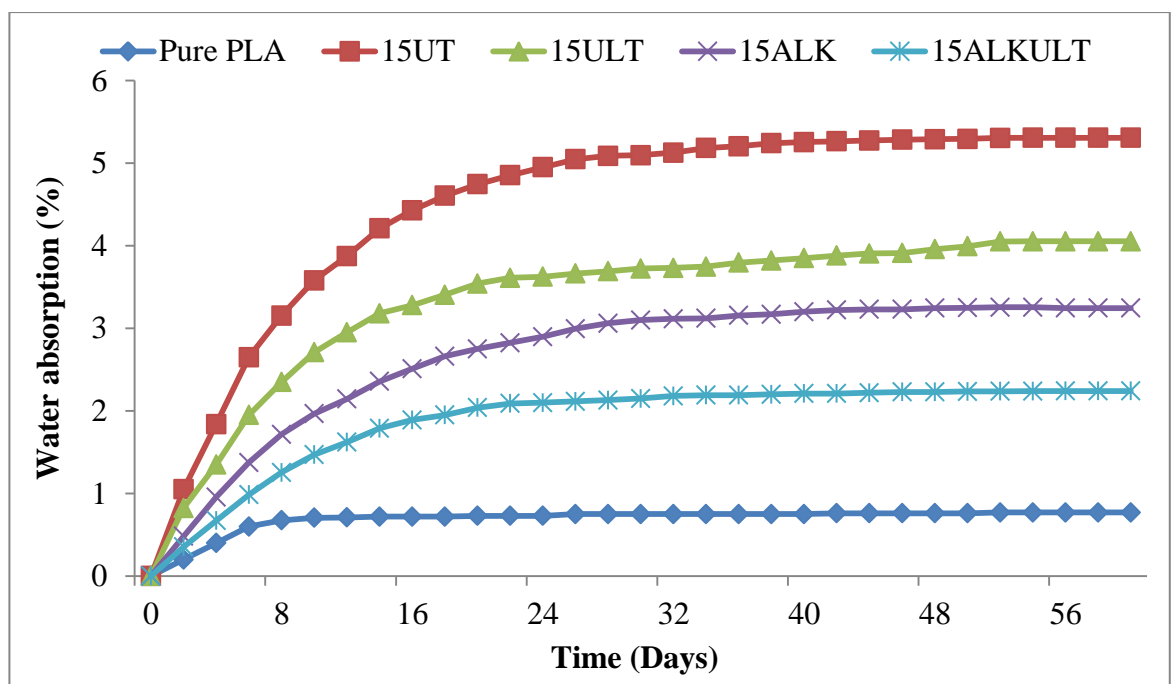


Fig. 5.17 Effect of high intensity ultrasound (ULT), alkali (ALK) and the combination of alkali and HIU (ALKULT) surface treatments on the water absorption of SF/PLA composites

Mohan and Kanny (2012) reported that after the surface treatment with alkali and the combination of alkali and clay treatments, the water absorption reduced to 11.5% and 10.3% respectively as compared to pure PP which was 12.5%. Ghosh et al. (2013) studied the effect of air bubbling through alkali solution and sonication on the water

absorption of banana fibre-vinyl ester composites. They reported that the combined treatment of air bubbling through alkali solution and sonication decreased the water absorption by 100% as compared to banana fibre composites treated only with an alkali solution.

These results proved that the surface treatments of natural fibres have considerable effects on the reduction of water absorption. The rate of diffusion of water in the composite materials was studied using Fick's steady state flow and the coefficient of diffusion (D) was calculated and the results have been summarised in **Table 5.3**. The coefficient of diffusion increased with an increase in the fibre loading in the composites which may be due to the following. First, similar to any other natural fibres, sisal fibres are highly hydrophilic in nature which favours the diffusion of water molecules into the composites. Second, due to an increase in the fibre loading in the composites, fibres become agglomerated within the composites which lead to the formation of voids and air bubbles. These voids and air bubbles allow rapid penetration of water molecules into the composites.

Generally polymer matrices are hydrophobic in nature and the natural fibres are hydrophilic which cause the incompatibility between polymer matrix and the natural fibres. This incompatibility caused poor interfacial adhesion between fibre and matrix phase which leads to an increase in the diffusion of water (Espert et al., 2004; Paul et al., 2015). The coefficient of diffusion decreased drastically for the treated SF/PLA composites (**Table 5.3**). The coefficient of diffusion was 0.6873 for 15 wt% of fibre loading with the combination of alkali and HIU treated sisal fibre composite which is 130% lower than the untreated fibre composite with the same fibre loading. This confirms the removal of amorphous materials from the surface of fibres which

significantly enhanced the interfacial adhesion between matrix and fibres. This observation is in agreement with the results obtained from FTIR and DMA.

Table 5.3 Water absorption properties of SF/PLA composites

S. No.	Samples	Fibre loading (wt %)	Type of surface treatment	Maximum water absorption (%)	Initial slope of plot (k) M(t) versus $t^{1/2}$	Diffusion coefficient, $D, \times 10^{-3}$ (mm^2/sec)
1	Pure PLA	0	-	0.78	0.01	0.13
2	10UT	10	Untreated	3.08	0.07	1.02
3	15UT	15	Untreated	5.30	0.15	1.56
4	20UT	20	Untreated	7.40	0.26	2.33
5	25UT	25	Untreated	8.84	0.37	3.20
6	30UT	30	Untreated	10.62	0.48	3.74
7	15ULT	15	HIU treated	4.05	0.09	0.87
8	15ALK	15	Alkali treated	3.24	0.06	0.68
9	15ALKULT	15	Alkali + HIU treated	2.24	0.04	0.58

5.10 Biodegradability analysis

Soil burial test was performed to evaluate the effect of different surface treatments and fibre loading on the biodegradability of SF/PLA composites. Samples of untreated and different surface treated SF/PLA composites were buried in open soil and the degradation experiments were carried out as described in the section 3.6. The percentage of weight loss was calculated for pure PLA and sisal fibre (untreated and surface treated) reinforced composites after the removal of composite samples from the soil. **Fig. 5.18** shows the percentage of weight loss with the function of fibre loading and different surface treatments. The biodegradation results revealed that the percentage weight loss for all the fibre reinforced composites was gradually increased

with increased fibre loading as well as number of days of soil burial. From **Fig. 5.18**, it could be seen that pure PLA shows the least degradation of 2.59% after 120 days of soil burial. However, the percentage of degradation increased with an increase in the fibre loading into PLA matrix. It is worth noted that the percentage weight loss increased with an increase in the fibre volume of the composites. After 180 days of soil burial, the percentage weight loss increased significantly by more than 180%, 400% and 550% with the addition of sisal fibres of 15, 20 and 30 wt% respectively as compared to pure PLA. An increase in the weight loss is mainly due to the exposure of cellulosic fibres to microbial degradation during soil burial.

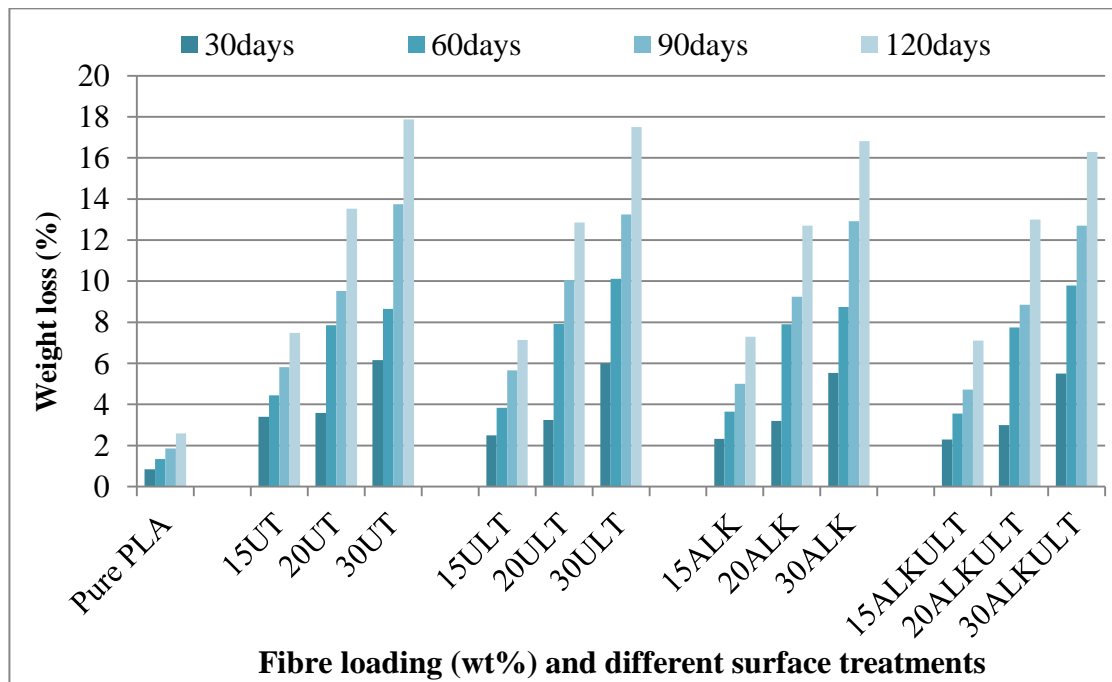


Fig. 5.18 Biodegradation of untreated (UT), HIU treated (ULT), alkali treated (ALK) and the combination of alkali and HIU treated (ALKULT) sisal fibre reinforced PLA composites with different weight percentage of fibre loading

Besides, it may be due to the hydrophilic nature of untreated sisal fibres which has the tendency to absorb more water into the composite materials leading to faster

degradation (Yussuf et al., 2010; Dong et al., 2014). On the other hand, different surface treated SF/PLA composites showed slower degradation as compared to untreated fibre composites (**Fig. 5.18**). For instance, 30 wt% of sisal fibre composites that were treated with the combination of alkali and HIU treatment showed 10% slower degradation than the untreated fibre composites. Fibre surface treatments make the fibres more hydrophobic and enhance the fibre-matrix interfacial adhesion which leads to slower degradation. Moreover, surface treatments remove the amorphous materials from the surface of fibres which significantly reduced the water absorption of the composites and leads to slower degradation as compared to untreated SF/PLA composites (Rajesh et al., 2015). In order to analyse and compare the morphological changes due to soil biodegradation, samples of pure PLA, untreated and surfaced treated SF/PLA composites were collected at different degradation stages and subjected to FE-SEM (**Fig. 5.19**).

As seen from **Fig. 5.19 A**, before soil burial, pure PLA shows a smooth and glassy surface. After 60 and 120 days the erosion and etching out of the surface of pure PLA clearly show gradual degradation (**Figs. 5.19 B-C**). In case of untreated SF/PLA composites with exposure to soil degradation (**Figs. 5.19 D-F**), it can be clearly seen that the fibres degrade rapidly as compared to PLA matrix. This is obvious as the cellulosic fibres are more prone to exposure and hence faster degradation than the matrix phase. Moreover, the untreated sisal fibres contain amorphous materials on the surface of fibres which undergo rapid degradation than the crystalline cellulose materials inside the fibre lumen (Alvarez et al., 2006; Zhao et al., 2008). In case of the combination of alkali and HIU treated SF/PLA composites (**Fig. 5.19 G-I**), the degradation was slower by 10% as compared to untreated fibre composites. This is mainly due to an improved compatibility between the treated sisal fibres and PLA

matrix that leads to an increased interfacial adhesion, due to which the degradation became slower as compared to untreated SF/PLA composites (Rajesh et al., 2015).

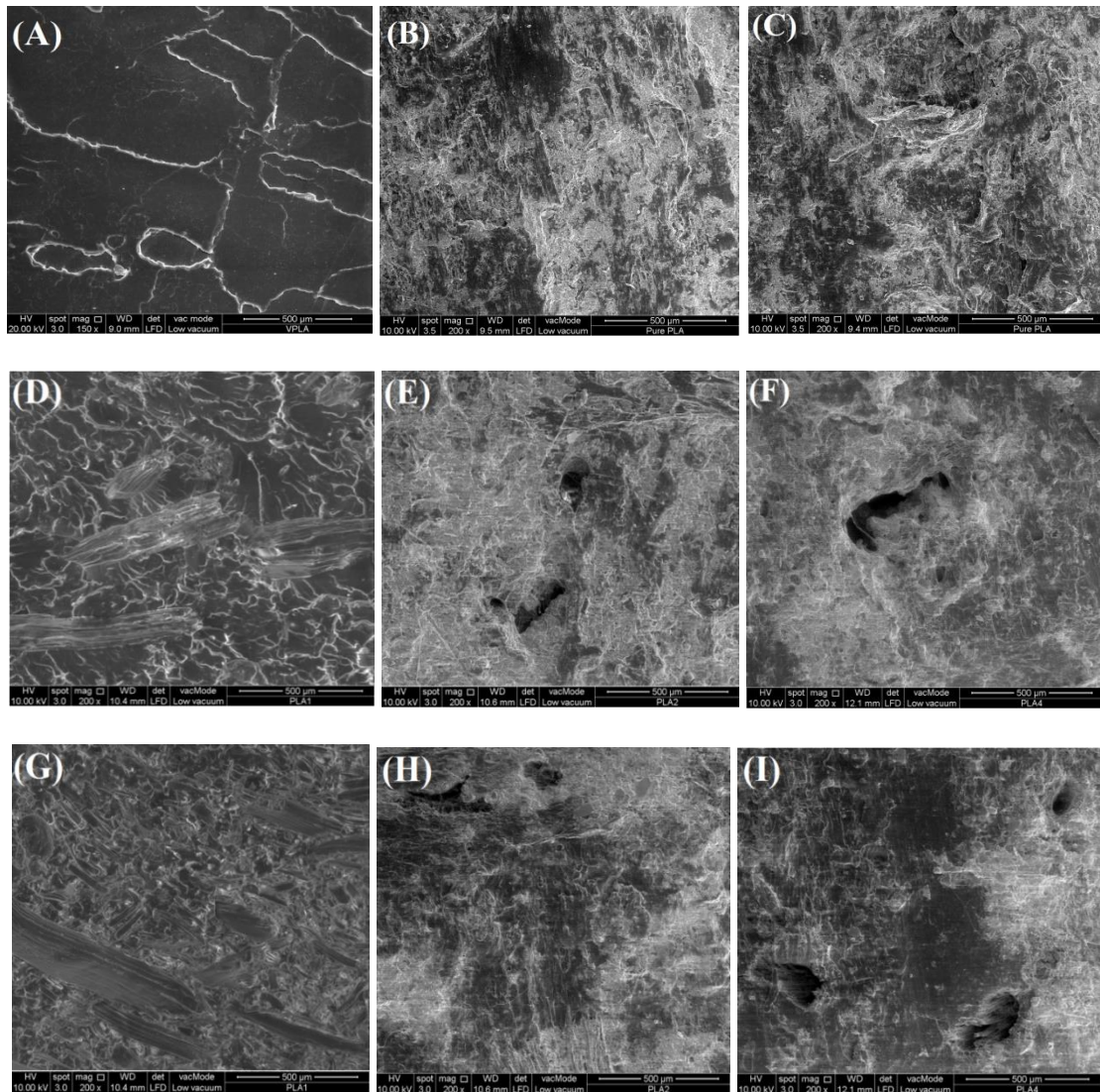


Fig. 5.19 FE-SEM images of outer surface of the soil buried samples (A) Pure PLA before soil burial, (B) Pure PLA after 60 days, (C) Pure PLA after 120 days, (D) 15 wt% untreated sisal fibre (UT) + PLA composites before soil burial, (E) 15UT+PLA after 60 days, (F) 15UT+PLA after 120 days, (G) 15 wt% of alkali and HIU treated sisal fibre (ALKULT) + PLA composites before soil burial, (H) 15ALKULT+PLA after 60 days, (I) 15ALKULT+PLA after 120 days

5.11 Conclusions

In this investigation, untreated and different surface treated sisal fibres reinforced PLA composites were successfully prepared by melt mixing and compression moulding techniques and the effect of fibre surface treatments on the morphology, mechanical, dynamic mechanical, thermal, water absorption and biodegradable properties were investigated. FE-SEM analysis indicated the well dispersion of fibres across the matrix after the combined treatment of alkali and HIU. FTIR studies confirm the surface treatments of sisal fibres and their addition into PLA matrix. Tensile strength, modulus and the impact strength increased by 10%, 75.4% and 42% respectively with the loading of surface treated sisal fibres as compared to the untreated fibres. The theoretical models were used to predict the effect of untreated and different surface treated short SF/PLA composites on Young's modulus and to fit the obtained experimental values. All the models except Bowyer and Bader model (BBM) show a reasonably good agreement with the experimental values particularly at lower fractions of fibres. The results of theoretical models revealed that the surface treatments of fibres influence the tensile properties of short SF/PLA composites. DMA analysis revealed that the increased fibre loading into PLA matrix significantly increased the storage modulus by 15% and 30% as compared to untreated fibre composites and pure PLA respectively. Thermal analysis showed an improved thermal stability by 12 °C and the crystallinity increased by 75% for the combined treatment of alkali and HIU as compared to untreated SF/PLA composites. Water absorption and soil biodegradation analysis were in favour of improved mechanical properties of SF/PLA composites with the incorporation of sisal fibres which were surface treated with the combination of alkali and HIU.

CHAPTER VI

Results and Discussion: Hal-PLA

Nanocomposites

6.1 Nitrogen adsorption-desorption analysis

Nitrogen adsorption-desorption isotherms of unmodified and APTES modified Hal nanotubes have been shown in **Fig. 6.1**. The specific surface area (S_{BET}), Langmuir surface area, pore volume (V_{pore}) and pore width (W_{pore}) values of unmodified and APTES modified Hal nanotubes have been shown in **Table 6.1**. Isotherms of both unmodified and APTES modified Hal nanotubes belong to type II with H3 hysteresis loop according to IUPAC classification (Sing, 1982; Thommes et al., 2015). It could be seen from **Fig. 6.1** that the untreated Hal nanotubes show a minor hysteresis loop which corresponds to the relatively large mesopores with non-uniform diameter of the Hal nanotubes lumen.

Table 6.1 Nitrogen adsorption and desorption data of surface area (S_{BET}), Langmuir surface area, volume (V_{pore}) and width (W_{pore}) for unmodified (uHal) and APTES modified Hal nanotubes (mHal)

Samples	S_{BET} (m^2/g)	Langmuir surface area (m^2/g)	V_{pore} (cm^3/g)		W_{pore} (\AA)	
			Adsorption	Desorption	Adsorption	Desorption
uHal	61.74	84.45	0.165	0.177	107.34	115.23
mHal	18.38	25.43	0.069	0.079	150.77	171.94

In case of APTES modified Hal nanotubes, there is a noticeable absorption of nitrogen which corresponds to the multilayer adsorption with uniform pore size. The BET specific surface area and pore volume of the unmodified Hal nanotubes were $61.74 \text{ cm}^3/\text{g}$ and $0.165 \text{ cm}^3/\text{g}$ respectively (**Table 6.1**) which indicate a larger surface area and pore volume. However, in case of APTES modified Hal nanotubes, the surface area, Langmuir surface area, and pore volume significantly decreased to $18.38 \text{ cm}^3/\text{g}$, $25.43 \text{ m}^2/\text{g}$ and $0.069 \text{ cm}^3/\text{g}$ respectively. This is due to the grafting of organo-silane compounds and the associated structural shrinkage in the APTES modified Hal nanotubes which lead to a significant decrease in the surface area (Yuan et al., 2008; Jin et al., 2015; Freire et al., 2016).

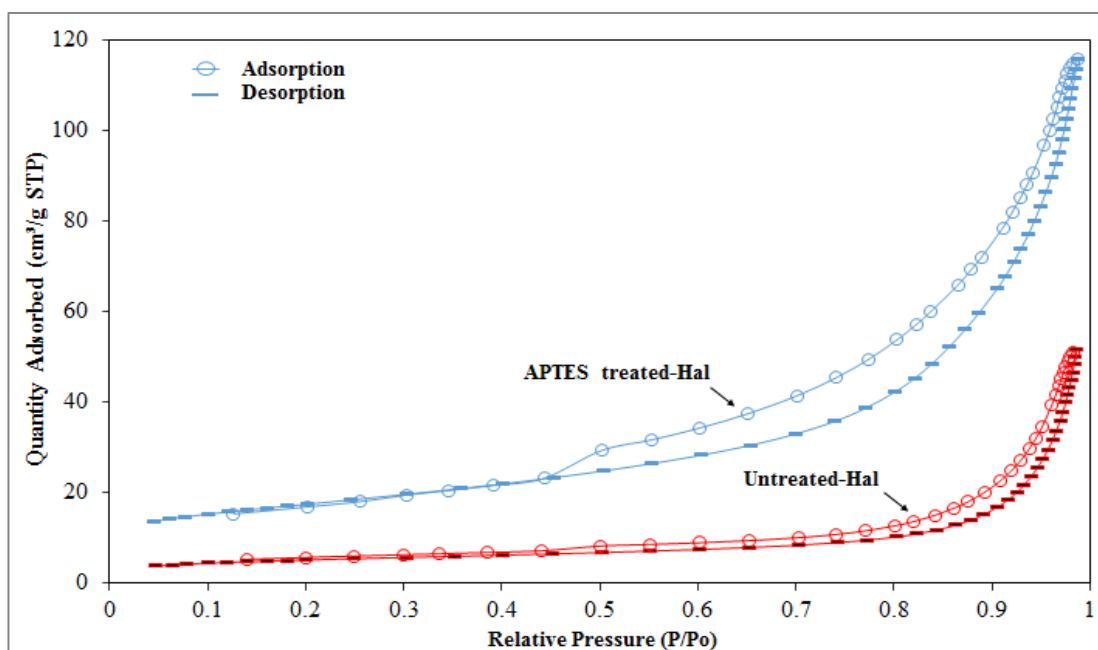


Fig. 6.1 Nitrogen adsorption-desorption isotherms of unmodified (uHal) and APTES modified Hal nanotubes (mHal)

6.2 FTIR analysis

Fig. 6.2 shows the FTIR spectra of unmodified (A) and surface modified Hal nanotubes (B) using the silane coupling agent, APTES. **Table 6.2** presents the

wavenumbers and assignments of FTIR spectra of unmodified Hal nanotubes, APTES modified Hal nanotubes and their PLA nanocomposites.

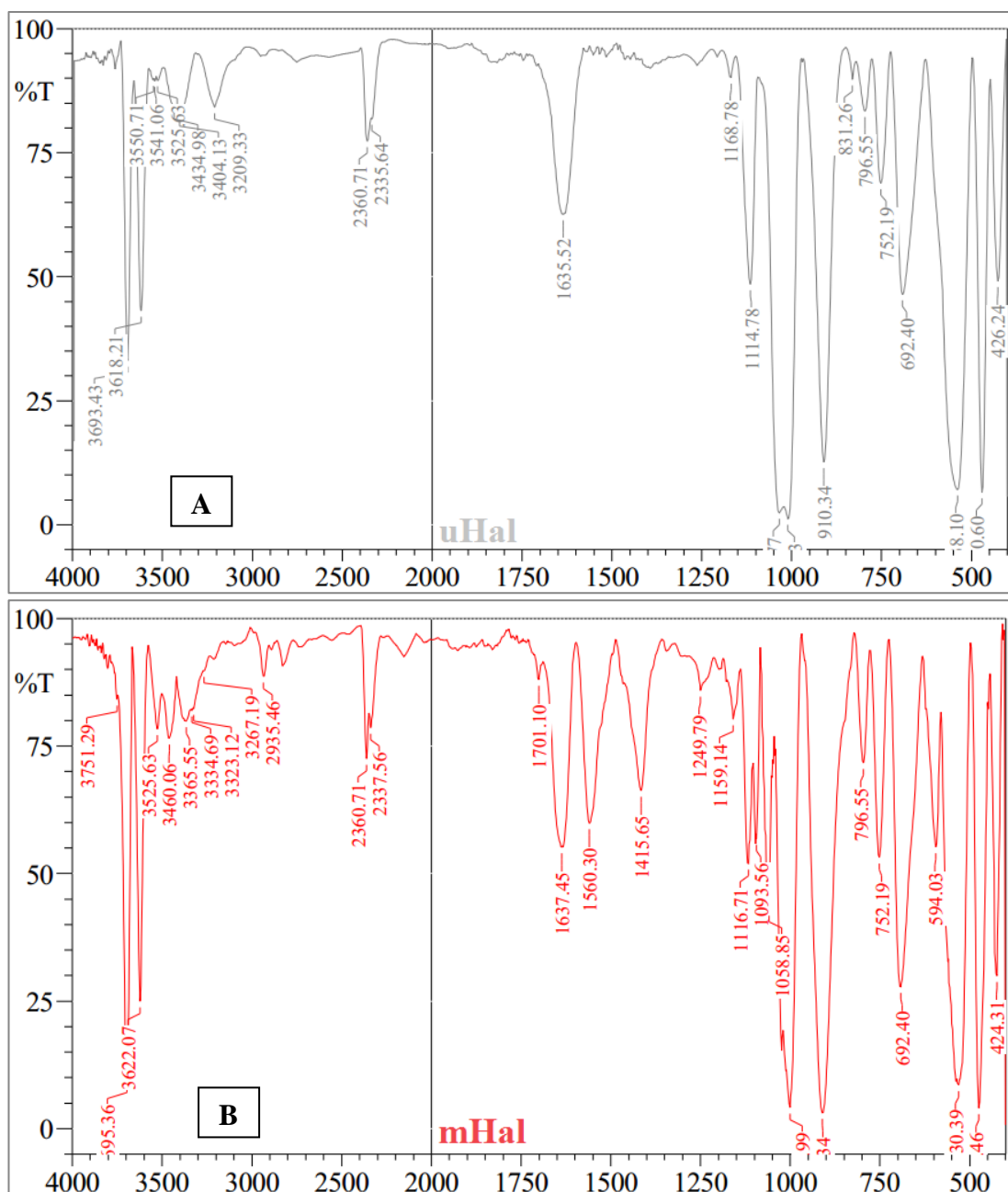


Fig. 6.2 FTIR spectra of unmodified (uHal) (A) and APTES modified Hal nanotubes (mHal) (B)

In the FTIR spectra of unmodified (uHal) and silane modified Hal nanotubes (mHal), the high intensity peaks at 3693 cm⁻¹, 3618 cm⁻¹, 3695 cm⁻¹ and 3622 cm⁻¹ are

associated with O-H stretching of Al-OH groups. In these OH groups, each OH linked to two Al atoms. The peaks at around 3434 cm^{-1} and 3460 cm^{-1} are attributed to intercalated water and OH groups on the surface of Hal nanotubes (Joussein et al., 2005). The bands in the region between 1000 and 1200 cm^{-1} are related to asymmetric stretching of siloxane groups in the Hal nanotubes (Barrientos-Ramirez et al., 2011). The peaks at around 470 cm^{-1} and 474 cm^{-1} are assigned to stretching vibrations of Si-O-Si groups (Yuan et al., 2008; Pasbakhsh et al., 2010; Albdiry and Yousif., 2014). As compared to unmodified Hal nanotubes, APTES modified Hal nanotubes (mHal) exhibit new FTIR bands.

The new peak at 3365 cm^{-1} for APTES modified Hal nanotubes is associated with asymmetric stretching of amino group. The deformation vibrations of CH_2 at 2935 cm^{-1} and the deformation peak of Si-CH_3 at around 1249 cm^{-1} have been noted. Due to silanisation, hydrolysis and condensation take place which lead to the generation of siloxane ($-\text{Si-O-Si}-$) and creates a bond between Hal nanotubes and the hydroxyl groups ($-\text{OH}$) on the surface of silane (**Scheme 2**). Hal nanotubes surface becomes hydrophobic due to these siloxanes (Albdiry and Yousif, 2014). Moreover, the new peak at 1560 cm^{-1} for APTES modified Hal nanotubes is attributed to the stretching vibration of amino group, which also proves the modification of APTES with Hal nanotubes. The high intensity peaks in the APTES modified Hal nanotubes from 3600 to 3700 cm^{-1} indicate the presence of inner hydroxyl groups as well as the hydroxyl groups located on the octahedral surfaces of Hal nanotubes. FTIR spectra of PLA with unmodified (A) and APTES modified (B) Hal nanocomposites have been represented in **Fig. 6.3**. The band at 3504 cm^{-1} indicates the interaction of hydroxyl groups of PLA with Si-O-Si groups of Hal nanotubes via hydrogen bonding (Liu et al., 2013).

The hydrogen bond interaction between PLA matrix and other nanofillers was reported by Matusik et al. (2011). The PLA shows absorption bands at 2999 cm^{-1} and at 2682 cm^{-1} arising from C-H stretching vibrations of CH_3 and CH groups respectively, whereas the stretching vibrations of carbonyl groups are appearing at 1755 cm^{-1} .

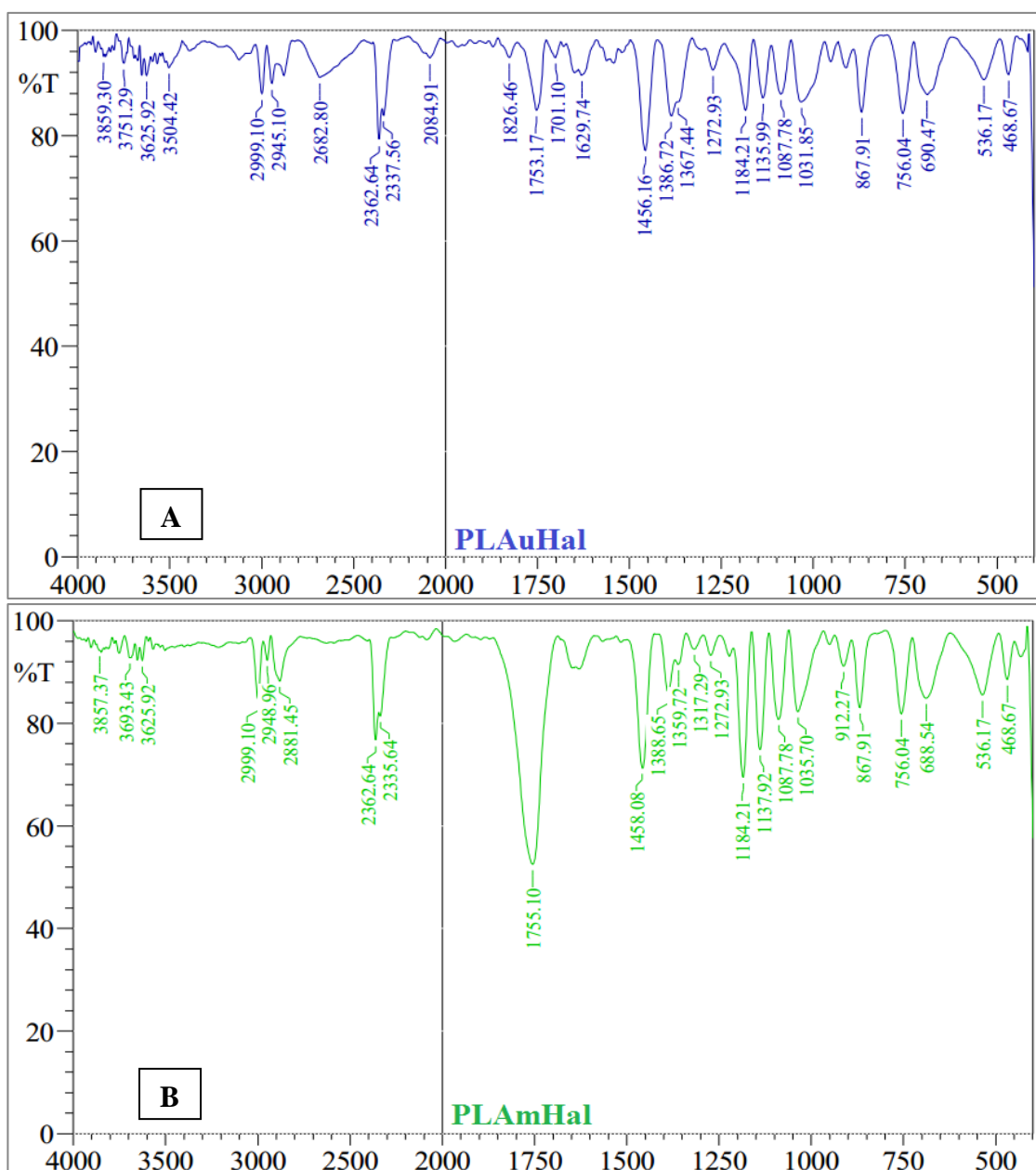


Fig. 6.3 FTIR spectra of PLA/unmodified Hal nanotubes (PLAuHal) (A) and PLA/APTES modified Hal nanotubes (PLAmHal) (B)

Table 6.2 FTIR bands and assignments for uHal, mHal and Hal-PLA nanocomposites
(Joussein et al., 2005; Yuan et al., 2008; Pasbakhsh et al., 2010; Carli et al., 2014)

Assignments	uHal	mHal	PLAuHal	PLAmHal
Positions (cm ⁻¹)				
O-H stretching of inner-surface hydroxyl groups	3693, 3618	3695, 3622	3625	3625, 3693
O-H stretching of inner hydroxyl groups	3618	3622	-	-
O-H stretching of water	3434	3460	-	-
Asymmetric stretching of N-H ₂	-	3365	-	-
Symmetric stretching of C-H ₂	-	2935	-	-
Stretching vibration of C-H ₃	-	-	2999, 2945	2999, 2948
Stretching vibration of C-H	-	-	2682	-
Stretching vibration of C=O	-	-	1753	1755
O-H deformation of water	1635	1637	-	-
Deformation (scissoring) of N-H ₂	-	1560	-	-
Bending vibration of C-H	-	-	1456	1458
Symmetric deformation of Si-CH ₃	-	1249	-	-
Asymmetric stretching of siloxanes	1033, 1010	1093, 1058, 1000	-	-
Deformation of Al-O-Si	538	530	536	536
Deformation of Si-O-Si	470	474	478	478
Deformation of Si-O	426	424	-	-

A high intensity peak appears at 536 cm^{-1} for APTES modified Hal-PLA nanocomposites is related to the deformation of Al-O-Si from Hal nanotubes which confirms the hydrogen bond interaction between APTES modified Hal nanotubes and PLA matrix. The intensity of the peak appearing at 1755 cm^{-1} for the carbonyl groups is higher for the APTES modified Hal nanotubes incorporated PLA nanocomposites as compared to unmodified Hal-PLA nanocomposites. The higher intensity of absorption bands at 3504 and 3691 cm^{-1} for the surface modified Hal-PLA nanocomposites confirm the formation of more hydrogen bonds between the APTES modified Hal nanotubes and PLA.

6.3 FE-SEM analysis

The FE-SEM image of Hal nanotubes is presented in **Fig. 6.4A**. Halloysite nanotubes are natural 1D nanomaterial having a cylindrical shape with hollow and open-ended tubular morphology. Impact fractured samples were used for the morphological studies to investigate the dispersion and interfacial features of fillers and matrix phase of Hal-PLA nanocomposites. The FE-SEM Image of impact fractured surface of pure PLA is presented in **Fig. 6.4B**, the glossy surface of which indicates the brittle nature of pure PLA (Liu et al., 2013). The large number of agglomeration could be seen in the FE-SEM image (**Fig. 6.4C**) of PLA nanocomposites with the addition of 4 wt% of unmodified Hal owing to the poor interfacial adhesion between Hal nanotubes and PLA. The above poor interfacial adhesion causes stress concentration and leads to reduced tensile and impact properties of Hal-PLA nanocomposites. The interfacial adhesion between Hal nanotubes and PLA matrix increased with APTES modified Hal-PLA nanocomposites (**Fig. 6.4D**).

Similar results were reported by Pasbakhsh et al. (2010) where they noticed more agglomeration in case of unmodified Hal nanotubes as compared to modified Hal nanotubes. An increase in the mechanical and thermal properties of the CPN is controlled by the reduction in the agglomeration which leads to an enhancement in the compatibility between matrix and filler. According to Carli et al. (2014), the mechanical and thermal properties of APTES modified Hal-PLA nanocomposites were purely dependent on the reaction between the functional groups of organo-silane modifier and the carbonyl groups of PLA matrix.

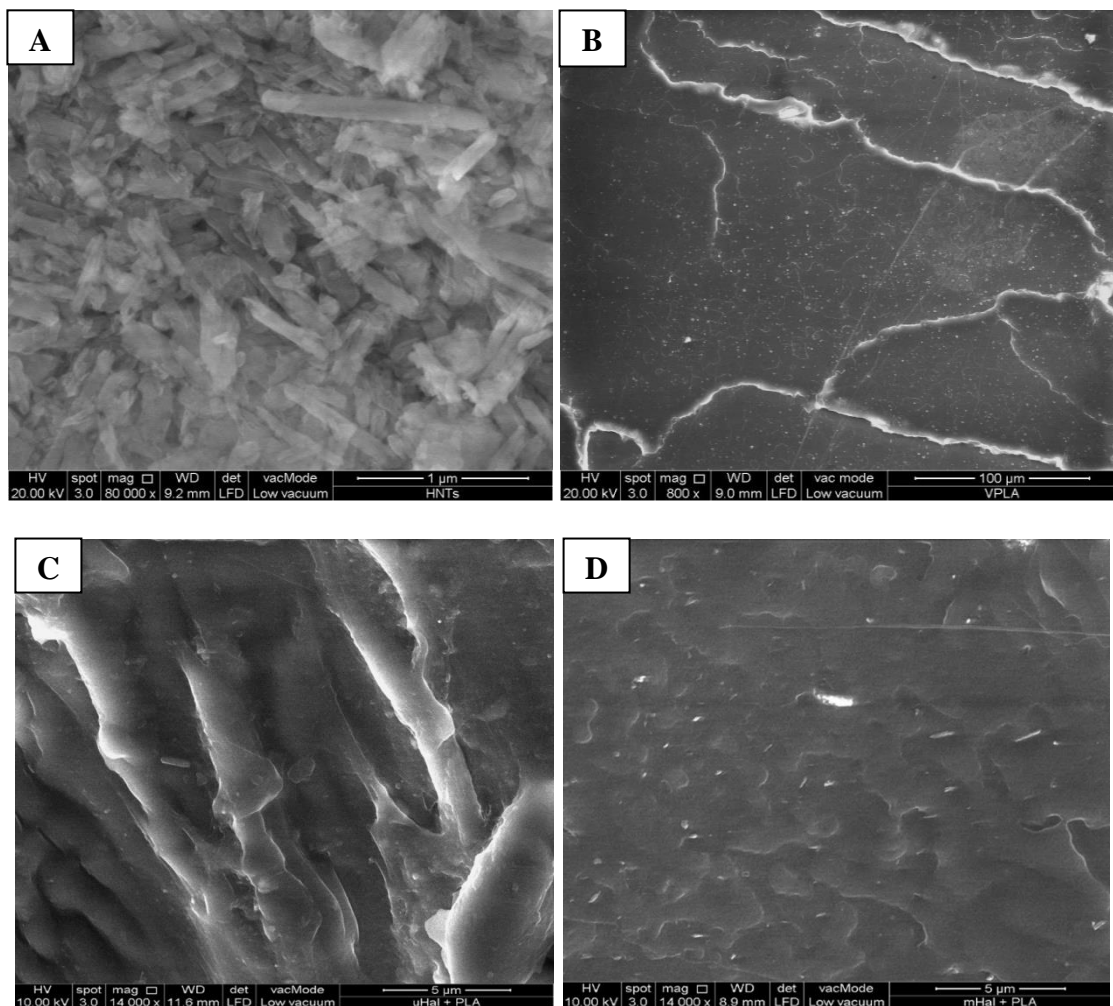


Fig. 6.4 FE-SEM images of impact fractured samples of unmodified (uHal) and APTES modified (mHal) Hal-PLA nanocomposites: (A) Hal nanotubes (B) Pure PLA (C) 4 wt% uHal (D) 4 wt% mHal

6.4 FE-SEM with EDX analysis for Hal nanotubes

The FE-SEM images and the EDX results of elemental analysis of unmodified and APTES modified Hal nanotubes are represented in **Fig. 6.5** and **Table 6.3**. These results revealed that Hal nanotube has a tubular structure with nanometer dimension. Besides, they show that Hal nanotubes were successfully modified with APTES.

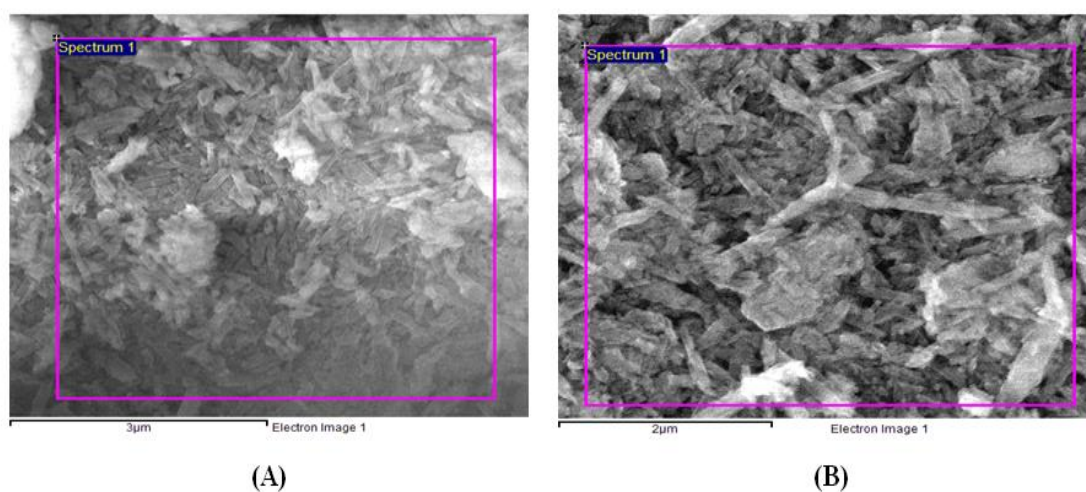


Fig. 6.5 FE-SEM images of (A) unmodified (uHal) and (B) APTES modified Hal nanotubes (mHal)

Table 6.3 EDX results of unmodified and APTES modified Hal nanotubes

S. No.	Samples	Elements (wt%)				
		Carbon	Oxygen	Silicon	Aluminium	Nitrogen
1	uHal	8.16	60.67	15.95	15.22	0.0
2	mHal	4.66	58.59	20.40	15.48	0.87

Silane grafting can be confirmed by the presence of nitrogen content and from an increase in the silane (APTES modified Hal nanotubes). However, according to Carli

et al. (2014), it is impossible to quantify the silane content using the EDX method. The quantity of amino groups in the APTES modified Hal nanotubes depends on the type of functionality of amino groups in the silane coupling agent (Yuan et al., 2008).

6.5 Tensile and impact properties

Tensile strength of unmodified and APTES modified Hal/PLA nanocomposites was shown in **Fig. 6.6**. The experimental values of tensile strength, elongation at break, tensile modulus and impact strength have been summarised in **Table 6.4**. The tensile strength increased with an increase in the loading of Hal nanotubes. Tensile strength of Hal-PLA nanocomposites with 2 wt% of APTES modified Hal nanotubes is 55.9 MPa which is 15% higher than pure PLA. Tensile strength further increased to 62.6 MPa for 4 wt% of silane modified Hal nanotubes i.e. 26.5% higher than pure PLA. This may be due to the presence of hydroxyl groups on the APTES modified Hal nanotubes which results in more hydrogen bond interactions between the modified Hal nanotubes and PLA matrix and consequently mHal are more uniformly dispersed across the PLA matrix. Thus, mHal are more effective in improving the mechanical properties of Hal-PLA nanocomposites. However, higher loading of Hal nanotubes led to decreased tensile strength.

In case of 8 wt% addition of APTES modified and unmodified Hal nanotubes into PLA show decreased tensile strength by more than 15%. This is mainly due to aggregation of Hal nanotubes across the PLA matrix which enhances the formation of stress concentration points lead to reduce mechanical properties (Liu et al., 2013). The decreased tensile strength of Hal-PLA nanocomposites with higher loading of Hal nanotubes may be due to the weakening of interfacial hydrogen bonding and also due to more agglomeration (as shown in the morphology results of **Fig. 6.4**). The

agglomeration of Hal nanotubes acts as the stress-concentration points which decreases the tensile strength. These observations corroborate the results obtained from FTIR and FE-SEM analyses. Thus, Hal nanotubes above 4 wt% decreased the tensile strength by more than 15%. Similar results have been reported (Du et al., 2006; Evagelia et al., 2011). Even a smaller loading (2 wt%) of nanosilica into PLA matrix increased the tensile strength and modulus by 15% and 37% respectively as compared to pure PLA (Evagelia et al., 2011).

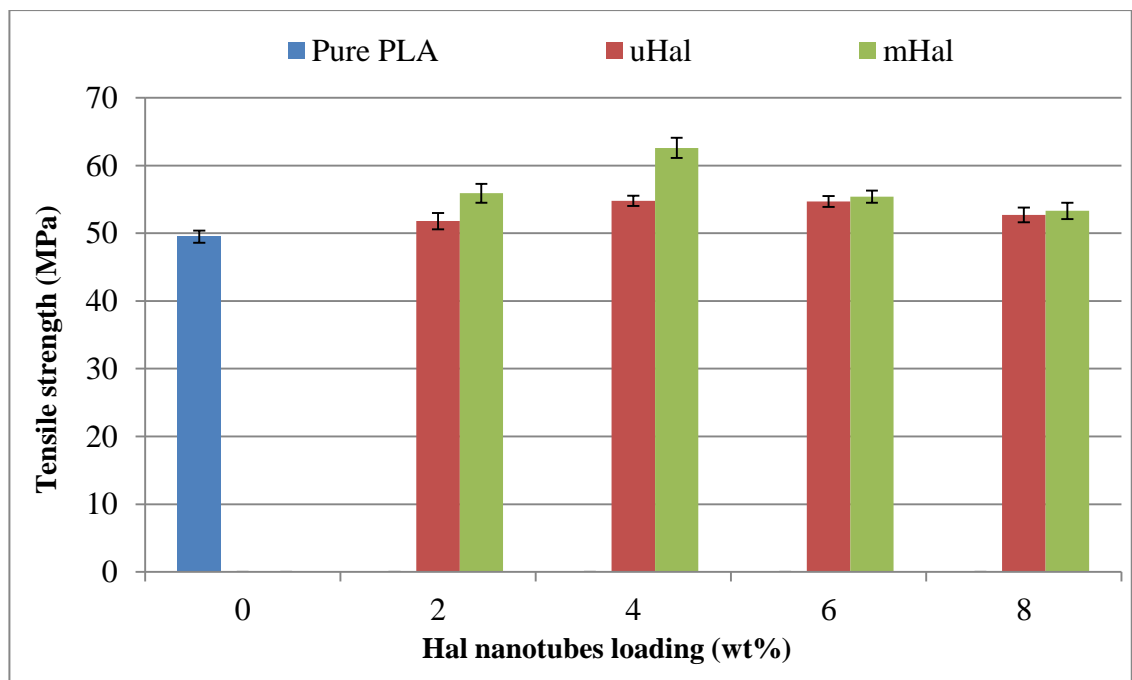


Fig. 6.6 Tensile strength of unmodified and APTES modified Hal-PLA nanocomposites

Tensile modulus (**Fig. 6.7**) increased gradually with the loading of Hal nanotubes into the PLA matrix. Tensile modulus increased to 1270 MPa for 8 wt% of APTES modified Hal nanotubes into PLA, which is 20% higher than pure PLA and approximately 5% higher than the unmodified Hal-PLA nanocomposites. Similar observations were reported by many other researchers (Wu et al., 2013). Prashantha et al. (2011) reported that the tensile strength and modulus increased from 22 to 35%

and 32 to 40% respectively, with the addition of quaternary ammonium salts modified Hal nanotubes into PP matrix as compared to pure PP. The addition of MAPTS (3-(trimethoxysilyl) propyl methacrylate) modified Hal nanotubes into polyamide 6 (PA6) matrix resulted in a significant improvement in the tensile properties, where the tensile strength increased by 21% with the addition of 10 wt% MAPTS modified Hal-PA6 nanocomposites as compared to unmodified Hal-PA6 nanocomposites (Guo et al., 2009).

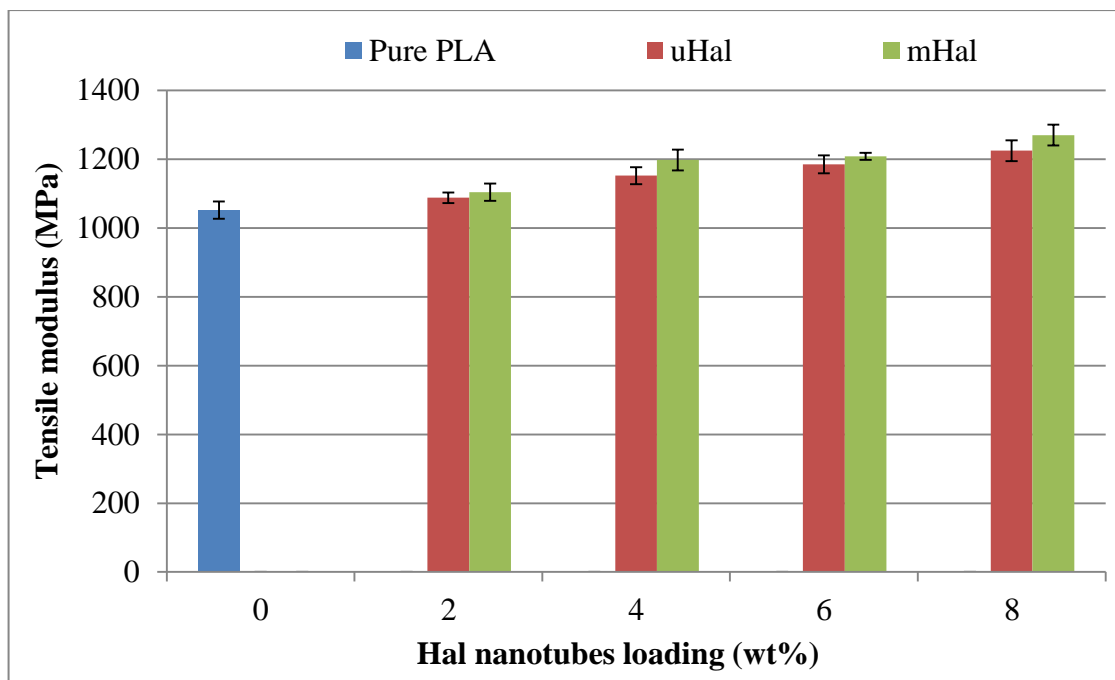


Fig. 6.7 Tensile modulus of Hal nanotubes (unmodified (uHal) and APTES modified Hal nanotubes (mHal)) PLA nanocomposites

Percentage of elongation at break are summarised in **Table 6.4**. Elongation at break increased significantly both for the unmodified and APTES modified Hal nanotubes (4 wt%) reinforced PLA nanocomposites as compared to pure PLA. Elongation at break reached 15.6% with the addition of 4 wt% APTES modified Hal nanotubes which is 50% higher than pure PLA.

An increase in the elongation at break clearly shows that the added Hal nanotubes (both unmodified and APTES modified) into PLA matrix act as plasticizer and dissipate the energy during fracture. Similar results were reported by Liu et al. (2013), where they noticed that the elongation at break increased significantly (>90%) with the addition of 20phr of unmodified Hal nanotubes into PLA matrix as compared to pure PLA. However, elongation at break reduced with the addition of Hal nanotubes above 20phr which clearly shows that small quantities of Hal nanotubes act as plasticizer of PLA.

Table 6.4 Mechanical properties of Hal nanotubes (unmodified and APTES modified) PLA nanocomposites (data in the parentheses indicate the standard deviation)

S. No.	Sample	Hal loading (wt%)	Tensile strength (MPa)	Elongation at break (%)	Tensile modulus (MPa)	Impact strength (J/m)
1	Pure PLA	0	49.5	9.2 (0.5)	1052	21.4
2	2uHal	2	51.8	10.5 (0.4)	1088	22.6
3	2mHal	2	55.9	13 (0.5)	1104	25.6
4	4uHal	4	54.8	12.9 (0.2)	1152	25.9
5	4mHal	4	62.6	15.6 (0.2)	1198	29.8
6	6uHal	6	54.7	9.1 (0.4)	1185	29.4
7	6mHal	6	55.4	9.5 (0.5)	1208	30.3
8	8uHal	8	52.7	9.5 (0.2)	1225	23.9
9	8mHal	8	53.3	10.3 (0.2)	1270	24.8

The impact strength of unmodified and APTES modified Hal nanotubes reinforced PLA nanocomposites measured according to ASTM 256 and the results have been shown in **Fig. 6.8**. The impact strength for the Hal-PLA nanocomposites increased by loading Hal nanotubes into PLA matrix and it was higher than pristine PLA. For instance, the impact strength of 6 wt% mHNT loading was 30.3 J/m, which is 41.5% higher than pure PLA. However, a further increase in Hal nanotubes loading (8 wt%) to PLA led to a decrease (up to 25%) in the impact strength, which may be due to more aggregation of Hal nanotubes as well as poor interactions between Hal nanotubes and PLA.

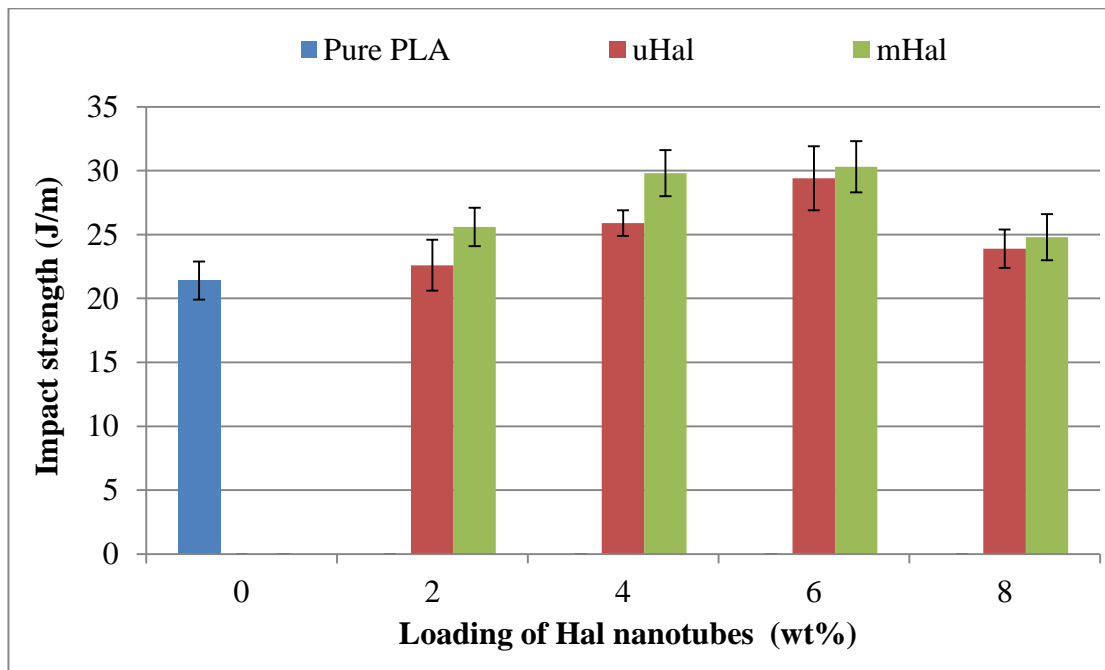


Fig. 6.8 Impact strength of Hal nanotubes (unmodified (uHal) and APTES modified (mHal)) PLA nanocomposites

Similar results were reported by Albdiry and Yousif (2013), where they noticed that the impact strength increased by 50% with the addition of 3 wt% APTES modified Hal nanotubes into unsaturated polyester as compared to neat unsaturated polyester. But, a further addition of Hal nanotubes decreased the impact strength of the CPN.

Liu et al. (2013) reported that the flexural and impact strength increased by 34% and 70% respectively with the addition of 30 phr of unmodified Hal nanotubes into PLA matrix as compared to pure PLA. However, a further addition of Hal nanotubes into the PLA matrix caused a reduction in the flexural and impact strength by 10% and 50% respectively. Lin et al. (2011) also reported similar results, where they noted that the addition of 5 wt% Hal nanotubes into polystyrene increased the impact strength by 300%. However, a further addition of Hal nanotubes (10 wt%) decreased the impact strength by 150%.

6.6 DMA analysis

The visco-elastic properties of unmodified and APTES modified Hal nanotubes filled PLA polymer nanocomposites were studied by dynamic mechanical analysis. This study is useful to evaluate the performance of materials under stress and temperature. The dynamic mechanical properties of 4 and 8 wt % of both the unmodified and APTES modified Hal nanotubes reinforced PLA nanocomposites as well as pure PLA were studied in terms of storage modulus (E') and damping factor ($\tan \delta$) as a function of temperature and the obtained results have been represented in **Figs. 6.9 and 6.10**.

At room temperature the Hal-PLA nanocomposites exhibit higher storage modulus (**Fig. 6.9 and Table 6.5**) as compared to pure PLA. The APTES modified Hal-PLA nanocomposites show higher storage modulus than unmodified Hal nanotubes and pure PLA. This is a clear evidence for the better dispersion of Hal nanotubes across the PLA matrix. APTES modified Hal nanotubes fillers have good interaction with PLA matrix and lead to the formation of stiffened interphase, which restricts the mobility of polymer chains resulting in an increase in the storage modulus.

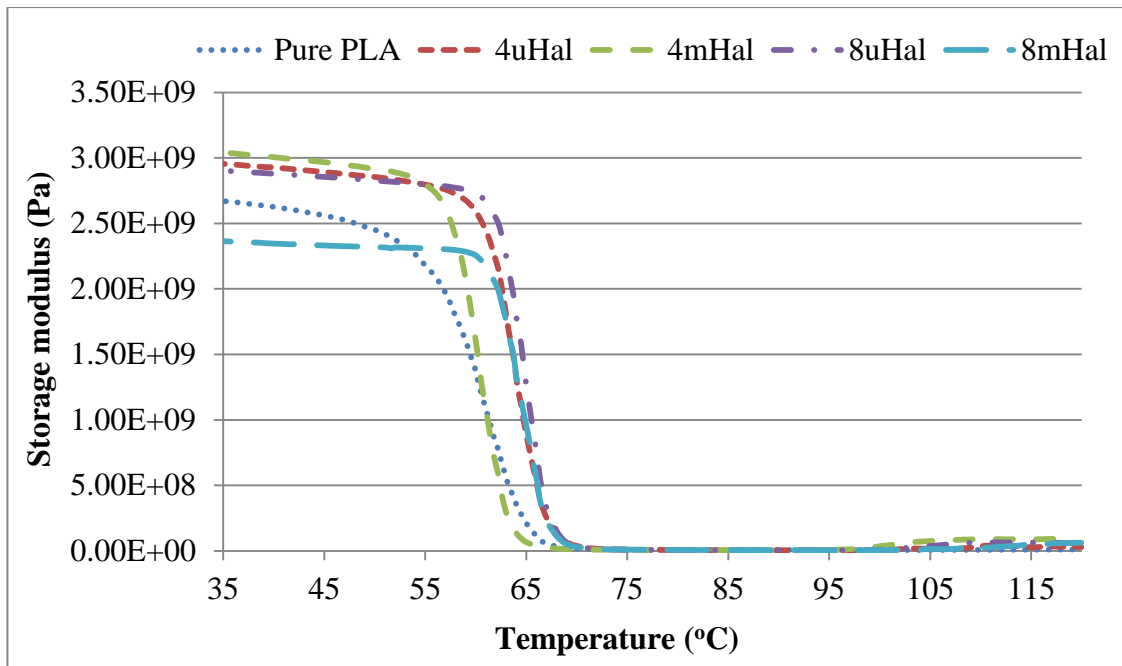


Fig. 6.9 storage modulus of Hal (unmodified (uHal) and APTES modified (mHal))
PLA nanocomposites

Storage modulus increased by more than 15% with the addition of 4 wt% of APTES modified Hal nanotubes as compared to pure PLA. Surprisingly there is only a slight increase (<5%) in the storage modulus with the addition of APTES modified Hal-PLA nanocomposites as compared to unmodified Hal nanotubes. A further addition of APTES modified Hal nanotubes (8 wt%) led to a decrease in the modulus, may be due to an increase in the aggregation of fillers. Filler aggregation in the CPN causes stress concentration points which lead to decrease the mechanical properties (Liu et al., 2013; Khonakdar, 2015). The elastic properties of CPN are measured by $\tan \delta$, which is the ratio of energy dissipated (loss modulus) to energy stored (storage modulus) per cycle. Hence, the elastic property of a material is inversely proportional to $\tan \delta$. The glass transition temperature (T_g) is determined by the maximum peak of $\tan \delta$ with respect to temperature (**Fig. 6. 10**).

The T_g of Hal-PLA nanocomposites is higher as compared to pure PLA due to the addition of unmodified Hal nanotubes into the PLA matrix which restricts the mobility of polymer chains resulting into an increase in T_g (Khonakdar, 2015).

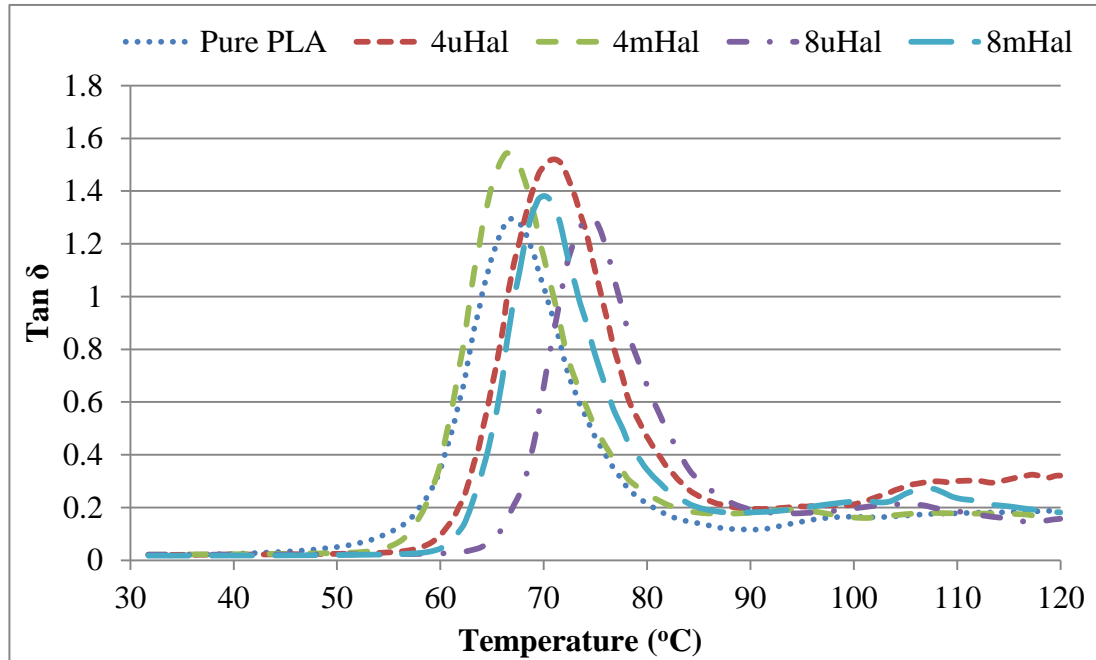


Fig. 6.10 Comparison of Tan delta values of Hal nanotubes (unmodified (uHal) and APTES modified (mHal)) PLA nanocomposites

However, this is not the case with APTES modified Hal-PLA nanocomposites, where a slight reduction in the T_g was observed as compared to pure PLA (**Table 6.5**). This again confirms the improvement in the elasticity of CPN with APTES modified Hal nanotubes which is in agreement with the tensile properties. Similar results have been reported by Rong et al. (2001), where they noticed that T_g of pure PP was 19.45 °C, but with the addition of 1 wt% clay filler T_g reduced to 12.54 °C. Pasbakhsh et al. (2010) and Shelley et al. (2001) were also reported similar reductions in the T_g with the addition of surface modified clay fillers into EPDM and nylon-6 CPN.

Table 6.5 storage modulus (at room temperature) and peak temperature of $\tan \delta$ (T_g) of Hal nanotubes (unmodified (uHal) and APTES modified (mHal)) PLA nanocomposites

S. No.	Pure PLA	4uHal	4mHal	8uHal	8mHal
Storage modulus (GPa)	2.69	2.98	3.06	2.92	2.37
T_g ($^{\circ}\text{C}$)	66.7	70.8	66.3	74.3	69.98

6.7 TGA analysis

The thermal stability of unmodified and APTES modified Hal nanotubes and their PLA nanocomposites were studied by TGA and the results have been reported in **Figs. 6.11 and 6.12 and Table 6.6**). The first mass loss for the unmodified Hal (uHal) reinforced PLA nanocomposites is in the temperature range from 60 to 180 $^{\circ}\text{C}$ (**Fig. 6.11**).

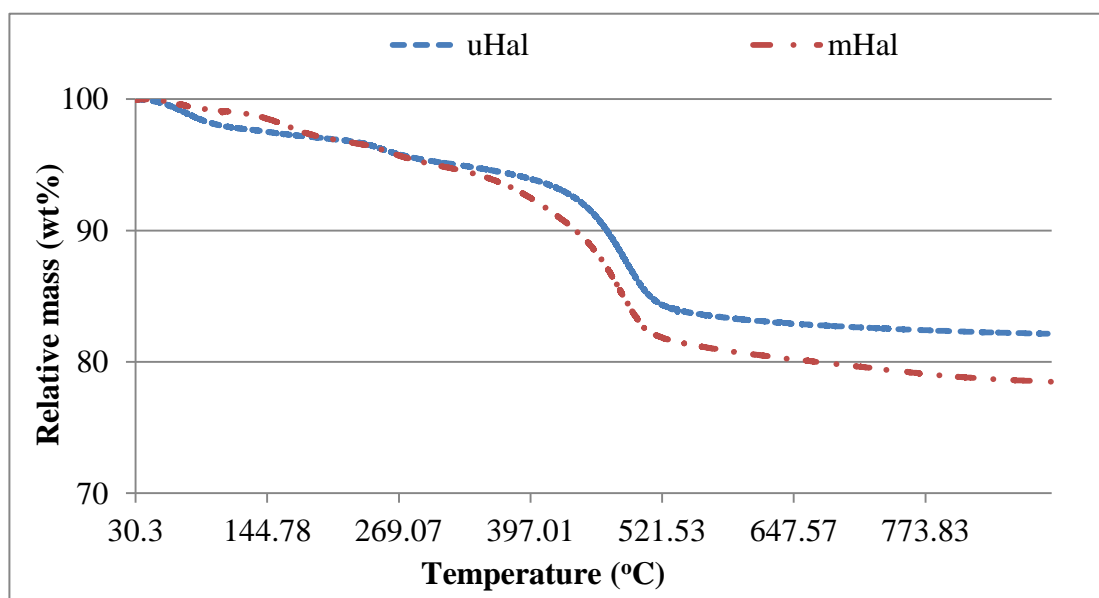


Fig. 6.11 TGA curves of (A) unmodified (uHal) and (B) APTES modified Hal nanotubes (mHal)

This mass loss corresponds to the evaporation of absorbed water from the surface and internal channels of Hal nanotubes. However, this mass loss curve has not been observed in case of APTES modified Hal nanotubes. This proves that the modification of Hal nanotubes with APTES leads to more water repellent property. The second mass loss in the temperature range between 200 and 330 °C is associated with the decomposition of hydrogen bond of Hal nanotubes by the secondary interaction or grafting onto Al-OH and Si-O-Si on the inner or outer surface of Hal nanotubes. These hydrogen bonds are much less thermally stable than the covalent bonding (Yuan et al., 2008). The final mass loss peak could be seen approximately from 330 to 550 °C which is related to the dehydroxylation of the residual structure of Al-OH and Si-O-Si groups of the inner and outer surface of Hal nanotubes (Yuan et al., 2008; Albdiry and Yousif, 2014; Carli et al., 2014).

It is also worth mention that APTES modified Hal nanotubes show higher mass loss as compared to unmodified Hal nanotubes. This is due to the decomposition of organic compounds of the APTES grafted onto Hal nanotubes. This again confirms the successful grafting of APTES with Hal nanotubes. Similar results have been reported by other researchers (Yuan et al., 2008; Barrientos-Ramirez et al., 2011; Carli et al., 2014). Thermal stability of both APTES modified and unmodified Hal nanotubes (4 and 8 wt%) filled PLA nanocomposites was studied (**Fig. 6.12**). The characteristic mass loss temperatures obtained from the TGA curves have been summarized in **Table 6.6**. The characteristic temperature at which 5% and 10% mass loss occurs is essential to evaluate the thermal stability of Hal-PLA nanocomposites. The obtained data reveal that the loading of unmodified Hal nanotubes and APTES modified Hal nanotubes have significant impact on the thermal stability of the resultant CPN. For pure PLA, 5% mass loss occurs at a temperature of 320 °C.

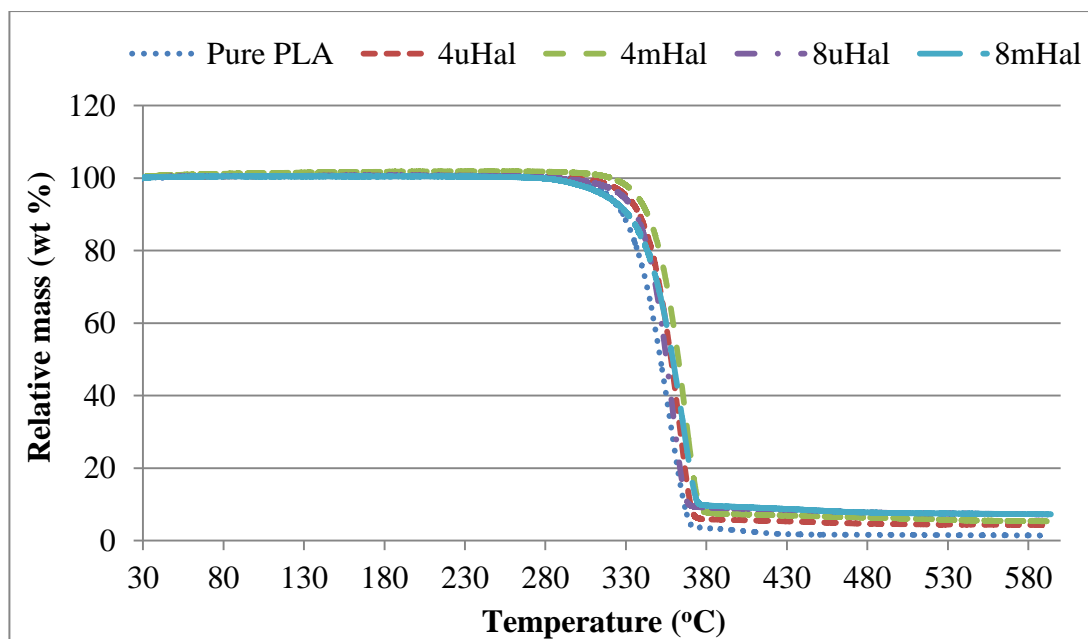


Fig. 6.12 TGA curves of Hal nanotubes (modified and unmodified) PLA nanocomposites

However, the same mass loss of 5% occurs when the temperature was increased to 330 °C, an increase of 10 °C by using 4 wt% unmodified Hal nanotubes filled CPN as compared to pure PLA (**Table 6.6**). This temperature is further increased to 337 °C, an increase of 17 °C for the CPN filled with 4 wt% APTES modified Hal nanotubes. Gilman (1999) reported that the thermal barrier of Hal nanotubes in the Hal-PLA nanocomposites protects the PLA polymer from contacting with fire which slows down the degradation of PLA during the degradation of CPN. It is also reported that the degradation products of polypropylene polymer may be entrapped inside the lumens of Hal nanotubes, resulting in an effective delay in mass transfer which remarkably improves the thermal stability of the nanocomposites (Du et al., 2006). It is mentioned that the intercalated layered silicate nanofillers had much better effects on the thermal stability of polymer matrix than the exfoliated layered silicate nanofillers (Gilman, 1999; Wang and Huang, 2013).

Table 6.6 Thermal properties of Hal nanotubes (unmodified (uHal) and APTES modified (mHal)) PLA nanocomposites

S. No.	Sample	Hal nanotubes loading (wt %)	T _{5% mass loss} (°C)	T _{10% mass loss} (°C)	T _{max mass loss} (°C)
1	Pure PLA	0	320	328	370
2	2uHal	2	325	333	375
3	2mHal	2	326	335	376
4	4uHal	4	330	338	377
5	4mHal	4	337	343	378
6	6uHal	6	329	337	374
7	6mHal	6	332	341	375
8	8uHal	8	328	336	373
9	8mHal	8	318	331	376

However, a further increase in Hal nanotubes (>6 wt%) decreased the thermal stability which is similar to the results observed in the previous investigations. A decrease in the thermal stability with a relatively higher Hal nanotubes loading due to the fact that Hal nanotubes started degradation at above 400 °C which caused higher weight loss. This is in agreement with the previous reported studies of PLA/montmorillonite (Jiang et al., 2007; Chen et al., 2015).

6.8 DSC analysis

PLA is a semicrystalline polymer and its mechanical and thermal properties depend on its crystal microstructure. Enhancement of crystallinity of PLA is an important task for its easy processability. It is reported that the addition of Hal nanotubes into PLA

increased the crystallinity of Hal-PLA nanocomposites. The cold crystallisation peak of PLA (T_{cc}) shifted to lower temperature with the addition of Hal nanotubes into PLA (Fig. 6.13 and Table 6.7).

The T_{cc} of 4 wt% loading of mHal was at 122.8 °C, which was 9.8 °C lower than 2 wt% loading of Hal nanotubes. The heterogeneous nucleating effect can be observed with the addition of Hal nanotubes on the PLA (Kontou et al., 2011; Liu et al., 2013; Wang and Qiu, 2011). With a small amount of Hal nanotubes, the nucleating effect of Hal nanotubes dominates and increases the cold crystallinity temperature. In case of higher loading of Hal nanotubes, the restriction of mobility of chains dominates in the PLA matrix which leads to decrease the crystallinity temperature.

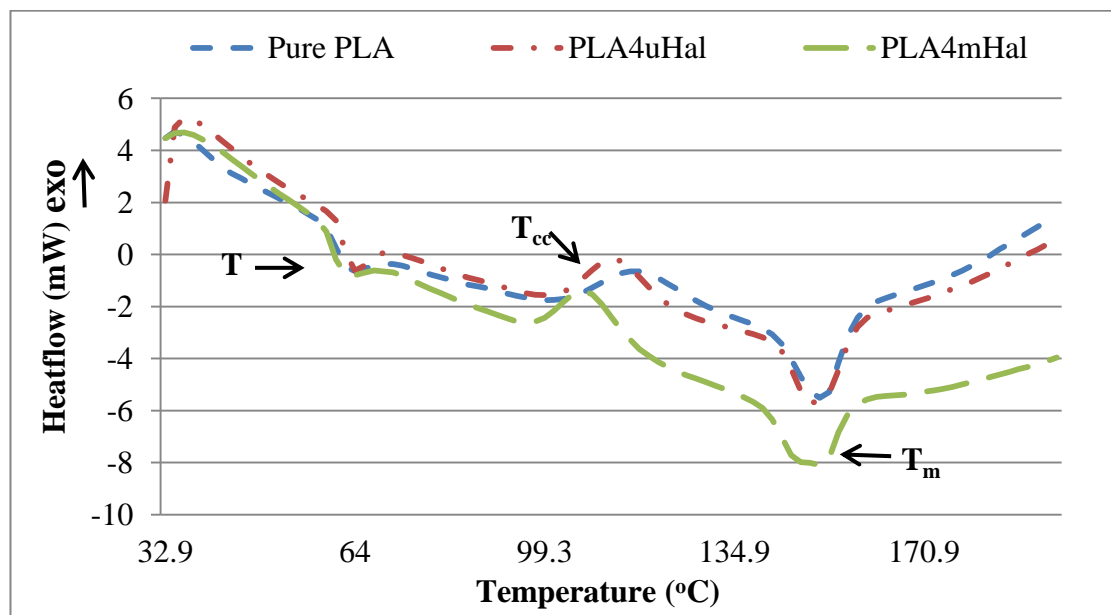


Fig. 6.13 DSC curves of Hal nanotubes (unmodified (uHal) and APTES modified (mHal)) PLA nanocomposites

Hal nanotubes play a dual role of improving the crystallinity of Hal-PLA nanocomposites. On one hand, it acts as a nucleating agent and on the other hand, the strong hydrogen bond interactions between Hal nanotubes and PLA chains restrict the

mobility of PLA chains. According to the reports by Krikorian and Pochan, (2005) and Liu et al., (2009) the exfoliated Hal/PLA nanocomposites form stable intercalated tactoids which act as heterogeneous nucleation sites, which significantly lower the crystallisation temperature. Addition of Hal nanotubes into PLA matrix increased the percentage crystallinity (%X_c).

Table 6.7 DSC results of Hal nanotubes (unmodified (uHal) and APTES modified (mHal)) PLA nanocomposites

S. No.	Sample	Hal nanotubes loading (wt%)	T _g (°C)	T _{cc} (°C)	T _m (°C)	X _c (%)
1	Pure PLA	0	58.4	117.9	153	15.25
2	2uHal	2	59.1	115.8	148.6	22.9
3	2mHal	2	59.7	116.2	151.34	17.20
4	4uHal	4	59.8	111.2	150.34	23.8
5	4mHal	4	60.2	106.4	150.25	19.82
6	6uHal	6	61.1	105.5	149.5	25.2
7	6mHal	6	61.8	105.18	149.0	23.5

The crystallinity increased significantly by 65% with the addition of 6 wt% of Hal nanotubes into Hal/PLA nanocomposites. A significant increase in the crystallinity (by 65%) could be seen in the Hal/PLA nanocomposites with the addition of Hal nanotubes due to nucleating effects. However, in case of APTES modified Hal/PLA nanocomposites, percentage of crystallinity slightly reduced with an increase in the loading of Hal nanotubes. This may be due to increased covalent bonding between Hal nanotubes and PLA matrix which leads to restricting the mobility of PLA

polymer chain around the Hal nanotubes and the crystal growth was retarded. Glass transition temperature (T_g) also increased by increasing the loading of Hal nanotubes in the Hal-PLA nanocomposites. All the Hal nanotubes filled CPN showed higher T_g at 59.7 °C, 60.2 °C and 61.8 °C for 2, 4 and 6 wt % of APTES modified Hal nanotubes respectively as compared to pure PLA. This supports the restriction of mobility in the polymer chain induced by the addition of Hal nanotubes and also the effective interfacial interaction between the Hal nanotubes and PLA matrix (Rittigstein et al., 2007).

6.9 Conclusions

In this investigation, halloysite (Hal) nanotubes were surface modified with 3-aminopropyltriethoxysilane (APTES) to enhance the surface interaction of Hal nanotubes with PLA and to achieve a good dispersion of Hal nanotubes across the PLA matrix. FTIR, Nitrogen adsorption-desorption analysis and FE-SEM with EDX analysis confirmed not only the grafting of APTES at the edges and surface of Hal nanotubes, but also confirmed the hydrogen bond interactions between PLA and Hal nanotubes. Morphological studies of the PLA nanocomposites with APTES modified Hal nanotubes using FE-SEM revealed good dispersion of nanofillers into PLA which lead to improving the mechanical and thermal properties. Tensile strength and modulus increased significantly by 26.5% and 20% with the addition of 4 and 8 wt% of APTES modified Hal nanotubes respectively as compared to pure PLA. Impact strength of 4 wt% APTES modified Hal-PLA nanocomposites was 29.8 MPa, which is 20% higher than the unmodified Hal-PLA nanocomposites and 40% higher than the pure PLA. DMA results showed a considerable increase (>10%) in the storage modulus after the addition of silane treated Hal nanotubes as compared to pure PLA. Thermal stability also increased by 17 °C as compared to pure PLA.

CHAPTER VII

Results and Discussion: Sisal-PP Composites

7.1 FE-SEM analysis

The morphology of untreated, alkali and HIU treated short sisal fibre reinforced PP (SF/PP) composites was studied by examining the fractured surfaces of tensile tested samples using FE-SEM. FE-SEM micrographs of fracture surface of untreated and treated SF/PP composites (containing 30 wt%) have been shown in **Fig. 7.1**. It could be seen that the sisal fibres are in unidirectional and well dispersed throughout PP matrix. Untreated SF/PP composites (**Fig. 7.1A**) exhibit fibre debonding due to the accumulation of moisture at the interface specifically from the surface of sisal fibres. It also indicates the number of voids between the fibre and matrix which is the evidence of poor adhesion responsible for the reduction in the mechanical properties. However, reduction of voids for alkali and HIU SF/PP composites confirmed the removal of amorphous materials after the treatment (**Figs. 7.1B, 7.1C and 7.1D**). HIU treated sisal fibre composites showed good dispersion across the matrix and the reduction of voids resulting in good mechanical properties (**Fig. 7.1B**). Morphology of alkali treated sisal fibre composites exhibits good dispersion as well as improved adhesion between fibre and matrix phase (**Fig. 7.1C**). **Fig. 7.1D** shows the FE-SEM image of combined alkali and HIU treated SF/PP composites. It could be seen that the fibres are well separated with the combined treatment of alkali and HIU which leads to enhancing the reactive surface area and resulting into good adhesion between fibre and matrix.

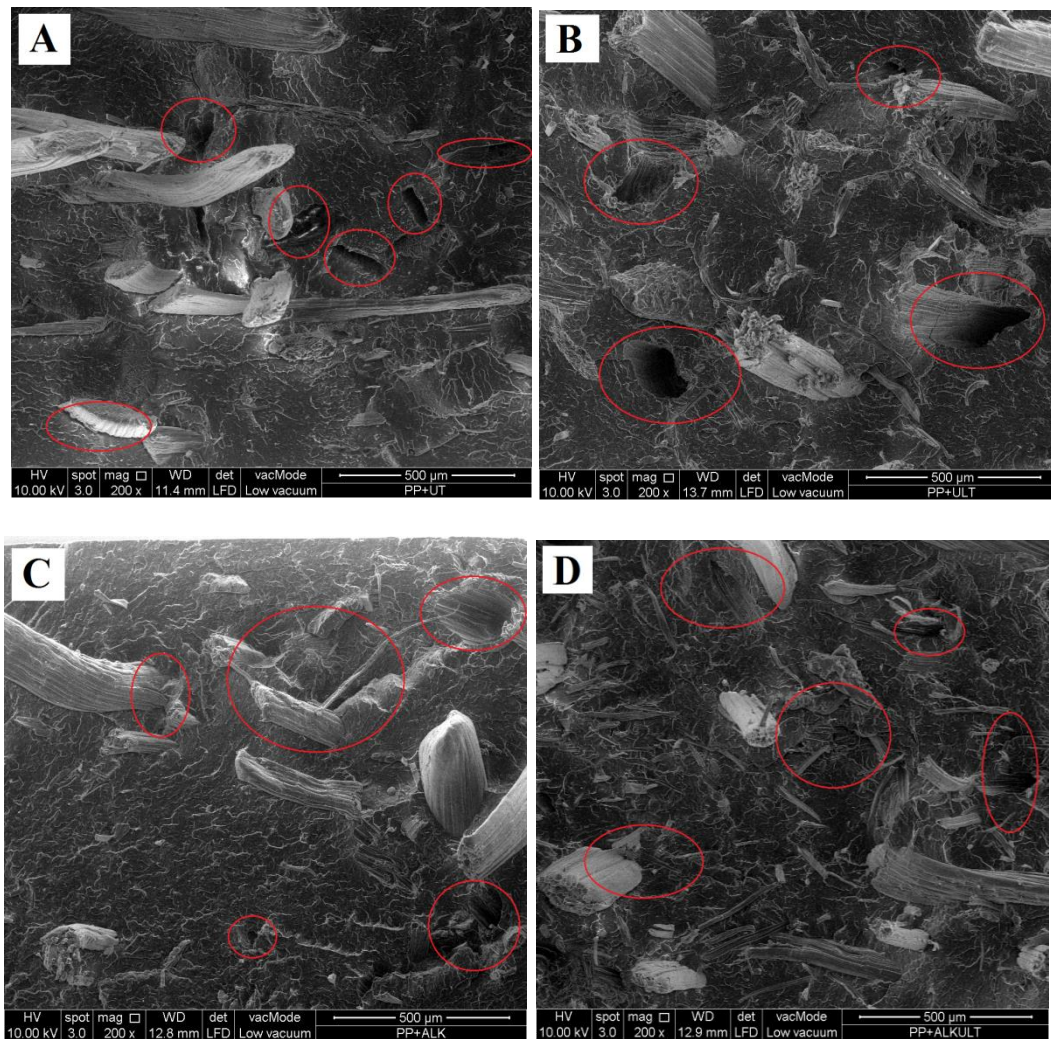


Fig. 7.1 FE-SEM micrographs of impact fractured SF/PP composites (A) Untreated (UT), (B) HIU treated (ULT), (C) Alkali treated (ALKT), (D) Combined treatment of alkali and HIU (ALKT-ULT)

7.2 Tensile properties

Tensile properties were studied to understand the effects of fibre loading and surface treatments on the mechanical properties of SF/PP composites. Tensile properties (tensile strength, modulus and elongation) of untreated and HIU treated, alkali treated and the combination of alkali and HIU treated SF/PP composites have been shown in **Figs. 7.2, 7.3 and 7.4**. It could be seen that the tensile strength is higher for 10 wt% fibre loading as compared to 15, 20 and 30 wt%. This is may be due to more number

of voids with higher filler content as well as weak interfacial adhesion between the hydrophilic filler and the hydrophobic polymer matrix with higher percentage of filler loading. Similar observations were found by other researchers. Paraparita et al. (2014) found that the tensile strength decreased significantly by more than 40% for 30 wt% of filler loading. Demir et al. (2006) observed a reduction in the tensile strength by 41% with more than 15 wt% of fibre loading in luffa fibres reinforced PP composites. Das and Satapathy (2011) observed similar results with cenosphere fibres reinforced PP composites. They indicated that the tensile strength decreased by the addition of filler. However, tensile modulus increased by more than 35% with the addition of 20 wt% of fibre fillers.

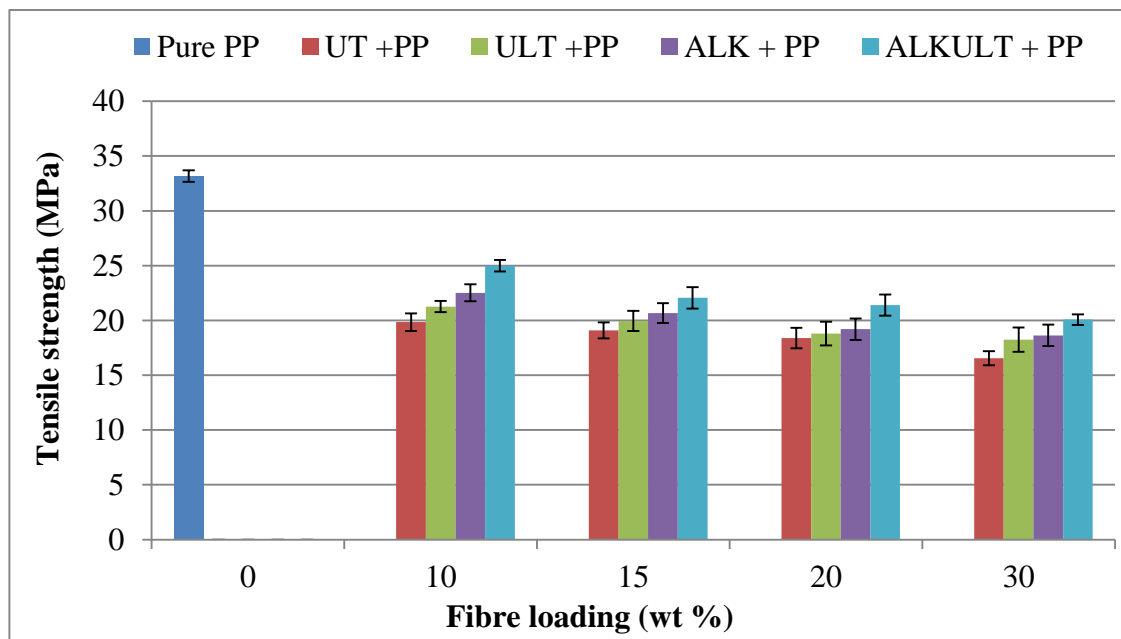


Fig. 7.2 Tensile strength of untreated and treated sisal fibre reinforced PP composites

- 1) Untreated (UT)
- 2) HIU treated (ULT)
- 3) Alkali treated (ALK)
- 4) combined treatment of alkali and HIU (ALK-ULT)

It could be seen from the **Fig. 7.2** the tensile strength of pure PP was 33.18 MPa. With the addition 10 wt% of untreated sisal fibres into PP matrix leads to significant

reduction of tensile strength by 67%. This is mainly due to presence of amorphous materials on the surface of the sisal fibres which are the responsible for water absorption and causing incompatibility with PP matrix which results of reduced mechanical properties. However, a significant increment of tensile strength could be observed with the addition of surface treated sisal fibres. Addition of 10 wt% of the combination of alkali and HIU treated sisal fibres into PP matrix increased the tensile strength by 25% as compared to untreated sisal fibre reinforced PP composites (**Fig. 7.2**). This is mainly due to an increase in the adhesion between treated fibres and matrix materials owing to the removal of amorphous materials by alkali and HIU treatments from the fibre surface whereby the fibre surface becomes clean and rough. Removal of amorphous materials from the fibre surface also reduces the moisture absorption which leads to an increase in the tensile strength and modulus of the fibre reinforced composites. Similar to tensile strength, elongation at break significantly decreased as the filler content increased (**Fig. 7.3**). Percentage elongation decreased by more than 65% with the addition of 10 wt% of untreated sisal fibres. This may be due to the restriction of molecular mobility with an increase in the filler in the matrix. However, only 35% of elongation at break was reduced for the combined treated alkali and HIU treated sisal fibres as compared to pure PP composites. This indicates that after the combined treatment with alkali and HIU, fibres surface become hydrophobic which improved the compatibility between fibre materials and hydrophobic polymer matrix. However, with higher filler content above 10 wt%, elongation decreased to the maximum of 80 % for 30 wt% of filler loading. This may be due to an increase in the fibre agglomeration and voids which lead to decrease the elongation.

Tensile modulus of untreated, HIU treated, alkali and the combination of alkali and HIU treated SF/PP composites is shown in **Fig. 7.4**. Tensile modulus significantly increased by more than 55% for 30 wt% addition of sisal fibres with the combined treatment of alkali and HIU as compared to pure PP. It is to be noted that the tensile modulus increased gradually with the addition of sisal fibres from 10 wt% onwards.

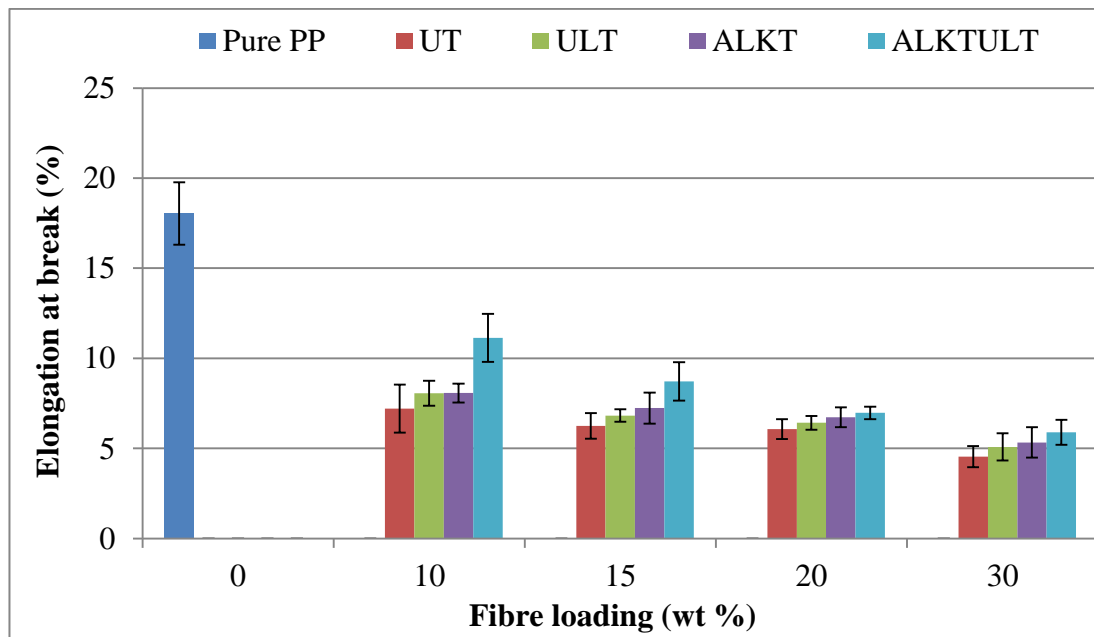


Fig. 7.3 Elongation at break of untreated and treated sisal fibre reinforced PP composites

Combination of alkali and HIU treated SF/PP composites show a significant increment in tensile modulus. This indicates that after the combined treatment of alkali and HIU a good interaction occurs between the sisal fibres and PP matrix which resulting into a good dispersion of fibre materials across the matrix and leads to an enhancement in the material stiffness. Kaewkuk et al. (2013) reported that the tensile modulus increased by two-fold for alkali treated SF/PP composites as compared to untreated fibres and considerable improvement was observed in the tensile strength for alkali treated sisal fibres. Elongation at break was reduced with increasing the

filler content. However, it slightly increased with alkali treated fibres composites as compared to untreated fibres.

Arrakhiz et al. (2012) and Elkhaoulani et al. (2013) studied the effects of alkali treatments on the mechanical and thermal properties of natural fibre reinforced polymer composites. They observed that the tensile modulus increased significantly by 145% with the addition of 30 wt% of treated Doum fibres reinforced low density polyethylene as compared to pure matrix. However, tensile strength significantly decreased with an increase in the filler. Mohan and Kanny (2012) reported that after alkali treatment tensile modulus increased by 30% with 20 wt% of filler content. Mwaikambo et al. (2007) reported that after alkali treatment the hemp fibres reinforced euphorbia composites showed an increase in the tensile strength and modulus by 31 and 13% respectively as compared to the untreated fibres.

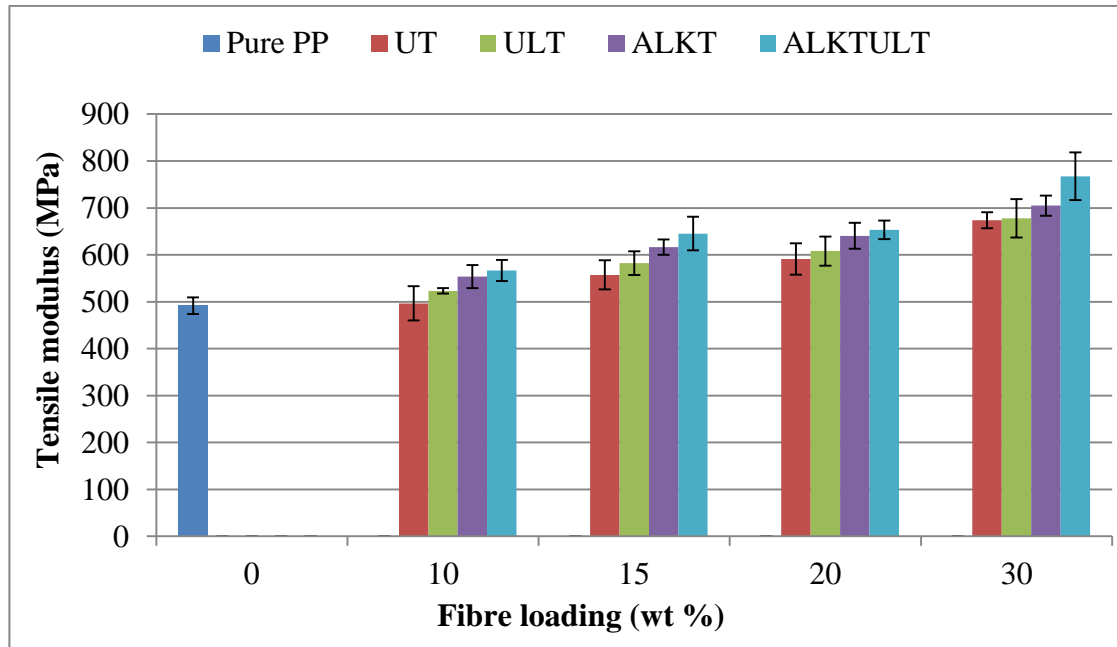


Fig. 7.4 Tensile modulus of untreated and treated sisal fibre reinforced PP composites

7.3 TGA analysis

The effect of different surface treatments on the thermal stability of SF/PP composites was evaluated. **Fig. 7.5** shows the TGA curves of pure PP, untreated and different surface treated SF/PP composites. Relatively a small degradation could be observed for the SF/PP composites in the temperature range from 90 to 150 °C are due to the presence of moisture in sisal fibres. However, this step could not be seen in case of pure PP. Pure PP has single stage degradation in the temperature range between 330 and 460 °C with the maximum degradation occurred at 450 °C.

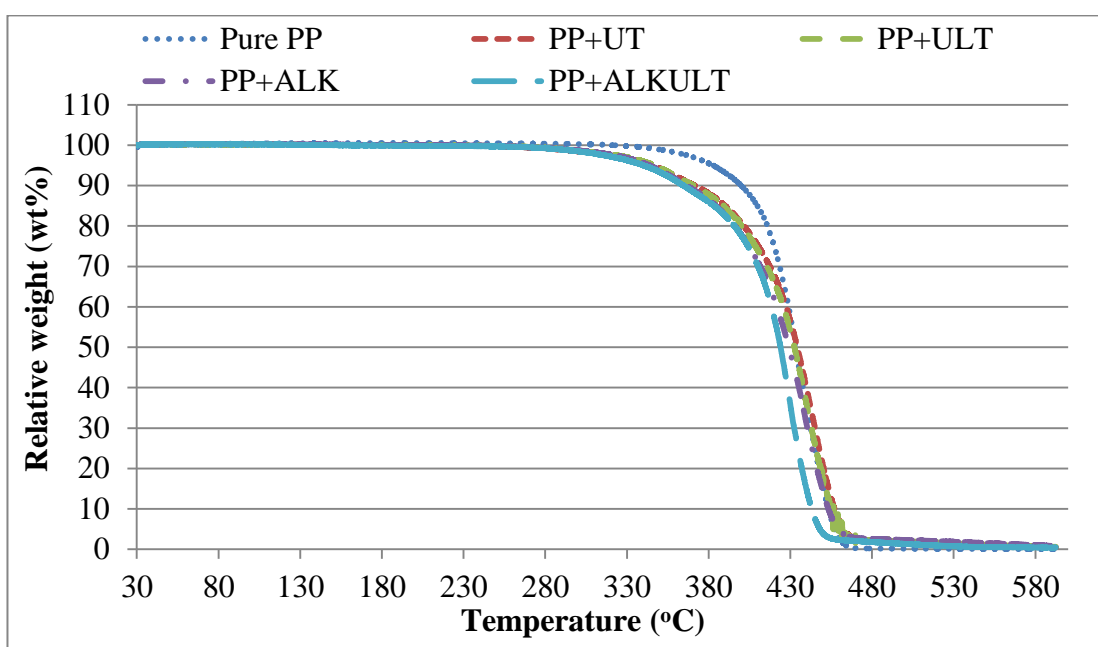


Fig. 7.5 TGA of untreated (UT), HIU treated (ULT), alkali treated (ALK) and the combination of alkali and HIU treated (ALKULT) SF/ PP composites

As seen in the **Fig. 7.5**, the thermal stability reduced significantly in the temperature range from 250 to 430 °C for the PP composites reinforced with untreated and surface treated sisal fibres as compared to pure PP. For instance, 10% weight loss could be noticed at 371.5 °C for the untreated SF/PP composites which is 28.5 °C higher than pure PP. This could be due to the presence of amorphous materials such as

hemicellulose, pectin and lignin in the untreated sisal fibres which are low in thermal stability as compared to pure PP matrix and thus leads to faster thermal degradation. Similar results were reported by other researchers.

Essabir et al. (2013b) studied the mechanical and thermal properties of PP based composites reinforced with argan particle net shells and observed that the thermal stability of argan particle reinforced PP composites was considerably reduced which is mainly due to the presence of amorphous materials on the surface of untreated fibres. Arrakhiz et al. (2012) studied the effect of different surface treatments (alkali, etherification and esterification treatments) on the mechanical and thermal properties of alfa fibre reinforced PP composites and reported a significant increment in the thermal stability for the surface treated alfa fibre reinforced PP composites as compared to untreated alfa fibre composites. The esterification (combination of alkali and ethyl ether) treatment showed better in removing the amorphous materials from the surface of alfa fibres and resulted in improving the thermal stability.

However, in case of surface treated sisal fibres (HIU (ULT), alkali (ALK) and the combination of alkali and HIU treated (ALKULT)) reinforced PP composites showed a marginal high thermal stability as compared to untreated SF/PP composites. Combination of alkali and HIU treated SF/PP composites showed 10% weight loss temperature at 372 °C which is 8 °C higher than untreated SF/PP composites. A significant increment in the thermal stability for the combination of alkali and HIU treated SF/PP composites proves that the amorphous materials from the surface of sisal fibres were removed significantly thereby increased the number of cellulose molecules on the surface of sisal fibres.

Kaewkuk et al. (2013) studied the effect of interfacial modification on the physical properties of SF/PP composites and found that alkali treated SF/PP composites showed higher thermal stability by more than 10 °C as compared to untreated SF/PP composites. Oza et al. (2014) also studied the effect of fibre surface treatment on the thermal stability of hemp fibres reinforced PLA composites and reported that the alkali treated hemp fibres reinforced PLA composites showed higher thermal stability by more than 6 °C as compared to untreated hemp fibres reinforced PLA composites. They also indicated that the increased thermal stability for the alkali treated fibre composites is due to the mercerisation which removed the amorphous materials from the surface of fibres and exposed more number of cellulose molecules.

7.4 DSC analysis

Pure PP, sisal fibres with surface treated and untreated reinforced PP composites were subjected to DSC analysis to evaluate the crystallisation and thermal properties. **Figs. 7.6 and 7.7** show the DSC thermograms of melting endotherm and cooling exotherm curves of PP and their sisal fibre composites with untreated and different surface treatments respectively. From **Fig. 7.7**, only a marginal effect of crystallisation temperature (T_{cc}) with the addition of fibres into PLA matrix could be noticed. However, melting temperature (T_m) increased with the addition of surface treated fibre to PP matrix. The combination of alkali and HIU treated SF/PP composite displayed a melting temperature around 166.25 °C which is 3.1 °C higher as compared to pure PP. This observation of higher melting temperature after the addition of surface treated sisal fibre is due to an increased interfacial adhesion between the surface treated sisal fibres and PP matrix.

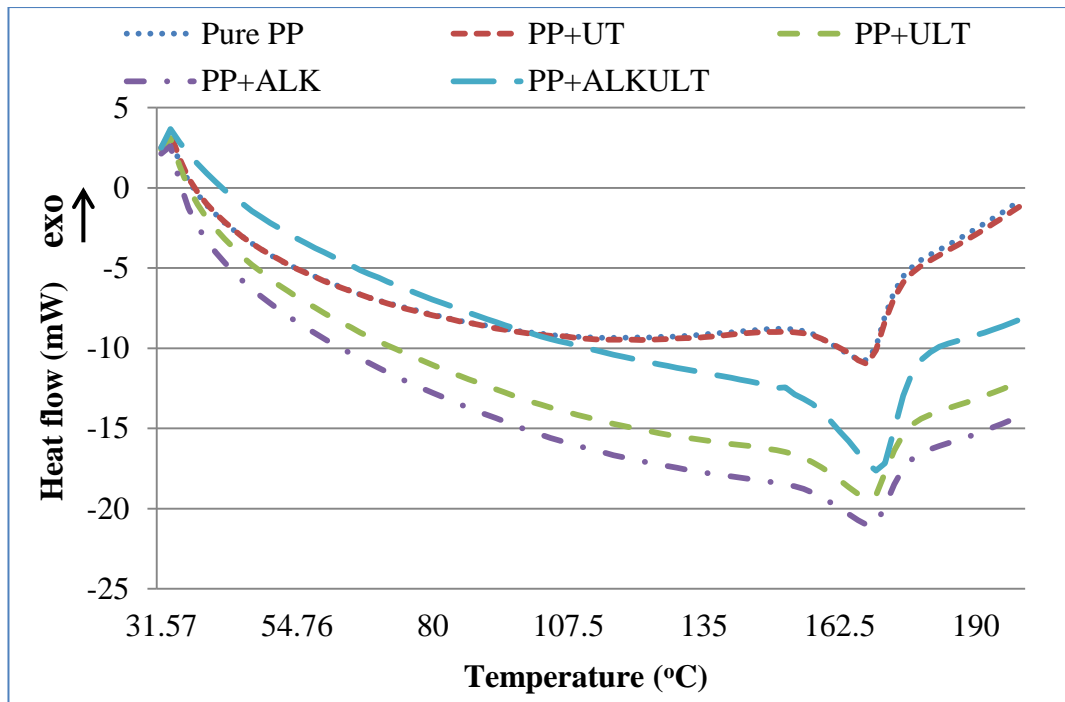


Fig. 7.6 DSC endothermic heating curves of untreated (UT), HIU treated (ULT), alkali treated (ALK), and the combination of alkali and HIU treated (ALKULT) SF/PP composites

Similar results have been reported by Joseph et al. (2003) where they noted an increase in the melting temperature by 14 °C after the addition of sisal fibres treated with maleic anhydride into PP composites. The percentage of crystallinity (X_c) shows that the pure PP has highest percentage of crystallinity which was 43.68%. However, loading of small quantity (10 wt%) of untreated sisal fibres into PP matrix results of disturbed in the crystalline structure of PP polymer which leads to significant reduction of percentage of crystallinity to 30.35%. However, addition of surface treated sisal fibres into PP leads to a considerable increment in the percentage of crystallinity could be observed. The percentage of crystallinity (X_c) is correlated with mechanical properties. In case of tensile strength, tensile strength of pure PP was slightly more than 33 MPa. With the addition 10 wt% of untreated sisal fibres into PP

matrix leads to significant reduction of tensile strength by 67%.

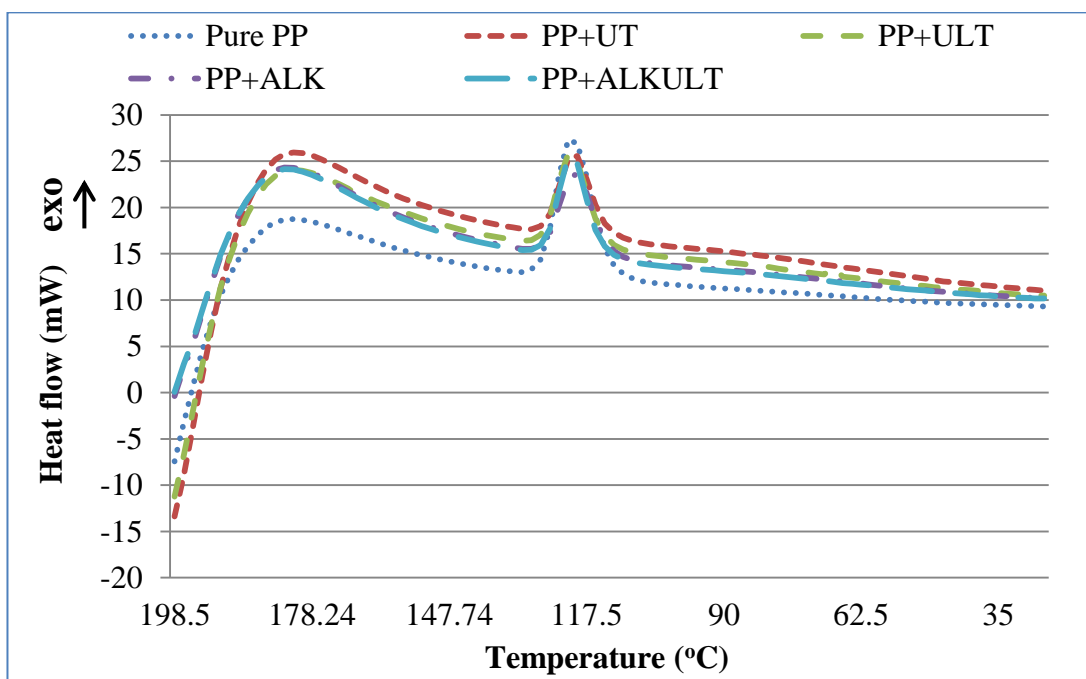


Fig. 7.7 DSC exothermic cooling curves of untreated (UT), HIU treated (ULT), alkali treated (ALK), and the combination of alkali and HIU treated (ALKULT) SF/PP composites

Table 7.1 Thermal properties of PP and untreated and different surface treated SF/PP composites

S. No.	Samples	T _c (°C)	T _m (°C)	X _c (%)
1	Pure PP	119.15	166.25	43.68
2	10UT+PP	119.45	166.34	30.35
3	10ULT+PP	120.62	167.01	32.40
4	10ALK+PP	120.37	168.08	35.63
5	10ALKULT+PP	120.85	169.35	38.13

This is mainly due to presence of amorphous materials on the surface of the sisal fibres which are the responsible for water absorption and causing incompatibility with PP matrix which results of reduced mechanical properties. However, a significant increment of tensile strength could be observed with the addition of surface treated sisal fibres. Addition of 10 wt% of the combination of alkali and HIU treated sisal fibres into PP matrix increased the tensile strength by 25% as compared to untreated sisal fibre reinforced PP composites. Increased tensile strength with the addition of combined treated sisal fibres confirms the removal of amorphous materials and increased the compatibility between sisal fibres and PP matrix. Increased the tensile strength for the combined treated sisal fibres also confirms the increased cellulose content.

7.5 DMA analysis

Storage modulus (E') is defined as the maximum energy stored during one cycle of oscillation. It also gives the material stiffness with the variation of temperature and load bearing capacity of the composite materials (Shinoj et al., 2011). **Fig. 7.8** shows the variations in the storage modulus of pure PP and untreated and different surface treated SF/PP composites with the fibre loading of 10 wt%. As seen in **Fig. 7.8**, at lower temperature the storage modulus (E') for pure PP and their composites filled with different surface treated sisal fibres exhibited higher values. It is worth noted that the storage modulus increased with the addition of sisal fibres into PP polymer. For instance, the storage modulus was 3.5 GPa for pure PP at $-51\text{ }^{\circ}\text{C}$. However, the storage modulus increased marginally to 4 GPa with the addition of 10 wt% of untreated sisal fibres into PP matrix. The increased storage modulus with the incorporation of sisal fibres is due to the reinforcement effect of the fibres that

allowed good stress transfer at the fibre-matrix interface in the composites (Joseph et al., 2003; Idicula et al., 2005; Vilay et al., 2008; Essabir et al., 2013a).

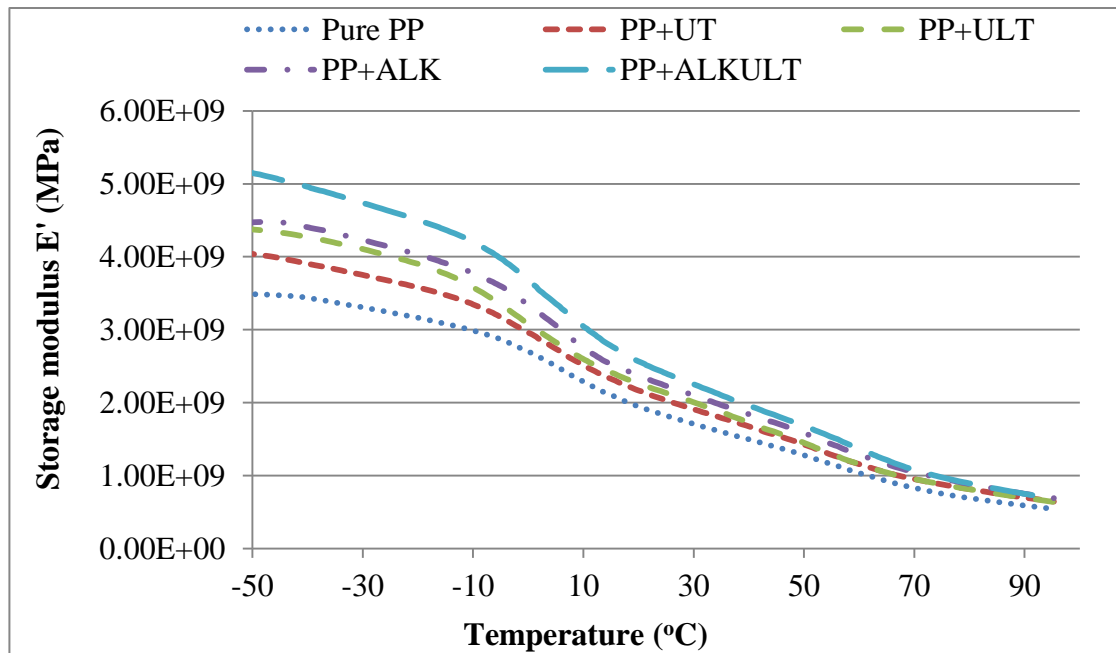


Fig. 7.8 Storage modulus (E') of untreated (UT), HIU treated (ULT), alkali treated (ALK), and the combination of alkali and HIU treated (ALKULT) SF/PP composites

In case of alkali treated and the combination of alkali and HIU treated SF/PP composites, the storage modulus (E') significantly increased by 27.5% and 50% respectively as compared to pure PP. These results proved that sisal fibres treated with alkali and the combination of alkali and HIU show better compatibility with polymer matrix and increased the interfacial adhesion as compared to untreated SF/PP composites (Pothan et al., 2006; Li et al., 2011; Sreenivasan et al., 2015).

Table 7.2 Storage modulus of SF/PP composites

Properties at 30°C	Pure PP	PP + UT	PP + ULT	PP + ALK	PP + ALKULT
Storage modulus	1.17	1.91	2.0	2.1	2.25

A similar trend has been observed by Ray et al. (2002) and Shinoj et al. (2011) for alkali treated jute fibre reinforced vinyl-ester composites and alkali treated oil palm fibre reinforced with LLDPE composites respectively. The damping factor ($\tan \delta$) is the ratio of storage modulus and the loss modulus (i.e. E'/E''). **Fig. 7.9** shows the curves of damping factor against temperature for pure PP and untreated as well as different surface treated SF/PP composites with 10% fibre loading. The damping peak reduced for sisal fibres composites as compared to pure PP which could be due to the incorporation of sisal fibres into the polymer matrix which restricts the mobility of polymer chain and leads to an increase in the storage modulus and a reduction in the viscoelastic lag between stress and the strain, thereby decreasing the damping factor with the addition of filler material (Jawaid et al., 2013; Ray et al., 2002; Sreenivasan et al., 2015).

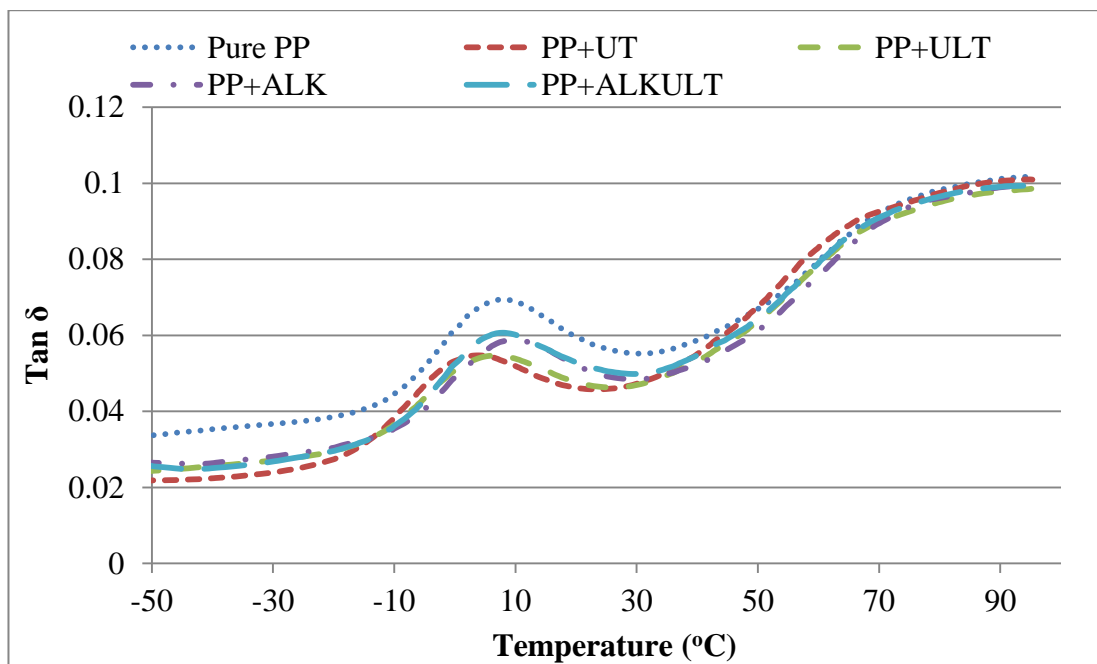


Fig. 7.9 $\tan \delta$ curves of untreated (UT), HIU treated (ULT), alkali treated (ALK), and the combination of alkali and HIU treated (ALKULT) SF/PP composites

It was also found that the peak of damping factor further decreased for the surface treatment of SF with HIU, alkali and the combination of alkali and HIU treatments. This further confirms the improved interfacial adhesion between surface treated sisal fibres and PP matrix after the surface treatment of sisal fibres with the combined alkali and HIU treatments (Ray et al., 2002; Pothan et al., 2003; Jawaid et al., 2013).

Loss modulus (E'') indicates the ability of a material to dissipate the absorbed energy within it in the form of heat or molecular rearrangements when force is applied. It shows the viscous nature of the polymer material (Saba et al., 2016). **Fig. 7.10** shows the loss modulus (E'') curves of pure PP and untreated as well as different surface treated SF/PP composites with 10% fibre loading. The results of loss modulus revealed that the incorporation of sisal fibres into PP matrix leads to an increase in the loss modulus which is due to the restriction in the molecular motion with an increase in the filler materials (Khonakdar, 2015; Sreenivasan et al., 2015). Broad peaks could be noticed in **Fig. 7.10** in the temperature range between -20 and 30 °C which represent the transition from glassy to rubbery state. The maximum temperature peak of loss modulus represents the maximum energy dissipation during the deformation occurred. It is observed that E'' curves reach maximum peak value and then decreased sharply with a further increase in the temperature which is due to free molecular motion of the polymer matrix. However, it is noticed that the sisal fibres composite obtained by the combination of alkali and HIU shows higher loss modulus (E'') by 0.9 GPa as compared to pure PP. This could be due to the increased stiffness after the combined treatment of alkali and HIU which is also an evidence of good compatibility between sisal fibres and PP matrix (Sreenivasan et al., 2015).

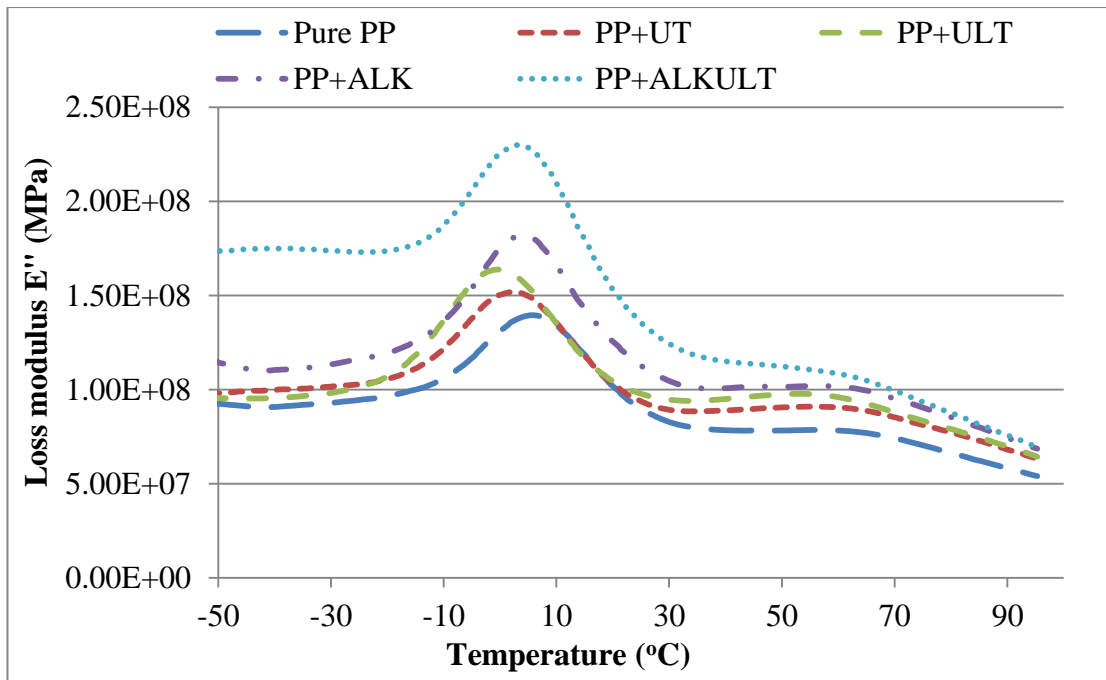


Fig. 7.10 Loss modulus curves of untreated (UT), HIU treated (ULT), alkali treated (ALK), and the combination of alkali and HIU treated (ALKULT) SF/PP composites

7.6 Water absorption studies

Water absorption characteristics of different weight percentage of untreated, HIU treated, alkali treated and the combination of alkali and HIU treated SF/PP composites have been evaluated. **Fig. 7.11** shows the effect of water absorption with increased fibre loading into PP matrix. It can be seen that the water absorption gradually increased with an increase in the fibre loading. In the initial stage of water immersion the composites showed very rapid diffusion of water absorption linearly. After reaching the equilibrium, the water absorption then slowed down and became constant. These findings indicate that the water absorption of SF/PP composites obeys the Fick's law of diffusion. Yew et al. (2005) reported the water absorption and enzymatic degradation of Polylactide (PLA) composites reinforced with rice starch where they observed a rapid water absorption in the first few days for the rice starch

reinforced PLA composites. The water absorption was as high as 5.7% for the fibre reinforced composites as compared to pure PLA which was 1%.

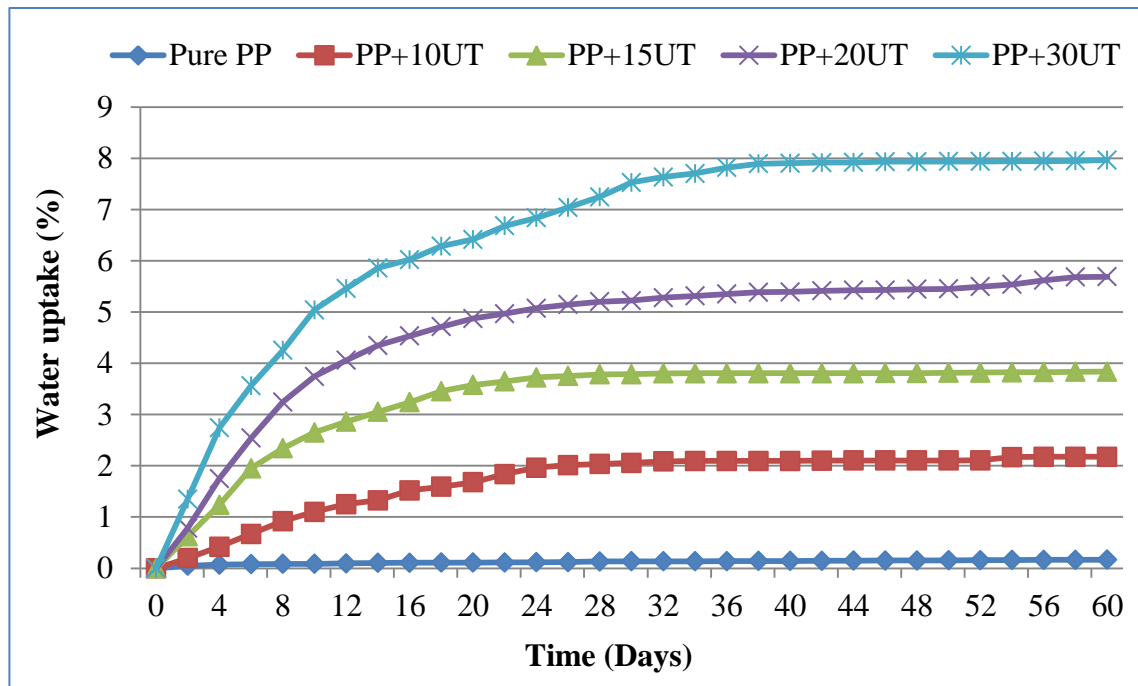


Fig. 7.11 Effect of fibre loading on the water absorption of untreated SF/PP composites

Alamri and Low (2013) studied the water absorption properties of cellulose fibre and nanoclay reinforced epoxy composites where they also noticed that the water absorption was higher in the initial time of immersion for all the fibre reinforced epoxy composites and then reached to a saturation point. As seen in **Fig. 7.11**, the rate of water absorption significantly increased with the addition of sisal fibres which is obvious that sisal fibres are hydrophilic in nature due to the presence of amorphous materials which allow the absorption of water molecules. It is observed that the water absorption rate increased by 8%, 5.69%, 3.83% and 2.17% with the addition of 30, 20, 15 and 10 wt% of untreated sisal fibres into PP matrix respectively after continued water immersion for 60 days. **Fig. 7.12** shows the comparison of the effect of different

surface treatments of SF/PP composites on water absorption. Rate of water absorption significantly decreased for the PP composites reinforced with sisal fibres treated with the combination of alkali and HIU.

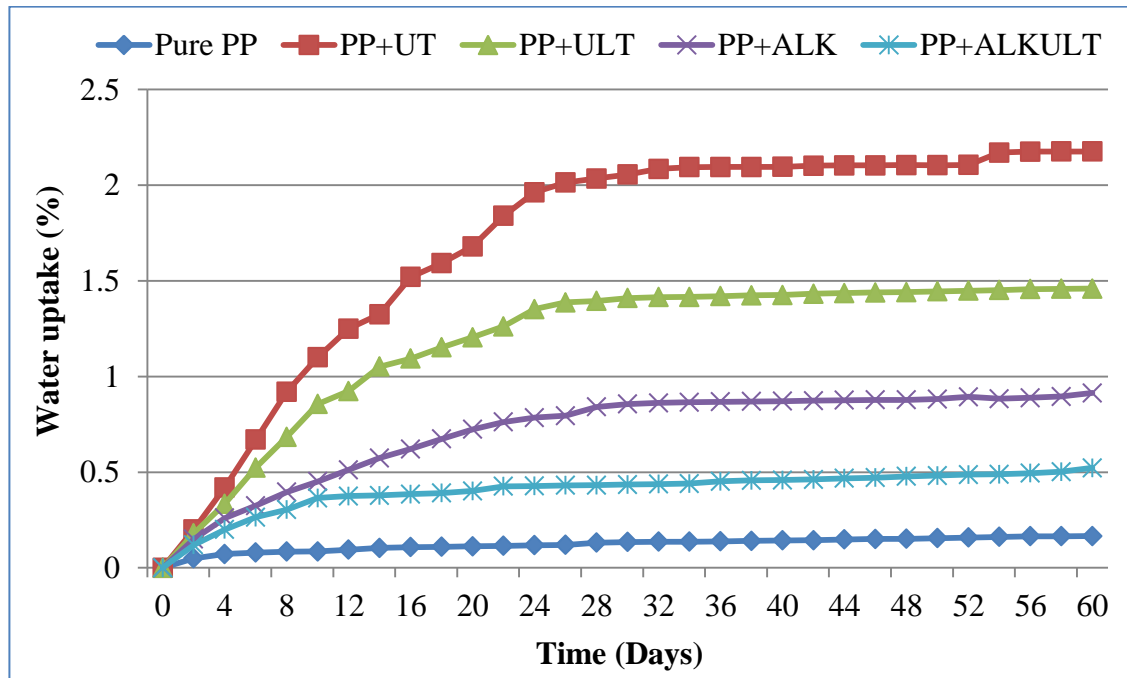


Fig. 7.12 Effect of HIU (ULT), alkali (ALK) and the combination of alkali and HIU (ALKULT) surface treatments on the water absorption of SF/PP composites

Water absorption for the combined alkali and HIU treated sisal fibres reduced to 0.52% which is more than a reduction of 300% as compared to untreated sisal fibre composites. This proves that the combined treatment of alkali and HIU significantly removed the amorphous materials from the surface of sisal fibres and increased the interfacial adhesion between PP matrix and sisal fibres in the composites and is in agreement with FTIR and FE-SEM results.

Rajesh et al. (2015) studied the effect of different weight percentage and surface treatments of SF loading on PLA composites and noticed an increase in the rate of water absorption by more than 9% with the addition of untreated sisal fibres (25 wt%)

into PLA matrix. However, the water absorption rate reduced to more than 3% in case of alkali treated sisal fibres (25 wt%) into PLA matrix. Also, with the addition of 30 wt% of sisal fibres into PP polymer matrix, the water absorption increased significantly by 600% as compared to 10 wt% of SF/PP composites (Chow et al., 2007). Mohan and Kanny (2012) studied the effect of alkali and clay treatments on water absorption for SF/PP composites and observed that the alkali and the combination of alkali and clay treated SF/PP composites show a considerable reduction in the water absorption by 8% and 17.6% as compared to untreated SF/PP composites.

The diffusion properties of SF/PP composites were explained by Fick's law and the values of percentage of water absorption and the coefficient of diffusion at room temperature for the untreated and different surface treated SF/PP composites have been calculated by using **eqns. 3.5 and 3.6** respectively and the obtained results have been given in **Table 7.2**. It can be seen that the diffusion coefficient increased with an increase in the fibre content. The diffusion coefficient increased by 3.42 mm²/sec with the addition of 30 wt% of untreated sisal fibres into PP matrix, which is 250% and 190% higher as compared to pure PP and 10 wt% addition of untreated SF/PP composites respectively. A significant increment in the rate of diffusion coefficient with higher loading of sisal fibres is due to an increase in the cellulose content. Similar results were reported by Dhakal et al. (2007a) where they noticed an increase in the rate of diffusion coefficient significantly by 180% with the addition of 26 wt% of hemp fibre/unsaturated polyester composites as compared to adding 10 wt% hemp fibre/unsaturated polyester composites. There is a considerable reduction in the rate of diffusion coefficient for the surface treated sisal fibre composites as compared to untreated fibre composites. The combination of alkali and HIU treated SF/PP

composites showed a decrease in the diffusion coefficient by 30% as compared to untreated SF/PP composites.

Table 7.3 Water absorption of SF/PP composites

Samples	Fibre loading (wt%)	Type of surface treatments	Maximum water absorption (%)	Initial slope of plot (k) M(t) versus $t^{1/2}$	Diffusion coefficient, D, $\times 10^{-3}$ (mm²/sec)
Pure PP	0	-	0.166	0.0038	0.9561
10UT	10	Untreated	2.176	0.0601	1.5495
15UT	15	Untreated	3.8368	0.0844	2.0451
20UT	20	Untreated	5.69	0.1287	2.6242
30UT	30	Untreated	7.966	0.1937	3.4251
10ULT	10	HIU treated	1.459	0.0378	1.3713
10ALK	10	Alkali treated	0.914	0.0238	1.1873
10ALKULT	10	Alkali + HIU treated	0.522	0.0105	1.0883

This again proved that the removal of amorphous materials from the surface of sisal fibres which are mainly responsible for the absorption of water. Mohan and Kanny (2012) studied the effect of chemical surface treatment on the water absorption of SF/PP composites where they noticed a reduction in the water absorption by 2.2% for the surface treated sisal fibre composites as compared to pure PP which is due to an improved interfacial adhesion between the sisal fibres and the matrix with the removal of hemicellulose, lignin and pectin from the surface of sisal fibres which are highly

hydrophilic in nature. Rajesh et al. (2015) and Yeh et al. (2015) also reported a significant reduction of water absorption for the chemically surface treated SF/PLA composites and rice husk/PP composites respectively as compared to their respective matrix.

7.7 Conclusions

In this investigation, halloysite (Hal) nanotubes were surface modified with 3-aminopropyltriethoxysilane (APTES) to enhance the surface interaction of Hal nanotubes with polylactide or poly (lactic acid) (PLA) and to achieve a good dispersion of Hal nanotubes across the PLA matrix. FTIR, Nitrogen adsorption-desorption analysis and FE-SEM with EDX analysis confirmed not only the grafting of APTES at the edges and surface of Hal nanotubes, but also confirmed the hydrogen bond interactions between PLA and Hal nanotubes. Morphological studies of the PLA nanocomposites with APTES modified Hal nanotubes using FE-SEM revealed good dispersion of nanofillers into PLA which lead to improving the mechanical and thermal properties. Tensile and impact properties significantly increased with the addition of APTES modified Hal nanotubes into PLA matrix. Tensile strength and modulus increased significantly by 26.5% and 20% with the addition of 4 and 8 wt% of APTES modified Hal nanotubes respectively as compared to pure PLA. Impact strength of 4 wt% APTES modified Hal-PLA nanocomposites was 29.8 MPa, which is 20% higher than the unmodified Hal-PLA nanocomposites and 40% higher than the pure PLA. DMA results showed a considerable increase (>10%) in the storage modulus after the addition of silane treated Hal nanotubes as compared to pure PLA. Thermal stability also increased by 17 °C as compared to pure PLA.

CHAPTER VIII

Results and Discussion: Hal-PP Composites

8.1 FE-SEM analysis

The surface morphology of the impact fractured samples of unmodified and APTES modified Hal nanotubes reinforced PP nanocomposites was investigated. **Figs. 8.1A and B** show the PP nanocomposites reinforced with unmodified and APTES modified Hal nanotubes respectively. The surface pore analysis, nitrogen absorption-desorption, FTIR and FE-SEM analysis of unmodified and APTES modified Hal nanotubes were investigated and discussed in sections 6.2, 6.3, 6.4 and 6.5 respectively.

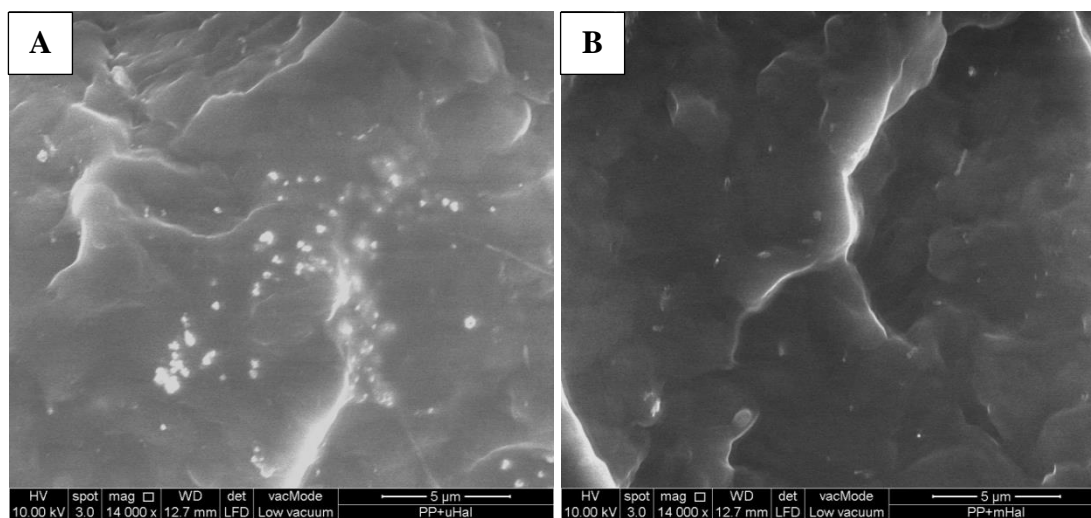


Fig. 8.1 FE-SEM images of impact fractured samples of unmodified (A) and APTES modified (B) Hal nanotubes reinforced PP nanocomposites

From **Fig. 8.1A**, it is clearly seen that the filler agglomeration and poor dispersion of unmodified Hal nanotubes across the PP matrix. As discussed in section 6.3, the filler agglomeration is due to the poor interfacial interaction between unmodified Hal

nanotubes and PP polymer matrix which causes stress concentration and hence leads to lowering the mechanical and thermal properties of Hal-PP nanocomposites. However, in case of APTES modified Hal-PP nanocomposites, nanotubes were well-dispersed across the PP matrix and relatively less agglomeration could be seen as compared to unmodified Hal-PP nanocomposites (**Fig. 8.1B**).

Surface modification of Hal nanotubes with APTES enhances the interfacial adhesion between Hal nanotubes and PP matrix which leads to improve the mechanical and thermal properties of Hal-PP nanocomposites. Moreover, modification of APTES significantly reduced the stress concentration points by increased filler dispersion across PP matrix which leads to good mechanical properties of the nanocomposites (Albdiry and Yousif, 2014; Carli et al., 2014).

8.2 Tensile and impact properties

Fig. 8.2 shows the tensile strength of pure PP and PP nanocomposites reinforced with untreated and APTES treated Hal nanotubes. It is clear from **Fig. 8.2** that a considerable increment of tensile strength with the addition of Hal nanotubes irrespective of their surface modification as compared to pure PP. Addition of 6 wt% of untreated and APTES modified Hal nanotubes into PP matrix increased the tensile strength by 16 and 31% respectively as compared to pure PP. It is observed that APTES modified Hal-PP nanocomposites showed good tensile properties as compared to untreated PP composites. This result proved the well dispersion of Hal nanotubes after the surface modification with APTES which enhances the efficient load transfer and thus good mechanical properties.

In addition to this, a number of hydrogen bond interaction between APTES modified Hal nanotubes and the PP polymer matrix due to the presence of hydroxyl groups on

the surface of APTES modified Hal nanotubes which enhances the compatibility between PP polymer matrix and APTES modified Hal nanotubes leads to increased tensile strength. In addition to the surface modification, high aspect ratio of Hal nanotubes promotes the high number of filler-matrix interaction which further leads to improve the mechanical properties of Hal-PP nanocomposites. These findings well correlate with other reports (Guo et al., 2009; Prashantha et al., 2011).

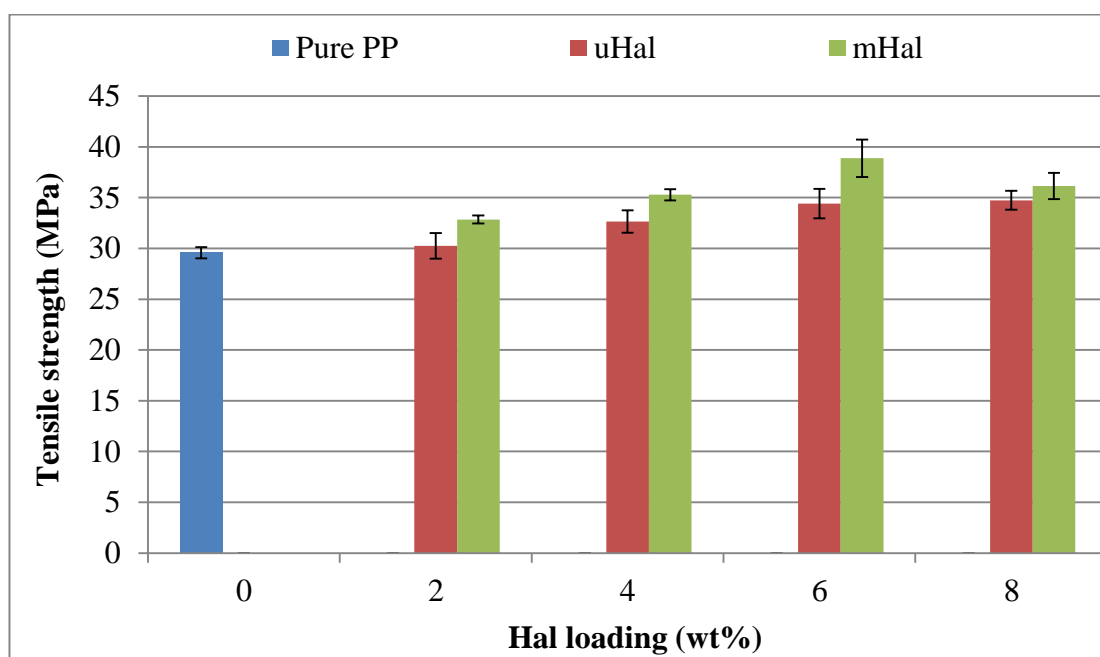


Fig. 8.2 Tensile strength of untreated and APTES modified Hal nanotubes reinforced PP nanocomposites

Guo et al. (2009) reported a significant increment of tensile strength by 21% with the addition of 10 wt% surface modified Hal-Polyamide 6 (PA6) nanocomposites as compared to pure PA6 resin. It is also reported that the tensile strength and modulus increased by 30.3 and 30.4% respectively with the incorporation of 6 wt% of Hal nanotubes into polyamide 6 (PA6) polymer matrix as compared to pure PA6 resin (Prashantha et al., 2011). However, PP nanocomposites with 8 wt% of Hal nanotubes loading show a slight decline in the tensile strength. This may be due to the increased

filler aggregation in the nanocomposites with a further addition of Hal nanotubes above 6 wt%. The filler aggregation with the addition of above optimum quantity of Hal nanotubes leads to poor interfacial adhesion between filler and polymer matrix. **Fig. 8.3** shows the tensile modulus of PP nanocomposites reinforced with unmodified and APTES modified Hal nanotubes. Similar to tensile strength, tensile modulus also significantly increased with an increase in Hal content into PP polymer matrix.

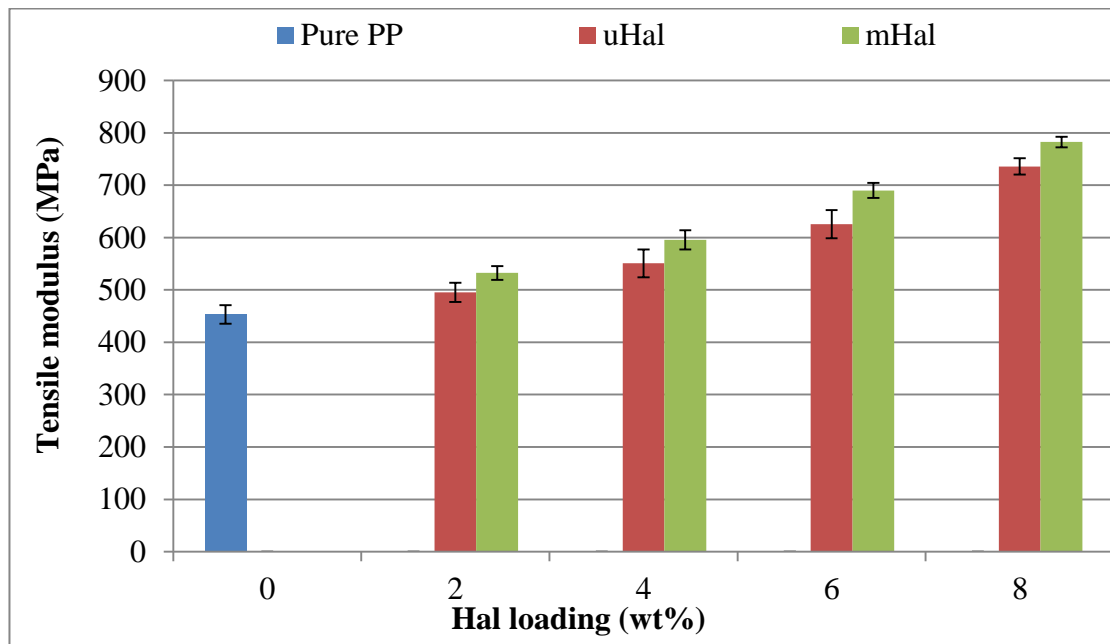


Fig. 8.3 Tensile modulus of unmodified and APTES modified Hal nanotubes reinforced PP nanocomposites

Similar trend was also reported by Albdiry and Yousif (2014) where they noticed that the tensile strength and modulus tend to decrease with a further addition (above 3 wt%) of Hal nanotubes into unsaturated polyester nanocomposites. It was found that the tensile modulus increased significantly by 72% with the addition of 8 wt% of APTES modified Hal-PP nanocomposites as compared to pure PP resin. This result again proved the good dispersion of surface modified Hal nanotubes with APTES across the PP matrix and improved the interfacial adhesion between fillers and the PP

polymer matrix. In contrast to the tensile strength and modulus, a slight reduction in the percentage of elongation at break could be seen with increased loading of Hal nanotubes into PP matrix. **Fig. 8.4** shows the percentage of elongation at break for PP nanocomposites reinforced with unmodified and APTES modified Hal nanotubes.

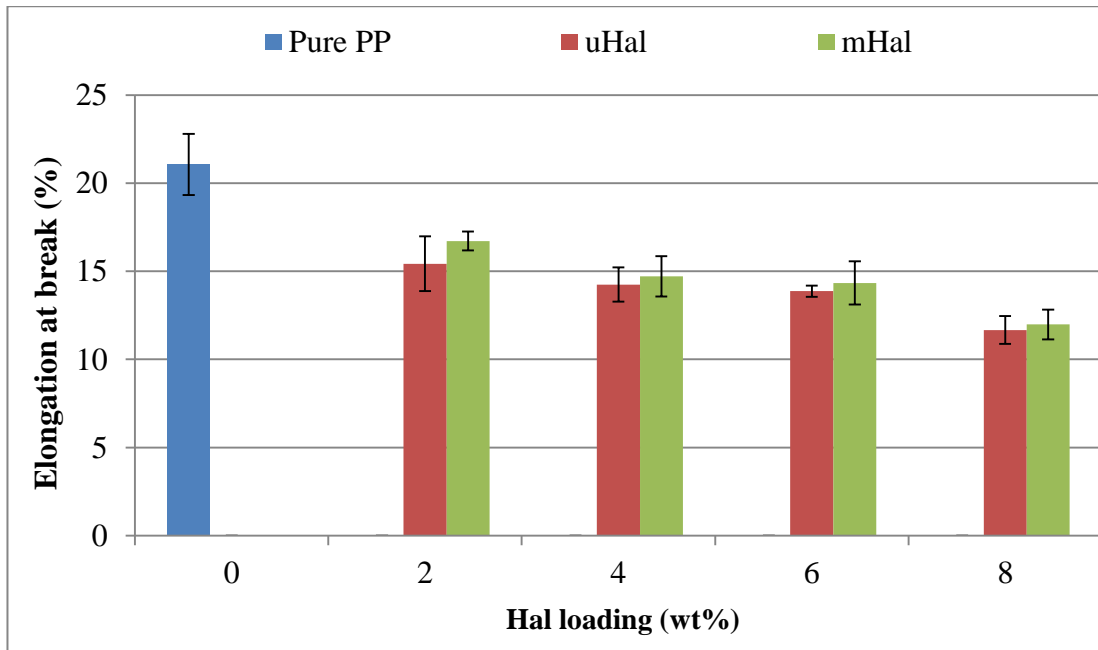


Fig. 8.4 Elongation at break of unmodified and APTES modified Hal nanotubes reinforced PP nanocomposites

The elongation at break decreased by 30% with 8 wt% loading of Hal nanotubes as compared to pure PP. This may be due to an increased rigidity of the polymer chain after the addition of filler. Similar trend has been reported by Prashantha et al. (2011) where they observed that 25% of elongation at break decreased with an increase in the Hal nanotubes by 8 wt% into PP polymer matrix. The effect of APTES modified Hal-PP nanocomposites on the impact property of Hal-PP nanocomposites was investigated. **Fig. 8.4** represents the impact strength of notched samples of unmodified and APTES modified Hal-PP nanocomposites.

A gradual increase in the impact strength could be observed with the addition of Hal nanotubes into PP matrix. It is noticed from **Fig. 8.5** that the impact strength of 6 wt% loading of APTES modified Hal-PP nanocomposites shows 27.8 J/m which is 44% higher than the impact strength of pure PP. It is also worth noted that the surface modified Hal-PP nanocomposites show better impact property as compared to unmodified Hal-PP nanocomposites. The small amount of Hal nanofillers acts as a plasticizer in the nanocomposites which helps to distribute the impact energy throughout the nanocomposites.

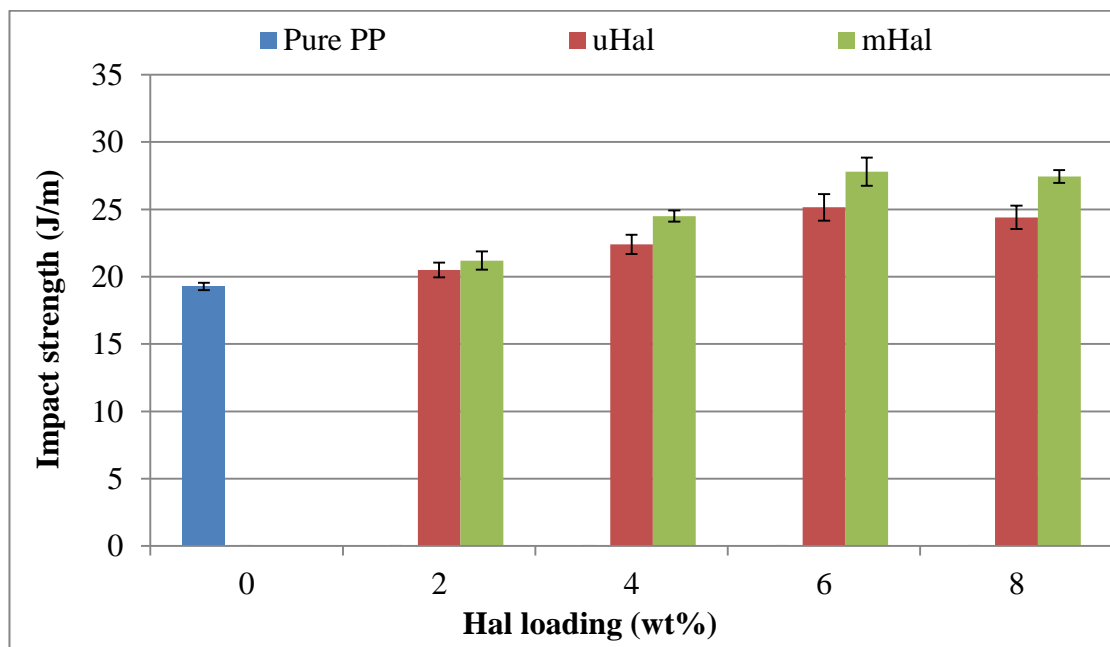


Fig. 8.5 Izod impact strength of notched samples of unmodified and APTES modified Hal-PP nanocomposites

However, decreased toughness could be observed for Hal-PP nanocomposites with a further increase in the filler loading above 6 wt%. Similar results were found out by other researchers (Liu et al., 2013). Prashantha et al. (2011) found that the impact toughness increased by more than 80% with the addition of quaternary ammonium salt modified Hal nanotubes reinforced PP nanocomposites as compared to pure PP.

8.3 TGA analysis

The thermal stability of PP nanocomposites reinforcement with unmodified and APTES modified Hal nanotubes was investigated using TGA. The TGA curves of pure PP and its nanocomposites reinforcement with unmodified and APTES modified Hal nanotubes have been shown in **Fig. 8.6**. It is noticed that only a slight increment in the thermal stability with the addition of Hal nanotubes into PP matrix. The values of temperature at which 50% weight loss occurred and percentage of char residue at maximum temperature (600 °C) are given in **Table 8.1**. It is worth noted that the thermal stability is considerably increased by 15 °C for the APTES modified Hal-PP nanocomposites as compared to pure PP.

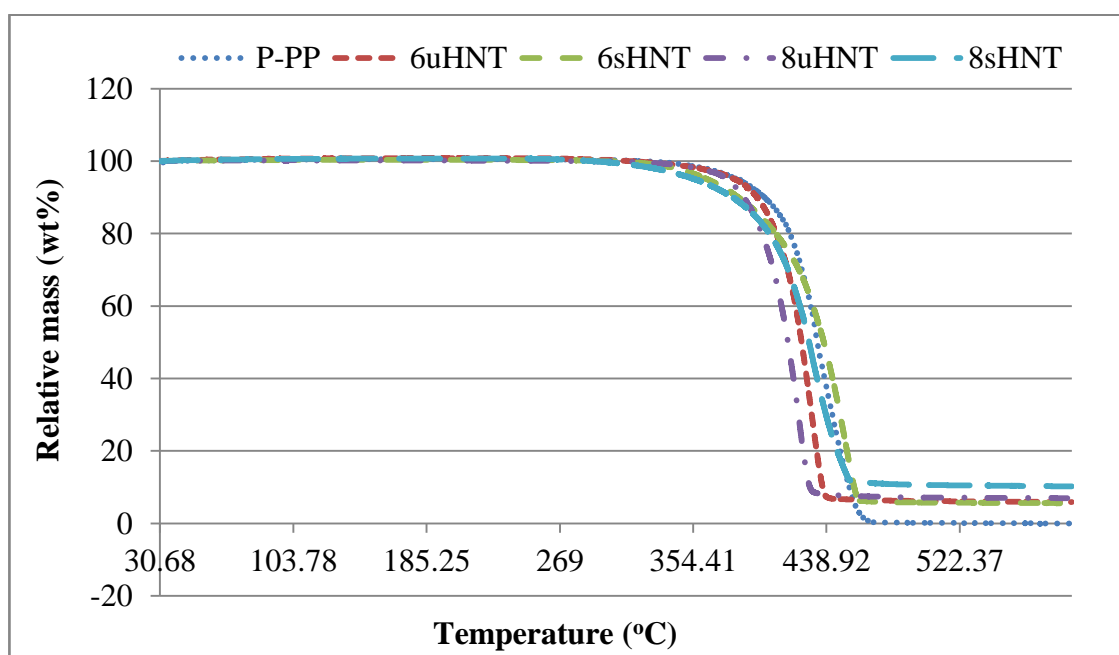


Fig. 8.6 TGA thermograms of pure PP, unmodified and APTES modified Hal-PP nanocomposites

The increased thermal stability shows the good interfacial adhesion between APTES modified Hal nanotubes and the PP matrix. However, it is also noted that a considerable decrease in the thermal stability for unmodified Hal nanotubes loaded PP

nanocomposites at maximum weight loss stage as compared to pure PP. Similar results were reported by Wang and Huang (2013). They indicated that the Hal nanotubes were acted as catalyst to enhance the degradation process during the volatilization. It is also believed that the Hal nanotubes weaken the PP polymer chain which influences the thermal oxidative degradation. The acidic groups present on the Hal nanotubes or the air entrapped inside the tubular lumen of the Hal nanotubes cause the thermal oxidative aging (Liu et al., 2010). It is important to mention that the char residue of Hal-PP nanocomposites was significantly higher than pure PP. No char residue could be observed for pure PP resin, whereas 6 and 8 wt% of Hal loading nanocomposites showed more than 5 and 10% of char residue respectively (**Table 8.1**). This result clearly shows the incorporation of Hal nanotubes and hence an improved thermal stability of the Hal-PP nanocomposites.

8.4 DSC analysis

A non-isothermal DSC analysis was carried out to investigate the effect of addition of unmodified and APTES modified Hal nanotubes into PP nanocomposites. **Figs. 8.7 and 8.8** show the melting temperature and cold crystallinity thermograms of Hal-PP nanocomposites respectively. **Table 8.1** shows the values of melting temperature (T_m), cold crystallization temperature (T_c) and percentage of crystallinity (X_c) for unmodified and APTES modified Hal-PP nanocomposites. The melting temperature (T_m) peak shows a considerable increment of melting temperature (**Fig. 8.7**). The melting temperature peak shifted to 169.83 °C with the addition of 8 wt% of APTES modified Hal nanotubes, whereas the melting temperature peak of pure PP was at 166.65 °C.

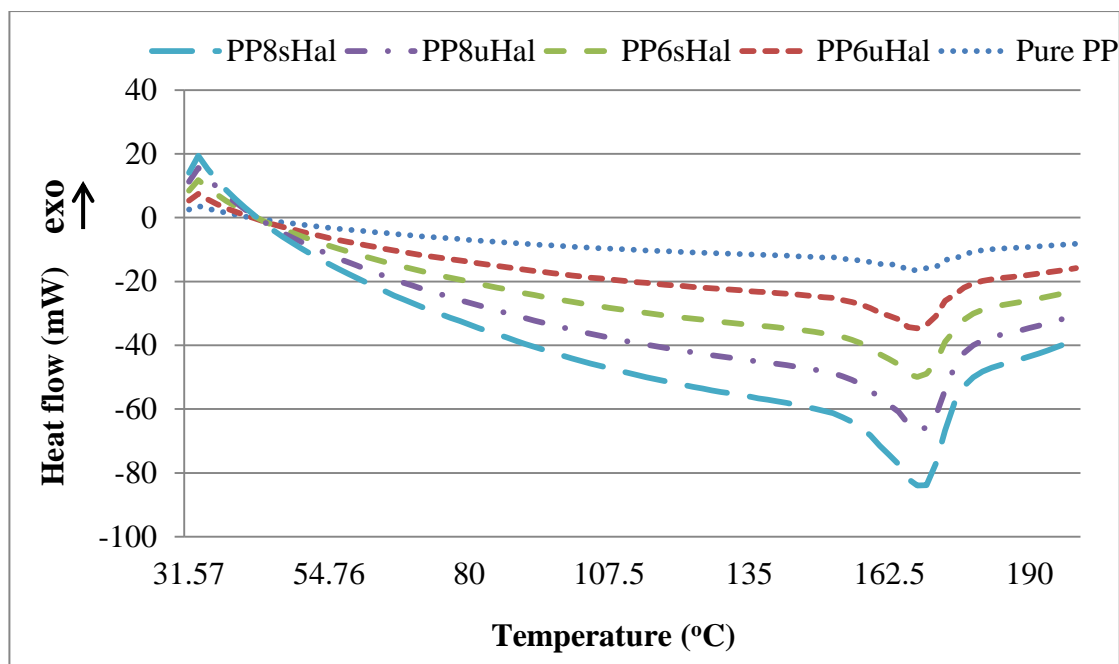


Fig. 8.7 DSC melting curves of pure PP, unmodified and APTES modified Hal-PP nanocomposites

The increment of melting temperature may be due to the reinforcement effect which restricts the free movement of polymer chain segments in the Hal-PP nanocomposites (Wang and Huang, 2013). It has been already reported that the addition of Hal nanotubes induced the nucleating effects in the nanocomposites which enhances the crystallinity of Hal-PP nanocomposites (Prashantha et al., 2011; Wang and Huang, 2013).

The cold crystalline temperature (T_{cc}) of Hal-PP nanocomposites shifted to lower temperature after the addition of Hal nanotubes. The T_{cc} for the pure PP was at 123.52 °C and with the addition of 8 wt% of Hal nanotubes into PP matrix the T_{cc} shifted to 121.02 °C. The lower the T_{cc} with respect to pure PP indicates the addition of nanofillers promoting the kinetics of nucleating effect in the Hal-PP nanocomposites and thus improved crystallinity (Kontou et al., 2011; Wang and Qiu, 2011).

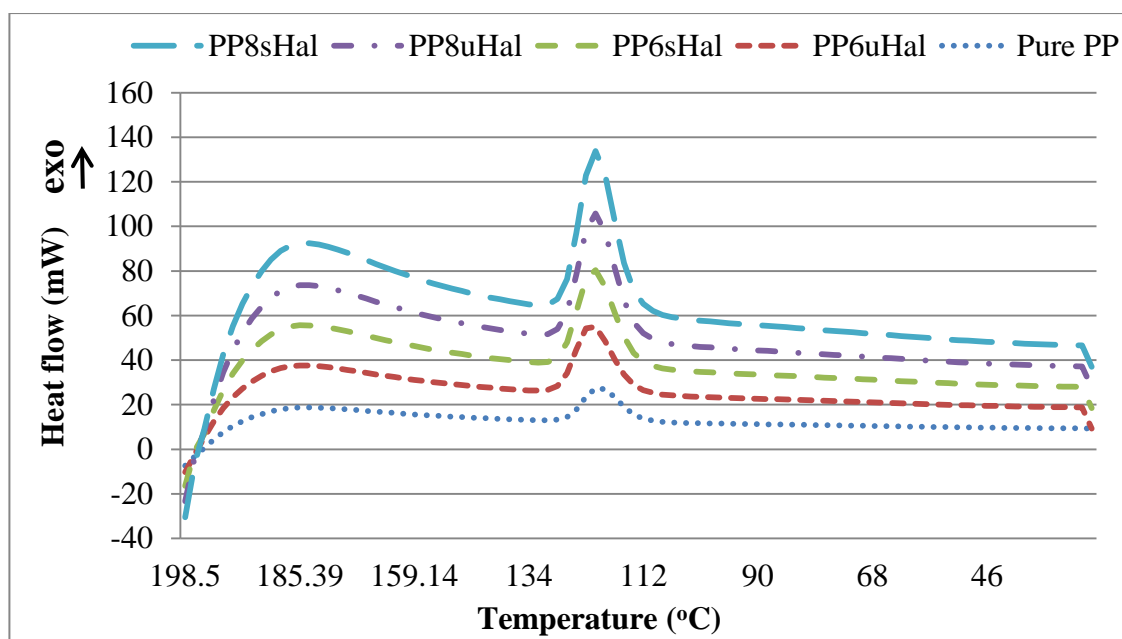


Fig. 8.8 DSC cooling curves of pure PP, unmodified and APTES modified Hal-PP nanocomposites

Table 8.1 TGA and DSC data of melting temperature (T_m), cold crystallization temperature (T_c) and percentage of crystallinity (X_c)

Samples	T_m (°C)	T_{cc} (°C)	X_c (%)	Temperature at	Char residue
				50% weight loss (°C)	(wt %)
Pure PP	166.65	123.52	38.5	433.14	0.0
PP + 6uHal	168.57	122.8	42.3	430.29	5.89
PP + 6sHal	168.8	121.56	46.8	445.24	7.25
PP + 8uHal	169.21	121.5	44.71	414.81	8.99
PP + 8sHal	169.83	121.02	47.1	427.97	10.2

8.5 DMA analysis

DMA analysis was carried out to study the effect of APTES modified Hal nanotubes reinforced PP nanocomposites on the visco-elastic properties. This analysis is useful

in the evaluation of composite dynamic mechanical performance under different temperature and mechanical stress (Saba et al., 2016). **Fig. 8.9** shows the curves of storage modulus (E') of unmodified and APTES modified Hal nanotubes reinforced PP composites. It is noticed from **Fig. 8.9** that the storage modulus was higher at lower temperature at around $-50\text{ }^{\circ}\text{C}$ and then a gradual decrease with increasing temperature could be noticed.

At lower temperature ($-51\text{ }^{\circ}\text{C}$) the storage modulus (E') was much higher for Hal-PP nanocomposites as compared to pure PP and even it increased significantly with the further addition of APTES modified Hal nanotubes into PP matrix. It was found that the addition of 6 wt% of APTES modified Hal nanotubes into PP matrix increased the storage modulus to 5.55 GPa which is 28% higher as compared to pure PP. Higher storage modulus for APTES modified Hal-PP nanocomposites as compared to pure PP clearly confirms the increased dispersion and interfacial interactions between the modified Hal nanofiller and the PP matrix. Similar results were reported by other researchers. Prashantha et al (2011) studied the effect of surface modification on the dynamic mechanical properties of Hal-PP nanocomposites and reported that the storage modulus increased with increased Hal nanotubes loading into PP matrix. They also noticed that the storage modulus was much higher for surface modified Hal-PP nanocomposites as compared to pure PP.

Lecouvet et al. (2013) studied the thermal and flammability properties of Hal nanotubes reinforced polyethersulfone (PES) nanocomposites prepared by melt compounding and found that the storage modulus significantly increased by more than 40% with the addition of 16 wt% of Hal-PES nanocomposites than pure PES resin. This may be due to higher intrinsic stiffness of Hal nanotubes, their orientation in the stretching direction and also their interfacial adhesion with PES polymer matrix

which lead to improved storage modulus higher for the Hal nanotubes reinforced PES nanocomposites than pure polymer resin.

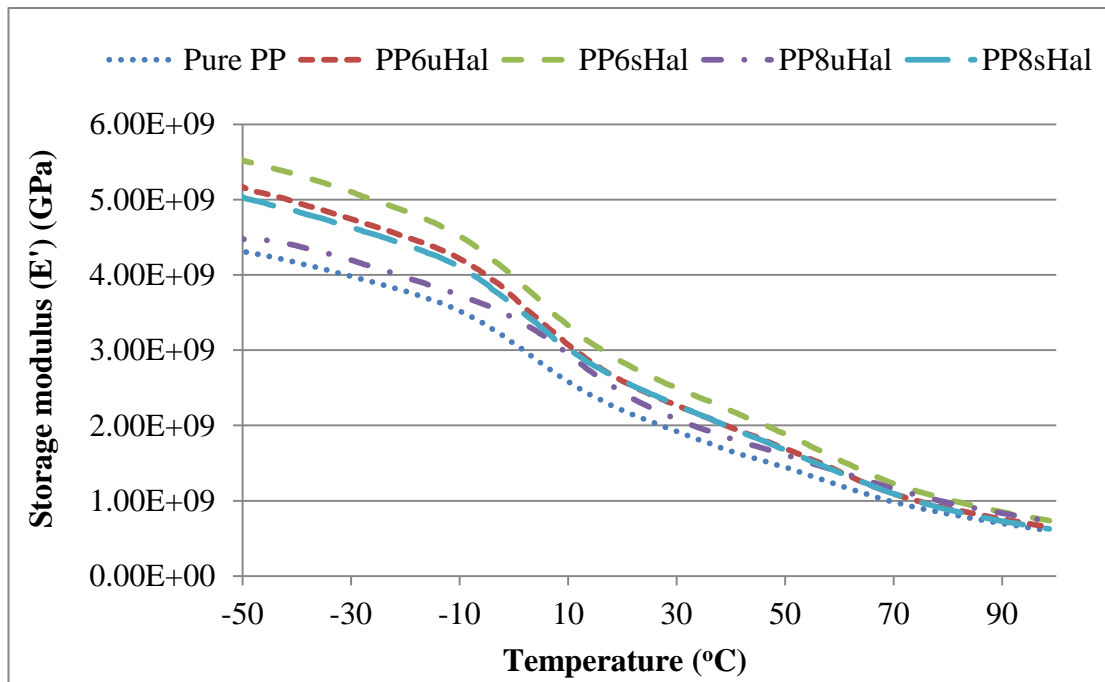


Fig. 8.9 Storage modulus (E') curves of unmodified and APTES modified Hal nanotubes reinforced PP nanocomposites

Loss modulus (E'') is defined as the capacity of the composite materials to dissipate the absorbed energy within the system as heat or intermolecular rearrangements when force is applied. It shows the viscous property of polymeric materials. Loss modulus is a sensitive property of the composite materials with molecular motions, transitions and relaxation process within the same system. With a gradual increase in the temperature, the materials change from rigid state to more elastic and the rate of change purely depends on the nature of fillers and polymer matrices (Saba et al., 2016). **Fig. 8.10** shows the loss modulus (E'') of the unmodified and APTES modified Hal-PP nanocomposites with different filler loading as a function of temperature. It is noticed that the peak of loss modulus curve was seen to be broad

and the peak height was relatively higher for pure PP resin as compared to Hal loaded nanocomposites.

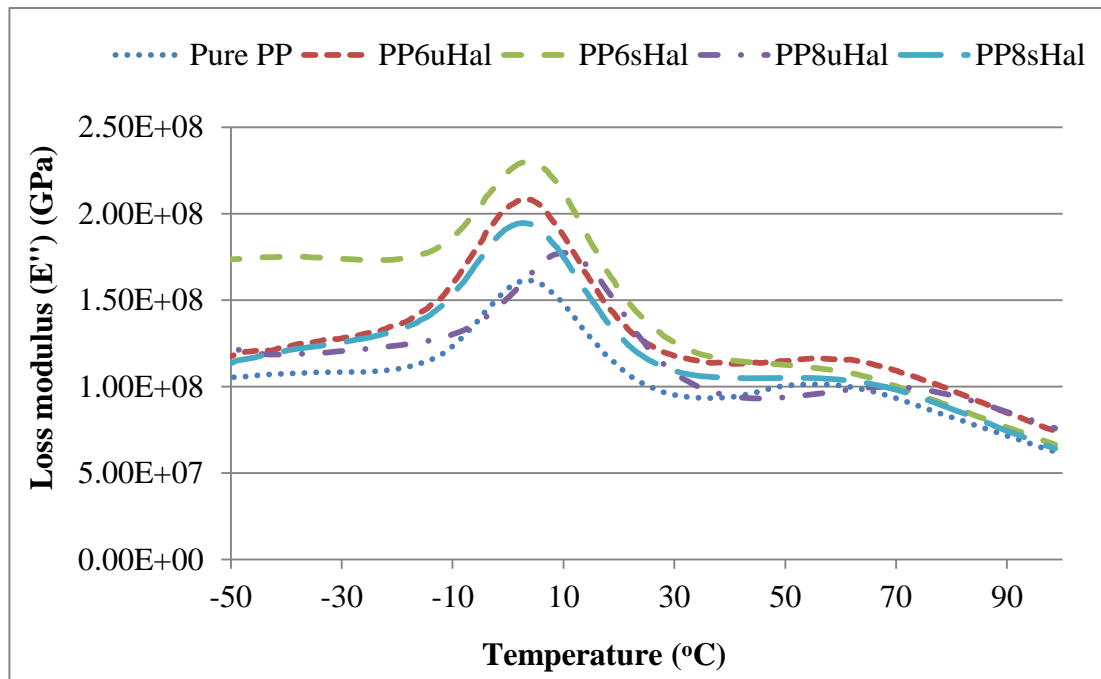


Fig. 8.10 Loss modulus curves of unmodified and APTES modified Hal nanotubes reinforced PP nanocomposites

The lower the peak height of the loss modulus for the APTES modified Hal-PP nanocomposites shows the increased storage modulus and decreased loss factor. This may be due to an increased interfacial adhesion and well dispersed Hal nanotubes across the PP matrix (Khonakdar, 2015). The damping factor which is also called as tan delta (δ) is the ratio of storage modulus (E') and loss modulus (E'') and has no dimension.

It is believed that the temperature at the peak of tan delta is considered as the glass transition temperature (T_g) of the material (Liu et al., 2013). It could be noticed from **Fig. 8.11** that there is a considerable increment in the T_g with the addition of Hal nanotubes into Hal-PP nanocomposites than pure PP.

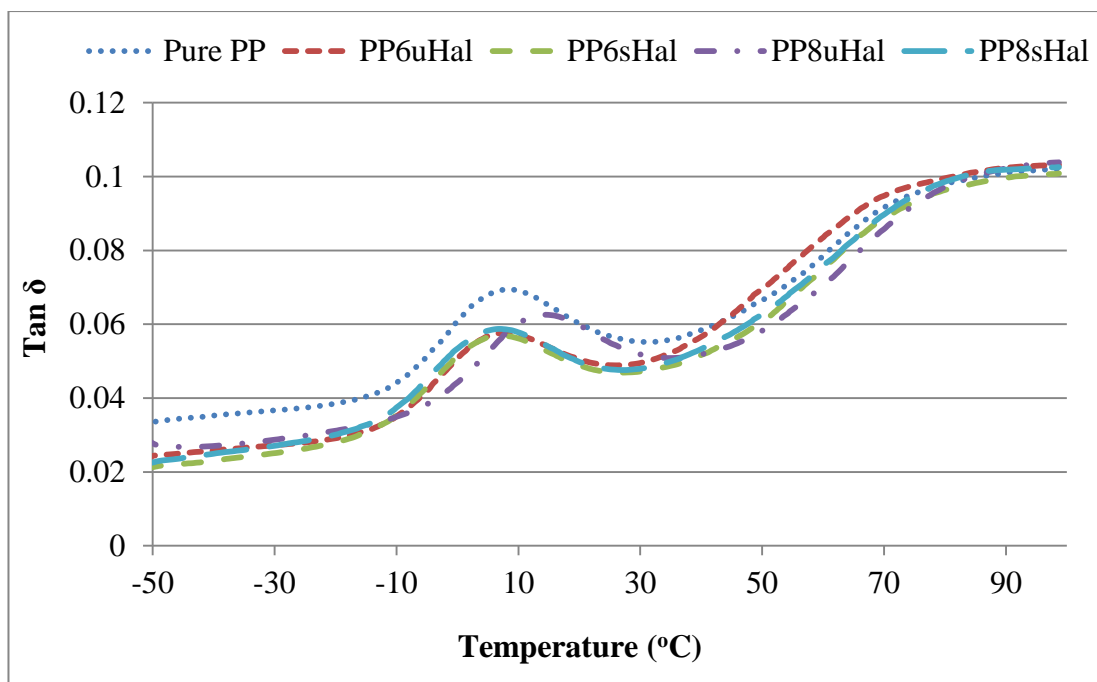


Fig. 8.11 Tan δ curves of unmodified and APTES modified Hal nanotubes reinforced PP nanocomposites

The T_g for pure PP was at 6.8 °C whereas the T_g for the addition of APTES modified Hal nanotubes of 6 and 8 wt% were at 7.2 and 8.3 °C respectively. This may be due to the restriction of segment motion in the polymer chain after the addition of Hal nanotubes which causes the increased modulus and leads to increased T_g of the composite materials (Russo et al., 2014).

8.6 Conclusions

The effect of APTES modified Hal nanotubes on mechanical and thermal properties of Hal-PP nanocomposites was studied. Morphological investigation revealed that the surface modified Hal nanotubes were better dispersed across the PP matrix and less agglomeration as compared to unmodified Hal-PP nanocomposites. Mechanical properties of the APTES modified Hal-PP nanocomposites were found to be superior to the unmodified Hal-PP nanocomposites. The tensile strength, modulus and impact

strength increased by 31, 72% and 44% respectively with the addition of 6 wt% of APTES modified Hal-PP nanocomposites as compared to pure PP. Thermal analysis revealed that the thermal stability and percentage crystallinity increased by 15 and 22% respectively for the Hal-PP nanocomposites with surface modification by APTES. DMA analysis showed the improved storage modulus by 28% as compared to pure PP. Overall, the investigation confirms the surface modification of Hal nanotubes with APTES which helps to enhance the mechanical and thermal properties of Hal-PP nanocomposites.

CHAPTER IX

Conclusions and future work

9.1 Conclusions

In this work, firstly, sisal fibres were surface treated with alkali, high intensity ultrasound (HIU) and the combination of alkali and HIU treatments to study the effective removal of amorphous materials such as hemicellulose, pectin, lignin and other waxy materials from the surface of sisal fibres. FE-SEM and FTIR analysis of surface treated sisal fibres revealed that the combination of alkali and HIU treatment was more effective in the removal of amorphous materials from the surface of sisal fibres and increased the fibre aspect ratio which plays an important role in achieving good mechanical properties of the resultant composites. XRD analysis confirmed a significant increase in the crystallinity in case of combined treated sisal fibres. TGA analysis indicated that the combination of alkali and HIU treated sisal fibres have high thermal stability as compared to untreated sisal fibres. However, due to the removal of amorphous materials from the fibre surface, tensile properties decreased significantly which may be due to the removal of amorphous materials which bind the cellulose materials tightly on the surface of fibres.

Second, PLA composites reinforced with sisal fibres were successfully prepared and the effect of different surface treatments of sisal fibres on the morphology, mechanical, thermal and biodegradability properties was studied. Morphological analysis showed that the surface treated sisal fibres were well dispersed across the PLA matrix and increased the interfacial adhesion which is a crucial property for the improvement of mechanical and thermal properties of composites. A significant

increment in the tensile properties could be observed for the combination of alkali and HIU treated sisal fibre composites as compared to untreated and pure PLA matrix. TGA and DSC analysis revealed that the improved thermal stability and crystallinity by 12 °C and 75% respectively with the combined treated sisal fibre reinforced PLA composites. DMA results showed that the stiffness increased significantly by 30% as compared to pure PLA. Water absorption and soil biodegradation analysis were also in favour of improved mechanical and thermal properties of SF/PLA composites with the incorporation of the combined treated sisal fibre.

Apart from sisal fibres, halloysite (Hal) nanotubes were also used as nano-fillers in order to tune the mechanical and thermal properties of PLA composites. Hal nanotubes were successfully surface modified with APTES silane coupling agent and the effects of APTES modified Hal/PLA nanocomposites on the morphology, mechanical and thermal properties of Hal/PLA composites were studied. Nitrogen adsorption-desorption, FTIR analysis confirmed the well dispersion of Hal nanotubes across the PLA matrix which improved the interfacial adhesion. Tensile and impact properties were significantly increased with the incorporation of APTES modified Hal/PLA nanocomposites. TGA analysis showed that the thermal stability improved significantly for APTES modified Hal/PLA nanocomposites as compared to pure PLA matrix. In this investigation, PP composites reinforced with sisal fibre and halloysite nanotubes were also prepared and the effect of surface modification on the mechanical and thermal properties of PP composites was studied. Similar to PLA composites, PP/Sisal fibre composites showed better improved mechanical and thermal properties as compared to pure PP.

Finally, sisal fibres and Hal nanotubes have significant effects to overcome the drawbacks of PLA polymer and improved the mechanical and thermal properties.

Surface modification of sisal fibres as well as Hal nanotubes was playing an important role in order to tune the mechanical and thermal properties of PLA composites. PLA polymer has the potential to replace PP polymer not only in the medical applications but also in automotive and other structural engineering applications.

9.2 Suggestions for future work

The results obtained from this investigation lead to confirm that the combination of alkali and HIU treatment could be very effective in order to remove the amorphous materials from the surface of fibres which improved the overall properties of fibre reinforced composites. It is suggested that in order to achieve industrial scale production of sisal fibre reinforced PLA composites a detailed process optimisation is needed. In this study, we revealed that the fibre orientation or alignment is one of the important factors which directly affect the mechanical properties of the composites. Therefore, it will be a good choice of development of uniaxially aligned fibre composites for the better performance of composites. Different types of coupling agents could be proposed in order to obtain more improved mechanical and thermal properties of the natural fibre reinforced polymer composites. Addition of coupling agents in the generation of polymer composites is another effective method to enhance the interfacial bonding between fibres and the matrices. Fire-retardant additives could be used in PLA nanocomposites along with Hal nanotubes in order to achieve good thermally stabilised composites which are required in specific applications such as aerospace, outdoor fabrications etc. PLA is very brittle and thus plasticisers and compatibilisers could be used for a further reduction in the brittleness as per the end use requirements.

References:

- Abdul Khalil, H.P.S., Bhat, A.H., Ireana Yusra, A.F., 2012. Green composites from sustainable cellulose nanofibrils: A review. *Carbohydr. Polym.* 87, 963–979.
- Abdul Khalil, H.P.S., Davoudpour, Y., Islam, M.N., Mustapha, A., Sudesh, K., Dungani, R., Jawaid, M., 2014. Production and modification of nanofibrillated cellulose using various mechanical processes: A review. *Carbohydr. Polym.* 99, 649–665.
- Abidi, N., Cabrales, L., Haigler, C.H., 2014. Changes in the cell wall and cellulose content of developing cotton fibers investigated by FTIR spectroscopy. *Carbohydr. Polym.* 100, 9–16.
- Alamri, H., Low, I.M., 2013. Effect of water absorption on the mechanical properties of nanoclay filled recycled cellulose fibre reinforced epoxy hybrid nanocomposites. *Compos. Part A Appl. Sci. Manuf.* 44, 23–31.
- Albdiry, M.T., Yousif, B.F., 2014. Role of silanized halloysite nanotubes on structural, mechanical properties and fracture toughness of thermoset nanocomposites. *Mater. Des.* 57, 279–288.
- Albdiry, M.T., Yousif, B.F., 2013. Morphological structures and tribological performance of unsaturated polyester based untreated/silane-treated halloysite nanotubes. *Mater. Des.* 48, 68–76.
- Alvarez, V.A., Ruseckaite, R.A., Va, A., 2006. Degradation of sisal fibre/Mater Bi-Y biocomposites buried in soil. *Polym. Degrad. Stab.* 91, 3156–3162.
- Arbelaiz, A., Fernández, B., Ramos, J.A., Mondragon, I., 2006. Thermal and

- crystallization studies of short flax fibre reinforced polypropylene matrix composites: Effect of treatments. *Thermochim. Acta* 440, 111–121.
- Arkles, B., 1977. Tailoring surfaces with silanes. *Chemtech* 7, 766-772.
- Arkles, B., Steinmetz, J.R., Zazyczny, J., Mehta, P., 1992. Factors contributing to the stability of alkoxy silanes in aqueous solution. *J. Adhes. Sci. Technol.* 1. 91-104.
- Arrakhiz, F.Z., Elachaby, M., Bouhfid, R., Vaudreuil, S., Essassi, M., Qaiss, A., 2012. Mechanical and thermal properties of polypropylene reinforced with Alfa fibre under different chemical treatment. *Mater. Des.* 35, 318–322.
- Arrieta, M.P., Lopez, J., Hernandez, A., Rayon, E., 2014. Ternary PLA-PHB-Limonene blends intended for biodegradable food packaging applications. *Eur. Polym. J.* 50, 255–270.
- Ashori, A., Nourbakhsh, A., 2010. Reinforced polypropylene composites: Effects of chemical compositions and particle size. *Bioresour. Technol.* 101, 2515–2519.
- Asumani, O.M.L., Reid, R.G., Paskaramoorthy, R., 2012. The effects of alkali-silane treatment on the tensile and flexural properties of short fibre non-woven kenaf reinforced polypropylene composites. *Compos. Part A Appl. Sci. Manuf.* 43, 1431–1440.
- Avella, M., Volpe, G. Della, Martuscelli, E., 1992. Transcrystallinity phenomena in a polypropylene/kevlar fibre system I: influence of crystallisation conditions. *Polym. Eng. Sci.* 32, 376–382.
- Azwa, Z.N., Yousif, B.F., Manalo, A.C., Karunasena, W., 2013. A review on the degradability of polymeric composites based on natural fibres. *Mater. Des.* 47,

424–442.

B. C. Barkakaty, 1976. Some structural aspects of sisal fibres. *J. Appl. Polym. Sci.* 20, 2921–2940.

Badia, J.D., Kittikorn, T., Strömberg, E., Santonja-Blasco, L., Martínez-Felipe, A., Ribes-Greus, A., Ek, M., Karlsson, S., 2014. Water absorption and hydrothermal performance of PHBV/sisal biocomposites. *Polym. Degrad. Stab.* 108, 166–174.

Barrientos-Ramirez, S., Oca-Ramirez, G.M. De, Ramos-Fernandez, E. V., Sepulveda-Escribano, A., Pastor-Blas, M.M., Gonzalez-Montiel, A., 2011. Surface modification of natural halloysite clay nanotubes with aminosilanes. Application as catalyst supports in the atom transfer radical polymerization of methyl methacrylate. *Appl. Catal. A Gen.* 406, 22–33.

Batalha, L.A.R., Silva, J.C. da, Jardim, C.M., Oliveira, R.C., Colodette, J.L., 2011. Effect of ultrasound and xylanase treatment on the physical-mechanical properties of bleached eucalyptus kraft pulp. *Nat. Resour.* 2, 125–129.

Battegazzore, D., Bocchini, S., Frache, A., 2011. Crystallization kinetics of poly(lactic acid)-talc composites. *Express Polym. Lett.* 5, 849–858.

Beg, M.D.H., Akindoyo, J.O., Ghazali, S., Mamun, A.A., 2015. Impact modified oil palm empty fruit bunch fibre/poly(lactic) acid composite. *Int. J. Chem. Mol. Nucl. Mater. Metallurgical Eng.* 9, 165–170.

Belaadi, A., Bezazi, A., Bouchak, M., Scarpa, F., Zhu, C., 2014. Thermochemical and statistical mechanical properties of natural sisal fibres. *Compos. Part B Eng.* 67, 481–489.

- Bledzki, A.K., Gassan, J., 1999. Composites reinforced with cellulose based fibres. *Prog. Polym. Sci.* 24, 221–274.
- Boopathi, L., Sampath, P.S., Mylsamy, K., 2012. Investigation of physical, chemical and mechanical properties of raw and alkali treated Borassus fruit fibre. *Compos. Part B Eng.* 43, 3044–3052.
- Cabral, H., 2005. Structure-properties relationship of short jute fibre reinforced polypropylene composites. *J. Compos. Mater.* 39, 51–65.
- Cai, M., Takagi, H., Nakagaito, A.N., Katoh, M., Ueki, T., Waterhouse, G.I.N., Li, Y., 2015. Influence of alkali treatment on internal microstructure and tensile properties of abaca fibres. *Ind. Crops Prod.* 65, 27–35.
- Cao, Y., Chan, F., Chui, Y.H., Xiao, H., 2012. Characterization of flax fibres modified by alkaline, enzyme, and steam-heat treatments. *BioResources* 7, 4109–4121.
- Carli, L.N., Daitx, T.S., Soares, G. V., Crespo, J.S., Mauler, R.S., 2014. The effects of silane coupling agents on the properties of PHBV/halloysite nanocomposites. *Appl. Clay Sci.* 87, 311–319.
- Carrasco, F., Pagès, P., Gámez-pérez, J., Santana, O.O., MasPOCH, M.L., 2010. Processing of poly (lactic acid): Characterization of chemical structure, thermal stability and mechanical properties. *Polym. Degrad. Stab.* 95, 116–125.
- Carrillo, F., Colom, X., Suñol, J.J., Saurina, J., 2004. Structural FTIR analysis and thermal characterisation of lyocell and viscose-type fibres. *Eur. Polym. J.* 40, 2229–2234.

- Chen, W., Yu, H., Liu, Y., 2011a. Preparation of millimeter-long cellulose nanofibres with diameters of 30-80 nm from bamboo fibers. *Carbohydr. Polym.* 86, 453–461.
- Chen, W., Yu, H., Liu, Y., Chen, P., Zhang, M., Hai, Y., 2011b. Individualization of cellulose nanofibres from wood using high-intensity ultrasonication combined with chemical pretreatments. *Carbohydr. Polym.* 83, 1804–1811.
- Cheng, Q., Wang, S., Han, Q., 2010. Novel process for isolating fibrils from cellulose fibres by high-intensity ultrasonication. II. Fibril characterization. *J. Appl. Polym. Sci.* 115, 2756–2762.
- Cheng, Q., Wang, S., Rials, T.G., 2009. Poly(vinyl alcohol) nanocomposites reinforced with cellulose fibrils isolated by high intensity ultrasonication. *Compos. Part A Appl. Sci. Manuf.* 40, 218–224.
- Chikouche, M.D.L., Merrouche, A., Azizi, A., Rokbi, M., Walter, S., 2015. Influence of alkali treatment on the mechanical properties of new cane fibre/polyester composites. *J. Reinf. Plast. Compos.* 34, 1329–1339.
- Chow, C.P.L., Xing, X.S., Li, R.K.Y., 2007. Moisture absorption studies of sisal fibre reinforced polypropylene composites. *Compos. Sci. Technol.* 67, 306–313.
- Cran, M.J., Bigger, S.W., S.M.A., I., 2014. Effect of kenaf fibre loading and thymol concentration on the mechanical and thermal properties of PLA/kenaf/thymol composites. *Ind. Crops Prod.* 61, 74–83.
- Das, A., Satapathy, B.K., 2011. Structural, thermal, mechanical and dynamic mechanical properties of cenosphere filled polypropylene composites. *Mater. Des.* 32, 1477–1484.

- De Rosa, I.M., Kenny, J.M., Puglia, D., Santulli, C., Sarasini, F., 2010. Morphological, thermal and mechanical characterization of okra (*Abelmoschus esculentus*) fibres as potential reinforcement in polymer composites. *Compos. Sci. Technol.* 70, 116–122.
- Demir, H., Atikler, U., Balköse, D., Tihmınlıođlu, F., 2006. The effect of fibre surface treatments on the tensile and water sorption properties of polypropylene–luffa fibre composites. *Compos. Part A Appl. Sci. Manuf.* 37, 447–456.
- Dhakal, H.N., Zhang, Z.Y., Richardson, M.O.W., 2007a. Effect of water absorption on the mechanical properties of hemp fibre reinforced unsaturated polyester composites. *Compos. Sci. Technol.* 67, 1674–1683.
- Dhakal, H.N., Zhang, Z.Y., Richardson, M.O.W., Alhuthali, A., Low, I.M., Dong, C., Ghosh, R., Ramakrishna, A., Reena, G., Mohan, T.P., Kanny, K., Ramadevi, P., Sampathkumar, D., Srinivasa, C.V., Bennehalli, B., Dhakal, H.N., Zhang, Z.Y., Richardson, M.O.W., 2007b. Effect of water absorption on the mechanical properties of hemp fibre reinforced unsaturated polyester composites. *Compos. Sci. Technol.* 67, 1674–1683.
- Dicker, M.P.M., Duckworth, P.F., Baker, A.B., Francois, G., Hazzard, M.K., Weaver, P.M., 2014. Green composites: A review of material attributes and complementary applications. *Compos. Part A* 56, 280–289.
- Diez-Pascual, A.M., Naffakh, M., Marco, C., Gomez-Fatou, M.A., Ellis, G.J., 2014. Multiscale fibre reinforced thermoplastic composites incorporating carbon nanotubes: A review. *Curr. Opin. Solid State Mater. Sci.* 18, 62–80.
- Dittenber, D.B., Gangarao, H.V.S., 2012. Critical review of recent publications on use

- of natural composites in infrastructure. *Compos. Part A Appl. Sci. Manuf.* 43, 1419–1429.
- Dong, Y., Ghataura, A., Takagi, H., Haroosh, H.J., Nakagaito, A.N., Lau, K.-T., 2014. Polylactic acid (PLA) biocomposites reinforced with coir fibres: Evaluation of mechanical performance and multifunctional properties. *Compos. Part A Appl. Sci. Manuf.* 63, 76–84.
- Du, M., Guo, B., Jia, D., 2010. Newly emerging applications of halloysite nanotubes: a review. *Polym. Int.* 59, 574–582.
- Du, M., Guo, B., Jia, D., 2006. Thermal stability and flame retardant effects of halloysite nanotubes on poly(propylene). *Eur. Polym. J.* 42, 1362–1369.
- Eichhorn, S., Thielemans, W., Benight, A.B., 2010. Review : Current international research into cellulose nanofibres and nanocomposites. *J. Mater. Sci.* 45, 1–33.
- El-Sabbagh, A., 2014. Effect of coupling agent on natural fibre in natural fibre/polypropylene composites on mechanical and thermal behaviour. *Compos. Part B Eng.* 57, 126–135.
- Elkhaoulani, A., Arrakhiz, F.Z., Benmoussa, K., Bouhfid, R., Qaiss, A., 2013. Mechanical and thermal properties of polymer composite based on natural fibres: Moroccan hemp fibres/polypropylene. *Mater. Des.* 49, 203–208.
- Espert, A., Vilaplana, F., Karlsson, S., 2004. Comparison of water absorption in natural cellulosic fibres from wood and one-year crops in polypropylene composites and its influence on their mechanical properties. *Compos. Part A Appl. Sci. Manuf.* 35, 1267–1276.

- Espinach, F.X., Julian, F., Verdaguer, N., Torres, L., Pelach, M.A., Vilaseca, F., Mutje, P., 2013. Analysis of tensile and flexural modulus in hemp strands/polypropylene composites. *Compos. Part B Eng.* 47, 339–343.
- Essabir, H., Elkhaoulani, A., Benmoussa, K., Bouhfid, R., Arrakhiz, F.Z., Qaiss, A., 2013a. Dynamic mechanical thermal behavior analysis of doum fibres reinforced polypropylene composites. *Mater. Des.* 51, 780–788.
- Essabir, H., Hilali, E., Elgharad, A., El Minor, H., Imad, A., Elamraoui, A., Al Gaudi, O., 2013b. Mechanical and thermal properties of bio-composites based on polypropylene reinforced with Nut-shells of Argan particles. *Mater. Des.* 49, 442–448.
- Evagelia, K., Michael, N., Panayiotis, G., 2011. Comparative study of PLA nanocomposites reinforced with clay and silica nanofillers and their mixtures. *J. Appl. Polym. Sci.* 122, 1519–1529.
- Faruk, O., Bledzki, A.K., Fink, H.P., Sain, M., 2012. Biocomposites reinforced with natural fibers: 2000-2010. *Prog. Polym. Sci.* 37, 1552–1596.
- Fiore, V., Di Bella, G., Valenza, A., 2015. The effect of alkaline treatment on mechanical properties of kenaf fibres and their epoxy composites. *Compos. Part B Eng.* 68, 14–21.
- Freire, C., Peixoto, A.F., Fernandes, A.C., Pereira, C., 2016. Microporous and mesoporous materials physicochemical characterization of organosilylated halloysite clay nanotubes. *Microporous Mesoporous Mater.* 219, 145–154.
- Fu, S.Y., Lauke, B., 1996. Effects of fibre length and fiber orientation distributions on the tensile strength of short fibre reinforced polymers. *Compos. Sci. Technol.* 56,

1179–1190.

Gareth Beckermann, 2007. Performance of Hemp-Fibre Reinforced Polypropylene Composite Materials. PhD Thesis, The University of Waikato.

Ghosh, R., Ramakrishna, A., Reena, G., 2013. Effect of air bubbling and ultrasonic processing on water absorption property of banana fibre-vinylester composites. *J. Compos. Mater.* 48 (14), 1691-1697.

Ghosh, R., Ramakrishna, A., Reena, G., Ravindra, A., Verma, A., 2014. Water absorption kinetics and mechanical properties of ultrasonic treated banana fibre reinforced-vinyl ester composites. *Procedia Mater. Sci.* 5, 311–315.

Gibson, R.F., 2010. A review of recent research on mechanics of multifunctional composite materials and structures. *Compos. Struct.* 92, 2793–2810.

Gilman, J., 1999. Flammability and thermal stability studies of polymer layered-silicate (clay) nanocomposites. *Appl. Clay Sci.* 15, 31-49.

Granda, L.A., Espinach, X., López, F., García, J.C., Delgado-Aguilar, M., Mutjé, P., 2016. Semichemical fibres of *Leucaena collinsii* reinforced polypropylene: Macromechanical and micromechanical analysis. *Compos. Part B Eng.* 92, 332–337.

Guo, B., Zou, Q., Lei, Y., Jia, D., 2009. Structure and performance of polyamide 6/halloysite nanotubes nanocomposites. *Polym. J.* 41, 835–842.

Gurunathan, T., Mohanty, S., Nayak, S.K., 2015. A review of the recent developments in biocomposites based on natural fibres and their application perspectives. *Compos. Part A Appl. Sci. Manuf.* 77, 1–25.

- Haameem J.A., M., Abdul Majid, M.S., Afendi, M., Marzuki, H.F.A., Fahmi, I., Gibson, A.G., 2016. Mechanical properties of Napier grass fibre/polyester composites. *Compos. Struct.* 136, 1–10.
- Herrmann, A.S., Nickel, J., Riedel, U., 1998. Construction materials based upon biologically renewable resources from components to finished parts. *Polym. Degrad. Stab.* 59, 251–261.
- Ho, M., Wang, H., Lee, J., Ho, C., Lau, K., Leng, J., Hui, D., 2012. Critical factors on manufacturing processes of natural fibre composites. *Compos. Part B* 8, 3549–3562.
- Hossain, M.K., Karim, M.R., Chowdhury, M.R., Imam, M.A., Hosur, M., Jeelani, S., Farag, R., 2014. Comparative mechanical and thermal study of chemically treated and untreated single sugarcane fibre bundle. *Ind. Crops Prod.* 58, 78–90.
- I.M. De Rosa, A. Iannoni, J.M. Kenny, D. Puglia, C. Santulli, F. Sarasini, A.T., 2011. Poly(lactic acid)/phormium tenax composites: Morphology and thermo-mechanical behavior. *Polym. Compos.* 1362-1368.
- Idicula, M., Malhotra, S.K., Joseph, K., Thomas, S., 2005. Dynamic mechanical analysis of randomly oriented intimately mixed short banana/sisal hybrid fibre reinforced polyester composites. *Compos. Sci. Technol.* 65, 1077–1087.
- Iskalieva, A., Yimmou, B.M., Gogate, P.R., Horvath, M., Horvath, P.G., Csoka, L., 2012. Cavitation assisted delignification of wheat straw: A review. *Ultrason. Sonochem.* 19, 984–993.
- Jawaid, M., Abdul Khalil, H.P.S., Hassan, A., Dungani, R., Hadiyane, A., 2013. Effect of jute fibre loading on tensile and dynamic mechanical properties of oil

- palm epoxy composites. *Compos. Part B Eng.* 45, 619–624.
- Jambeck, J.R., Geyer, R., Wilcox, C., Siegler, T.R., Perryman, M., Andrady, A., Narayan, R., Law, K.L., 2015. Plastic waste inputs from land into the ocean. *Science* 80. 347-352.
- Jiang, L., Zhang, J., Wolcott, M.P., 2007. Comparison of polylactide/nano-sized calcium carbonate and polylactide/montmorillonite composites: Reinforcing effects and toughening mechanisms. *Polymer*. 48, 7632–7644.
- Jin, J., Fu, L., Yang, H., Ouyang, J., 2015. Carbon hybridized halloysite nanotubes for high-performance hydrogen storage capacities. *Sci. Rep.* 5, 1-10.
- John, M.J., Anandjiwala, R.D., 2009. Chemical modification of flax reinforced polypropylene composites. *Compos. Part A Appl. Sci. Manuf.* 40, 442–448.
- John, M.J., Anandjiwala, R.D., 2008. Recent developments in chemical modification and characterization of natural fiber-reinforced composites. *Polym. Compos.* 29, 187–207.
- John, M.J., Thomas, S., 2008. Biofibres and biocomposites. *Carbohydr. Polym.* 71, 343–364.
- Joseph, K., James, B., Thomas, S., Carvalho, L.H. De, 1999. A review on sisal fiber reinforced polymer composites. *Eng. Agrícola* 3, 367–379.
- Joseph, K., Varghese, S., Kalaprasad, G., Thomas, S., Prasannakumari, L., Koshy, P., Pavithran, C., 1996. Influence of interfacial adhesion on the mechanical properties and fracture behaviour of short sisal fibre reinforced polymer composites. *Eur. Polym. J.* 32, 1243–1250.

- Joseph, P.V., Joseph, K., Thomas, S., Pillai, C.K.S., Prasad, V.S., Groeninckx, G., Sarkissova, M., 2003. The thermal and crystallisation studies of short sisal fibre reinforced polypropylene composites. *Compos. Part A Appl. Sci. Manuf.* 34, 253–266.
- Joseph, P. V., Mathew, G., Joseph, K., Thomas, S., Pradeep, P., 2003. Mechanical properties of short sisal fibre reinforced polypropylene composites: Comparison of experimental data with theoretical predictions. *J. Appl. Polym. Sci.* 88, 602–611.
- Joseph, P. V, Joseph, K., Thomas, S., 1999. Effect of processing variables on the mechanical properties of sisal fibre reinforced polypropylene composites. *Compos. Part B Eng.* 59, 1625–1640.
- Joseph, P. V, Mathew, G., Joseph, K., Groeninckx, G., Thomas, S., 2003. Dynamic mechanical properties of short sisal fibre reinforced polypropylene composites. *Compos. Part A Appl. Sci. Manuf.* 34, 275–290.
- Joussein, E., Petit, S., Churchman, J., Theng, B., Righi, D., Delvaux, B., 2005. Halloysite clay minerals – a review. *Clay Miner.* 40, 383–426.
- Kabir, M.M., Wang, H., Lau, K.T., Cardona, F., 2013a. Tensile properties of chemically treated hemp fibres as reinforcement for composites. *Compos. Part B Eng.* 53, 362–368.
- Kabir, M.M., Wang, H., Lau, K.T., Cardona, F., 2013b. Effects of chemical treatments on hemp fibre structure. *Appl. Surf. Sci.* 276, 13–23.
- Kabir, M.M., Wang, H., Lau, K.T., Cardona, F., 2012. Chemical treatments on plant-based natural fibre reinforced polymer composites: An overview. *Compos. Part*

B Eng. 43, 2883–2892.

Kaewkuk, S., Sutapun, W., Jarukumjorn, K., 2013. Effects of interfacial modification and fiber content on physical properties of sisal fibre/polypropylene composites. *Compos. Part B Eng.* 45, 544–549.

Kalaprasad, G., Joseph, K., Thomas, S., Pavithran, C., 1997. Theoretical modelling of tensile properties of short sisal fibre-reinforced low-density polyethylene composites. *J. Mater. Sci.* 32, 4261–4267.

Kaushik, V.K., Kumar, A., Kalia, S., 2012. Effect of mercerization and benzoyl peroxide treatment on morphology, thermal stability and crystallinity of sisal fibres. *Int. J. Text. Sci.* 1, 101–105.

Khonakdar, H.A., 2015. Dynamic mechanical analysis and thermal properties of LLDPE/EVA/modified silica nanocomposites. *Compos. Part B Eng.* 76, 343–353.

Kim, H., Yang, H., Kim, H., 2005. Biodegradability and mechanical properties of agro-flour – filled polybutylene succinate biocomposites. *J. Appl. Phys.* 97, 1513–1521.

Kim, I.-H.H., Jeong, Y.G., 2010. Polylactide/exfoliated graphite nanocomposites with enhanced thermal stability, mechanical modulus, and electrical conductivity. *J. Polym. Sci. Part B Polym. Phys.* 48, 850–858.

Kontou, E., Niaounakis, M., Georgiopoulos, P., Evagelia, K., Michael, N., Panayiotis, G., Kontou, E., Niaounakis, M., Georgiopoulos, P., 2011. Comparative study of PLA nanocomposites reinforced with clay and silica nanofillers and their mixtures. *J. Appl. Polym. Sci.* 122, 1519–1529.

- Koronis, G., Silva, A., Fontul, M., 2013a. Green composites: A review of adequate materials for automotive applications. *Compos. Part B Eng.* 44, 120–127.
- Koronis, G., Silva, A., Fontul, M., 2013b. Green composites : A review of adequate materials for automotive applications. *Compos. Part B* 44, 120–127.
- Krikorian, V., Pochan, D., 2005. Crystallization behavior of poly(lactic acid) nanocomposites: nucleation and growth probed by infrared spectroscopy. *Macromolecules* 38, 6520–6527.
- Krishnaiah, P., Ratnam, C.T., Manickam, S., 2017. Enhancements in crystallinity, thermal stability, tensile modulus and strength of sisal fibres and their PP composites induced by the synergistic effects of alkali and high intensity ultrasound (HIU) treatments. *Ultrason. Sonochem.* 34, 729–742.
- Lacroix, T., Tilmans, B., Keunings, R., Desaegeer, M., Verpoest, I., 1992. Modelling of critical fibre length and interfacial debonding in the fragmentation testing of polymer composites. *Compos. Sci. Technol.* 43, 379–387.
- Lavoratti, A., Scienza, L.C., Zattera, A.J., 2015. Dynamic-mechanical and thermomechanical properties of cellulose nanofibre/polyester resin composites. *Carbohydr. Polym.* 136, 955–963.
- Le Troedec, M., Sedan, D., Peyratout, C., Bonnet, J.P., Smith, A., Guinebretiere, R., Gloaguen, V., Krausz, P., 2008. Influence of various chemical treatments on the composition and structure of hemp fibres. *Compos. Part A Appl. Sci. Manuf.* 39, 514–522.
- Lecouvet, B., Sclavons, M., Bourbigot, S., Bailly, C., 2013. Thermal and flammability properties of polyethersulfone/halloysite nanocomposites prepared by melt

- compounding. *Polym. Degrad. Stab.* 98, 1993–2004.
- Lee, H.S., Cho, D., Han, S.O., 2008. Effect of natural fiber surface treatments on the interfacial and mechanical properties of henequen/polypropylene biocomposites. *Macromol. Res.* 16, 411–417.
- Lee, K.-Y.Y., Bharadia, P., Blaker, J.J., Bismarck, A., 2012. Short sisal fibre reinforced bacterial cellulose polylactide nanocomposites using hairy sisal fibres as reinforcement. *Compos. Part A Appl. Sci. Manuf.* 43, 2065–2074.
- Li, W., Yue, J., Liu, S., 2012. Preparation of nanocrystalline cellulose via ultrasound and its reinforcement capability for poly (vinyl alcohol) composites. *Ultrason-Sonochem.* 19, 479–485.
- Li, X., Tabil, L.G., Panigrahi, S., 2007. Chemical treatments of natural fibre for use in natural fiber-reinforced composites: A review. *J. Polym. Environ.* 15, 25–33.
- Li, Y., Mai, Y.-W., Ye, L., 2000. Sisal fibre and its composites: A review of recent developments. *Compos. Sci. Technol.* 60, 2037–2055.
- Li, Y., Pickering, K.L., 2009. The effect of chelator and white rot fungi treatments on long hemp fibre-reinforced composites. *Compos. Sci. Technol.* 69, 1265–1270.
- Li, Y., Pickering, K.L., Farrell, R.L., 2009. Determination of interfacial shear strength of white rot fungi treated hemp fibre reinforced polypropylene. *Compos. Sci. Technol.* 69, 1165–1171.
- Li, Z., Zhou, X., Pei, C., 2011. Effect of sisal fibre surface treatment on the properties of sisal fibre reinforced polylactide composites. *Int. J. Polym. Sci.* 2011, 1–7.
- Lim, L.-T., Auras, R., Rubino, M., 2008. Processing technologies for poly (lactic

- acid). *Prog. Polym. Sci.* 33, 820–852.
- Lin, Y., Ng, K.M., Chan, C.-M., Sun, G., Wu, J., 2011. High-impact polystyrene/halloysite nanocomposites prepared by emulsion polymerization using sodium dodecyl sulfate as surfactant. *J. Colloid Interface Sci.* 358, 423–429.
- Liu, M., Guo, B., Du, M., Chen, F., Jia, D., 2009. Halloysite nanotubes as a novel β -nucleating agent for isotactic polypropylene. *Polymer.* 50, 3022–3030.
- Liu, M., Jia, Z., Jia, D., Zhou, C., 2014. Recent advance in research on halloysite nanotubes-polymer nanocomposite. *Prog. Polym. Sci.* 39, 1498–1525.
- Liu, M., Jia, Z., Liu, F., Jia, D., Guo, B., 2010. Tailoring the wettability of polypropylene surfaces with halloysite nanotubes. *J. Colloid Interface Sci.* 350, 186–193.
- Liu, M., Zhang, Y., Zhou, C., 2013. Nanocomposites of halloysite and polylactide. *Appl. Clay Sci.* 75–76, 52–59.
- López, J.P., Boufi, S., Mansouri, N.E. El, Mutjé, P., Vilaseca, F., 2012. PP composites based on mechanical pulp, deinked newspaper and jute strands: A comparative study. *Compos. Part B* 43, 3453–3461.
- López, J.P., Mutjé, P., Carvalho, A.J.F., Curvelo, A.A.S., Gironès, J., 2013. Newspaper fibre-reinforced thermoplastic starch biocomposites obtained by melt processing: Evaluation of the mechanical, thermal and water sorption properties. *Ind. Crop. Prod.* 44, 300–305.
- Lu, T., Jiang, M., Jiang, Z., Hui, D., Wang, Z., Zhou, Z., 2013. Effect of surface

- modification of bamboo cellulose fibres on mechanical properties of cellulose/epoxy composites. *Compos. Part B Eng.* 51, 28–34.
- Luo, H., Xiong, G., Ma, C., Chang, P., Yao, F., Zhu, Y., Zhang, C., Wan, Y., 2014. Mechanical and thermo-mechanical behaviors of sizing-treated corn fibre/polylactide composites. *Polym. Test.* 39, 45–52.
- Ma, H., Whan Joo, C., 2011. Influence of surface treatments on structural and mechanical properties of bamboo fibre-reinforced poly(lactic acid) biocomposites. *J. Compos. Mater.* 45, 2455–2463.
- MacMillan, J., 2009. Using Silanes as Adhesion Promoters. United Chem. Technol. Inc. 4–23.
- Mahjoub, R., Yatim, J.M., Mohd Sam, A.R., Hashemi, S.H., 2014. Tensile properties of kenaf fibre due to various conditions of chemical fiber surface modifications. *Constr. Build. Mater.* 55, 103–113.
- Majeed, K., Jawaid, M., Hassan, A., Abu Bakar, A., Abdul Khalil, H.P.S., Salema, A.A., Inuwa, I., 2013. Potential materials for food packaging from nanoclay/natural fibres filled hybrid composites. *Mater. Des.* 46, 391–410.
- Malhotra, S., Goda, K., Sreekala, M.S., 2012. Advances in polymer composites: Macro- and microcomposites – state of the art, new challenges and opportunities, in: *Introduction to Polymer Composites*. 1. 1–16.
- Mantia, F.P. La, Morreale, M., 2011. Green composites : A brief review. *Compos. Part A* 42, 579–588.
- Matusik, J., Stodolak, E., Bahranowski, K., 2011. Synthesis of polylactide/clay

- composites using structurally different kaolinites and kaolinite nanotubes. *Appl. Clay Sci.* 51, 102–109.
- Mishra, S., Mohanty, A.K., Drzal, L.T., Misra, M., Hinrichsen, G., 2004. A review on pineapple leaf fibres, sisal fibres and their biocomposites. *Macromol. Mater. Eng.* 289, 955–974.
- Mishra, S., Rathore, D.K., Ray, B.C., 2014. A recent understanding on theories of moisture ingress and its effect on FRP composites. *J. Adv. Res. Manuf. Mater. Sci. Metall. Eng.* 1, 29–52.
- Mitra, Basak, Sarkar, 1998. Studies on jute-reinforced composites, its limitations, and some solutions through chemical modifications of fibres. *J. Appl. Polym. Sci.* 67, 1093–1100.
- Mohan, T.P., Kanny, K., 2012. Chemical treatment of sisal fibre using alkali and clay method. *Compos. Part A Appl. Sci. Manuf.* 43, 1989–1998.
- Mokaloba, N., Batane, R., 2014. The effects of mercerization and acetylation treatments on the properties of sisal fibre and its interfacial adhesion characteristics on polypropylene. *Int. J. Eng. Sci. Technol.* 6, 83–97.
- Moshiul Alam, A.K.M., Beg, M.D.H., Reddy Prasad, D.M., Khan, M.R., Mina, M.F., 2012. Structures and performances of simultaneous ultrasound and alkali treated oil palm empty fruit bunch fibre reinforced poly(lactic acid) composites. *Compos. Part A Appl. Sci. Manuf.* 43, 1921–1929.
- Mwaikambo, L.Y., Ansell, M.P., 2002. Chemical modification of hemp, sisal, jute, and kapok fibres by alkalization. *J. Appl. Polym. Sci.* 84, 2222–2234.

- Mwaikambo, L.Y., Ansell, M.P., 1999. The effect of chemical treatment on the properties of hemp, sisal, jute and kapok for composite reinforcement. *Angew. Makromol. Chemie* 272, 108–116.
- Mwaikambo, L.Y., Tucker, N., Clark, A.J., 2007. Mechanical properties of hemp-fibre-reinforced euphorbia composites. *Macromol. Mater. Eng.* 292, 993–1000.
- Nair, K.C.M., Thomas, S., Groeninckx, G., 2001. Thermal and dynamic mechanical analysis of polystyrene composites reinforced with short sisal fibres. *Compos. Sci. Technol.* 61, 2519–2529.
- Nampoothiri, K.M., Nair, N.R., John, R.P., 2010. An overview of the recent developments in polylactide (PLA) research. *Bioresour. Technol.* 101, 8493–8501.
- NatureWorks LLC, 2013. Ingeo™ Biopolymer 2003D Technical Data Sheet For Fresh Food Packaging and Food Serviceware.
- Nayak, S.K., Dixit, G., Appu Kuttan, K.K., 2013. Mechanical properties of eco-friendly recycled polymer composites: A comparative study of theoretical and experimental results. *Int. J. Plast. Technol.* 17, 75–93.
- Nel, A., 2007. Toxic Potential of Materials. *Science*. 311, 622–627.
- Nishiyama, Y., Kuga, S., Okano, T., 2000. Mechanism of mercerization revealed by X-ray diffraction. *J. Wood Sci.* 46, 452–457.
- Notta-cuvier, D., Odent, J., Delille, R., Murariu, M., Lauro, F., Raquez, J.M., 2014. Tailoring polylactide (PLA) properties for automotive applications: Effect of addition of designed additives on main mechanical properties. *Polym. Test.* 36,

1–9.

- Oh, S.Y., Dong, I.Y., Shin, Y., Hwan, C.K., Hak, Y.K., Yong, S.C., Won, H.P., Ji, H.Y., 2005. Crystalline structure analysis of cellulose treated with sodium hydroxide and carbon dioxide by means of X-ray diffraction and FTIR spectroscopy. *Carbohydr. Res.* 340, 2376–2391.
- Ohkita, T., Lee, S.H., 2006. Thermal degradation and biodegradability of poly (lactic acid)/corn starch biocomposites. *J. Appl. Polym. Sci.* 100, 3009–3017.
- Orue, A., Jauregi, A., Peña-Rodriguez, C., Labidi, J., Eceiza, A., Arbelaiz, A., 2015. The effect of surface modifications on sisal fibre properties and sisal/poly(lactic acid) interface adhesion. *Compos. Part B Eng.* 73, 132–138.
- Orue, A., Jauregi, A., Unsuain, U., Labidi, J., Eceiza, A., Arbelaiz, A., 2016. The effect of alkaline and silane treatments on mechanical properties and breakage of sisal fibres and poly (lactic acid)/ sisal fibre composites. *Compos. - Part A Appl. Sci. Manuf.* 84, 186–195.
- Oujai, S., Shanks, R.A., 2005. Composition, structure and thermal degradation of hemp cellulose after chemical treatments. *Polym. Degrad. Stab.* 89, 327–335.
- Oza, S., Ning, H., Ferguson, I., Lu, N., 2014. Effect of surface treatment on thermal stability of the hemp-PLA composites: Correlation of activation energy with thermal degradation. *Compos. Part B Eng.* 67, 227–232.
- Pandey, J.K., Raghunatha Reddy, K., Pratheep Kumar, A., Singh, R.P., 2005. An overview on the degradability of polymer nanocomposites. *Polym. Degrad. Stab.* 88, 234–250.

- Paraparita, E., Darie, R.N., Popescu, C.M., Uddin, M.A., Vasile, C., 2014. Structure-morphology-mechanical properties relationship of some polypropylene/lignocellulosic composites. *Mater. Des.* 56, 763–772.
- Park, S., Baker, J.O., Himmel, M.E., Parilla, P.A., Johnson, D.K., 2010. Cellulose crystallinity index: measurement techniques and their impact on interpreting cellulase performance. *Biotechnol. Biofuels.* 3, 1-10.
- Park, S.H., Lee, S.G., Kim, S.H., 2013. Isothermal crystallization behavior and mechanical properties of polylactide/carbon nanotube nanocomposites. *Compos. Part A Appl. Sci. Manuf.* 46, 11–18.
- Pasbakhsh, P., Ismail, H., Fauzi, M.N.A., Bakar, A., 2010. EPDM/modified halloysite nanocomposites. *Appl. Clay Sci.* 48, 405–413.
- Paul, V., Kanny, K., Redhi, G.G., 2015. Mechanical, thermal and morphological properties of a bio-based composite derived from banana plant source. *Compos. Part A Appl. Sci. Manuf.* 68, 90–100.
- Pérez, E., Alvarez, V., Pérez, C.J., Bernal, C., 2013. A comparative study of the effect of different rigid fillers on the fracture and failure behavior of polypropylene based composites. *Compos. Part B Eng.* 52, 72–83.
- Petinakis, E., Yu, L., Edward, G., Dean, K., Liu, H., Scully, A.D., 2009. Effect of matrix-particle interfacial adhesion on the mechanical properties of poly(lactic acid)/wood-flour micro-composites. *J. Polym. Environ.* 17, 83–94.
- Pickering, K.L., Efendy, M.G.A., Le, T.M., 2016. A review of recent developments in natural fibre composites and their mechanical performance. *Compos. Part A Appl. Sci. Manuf.* 83, 98–112.

- Porras, A., Maranon, A., 2012. Development and characterization of a laminate composite material from polylactic acid (PLA) and woven bamboo fabric. *Compos. Part B* 43, 2782–2788.
- Pothan, L.A., Oommen, Z., Thomas, S., 2003. Dynamic mechanical analysis of banana fibre reinforced polyester composites. *Compos. Sci. Technol.* 63, 283–293.
- Pothan, L.A., Thomas, S., Groeninckx, G., 2006. The role of fibre/matrix interactions on the dynamic mechanical properties of chemically modified banana fibre/polyester composites. *Compos. Part A Appl. Sci. Manuf.* 37, 1260–1269.
- Prashantha, K., Lacrampe, M. F., Krawczak, P., 2011. Processing and characterization of halloysite nanotubes filled polypropylene nanocomposites based on a masterbatch route: effect of halloysites treatment on structural and mechanical properties. *Express Polym. Lett.* 5, 295–307.
- Prashantha, K., Schmitt, H., Lacrampe, M.F., Krawczak, P., 2011. Mechanical behaviour and essential work of fracture of halloysite nanotubes filled polyamide 6 nanocomposites. *Compos. Sci. Technol.* 71, 1859–1866.
- Ragoubi, M., George, B., Molina, S., Bienaimé, D., Merlin, A., Hiver, J.M., Dahoun, A., 2012. Effect of corona discharge treatment on mechanical and thermal properties of composites based on miscanthus fibres and polylactic acid or polypropylene matrix. *Compos. Part A Appl. Sci. Manuf.* 43, 675–685.
- Rajesh, G., Prasad, A.R., Gupta, A., 2015. Mechanical and degradation properties of successive alkali treated completely biodegradable sisal fibre reinforced poly lactic acid composites. *J. Reinf. Plast. Compos.* 34, 951–961.

- Ramadevi, P., Sampathkumar, D., Srinivasa, C.V., Bennehalli, B., 2012. Effect of alkali treatment on water absorption of single cellulosic abaca fibre. *BioResources* 7, 3515–3524.
- Raquez, J.-M., Habibi, Y., Murariu, M., Dubois, P., 2013. Polylactide (PLA)-based nanocomposites. *Progr Polym Sci* 38, 1504–1542.
- Rasal, R.M., Janorkar, A. V., Hirt, D.E., 2010. Poly(lactic acid) modifications. *Prog. Polym. Sci.* 35, 338–356.
- Rathin Datta and Michael Henry, 2006. Lactic acid: recent advances in products, processes and technologies – a review. *J. Chem. Technol. Biotechnol.* 81, 1119–1129.
- Ray, D., Sarkar, B.K., Das, S., Rana, A.K., 2002. Dynamic mechanical and thermal analysis of vinylester-resin-matrix composites reinforced with untreated and alkali-treated jute fibres. *Compos. Sci. Technol.* 62, 911–917.
- Rittigstein, P., Priestley, R.D., Broadbelt, L.J., Torkelson, J.M., 2007. Model polymer nanocomposites provide an understanding of confinement effects in real nanocomposites. *Nat. Mater.* 6, 278–282.
- Rong, M.Z., Zhang, M.Q., Liu, Y., Yang, G.C., Zeng, H.M., 2001. The effect of fibre treatment on the mechanical properties of unidirectional sisal-reinforced epoxy composites. *Compos. Sci. Technol.* 61, 1437–1447.
- Rooj, S., Das, A., Thakur, V., Mahaling, R.N., Bhowmick, A.K., Heinrich, G., 2010. Preparation and properties of natural nanocomposites based on natural rubber and naturally occurring halloysite nanotubes. *Mater. Des.* 31, 2151–2156.

- Rosa, M.F., Chiou, B. S, Medeiros, E.S., Wood, D.F., Williams, T.G., Mattoso, L.H.C., Orts, W.J., Imam, S.H., 2009. Effect of fibre treatments on tensile and thermal properties of starch/ethylene vinyl alcohol copolymers/coir biocomposites. *Bioresour. Technol.* 100, 5196–5202.
- Russo, P., Acierno, D., Rosa, R., Leonelli, C., Corradi, A., Rizzuti, A., 2014. Mechanical and dynamic-mechanical behavior and morphology of polystyrene/perovskite composites: Effects of filler size. *Surf. Coatings Technol.* 243, 65–70.
- Saba, N., Jawaid, M., Allothman, O.Y., Paridah, M.T., 2016. A review on dynamic mechanical properties of natural fibre reinforced polymer composites. *Constr. Build. Mater.* 106, 149–159.
- Saeidlou, S., Huneault, M.A., Li, H., Park, C.B., 2012. Poly (lactic acid) crystallization. *Prog. Polym. Sci.* 37, 1657–1677.
- Sanomura, Y., Kawamura, M., 2003. Fiber orientation control of short-fibre reinforced thermoplastics by ram extrusion. *Polym. Compos.* 24, 587–596.
- Satyanarayana, K.G., Arizaga, G.G.C., Wypych, F., 2009. Biodegradable composites based on lignocellulosic fibres-An overview. *Prog. Polym. Sci.* 34, 982–1021.
- Sawpan, M.A., 2009. Mechanical Performance of Industrial Hemp Fibre Reinforced Polylactide and Unsaturated Polyester Composites. PhD Thesis, The University of Waikato.
- Sawpan, M.A., Pickering, K.L., Fernyhough, A., 2011. Effect of fibre treatments on interfacial shear strength of hemp fibre reinforced polylactide and unsaturated polyester composites. *Compos. Part A Appl. Sci. Manuf.* 42, 1189–1196.

- Semba, T., Kitagawa, K., Ishiaku, U.S., Hamada, H., 2006. The effect of crosslinking on the mechanical properties of polylactic acid/polycaprolactone blends. *J. Appl. Polym. Sci.* 101, 1816–1825.
- Serrano, A., Espinach, F.X., Tresserras, J., del Rey, R., Pellicer, N., Mutje, P., 2014. Macro and micromechanics analysis of short fibre composites stiffness: The case of old newspaper fibres-polypropylene composites. *Mater. Des.* 55, 319–324.
- Shanmugam, D., Thiruchitrambalam, M., 2013. Static and dynamic mechanical properties of alkali treated unidirectional continuous palmyra palm leaf stalk fibre/jute fiber reinforced hybrid polyester composites. *Mater. Des.* 50, 533–542.
- Shelley, J.S., Mather, P.T., DeVries, K.L., 2001. Reinforcement and environmental degradation of nylon-6/clay nanocomposites. *Polymer (Guildf.)* 42, 5849–5858.
- Shinoj, S., Visvanathan, R., Panigrahi, S., Varadharaju, N., 2011. Dynamic mechanical properties of oil palm fibre (OPF)-linear low density polyethylene (LLDPE) biocomposites and study of fibre-matrix interactions. *Biosyst. Eng.* 109, 99–107.
- Shukor, F., Hassan, A., Saiful Islam, M., Mokhtar, M., Hasan, M., 2014. Effect of ammonium polyphosphate on flame retardancy, thermal stability and mechanical properties of alkali treated kenaf fibre filled PLA biocomposites. *Mater. Des.* 54, 425–429.
- Silva, F. de A., Chawla, N., de Toledo Filho, R.D., 2009. An experimental investigation of the fatigue behavior of sisal fibres. *Mater. Sci. Eng. A* 516, 90–95.
- Silva, F.D.A., Chawla, N., Filho, R.D.D.T., 2008. Tensile behavior of high

- performance natural (sisal) fibres. *Compos. Sci. Technol.* 68, 3438–3443.
- Sing, K.S.W., 1982. Reporting physisorption data for gas/solid systems with special reference to the determination of surface area and porosity. *Pure Appl. Chem.* 54, 2201–2218.
- Sinha Ray, S., Okamoto, M., 2003. Polymer/layered silicate nanocomposites: A review from preparation to processing. *Prog. Polym. Sci.* 28, 1539–1641.
- Siquan Wang, Q.C., 2009. A novel process to isolate fibrils from cellulose fibres by high-intensity ultrasonication, part 1: Process optimization. *J. Appl. Polym. Sci.* 113, 1270–1275.
- Somerville, C.R., Bauer, S., Brininstool, G., Facette, M., Hamann, T., Milne, J., Osborne, E., Paredes, A.R., Persson, S., Raab, T., Vorwerk, S., Youngs, H., 2004. Toward a Systems Approach to Understanding Plant Cell Walls. *ScienceMag* 306, 2206–2211.
- Sperling, L.H., 2005. Introduction to physical polymer science, Introduction to Physical Polymer Science.
- Sreekala, M.S., Thomas, S., 2003. Effect of fibre surface modification on water-sorption characteristics of oil palm fibres. *Compos. Sci. Technol.* 63, 861–869.
- Sreenivasan, V.S., Rajini, N., Alavudeen, A., Arumugaprabu, V., 2015. Dynamic mechanical and thermo-gravimetric analysis of *Sansevieria cylindrica*/polyester composite: Effect of fibre length, fibre loading and chemical treatment. *Compos. Part B Eng.* 69, 76–86.
- Stephanie, L.A., 2014. Chemical modification of lignins: Towards biobased polymers.

Prog. Polym. Sci. 39, 1266–1290.

Sudhakara, P., Jagadeesh, D., Wang, Y., Venkata Prasad, C., Devi, A.P.K., Balakrishnan, G., Kim, B.S., Song, J.I., 2013. Fabrication of Borassus fruit lignocellulose fibre/PP composites and comparison with jute, sisal and coir fibres. Carbohydr. Polym. 98, 1002–1010.

Šutka, A., Kukle, S., Gravitis, J., Grave, L., 2013. Characterization of cellulose microfibrils obtained from hemp. Conf. Pap. Mater. Sci. 2013, 1–5.

Thomason, J.L., 1997. Thomason J. L., Vlugg M. A. Influence of fibre length and concentration on the properties of glass fibre-reinforced polypropylene: Part 4. Impact Properties. Compos. Part A 28A, 277–88.

Thommes, M., Kaneko, K., Neimark, A. V., Olivier, J.P., Rodriguez-Reinoso, F., Rouquerol, J., Sing, K.S.W., 2015. Physisorption of gases, with special reference to the evaluation of surface area and pore size distribution (IUPAC Technical Report). Pure Appl. Chem. 87, 1051–1069.

Tischer, P.C.S.F., Sierakowski, M.R., Westfahl, H., Tischer, C.A., 2010. Nanostructural reorganization of bacterial cellulose by ultrasonic treatment. Biomacromolecules 11, 1217–1224.

Tisserat, B., Joshee, N., Mahapatra, A.K., Selling, G.W., Finkenstadt, V.L., 2013. Physical and mechanical properties of extruded poly(lactic acid)-based Paulownia elongata biocomposites. Ind. Crops Prod. 44, 88–96.

Tjong, S.C., 2013. Recent progress in the development and properties of novel metal matrix nanocomposites reinforced with carbon nanotubes and graphene nanosheets. Mater. Sci. Eng. R Reports 74, 281–350.

- Vilaseca, F., Valadez-Gonzalez, A., Herrera-Franco, P.J., Pelach, M.A., Lopez, J.P., Mutje, P., 2010. Biocomposites from abaca strands and polypropylene. Part I: Evaluation of the tensile properties. *Bioresour. Technol.* 101, 387–395.
- Vilay, V., Mariatti, M., Mat Taib, R., Todo, M., 2008. Effect of fibre surface treatment and fibre loading on the properties of bagasse fibre-reinforced unsaturated polyester composites. *Compos. Sci. Technol.* 68, 631–638.
- Wang, B., Huang, H.-X., 2013. Effects of halloysite nanotube orientation on crystallization and thermal stability of polypropylene nanocomposites. *Polym. Degrad. Stab.* 98, 1601–1608.
- Wang, H., Qiu, Z., 2011. Crystallization behaviors of biodegradable poly(l-lactic acid)/graphene oxide nanocomposites from the amorphous state. *Thermochim. Acta* 526, 229–236.
- Wootthikanokkhan, J., Cheachun, T., Sombatsompop, N., Thumsorn, S., Kaabbuathong, N., Wongta, N., Wong-On, J., Na Ayutthaya, S.I., Kositchaiyong, A., 2013. Crystallization and thermomechanical properties of PLA composites: Effects of additive types and heat treatment. *J. Appl. Polym. Sci.* 129, 215–223.
- Wu, W., Cao, X., Zhang, Y., He, G., 2013. Polylactide/halloysite nanotube nanocomposites: Thermal, mechanical properties, and foam processing. *J. Appl. Polym. Sci.* 130, 443–452.
- Yan, L., Chouw, N., Huang, L., Kasal, B., 2016a. Effect of alkali treatment on microstructure and mechanical properties of coir fibres , coir fibre reinforced-polymer composites and reinforced-cementitious composites. *Constr. Build.*

Mater. 112, 168–182.

Yan, L., Kasal, B., Huang, L., 2016b. A review of recent research on the use of cellulosic fibres, their fibre fabric reinforced cementitious, geo-polymer and polymer composites in civil engineering. *Compos. Part B* 92, 94–132.

Yao, Z.T., Chen, T., Li, H.Y., Xia, M.S., Ye, Y., Zheng, H., 2013. Mechanical and thermal properties of polypropylene (PP) composites filled with modified shell waste. *J. Hazard. Mater.* 262, 212–217.

Yeh, S.K., Hsieh, C.C., Chang, H.C., Yen, C.C.C., Chang, Y.C., 2015. Synergistic effect of coupling agents and fiber treatments on mechanical properties and moisture absorption of polypropylene-rice husk composites and their foam. *Compos. Part A Appl. Sci. Manuf.* 68, 313–322.

Yew, G.H., Mohd Yusof, A.M., Mohd Ishak, Z.A., Ishiaku, U.S., 2005. Water absorption and enzymatic degradation of poly(lactic acid)/rice starch composites. *Polym. Degrad. Stab.* 90, 488–500.

Yu, T., Jiang, N., Li, Y., 2014. Study on short ramie fibre/poly(lactic acid) composites compatibilized by maleic anhydride. *Compos. Part A Appl. Sci. Manuf.* 64, 139–146.

Yuan, P., Southon, P.D., Liu, Z., Green, M.E.R., Hook, J.M., Antill, S.J., Kepert, C.J., 2008. Functionalization of halloysite clay nanotubes by grafting with 3-aminopropyltriethoxysilane. *J. Phys. Chem. C* 112, 15742–15751.

Yuan, P., Tan, D., Annabi-Bergaya, F., 2015. Properties and applications of halloysite nanotubes: recent research advances and future prospects. *Appl. Clay Sci.* 112–113, 75–93.

- Yussuf, A.A., Massoumi, I., Hassan, A., 2010. Comparison of polylactic Acid/Kenaf and polylactic Acid/Rise husk composites: The influence of the natural fibres on the mechanical, thermal and biodegradability properties. *J. Polym. Environ.* 18, 422–429.
- Zhang, L., Ye, X., Xue, S.J., Zhang, X., Liu, D., Meng, R., Chen, S., 2013. Effect of high-intensity ultrasound on the physicochemical properties and nanostructure of citrus pectin. *J. Sci. Food Agric.* 93, 2028–2036.
- Zhao, Q., Tao, J., Yam, R.C.M., Mok, A.C.K., Li, R.K.Y., Song, C., 2008. Biodegradation behavior of polycaprolactone/rice husk eco-composites in simulated soil medium. *Polym. Degrad. Stab.* 93, 1571–1576.
- Zhong, L.X., Fu, S.Y., Zhou, X.S., Zhan, H.Y., 2011. Effect of surface microfibrillation of sisal fibre on the mechanical properties of sisal/aramid fibre hybrid composites. *Compos. Part A Appl. Sci. Manuf.* 42, 244–252.
- Zhou, F., Cheng, G., Jiang, B., 2014. Effect of silane treatment on microstructure of sisal fibres. *Appl. Surf. Sci.* 292, 806–812.
- Zhu, C., Richardson, R.M., Potter, K., Koutsomitopoulou, A., Van Duijneveldt, J.S., Vincent, S.R., Wanasekara, N.D., Eichhorn, S.J., Rahatekar, S.S., 2016. High Modulus Regenerated Cellulose Fibres Spun from a Low Molecular Weight Microcrystalline Cellulose Solution. *ACS Sustain. Chem. Eng.* 4, 4545–4553.

Appendices

Appendix – A

Calculation of the volume fraction of fibres for 10 wt% of sisal fibre loading

Volume fraction of fibres (V_f) can be calculated by using the following equation

1(Messiry, 2013):

$$V_f = \frac{W_f \times \rho_m}{(\rho_m \times W_f) + (\rho_f \times W_m)}$$

Whereas ρ_f and ρ_m are the density of fibres and matrix respectively. W_f and W_m are the weight of the fibres and matrix respectively.

$$\rho_f = 1.41 \text{ g/cm}^3$$

$$\rho_m = 1.25 \text{ g/cm}^3$$

$$W_f = 0.01 \text{ kg}$$

$$W_m = 0.09 \text{ kg}$$

$$V_f = \frac{0.01 \times 1.25}{(1.25 \times 0.01) + (1.41 \times 0.09)}$$

$$V_f = 0.089$$

Calculation of the tensile modulus by Parallel and Series models:

Tensile modulus was calculated by using the equation 2.1 and 2.2

$$M_c = \eta_e * M_f * V_f + (1 - V_f) * M_m$$

Where, M_c , M_f and M_m are the modulus of composites, fibre and matrix respectively.

η_e and V_f is the efficiency factor and volume fractions of fibres respectively.

The fibre efficiency factor (η_e) is the product of fibre orientation efficiency factor (η_0)

and fibre length efficiency factor (η_1). It can be calculated by using eqn 2.3, 2.4, 2.5

and 2.6.

$$M_f = 16.3 \text{ GPa}$$

$$M_m = 1.052 \text{ GPa}$$

$$V_f = 0.089$$

$$\eta_e = 0.43$$

Parallel model:

$$M_c = \eta_e * M_f * V_f + (1 - V_f) * M_m$$

$$M_c = 0.43 \times 16.3 \times 0.089 + (1 - 0.089) \times 1.052$$

$$M_c = 1.03 \text{ GPa}$$

Series model:

$$M_c = \frac{M_m \times M_f}{(M_m \times V_f) + M_f(1 - V_f)}$$

$$M_c = \frac{1.052 \times 16.3}{(1.052 \times 0.089) + 16.3(1 - 0.089)}$$

$$M_c = 1.147 \text{ GPa}$$

Hirsch model:

$$M_c = x (M_f V_f + M_m (1 - V_f)) + (1 - x) \frac{M_m \times M_f}{(M_m \times V_f) + M_f (1 - V_f)}$$

The factors which control the x values are: fibre orientation, fibre length and the effect of stress concentration of the fibres. The stress transfer factor x is approximately 0.4 which is in agreement with the semi-aligned short fibre reinforced polymer composites (Kalaprasad et al., 1997).

$$M_c = 0.4 (16.3 \times 0.089 + 1.052(0.911)) + (0.6) \frac{1.052 \times 16.3}{(1.052 \times 0.089) + 16.3 (0.911)}$$

$$M_c = 1.652 \text{ GPa}$$

Appendix – B

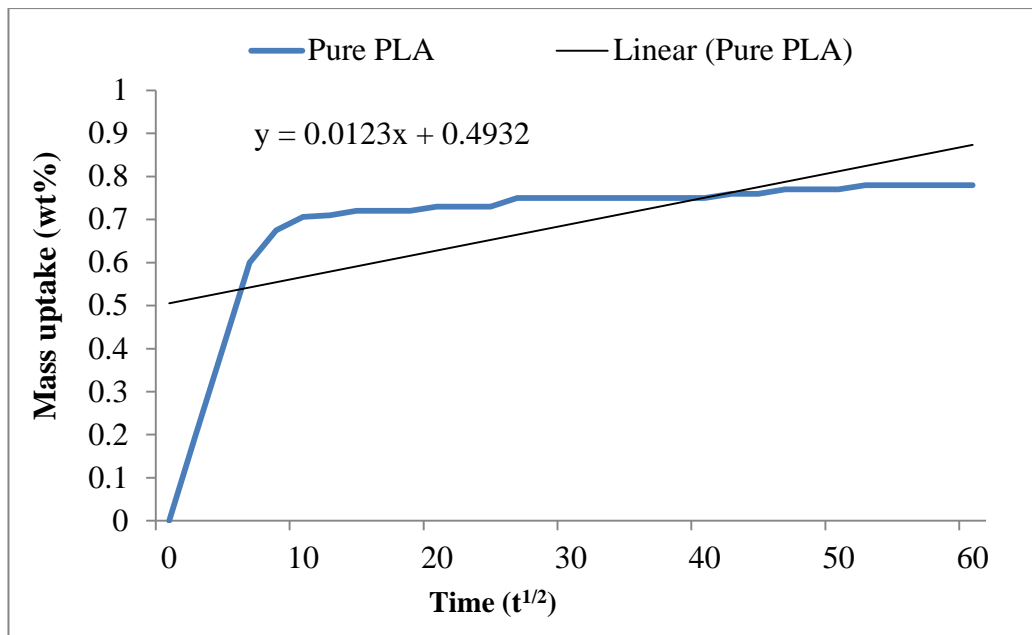


Fig. 1.1 Slope of diffusion coefficient of water uptake for pure PLA

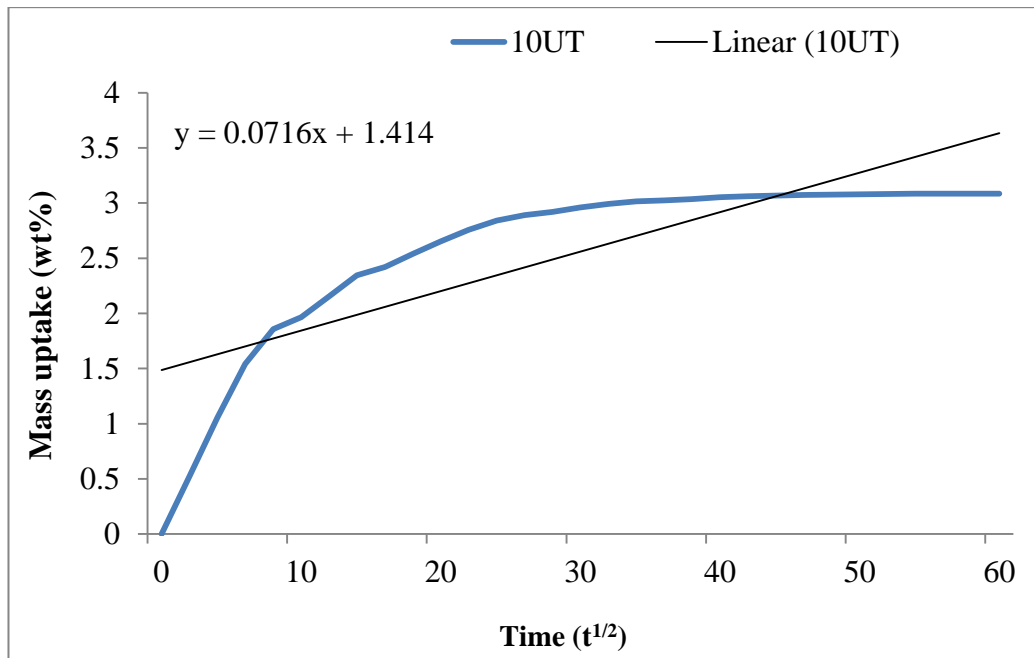


Fig. 1.2 Slope of diffusion coefficient of water uptake for PLA + untreated sisal fibre (10 wt%) composites

10UT: 10 wt% untreated sisal fibres